Synthesis of Filters for Digital Wireless Communications

Evaristo Musonda

Submitted in accordance with the requirements for the degree of
Doctor of Philosophy

The University of Leeds

Institute of Microwave and Photonics

School of Electronic and Electrical Engineering

December, 2015

The candidate confirms that the work submitted is his own, except where work which has formed part of jointly-authored publications has been included. The contribution of the candidate and the other authors to this work has been explicitly indicated below. The candidate confirms that appropriate credit has been given within the report where reference has been made to the work of others.

Chapter 2 to Chapter 6 are partly based on the following two papers:

Musonda, E. and Hunter, I.C., *Synthesis of general Chebyshev characteristic function for dual (single) bandpass filters*. *In Microwave Symposium (IMS), 2015 IEEE MTT-S International*. 2015.

Snyder, R.V., et al., *Present and Future Trends in Filters and Multiplexers.* Microwave Theory and Techniques, IEEE Transactions on, 2015. **63**(10): p. 3324-3360

E. Musonda developed the synthesis technique and wrote the first paper and section IV of the second invited paper. Professor Ian Hunter provided useful editorial comments, suggestions and corrections to the work.

Chapter 3 is based on the following two papers:

Musonda, E. and Hunter I.C., *Design of generalised Chebyshev lowpass filters using coupled line/stub sections*. *In Microwave Symposium (IMS), 2015 IEEE MTT-S International*. 2015.

Musonda, E. and I.C. Hunter, *Exact Design of a New Class of Generalised Chebyshev Low-Pass Filters Using Coupled Line/Stub Sections*. Microwave Theory and Techniques, IEEE Transactions on, 2015. PP(99): p. 1-11.

Supervisor (Professor Ian Hunter) proposed the initial physical realisation of a basic section and reviewed the final papers. E. Musonda developed the initial idea, developed the complete synthesis technique including the required transfer functions and circuit transformations, and wrote the papers.

Chapter 4 is based on the following paper:

Musonda, E. and Hunter I.C., *Microwave Bandpass Filters Using Re-Entrant Resonators.* Microwave Theory and Techniques, IEEE Transactions on, 2015. **63**(3): p. 954-964.

Supervisor (Professor Ian Hunter) proposed the idea of integrated resonance and transmission zero using the re-entrant transmission line and reviewed the final paper. E. Musonda developed the equivalent circuits, synthesis and design theory and wrote the paper.

Acknowledgements

My utmost gratitude goes to Professor Ian Hunter, my supervisor and research chair of Royal Academy of Engineering/Radio Design Ltd - Microwave Signal Processing, for his exemplary role and encouragement during my PhD research work.

I am grateful to Radio Design Limited for their technical support toward our research group at the University of Leeds. I am grateful to various individual supports from within School of Electronic and Electrical at Leeds University and my colleagues.

I also incessantly thank my PhD sponsors namely the University of Leeds under the oversight of Professor Ian Hunter, the Beit Trust for part funding towards my PhD and RS Microwave for providing equipment funding.

Lastly, I thank my family, my wife Caroline, my son Crescens, and daughters Whitney and Charlotte, for their endurance, emotional support and comfort rendered to me during the course of my research. I am forever indebted to my sister Mable, who has been like my mother and always been there for me whenever I needed someone to lean on.

Abstract

Firstly, a new synthesis method for the generation of the generalized Chebyshev characteristic polynomials has been presented. The general characteristic function is generated by a linear combination of Chebyshev basis characteristic functions. The basis functions for different filtering functions may easily be determined based on the number and position of reflection and transmission zeros. These basis functions enable direct synthesis of both lumped and distributed filter networks. Different filter functions including but not limited to low-pass, bandpass and dual bandpass filters, have been synthesised to demonstrate the general application of the synthesis method.

Secondly, a new method for the design of a new class of distributed low-pass filter has been presented that enables exact realisation of the series short circuited transmission lines which are normally approximated via unit elements in other filter realisations. The filters are based on parallel coupled high impedance transmission lines which are terminated at one end in open-circuited stubs. The approach enables realisation of both finite and quarter-wave frequency transmission zeros hence giving improved stopband performance. A complete design is presented and the fabricated low-pass filter demonstrates excellent performance in good agreement with theory.

Finally, design techniques for microwave bandpass filters using re-entrant resonators are presented. The key feature is that each re-entrant resonator in the filter generates a passband resonance and a finite frequency transmission zero, above the passband. Thus an N^{th} degree filter can have N finite frequency transmission zeros with a simple physical realization. A new synthesis technique for pseudo-elliptic low-pass filters suitable for designing re-entrant bandpass filter has also been show-cased. A physically symmetrical 5 pole re-entrant bandpass prototype filter with 5 transmission zeros above the passband was designed and fabricated. Measured results showed good correspondence with theories.

Table of Contents

Acknowledgements ..... **iv**

Abstract ..... **v**

Table of Contents ..... **vi**

List of Tables ..... **x**

List of Figures ..... **xv**

Motivation ..... **xxi**

Thesis Organisation ..... **xxv**

Chapter 1 Microwave Filters – Fundamentals **1**

1.1 Microwave Filter Networks – Analysis and Synthesis 1

1.1.1 Filter Transfer Function, Characteristic Function and Characteristic Polynomials 2

1.1.2 S-Parameters, ABCD Matrix and Y Admittance Matrix 8

1.1.3 Coupling Matrix Synthesis Method 13

1.1.4 Cascaded Synthesis Method 30

1.2 Design of Microwave Filters 38

1.2.1 Lumped Lowpass Prototype Filters 38

1.2.2 Frequency Transformation and Impedance Scaling 39

1.2.3 Distributed Elements Filters 39

1.2.4 Numerical EM Techniques 40

1.2.5 Other Design Considerations 52

1.3 Conclusion 53

Chapter 2 Method for Generating Generalised Chebyshev Polynomials **54**

2.1 Introduction 54

2.2 Generalised Chebyshev Characteristic Function 54

2.3 General Recursive Technique - Determining the characteristic polynomials 57

2.4 Basis Characteristic Functions 58

2.4.1 Lumped Generalised Chebyshev Low-pass Filters 60

2.4.2 Distributed Generalised Chebyshev Low-pass Filters 65

2.4.3 Lumped Generalised Chebyshev Bandpass Filters 66

2.4.4 Lumped Chebyshev Low-pass Prototype Filter for Interdigital Bandpass Filter 78
2.4.5 Distributed Generalised Chebyshev Bandpass Filters 83
2.4.6 Lumped Chebyshev Narrow Dual Bandpass Filters 86
2.4.7 Lumped Generalised Chebyshev Dual Bandpass Filters 89
2.5 Procedure for Generating the Filter Characteristic Polynomials 101
2.6 Examples 101
2.6.1 Direct Synthesis of Generalised Distributed Chebyshev Low-pass Filter 102
2.6.2 Direct Synthesis of Generalised Distributed Bandpass Filter 104
2.7 Conclusion 106
Chapter 3 Synthesis and Realisation of a New Class of Distributed Low-pass Filters 108
3.1 Introduction 108
3.2 Design Theory 109
Physical Realisation I 112
3.2.2 Physical Realisation II – 'Meander-like' Low-pass Filter 115
3.2.3 Comparison based on theory and simulations 129
3.3 Conclusion 131
Chapter 4 Synthesis and Design of Bandpass Filters with 'Integrated' Transmission Zeros Using Re-entrant Transmission Lines 132
4.1 Introduction 132
4.2 Transmission Zeros Generation Methods 133
4.3 Lowpass Prototype Filter Circuits for Pseudo-elliptic Bandpass Filters 134
4.3.1 Asymmetrical-Frequency-Transformed Pseudo-elliptic Lowpass Prototype Filter 134
4.3.2 General Synthesis for Pseudo-elliptic Lowpass Prototype Filter 139
4.3.3 Synthesis Illustrative Example 145
4.4 Re-entrant Resonators 147
4.4.1 Re-entrant Resonator producing a transmission zero above the passband 152
4.4.2 Re-entrant Resonator producing a transmission zero below the passband 157

4.5 Design Theory for Re-entrant Bandpass Filter.....159
4.5.1 Re-entrant Bandpass Filter Equivalent Circuit.....159
4.5.2 Pseudo-elliptic Lowpass Prototype filter to Bandpass filter Frequency Transformation.....160
4.5.3 Close-to-Band Transmission Zeroes.....163
4.5.4 Physical dimensions.....164
4.6 Design Examples.....166
4.6.1 Design Example I.....166
4.6.2 Design Example II.....168
4.7 Discussion.....171
4.7.1 High Selectivity.....172
4.7.2 Symmetrical Design.....172
4.7.3 Tunability.....173
4.7.4 Compact In-Line Filter Structure.....173
4.8 Conclusion.....174
Chapter 5 Synthesis Methods for Single Bandpass and (Narrow) Dual Bandpass Filters.....175
5.1 Introduction.....175
5.2 Direct synthesis of bandpass filters.....175
5.2.1 Pseudo-combline Bandpass Filter Design.....175
5.2.2 Synthesis of the interdigital bandpass filter.....188
5.2.3 Direct Synthesis for Combline Bandpass Filter.....194
5.3 Synthesis of Narrow Dual Bandpass Filters.....199
5.3.1 Synthesis Illustrative Example.....200
5.4 Conclusion.....202
Chapter 6 Direct Synthesis and Design for Dual Band Filters.....203
6.1 Introduction.....203
6.2 Existing Methods for Dual Bandpass Synthesis.....204
6.3 Cascaded quadruplets (CQ) Dual Bandpass Filters.....205
6.3.1 Symmetric Dual Bandpass Filter Example.....206
6.3.2 Asymmetric Dual Bandpass Filter Example.....209
6.4 Decomposition into Parallel Connected Filters.....214
6.4.1 Dual Bandpass Filter Analysis.....214

6.4.2 Parallel Connected Bandpass Filters 216
6.4.3 Parallel Connected Dual Bandpass Filter Example 1 218
6.4.4 Parallel Connected Dual Bandpass Filter Example 2 225
6.4.5 Comparison Between Cascaded N-tuplets and Parallel Connected Dual Bandpass Realisations 230
6.5 Dual Bandpass Filter Design Example 233
6.6 Conclusion 239
Chapter 7 Conclusion and Future Work 240
List of References 245

List of Tables

Table I Typical Specifications of GSM 900 and 1800 Base Station Filters ……xxii

Table 1-1 Values of n and m for a Quadruplet.....26

Table 1-2 Cascaded Synthesis Using ABCD Matrices Extraction for Commonly Used Elements.....33

Table 1-3 Summary of Synthesis and Design of Microwave Filters 52

Table 2-1 Examples of Cutoff Polynomial V 55

Table 2-2: Normalised Basis Function Polynomials for Synthesis of Common Chebyshev Low-pass Filters.....65

Table 2-3 Basis Function Polynomials for Synthesis of Distributed Chebyshev Low-pass Filters 65

Table 2-4 Possible Values for Weighting Numbers α, β and γ 74

Table 2-5 Minimum Phase Bandpass Filter Family of Solutions 74

Table 2-6 Basis Functions for Direct Synthesis of Lumped Bandpass Filters or Symmetrical Low-pass Prototype Filter for Dual Bandpass Filter.....77

Table 2-7 Basis Functions for Direct Synthesis of Distributed Bandpass Filters or Symmetrical Low-pass Prototype Filter for Dual Bandpass Filter (N-$NFTZ$-$N0o$).....84

Table 2-8 Quarter-wavelength Bandpass Filter Basis Functions (N-$NFTZ$-$N0o$).....85

Table 2-9 Asymmetrical Narrow Dual Bandpass Prototype Filter Basis Functions.....87

Table 2-10 Normalized 4th Degree Basis Functions for Direct Synthesis of Dual Bandpass Filters.....90

Table 2-11 Normalized 6th Degree Basis Functions for Direct Synthesis of Dual Bandpass Filters.....93

Table 2-12 Normalized 8th Degree Basis Functions for Direct Synthesis of Dual Bandpass Filters.....97

Table 2-13 Specification for a Distributed Low-pass Filter Example 2.6.1 102

Table 2-14 Basis Functions for a Distributed Chebyshev Low-pass Filter 103

Table 2-15 $9-2-6$ Distributed Low-pass Filter Polynomials 103

Table 2-16 Distributed Bandpass Filter Specifications 104

Table 2-17 Basis Functions for a Distributed Chebyshev Bandpass Filter.....104

Table 2-18 12-4-1 Distributed Bandpass Filter Polynomials 105

Table 2-19 $Nr \times Nr$ Coupling Matrix of a 12-4-1 Distributed Bandpass Filter.....106

Table 2-20 Final Element Values of a Capacitively Loaded Distributed Bandpass Filter.....107

Table 3-1 7th Degree Low-pass Filter Synthesised Admittance Values $\mho$ 114

Table 3-2 7th Degree Low-pass Filter Impedance Values Ω After Transformation II (A)-(C) in $50\ \Omega$ system.....114

Table 3-3 7th Degree Canonical Low-pass Filter Impedance Values Ω122

Table 3-4 7th Degree Meander-Like Low-pass Filter Impedance Values Ω 122

Table 3-5 Synthesised 9th Degree Canonical Low-pass Filter Impedance Values 124

Table 3-6 Synthesised 9th Degree Meander-Like Low-pass Filter Impedance Values 124

Table 3-7 9th Degree Low-pass Filter optimised Dimensions (mm)....124

Table 3-8 Improved 9th Degree Low-pass Filter optimised Dimensions (mm).....128

Table 4-1 ABCD Polynomials Of The Synthesis Example 0 144

Table 4-2 Element Values Of The General Pseudo-elliptic Lowpass Prototype Filter 145

Table 4-3 Equivalent Circuits Under Different Terminations Of Re-Entrant Transmission Line.....150

Table 4-4 Re-entrant Resonator vs Coaxial Resonator 165

Table 4-5 Elliptic Lowpass Filter Element Values 167

Table 4-6 Re-entrant Bandpass Filter Element Values $Zri = 77\ \Omega$.....167

Table 4-7 Re-entrant Bandpass Filter Element Values 169

Table 4-8 Filter Theoretical (Calculated) Physical Dimensions (mm).169

Table 4-9 Filter Physical Dimensions after Optimization (mm).....169

Table 5-1 Pseudo-combline Bandpass Filter Specifications.....183

Table 5-2 5th Degree Lumped Bandpass Filter Characteristic Polynomials.....183

Table 5-3 5^{th} Degree Lumped Bandpass Filter Synthesized Element Values 183

Table 5-4 5^{th} Degree Pseudo-combline Bandpass Filter Impedance Values Ω 184

Table 5-5 5^{th} degree Pseudo-combline Bandpass Filter Dimensions (mm) 184

Table 5-6 4^{th} degree interdigital bandpass specifications: 193

Table 5-7 4^{th} Degree Lumped Bandpass Filter Characteristic Polynomials.....193

Table 5-8 4^{th} Degree Distributed Interdigital Bandpass Filter Characteristic Polynomials.....194

Table 5-9 4^{th} Degree Interdigital Bandpass Filter Synthesised Impedances Ω 194

Table 5-10 4^{th} Degree Interdigital Bandpass Filter Final Impedance Values Ω 194

Table 5-11 Basis Functions Selection for Combline Bandpass Filters195

Table 5-12 Specification for Combline Bandpass Filter Synthesis Example 5.2.3.2 195

Table 5-13 Final Coupling Matrix for Distributed Bandpass Filter in 1 Ohm System 196

Table 5-14 Final Combline Bandpass Filter Element Values.....197

Table 5-15 10-0-1 Combline Bandpass Filter Resonance Frequencies197

Table 5-16 10-0-1 Combline Bandpass Filter Inter-resonator Couplings using two combline resonators model 197

Table 5-17 10-0-1 Combline Bandpass Filter Input/Output Couplings197

Table 5-18 Physical Dimensions (mm).....198

Table 5-19 Basis Functions Selection for a Dual Band Lowpass Characteristic Function.....200

Table 5-20 10-4-1 Lowpass Filter Prototype Characteristic Polynomials 201

Table 5-21 10-4-1 Lowpass Filter Prototype Coupling Matrix 201

Table 6-1 Symmetrical Dual Bandpass Filter Specifications 206

Table 6-2 Basis Functions Selection 16-8-1 Direct Synthesised Dual Bandpass Filter.....206

Table 6-3 16-8-2 Dual Bandpass Filter Characteristic Polynomials....207

Table 6-4 $Nr \times Nr$ Normalised Coupling Matrix of a Symmetrical 16-8-1 Dual Bandpass Filter 208

Table 6-5 Asymmetrical Dual Bandpass Filter Specifications 209

Table 6-6 Basis Functions Selection 16-8-1 Direct Synthesised Asymmetrical Dual Bandpass Filter.....210

Table 6-7 16-8-1 Dual Bandpass Filter Polynomials 211

Table 6-8 $Nr \times Nr$ Coupling Matrix of an Asymmetrical 16-8-1 Dual Bandpass Filter.....212

Table 6-9 Final Element Values of a Capacitively Loaded Dual Bandpass Filter.....213

Table 6-10 Parallel Connected Dual Bandpass Filter Example 1 Specifications 218

Table 6-11 16-12-1 Parallel Connected Dual Bandpass Filter Basis Functions.....220

Table 6-12 16-12-1 Parallel Connected Dual Bandpass Filter Polynomials 221

Table 6-13 $Nr + 2 \times Nr + 2$ Coupling Matrix of a 16-12-1 Dual Bandpass Filter.....222

Table 6-14 Final Element Values of a Capacitively Loaded Parallel Connected Dual Bandpass Filter.....223

Table 6-15 Parallel Connected Dual Bandpass Filter Example 2 Specifications 225

Table 6-16 14-10-1 Parallel Connected Dual Bandpass Filter Basis Functions.....226

Table 6-17 14-10-1 Parallel Connected Dual Bandpass Filter Polynomials 227

Table 6-18 $Nr + 2 \times Nr + 2$ Coupling Matrix of a 14-10-1 Dual Bandpass Filter.....228

Table 6-19 Dual Bandpass Filter Resonance Frequencies.....231

Table 6-20 14-6-1 Cascaded N-tuplets Dual Bandpass Filter Inter-resonator Couplings using two combline resonators model 231

Table 6-21 14-10-1 Parallel Connected Dual Bandpass Filter Inter-resonator Couplings using two combline resonators model 232

Table 6-22 Dual Bandpass Filter Input/Output Couplings Bandwidths Comparisons (MHz).....232

Table 6-23 Dual Bandpass Filter Specifications.....233

Table 6-24 12-4-1 Dual Bandpass Filter Basis Functions.....233

Table 6-25 12-4-1 Dual Bandpass Filter Polynomials 235

Table 6-26 $Nr \times Nr$ Coupling Matrix of a 12-4-1 Dual Bandpass Filter235

Table 6-27 Final Element Values of a Capacitively Loaded Dual Bandpass Filter.....236

Table 6-28 12-4-1 Dual Bandpass Filter Resonance Frequencies 237

Table 6-29 12-4-1 Dual Bandpass Filter Inter-resonator Couplings using two combline resonators model.....237

Table 6-30 12-4-1 Dual Bandpass Filter Input/Output Couplings.....237

List of Figures

Fig. I Spectrum allocations in UK for 2010 xix

Fig. II Typical duplexer architecture for cellular base station xx

Fig. 1-1 Filter Synthesis and Design Process.....1

Fig. 1-2 Scattering parameters for a two port filter network 3

Fig. 1-3 Transversal array lowpass filter network.....15

Fig. 1-4 An ith branch of a transverse network 19

Fig. 1-5 A bandpass trisection with all inductive couplings centred at node k.....21

Fig. 1-6 Alternative forms of a quadruplet with all inductive couplings26

Fig. 1-7 Resonators.....28

Fig. 1-8 Nodal representation of filter networks.....29

Fig. 1-9 Short hand representation of coupling elements between node r and $r+1$.....30

Fig. 1-10 An example of 3D EM resonator model and its equivalent circuit for determining the input coupling 3 dB Bandwidth.....42

Fig. 1-11 An example of a two resonator EM model used to compute magnetic inter-resonator couplings.....45

Fig. 1-12 Equivalent circuit of a two combline resonator EM model for computing magnetic inter-resonator couplings 46

Fig. 1-13 An example of a two resonator EM model used to compute electric inter-resonator couplings.....48

Fig. 1-14 Equivalent circuit of a two combline resonator EM model for computing electric inter-resonator couplings.....49

Fig. 2-1 Normalised minimum phase bandpass network characteristic function plot for $N=6$ and $\omega c=0.5$ 67

Fig. 2-2 Lumped element low-pass prototype filter used for design of bandpass filters with $NTZ=N-1$ 75

Fig. 2-3 Example of a plot of normalised (with $\delta=1$) $X2-2-0\omega$ basis characteristic function 76

Fig. 2-4 General distributed equivalent circuit for interdigital bandpass filter.....78

Fig. 2-5 Simulated response of design example 2.6.1 102

Fig. 2-6 Illustration of a 6th degree bandpass filter example 2.6.2 implemented using two cascaded trisections showing inductively and capacitively coupled shunt LC resonator nodes (circled) 106

Fig. 2-7 Simulated response of the distributed bandpass example 2.6.2 107

Fig. 3-1 Proposed layout of meander-like low-pass filter (a) composed of a section of high impedance parallel coupled lines short circuited by a low impedance open circuited stub at alternate ends (b) graphical line equivalent circuit.....109

Fig. 3-2 Derived equivalent circuit transformations (*May be a hanging node).....110

Fig. 3-3 Generalised Chebyshev distributed low-pass prototype filter112

Fig. 3-4 Graphical representation of the equivalent circuit of Fig. 3-3 after transformation of the 3rd degree basic sections 112

Fig. 3-5 A basic section containing a pair of coupled line and a stub and its equivalent circuits 113

Fig. 3-6 Physical layout for generalised Chebyshev distributed low-pass filter 113

Fig. 3-7 Circuit and HFSS simulation response for design example 3.2.1.1.....114

Fig. 3-8 Physical layout of the striplines for the general meander-like low-pass filter.....116

Fig. 3-9 Graphical representation of the equivalent circuit of Fig. 3-8 for a meander-like low-pass filter.....116

Fig. 3-10 Derived network transformation for $N = 3, 5, 7$ and 9 meander-like low-pass filters.....117

Fig. 3-11 Circuit simulation of a 7-2-5 meander-like low-pass filter in example 0 123

Fig. 3-12 Diagram showing the layout of the fabricated 9th degree meander-like low-pass filter. Dimensions shown are as given in Table 3-7 125

Fig. 3-13 Physical hardware of the fabricated 9th degree 'meander-like' low-pass Filter (top cover removed) 125

Fig. 3-14 Comparison of simulated response of the synthesized, HFSS and measurement of meander-like low-pass filter.....126

Fig. 3-15 Comparison of insertion losses between HFSS simulations for b=15 mm and b=25 mm and measured response with b=25 mm 127

Fig. 3-16 Comparison of optimised equivalent circuit simulation and HFSS simulations of meander-like low-pass filter with ground plane spacing of 15 mm and 25 mm.....127

Fig. 3-17 Modified Meander-like structure obtained from Fig. 3-12 by shortening the open ends of the open circuited stubs 128

Fig. 3-18 Improvement in stopband performance of the meander-like low-pass filter by shortening the open ends of the open circuited stubs 129

Fig. 3-19 Circuit simulation comparison of 9th degree meander-like low-pass filter with a 9th degree generalised Chebyshev low-pass filter and 15th degree stepped impedance low-pass filter 130

Fig. 3-20 Circuit insertion loss simulation comparison of 9th degree meander-like low-pass filter with a 9th degree generalised Chebyshev low-pass filter and 15th degree stepped impedance low-pass filter.....130

Fig. 4-1 Asymmetrical-frequency-transformed elliptic lowpass prototype filter (a) all-pole Chebyshev lowpass prototype filter (b) asymmetrical-frequency-transformed pseudo elliptical lowpass prototype filter where $Yr = j1 - \omega o\omega\omega - \omega oCr,\ r = 1, 2, \dots, N$ 135

Fig. 4-2 The dual circuit transformation of a capacitor (a) and an inductor (b).....139

Fig. 4-3 TZG element.....139

Fig. 4-4 Circuit transformation for the series FIRs and inverters 142

Fig. 4-5 Circuit transformation for the input series FIRs.....142

Fig. 4-6 Further circuit transformation at the input (output) of the network.....143

Fig. 4-7 Simulated response of the 3rd degree general elliptic lowpass prototype filter 146

Fig. 4-8 General pseudo-elliptic lowpass prototype filter circuit after the 3 circuit transformations.....147

Fig. 4-9 General pseudo-elliptic lowpass prototype filter in its final circuit form.....147

Fig. 4-10 A physical re-entrant transmission line: (a) top and cross section view (b) isometric view 148

Fig. 4-11 A re-entrant line equivalent circuit (a) Physical transmission line (b) Graph representation (c) two series-connected transmission lines 148

Fig. 4-12 Graph representation of the equivalent circuit of re-entrant line using Sato's equivalent circuit of two coupled lines.....149

Fig. 4-13 Case 1 - Re-entrant resonator realizing a transmission zero above the passband (a) derivation of the equivalent circuit (b) resonance circuit. 152

Fig. 4-14 Cross section of a physical realization of circuit of Fig. 4-13(b) 152

Fig. 4-15 Reactance function $Xin\omega$ plot corresponding to circuit of Fig. 4-13 153

Fig. 4-16 Case 2 - Re-entrant resonator circuit realizing a transmission zero above passband (a) equivalent circuit (b) resonance circuit156

Fig. 4-17 Cross section of a physical realization of circuit of Fig. 4-16(b) 156

Fig. 4-18 Reactance function $Xin\omega$ plot corresponding to circuit of Fig. 4-16(b).....156

Fig. 4-19 Re-entrant resonator circuit that realizes transmission zero below the passband (a) equivalent circuit (b) resonance circuit.158

Fig. 4-20 Cross section of a physical realization of circuit of Fig. 4-19(b) 158

Fig. 4-21 Reactance function $Xin\omega$ plot corresponding to circuit of Fig. 4-19 (b).....158

Fig. 4-22 Equivalent circuit of an Nth degree re-entrant bandpass filter 160

Fig. 4-23 Formation of admittance inverters between node r and $r+1$ 160

Fig. 4-24 Final equivalent circuit of an Nth degree re-entrant bandpass filter with admittance inverters.....160

Fig. 4-25 Nth degree all-pole pseudo-elliptic lowpass prototype filter with admittance inverters (input and output inverters not shown) 161

Fig. 4-26 Nth degree all-pole Chebyshev lowpass filter.....161

Fig. 4-27 Frequency mapping of the admittances at rth node 163

Fig. 4-28 (a) Element values vs transmission zero positions $fo = 1\ GHz$, and $\theta o = 30o$and $Zri = 77\ \Omega$ (b) Element values vs transmission zero positions $fo = 1\ GHz$, and $\theta o = 45o$and $Zri = 77\ \Omega$ 164

Fig. 4-29 Re-entrant resonator cross section corresponding to Fig. 4-17 structure of section 0 case 2 with square outer conductor and circular middle and inner conductors and height H (not shown)165

Fig. 4-30 Circuit simulation of the 5th degree re-entrant bandpass filter of example 4.6.2 168

Fig. 4-31 Circuit simulation of the 5th degree re-entrant bandpass filter example 4.6.2 vs HFSS simulation 170

Fig. 4-32 Diagram showing the layout of the re-entrant resonators in the design example 4.6.2: (a) Top view (b) Cross section of side view - dimensions shown are as given in Table 4-9 170

Fig. 4-33 Measured vs HFSS frequency response of the fabricated re-entrant bandpass filter 171

Fig. 4-34 Measured versus HFSS simulation of the fabricated re-entrant bandpass filter 172

Fig. 4-35 Photo showing a fabricated re-entrant bandpass filter (a) filter with top cover removed (b) assembled filter with input and output connectors 174

Fig. 5-1 Lumped element bandpass prototype filter used for design of pseudo-combline bandpass filter with $NTZ = 1$.....176

Fig. 5-2 Extraction of Γ section from the filter network 177

Fig. 5-3 Distributed circuit for pseudo-combline bandpass filter 182

Fig. 5-4 A unit length (UE) phase shifter and its equivalent circuit consisting of an inverter between short circuited shunt stubs...182

Fig. 5-5 Formulation of an inverter in the distributed pseudo-combline bandpass filter between node r and $r + 1$.....182

Fig. 5-6 Distributed pseudo-combline bandpass filter circuit after introduction of unit phase shifter at input/output and admittance inverters.....182

Fig. 5-7 Final distributed circuit for pseudo-combline bandpass filter after scaling internal nodes 182

Fig. 5-8 Physical layout of the hardware for 5th degree pseudo-combline bandpass filter (a) top view (b) side view 185

Fig. 5-9 HFSS physical model of the 5th degree pseudo-combline bandpass filter (a) side view (b) perspective view.....186

Fig. 5-10 HFSS simulated passband response of 5th degree pseudo-combline bandpass filter.....187

Fig. 5-11 HFSS vs synthesis wide band response of the pseudo-combline bandpass filter.....188

Fig. 5-12 General distributed equivalent circuit for interdigital bandpass filter.....188

Fig. 5-13 Extraction of the Γ section.....190

Fig. 5-14 Interdigital bandpass filter equivalent circuit after introduction of redundant unity phase shifters at input/output and formation of admittance inverters.....192

Fig. 5-15 Final interdigital bandpass filter equivalent circuit after scaling of internal nodes 193

Fig. 5-16 Topology of the 5th degree combline bandpass filter 198

Fig. 5-17 HFSS modelling of the combline bandpass filter in example 5.2.3.2 199

Fig. 5-18 Comparison between synthesised and HFSS fine-tuned simulation for combline bandpass filter response 199

Fig. 5-19 10th Degree Dual Bandpass Filter Topology 201

Fig. 5-20 10th Degree Dual Bandpass Filter Simulated Frequency Response 202

Fig. 6-1 Symmetrical 16-8-1 dual bandpass filter topology 208

Fig. 6-2 Simulated magnitude response for 16-8-2 symmetric dual bandpass filter 209

Fig. 6-3 Asymmetrical 16-8-1 dual bandpass filter topology 212

Fig. 6-4 Simulated magnitude response for 16-8-1 asymmetric dual bandpass filter 213

Fig. 6-5 Simulated magnitude response of a dual bandpass filter before and after decomposition into parallel connected filter networks 221

Fig. 6-6 16-12-1 Parallel Connected dual bandpass filter topology 223

Fig. 6-7 Individual filter's magnitude response for the 16-12-1 parallel connected dual bandpass filter 224

Fig. 6-8 Circuit simulation for the 16-12-1 parallel connected dual bandpass filter with element values of Table 6-14 224

Fig. 6-9 Simulated magnitude response of a dual bandpass filter before and after decomposition into parallel connected filter networks 227

Fig. 6-10 14-10-1 Parallel Connected dual bandpass filter topology .. 229

Fig. 6-11 Individual filter's magnitude response of the 14-10-1 parallel connected dual bandpass filter 229

Fig. 6-12 Two possible physical realisation of dual bandpass filter .. 230

Fig. 6-13 Simulated magnitude response of a 12-4-1 dual bandpass filter 234

Fig. 6-14 12-4-1 Dual Bandpass Filter Topology 236

Fig. 6-15 12-4-1 dual bandpass filter EM model 238

Fig. 6-16 Coarse EM vs Circuit simulation for the 12-4-1 dual bandpass filter 239

Motivation

In wireless cellular systems, the communication between the mobile station (MS) and a base transceiver station (BTS) is made possible by electromagnetic (EM) waves propagating in air, through physical structures such as walls and other media at a particular frequency or wavelength. Mobile networks are allocated particular frequencies according to the standard employed. Usually a frequency range, called bandwidth, is allocated from the available EM spectrum for a particular use. Fig I shows the frequency bandwidths allocations (lower microwave frequency range) for different applications including military, aeronautical, broadcasting, terrestrial and satellite communication, to mention just a few [1].

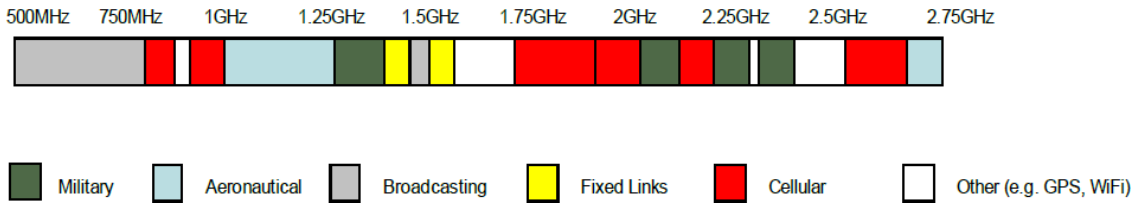

Fig. I Spectrum allocations in UK for 2010 (source [1])

Because the EM spectrum is a finite resource, the amount of bandwidth available for cellular systems is limited. This in turn limits capacity of the mobile networks and the data rates that may be supported. With more and more digital devices communicating wirelessly now than ever before, the demand for high data rates and subsequently the need for more bandwidth have increased. This means the use of high frequency is preferred to increase the capacity to carry information. Additionally, the high demand for spectrum has led to the proliferation of frequency bands leading to an overcrowded microwave spectrum. Because the microwave spectrum is divided and shared between different users and applications, microwave filters must be employed to efficiently manage this finite and important resource.

Radio Frequency (RF) and Microwave filters are an important integral part of modern digital wireless communication systems. Typically, these electrical filters are designed to allow certain frequency band(s) of signal to pass through and to

reject others. In general, they are primarily used to limit noise bandwidth and maximise the suppression of the unwanted signals in both transmitter and receiver architectures. Then also, various propagation effects degrade communication signals because of the unforgiving wireless environment. Thus transmitter and receiver front end RF and microwave filters must also have low loss to balance the system's power budget. The filter size (volume, weight and hence the cost) is another major driving variable with emphasis placed on reducing space that the filter take up in RF and microwave circuits. BTS filters have to meet with even more stringent performance requirement.

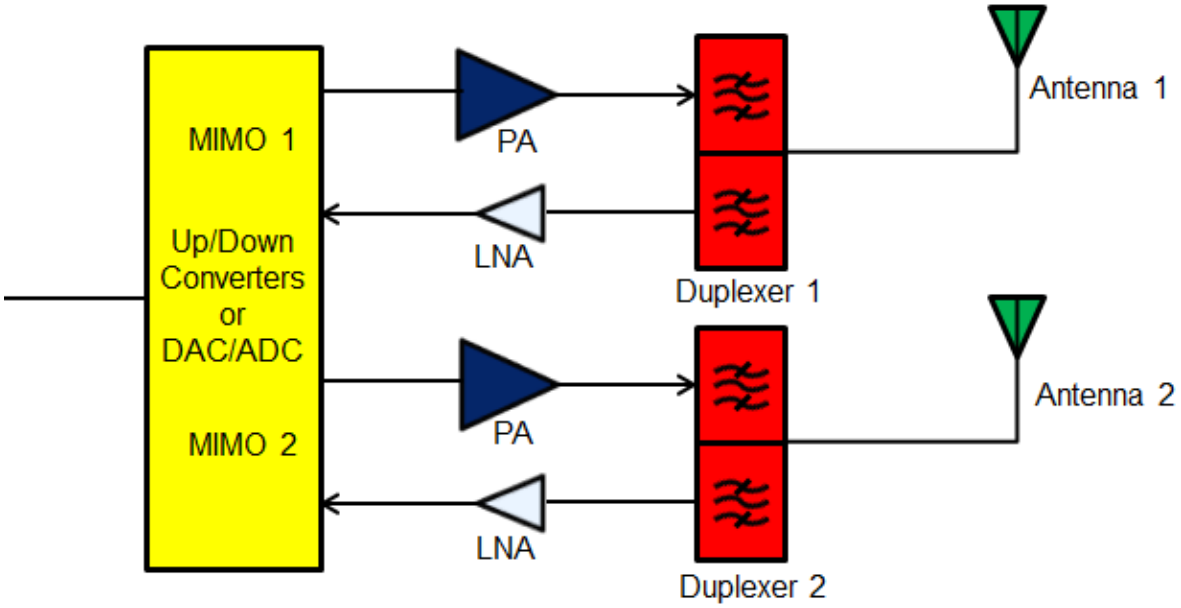

Fig. II Typical duplexer architecture for cellular base station with two MIMO paths – Courtesy of Radio Design Limited

Fig. II shows a typical duplexer used in a BTS with a 2X2 MIMO (multiple input and multiple output) for diversity. Each duplexer consists of transmitter and receiver channel filters that are connected at the common port which in turn is connected to the antenna. As well as cleaning up on unwanted signals generated by non-linear power amplifier in transmitters, there are strict guidelines to control the amount of spurious power emitted by transmitters. This means the transmitter filter must have a high rejection in the receiver band. Conversely, receiver filters must be designed not only to reject strong interference signals from external sources but also to reject strong transmitter signal that could potentially desensitise the receiver (self-

interference). Table I shows the typical specifications of GSM 900 and GSM 1800 base station filters. To achieve a high rejection of 90 dB of the transmitter band over the receiver band and vice versa in the duplexer, requires asymmetrical filters in which transmission zeros are placed on one side of the passband to increase rejection in transmitter or receiver filter [2]. In addition, there are other rejection requirements in the stopbands of each individual transmitter and receiver filter, such as 60 dB rejection in other cellular bands such as 800 band (791-821 MHz and 832-862 MHz) as well as the 2100 band (1920-1980 MHz and 2110-2170 MHz).

Table I Typical Specifications of GSM 900 and 1800 Base Station Filters

Passband	GSM 900	Receiver	880-915 MHz
		Transmitter	925-960 MHz
	GSM 1800	Receiver	1710-1785 MHz
		Transmitter	1805-1880 MHz
Maximum Passband Insertion Loss			1 dB
Mininimum Passband Return Loss			20 dB
Isolation between Transmitter and Receiver ports for duplexer			90 dB
System Impedance			50 Ω

To meet all the above stringent requirements, means that active research in microwave filters is required. Addressing most of these challenges is at the root of filter design – synthesis. Practical microwave filters can only be approximately designed. Circuit models are designed to approximate the real physical filter under various simplifications. This is because physical electrical filters (or EM models) do have second order effects. The extent to which the approximation satisfies the specifications depends on how well the circuit model synthesis and EM modelling is performed, and the material properties and tolerances required. The synthesis is thus as important as the EM modelling of microwave filters.

The past few decades has seen significant re-engineering to communication architectures and hardware. This has subsequently brought with it new and

evolving design methods for electrical filters to meet up with the dynamic system requirements. New novel techniques are needed beyond the established norms and often on the edge of physical practicality. Along with filter network synthesis, this thesis was an attempt to research new microwave base station filter design techniques that are capable of meeting various stringent requirements. The meander-like low-pass filter and re-entrant bandpass filter in Chapter 3 and Chapter 4 respectively are results of this driving factor. Numerous miniaturisation implementation techniques are used but effective filter design is primarily addressed by synthesis of suitable circuit networks.

Improvement in the transmitter and receiver architectures requires the use of multi-band filters. Available methods for multi-band filters do not enable exact synthesis of some of the desired transfer functions for arbitrary pass bands and separation bandwidths. A new synthesis method was therefore developed to provide a general solution to the exact synthesis of dual bandpass filters, with two alternative physical realisations.

In addition, most of the fundamental design of microwave filters has not changed over many decades now. While other technologies are keeping up with Moore's law, the improvement in base station filter design technology seems to have dwindled. It could even be argued that the design of microwave filters seems to have reached its fundamental physical performance limit. To rejuvenate the retarded growth, entails new synthesis and modelling techniques as well as new technologies in terms of materials used in the realisation of microwave filter to push the limit further.

It is believed that the synthesis techniques and novel physical realisations presented in this thesis will contribute to improving electrical filter synthesis and design to meet the challenges of the dynamic wireless communication systems.

Thesis Organisation

The first two Chapters cover a complete and systematic synthesis procedure for microwave filters employing Chebyshev characteristic functions. Chapter 1 highlights the basic theory on filter network synthesis and analysis upon which modern microwave filter designs are based. Using conventional synthesis approaches, it presents thorough prerequisite material on the novel synthesis technique used throughout the entire thesis. The procedure is presented in a clear and concise way suitable for direct application in computer aided designs. MATLAB programming was used for many of the filter synthesis and design algorithms developed throughout this thesis. The established methods have also been modified in line with the new synthesis technique to be presented in later Chapters. The material presented is both suitable for the synthesis of both lumped and distributed microwave filters. It includes a review of the coupling matrix for low-pass and bandpass filters. A brief description on microwave filter realisations is also given.

In Chapter 2, a concept of Chebyshev basis functions is introduced for the first time to show how this simplifies the synthesis of most microwave filters. This allows designers to synthesise Chebyshev filters in both lumped and distributed form without the need for frequency variable transformations. The Chapter shows by means of relevant filtering functions how the basis functions are determined and how they are applied in filter synthesis. This Chapter forms the foundation of synthesis of filters presented in the rest of the Chapters. As well as complementing the synthesis principles in Chapter 1, Chapter 2 presents a general recursive algorithm based on basis functions for computing the Chebyshev characteristic polynomials required in microwave filter synthesis.

Chapter 3 describes the novel synthesis technique of a new class of distributed low-pass filter that enables exact realisation of the distributed low-pass filter network. Starting with the canonical transfer functions, it is shown how different low-pass filter networks are transformed to more suitable networks for physical

realisation. A complete synthesis procedure is included together with a designed and fabricated low-pass prototype filter.

Chapter 4 presents another novel concept in which a re-entrant transmission line is used to provide for both resonance and transmission zeros. A new method of synthesising a pseudo-elliptic low-pass filter that enables realisation of re-entrant bandpass filters is also given. A thorough design description and analysis are given and validated with a design example.

The synthesis methods given in Chapter 1 and Chapter 2 were applied to single and dual bandpass filters in Chapter 5. It is shown how practical single bandpass filters may be directly synthesised using the proposed synthesis method. A narrow band approach to synthesis of dual bandpass filter is also demonstrated. Several detailed examples were used to demonstrate the new concepts introduced.

Finally, Chapter 6 presents the exact synthesis method for dual bandpass filter using the novel synthesis technique of Chapter 2. Two practical realisations of dual bandpass filters are highlighted including the decomposition into parallel connected bandpass filter networks. Design illustrative examples are given with typical and real specifications to authenticate the given methods.

A conclusion and suggestion for some future work are given in Chapter 7. Below is a list of publications the author has written and made contributions to.

List of Author's Publications

[1] Hunter, I., et al. Transversal directional filters for channel combining. in Microwave Symposium Digest (IMS), 2013 IEEE MTT-S International. 2013.

[2] Hunter, I.C., et al., *Transversal directional filters for channel combining.* Radar, Sonar & Navigation, IET, 2014. **8**(9): p. 1288-1294.

[3] Musonda, E. and I. Hunter. *Design of generalised Chebyshev lowpass filters using coupled line/stub sections*. in *Microwave Symposium (IMS), 2015 IEEE MTT-S International*. 2015.

[4] Musonda, E. and I. Hunter. *Synthesis of general Chebyshev characteristic function for dual (single) bandpass filters*. in *Microwave Symposium (IMS), 2015 IEEE MTT-S International*. 2015.

[5] Musonda, E. and I. Hunter, *Exact Design of a New Class of Generalised Chebyshev Low-Pass Filters Using Coupled Line/Stub Sections.* Microwave Theory and Techniques, IEEE Transactions on, 2015. **PP**(99): p. 1-11.

[6] Musonda, E. and I.C. Hunter, *Microwave Bandpass Filters Using Re-Entrant Resonators.* Microwave Theory and Techniques, IEEE Transactions on, 2015. **63**(3): p. 954-964.

[7] Snyder, R.V., et al., *Present and Future Trends in Filters and Multiplexers.* Microwave Theory and Techniques, IEEE Transactions on, 2015. **63**(10): p. 3324-3360.

Chapter 1 Microwave Filters – Fundamentals

1.1 Microwave Filter Networks – Analysis and Synthesis

An electrical filter is a fundamental component in microwave signal processing. It is a frequency selective device that allows only a band(s) of frequency of interest to pass through and attenuates any signal power out of this band(s). The design of electrical filters follows a well-established process as depicted in Fig. 1-1. The different facets of the design stages will be discussed in this Chapter. Firstly, the filter transfer function for either symmetrical or asymmetrical response is generated to satisfy the given attenuation levels in the filter specifications. Filter network synthesis involves determining a rational function based on the characteristic polynomials from which lumped or distributed parameter circuit models of the filter network can be realised. The circuit models are frequency mapped and element values may be scaled to suit the technology of implementation. EM modelling techniques allows the final circuit models to be approximated to the physical models (EM models). Finally, EM models are fine-tuned across a range of frequency to best match the circuit models before fabrication.

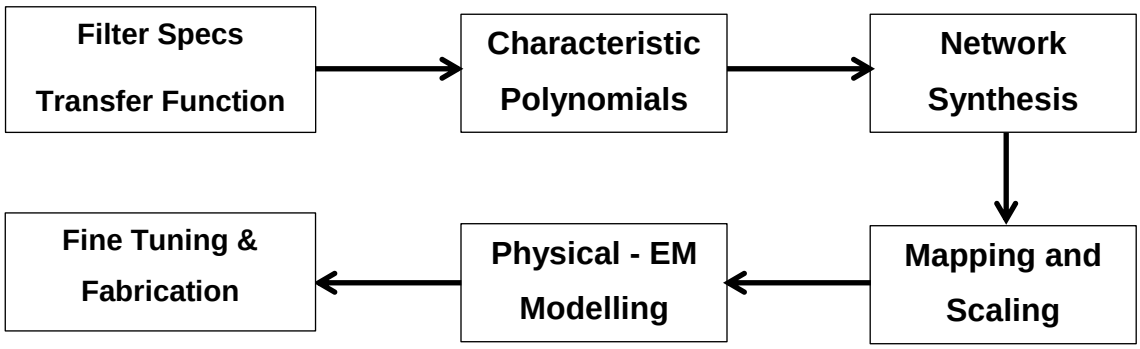

Fig. 1-1 Filter Synthesis and Design Process

The synthesis process is introduced in this Chapter and it forms the foundation for the work presented in the rest of the Chapters. The microwave filter network analysis and synthesis discussed here are based on well-known and exhausted

theories [3-6], and a revision of the underlying principles is given in the context of this work.

1.1.1 Filter Transfer Function, Characteristic Function and Characteristic Polynomials

1.1.1.1 Polynomial Definitions

It is assumed throughout this work that the filter network is a two port passive lossless network. This means that any signal incident at the source port of the network is either transmitted to the load port ($S_{21}(p)$) or reflected back at the source port ($S_{11}(p)$) as depicted in Fig. 1-2 and that the filter is realised with passive reactive elements. The input reflection (S_{11}) and forward transmission (S_{21}) coefficients of the S-parameters will be discussed in section 1.1.2.1. The characteristic polynomials are derived from the amplitude-squared filter network power transfer function defined as [3]

$$|S_{21}(\omega)|^2 = \frac{1}{1 + [T_N(\omega)]^2} \tag{1.1}$$

where $T_N(\omega)$ is a rational polynomial called the characteristic function [7, 8]. Furthermore, the characteristic function is defined as

$$T_N(\omega) = k\frac{F(\omega)}{P(\omega)} \tag{1.2}$$

where k is a constant and $F(\omega)$ and $P(\omega)$ are monic reflection and transmission characteristic polynomial respectively, all dependent on the radian frequency variable ω rad/s. The variable ω here is assumed without loss of generality although more general use would require the complex frequency variable p where

$$p = j\omega. \tag{1.3}$$

For synthesis of distributed filters, a real distributed variable t will be used instead where

$$t = tan\,\theta \tag{1.4}$$

and its corresponding complex variable ρ also known as Richard's variable [9] defined as

$$\rho = tanh(j\theta) = j\,tan\,\theta = jt \tag{1.5}$$

where the variable θ is the electrical length in radians. In addition θ is related to the more familiar radian frequency variable ω as

$$\theta = a\omega \tag{1.6}$$

The constant a is evaluated as

$$a = \frac{\theta_o}{\omega_o} \tag{1.7}$$

where θ_o is the electrical length at some frequency point ω_o normally taken to be the centre (or cutoff) frequency. With these simple variable changes, all the principles and techniques described in this Chapter apply to direct synthesis of distributed filter networks as well. Note that the variable ω (or t in distributed domain) is considered to be in a ω – plane (or t - plane) so that the characteristic polynomials may have complex singularities in ω (or t). Hence the singularities for the characteristic polynomials may be determined in the ω – plane (or t – plane) and using (1.3) (or (1.5)) converted to the conventional complex p - plane (or ρ – plane) singularities.

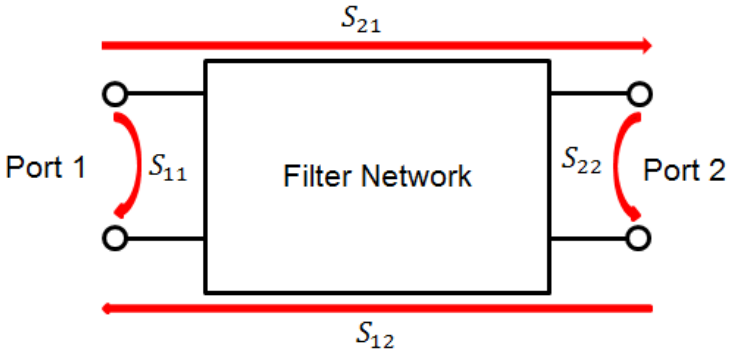

Fig. 1-2 Scattering parameters for a two port filter network

Because of the restrictions imposed on the physical realisation using lumped or distributed transmission line type elements, synthesis of transfer characteristic function are restricted to only certain transfer functions. This implies restrictions on the nature of the zeros and poles of characteristic function.

The zeros of the characteristic function $T_N(\omega)$ are also the zeros of the reflection characteristic polynomial $F(\omega)$ and are called the reflections zeros which are

frequency points of maximum power transfer. At these frequency points, all the power incident at the source is transferred to the load and the filter loss is zero. The degree of $F(\omega)$ is normally equal to the degree of the filter network, N. The poles of the characteristic function $T_N(\omega)$ are also the zeros of the transmission characteristic polynomial $P(\omega)$. These are called transmission zeros and represents frequency points of maximum reflection of energy. Thus no energy is transferred to the load port. At these points, all the signal power is attenuated and are thus also points of maximum attenuation. Normally the number and position of these zeros are controlled or prescribed so that desired attenuation occurs at some specific out-of-band frequencies. For convenient physical realisability, the degree of $P(\omega)$, N_{TZ} is chosen such that $N_{TZ} \leq N$. The goal of polynomial synthesis is to find the desired minimum degree characteristic function $T_N(\omega)$ which minimises filter losses in the passband and maximises attenuation in the stopband.

The characteristic polynomials are the starting point in the synthesis process. In fact all microwave prototype filters are characterised by the characteristic polynomials. The nature of their zeros define a particular prototype filter response, such as Butterworth, Chebyshev, Elliptic etc. The characteristic polynomials may be completely prescribed as is the case with Butterworth filter response (all reflection zeros are coincident at the origin and all the transmission zeros are at infinity), but as will be evident later on, only the transmission characteristic polynomial may be prescribed in the case of Chebyshev filter response. The reflection characteristic polynomial for Chebyshev response may be obtained from a recursive algorithm that ensures equal passband return loss ripples response. This algorithm will be discussed in Chapter 2. The Chebyshev response gives a good compromise between in band return loss and out-of-band rejection and is relatively not very sensitive to element value tolerance [10]. For this reason, they were used in this work.

There is one more polynomial used in filter synthesis, and thus it will be more instructive to define it now as it may be derived from the two characteristic polynomials described above. However, the reflection and transmission characteristic polynomials completely characterises any two port passive lossless

filter network. The third polynomial arises from the following definition of the input reflection (S_{11}) and forward transmission (S_{21}) coefficients of the S parameters:

$$S_{11}(\omega) = \frac{F(\omega)/\mu}{E(\omega)} \tag{1.8}$$

and

$$S_{21}(\omega) = \frac{P(\omega)/\varepsilon}{E(\omega)} \tag{1.9}$$

respectively, where in both cases the denominator polynomial $E(\omega)$ is the Hurwitz polynomial [3]. All the zeros of the Hurwitz polynomial $E(\omega)$ are in the left half-plane of the complex p plane. At this point all the polynomials $F(\omega)$, $P(\omega)$ and $E(\omega)$ are assumed to be monic polynomials (i.e. the coefficient of the highest power term is unity). For the numerator polynomials $F(\omega)$ and $P(\omega)$, μ and ε respectively are normalising parameters discussed in the next section. The degree of $E(\omega)$ is equal to the degree of the filter network, N. The Hurwitz polynomial $E(\omega)$ is normally found from alternating pole technique [11] when both $F(\omega)$ and $P(\omega)$ are known. In general, any one of the polynomials may be found given any two of the other polynomials. The technique used to find $E(\omega)$ polynomial in this work will be outlined in section 1.1.2.

1.1.1.2 Polynomial Normalisation

As mentioned in the previous section, it is assumed that the characteristic polynomials $F(\omega)$ and $P(\omega)$ and the Hurwitz polynomial $E(\omega)$ are monic. Consequently (1.1) is re-written as

$$|S_{21}(\omega)|^2 = \frac{1}{1+[T_N(\omega)]^2} = \frac{1}{1+\left(k\frac{F(\omega)}{P(\omega)}\right)^2} = \frac{1}{1+\left(\frac{F(\omega)/\mu}{P(\omega)/\varepsilon}\right)^2} \tag{1.10}$$

where the substitution $k = \varepsilon/\mu$ was made. In Chebyshev filter response, the scalar k is chosen to control the passband return loss ripple level. For monic polynomials $F(\omega)$ and $P(\omega)$ their normalizing parameter μ and ε respectively are computed at points in ω - plane (or θ – plane) where both $S_{11}(\omega)$ and $S_{21}(\omega)$ are known (e.g. $\omega = 1$ rad/s) so that the unitary condition [4]

$$|S_{21}(\omega)|^2 + |S_{11}(\omega)|^2 = 1 \tag{1.11}$$

and the prescribed passband return loss level are satisfied. Using (1.10) and (1.11), $S_{11}(\omega)$ may be expressed as,

$$|S_{11}(\omega)|^2 = \frac{\left(\frac{F(\omega)/\mu}{P(\omega)/\varepsilon}\right)^2}{1 + \left(\frac{F(\omega)/\mu}{P(\omega)/\varepsilon}\right)^2} \tag{1.12}$$

Also by definition the passband return loss (RL) evaluated at $\omega = \omega_c$ (where ω_c may be equal to any of the known cutoff points) is given by

$$RL = -10log|S_{11}(\omega)|^2|_{\omega=\omega_c}\, dB \tag{1.13}$$

By solving (1.12) and (1.13) simultaneously at any of the cutoff points, the constant $k = \varepsilon/\mu$ may be computed as

$$k = \frac{\varepsilon}{\mu} = \frac{1}{\sqrt{10^{(RL/10)} - 1}} \left|\frac{F(\omega)}{P(\omega)}\right|\Bigg|_{\omega=\omega_c} \tag{1.14}$$

It also follows using (1.8) and (1.9), and the unitary condition (1.11) that,

$$\left|\frac{F(\omega)/\mu}{E(\omega)}\right|^2 + \left|\frac{P(\omega)/\varepsilon}{E(\omega)}\right|^2 = 1 \tag{1.15}$$

Recall that the polynomials $F(\omega)$ and $E(\omega)$ are of degree N and the degree of $P(\omega)$ is N_{TZ}, then computing the limit of (1.15) as $\omega \to \infty$ yields

$$\begin{aligned} \mu &= \pm 1 \text{ for } N_{TZ} < N \\ \frac{1}{\mu^2} + \frac{1}{\varepsilon^2} &= 1 \text{ for } N_{TZ} = N \end{aligned} \tag{1.16}$$

Solving (1.14) and (1.16) simultaneously gives the two normalizing parameters. For $N_{TZ} < N$

$$\varepsilon = \pm \frac{1}{\sqrt{10^{(RL/10)} - 1}} \left| \frac{P(\omega)}{F(\omega)} \right|_{\omega=\omega_c} \tag{1.17}$$

$$\mu = \pm 1$$

and for $N_{TZ} = N$

$$\varepsilon = \pm\sqrt{1 + k^2} = \pm \sqrt{1 + \left(\frac{1}{\sqrt{10^{(RL/10)} - 1}} \left| \frac{P(\omega)}{F(\omega)} \right|_{\omega=\omega_c} \right)^2} \tag{1.18}$$

$$\mu = \pm \frac{\varepsilon}{k} = \pm \frac{\varepsilon}{\sqrt{\varepsilon^2 - 1}}$$

Note that the positive and negative sign on μ gives the dual network realisation [4]. Recall also that the above formulae apply for distributed filter networks as well with appropriate variable substitution. In some distributed filter networks, however, the degree of the polynomial $F(t)$ is less than the degree of the filter network N. If the degree of $E(t)$ is N and the degree of $P(t)$ is N_{TZ} such that $N = N_{TZ}$ then it follows using the above derivation that the normalising parameters take the following form,

$$\varepsilon = \pm 1$$

$$\mu = \pm \frac{\varepsilon}{k} = \pm \frac{1}{\frac{1}{\sqrt{10^{(RL/10)} - 1}} \left| \frac{F(t)}{P(t)} \right|_{t=t_c}} \tag{1.19}$$

where $t_c = tan\, \theta_c$ is the cutoff point.

One more important filter characterisation not discussed in great detail is the transmission group delay (τ) obtained from the transmission coefficient as

$$\tau = -\frac{d\emptyset_{21}}{d\omega} \tag{1.20}$$

where $\emptyset_{21}$ is the phase of the transmission coefficient S_{21}. The group delay shows how different frequent signal components are delayed as they travel through the

filter network. In some applications it becomes important to have at least constant passband group delay to minimise signal distortion.

1.1.2 S-Parameters, ABCD Matrix and Y Admittance Matrix

1.1.2.1 S-Parameters

S-parameters or scattering parameters are a useful way to characterise a microwave filter network and may be defined conventionally as rational polynomials as follows

$$S_{11}(p) = \frac{F_{11}}{E_s} \qquad S_{12}(p) = \frac{P_{12}}{E_s} \qquad S_{21}(p) = \frac{P_{21}}{E_s} \qquad S_{22}(p) = \frac{F_{22}}{E_s} \tag{1.21}$$

where $S_{11}(p)$, $S_{12}(p)$, $S_{21}(p)$ and $S_{22}(p)$ are the input reflection, reverse transmission, forward transmission and output reflection coefficients as depicted in Fig. 1-2. The polynomials F_{11}(and F_{22}), P_{12} (and P_{21}) and E_s are functions of the complex frequency variable p corresponding to the reflection characteristic polynomial $F(\omega)$, transmission characteristic polynomial $P(\omega)$ and Hurwitz polynomial $E(\omega)$ defined in the ω – plane as in section 1.1.1.1. They are related by

$$\begin{aligned} P_{21} = P_{21}(p) &= (j)^{N_{TZ}} P(-jp) \\ F_{11} = F_{11}(p) &= (j)^{N} F(-jp) \\ E_s = E_s(p) &= (j)^{N} E\,(-jp) \end{aligned} \tag{1.22}$$

Note here that, the complex frequency variable p is used without loss of generality. The formulae in this section apply to the distributed filter synthesis as well where the variable ρ would be used instead of p. For this reason, the polynomials would be written without the variable dependence indicated e.g. P_{21} to mean $P_{21}(p)$ or $P_{21}(\rho)$. Additionally, from the orthogonality unitary condition [3],

$$P_{21} = (j)^{mod\left(\frac{N-N_{TZ}+1}{2}\right)} P_{21} \tag{1.23}$$

The modulo operation (mod) simply corresponds to multiplication of the transmission polynomial P_{21} by a j to normalise the phase relationship for the s-parameters when $N - N_{TZ}$ is even. For a lossless passive reciprocal filter network it is assumed that,

$$F_{11} = F_{22} = (-1)^N {F_{11}}^* \tag{1.24}$$

i.e. all reflection zeros are on the imaginary axis and

$$P_{12} = P_{21} = (-1)^{N_{TZ}} {P_{21}}^* \tag{1.25}$$

i.e. all transmission zeros must exist on the imaginary axis or as complex paraconjugated pairs (i.e. $p_z = \pm\sigma + j\omega$) to ensure physical realisability. The asterisks * is a paraconjugation operation (the reflection of a function symmetrically on the imaginary axis. For example, $F(p)^* = F^*(-p) = {a_0}^* \times (-p)^N + {a_1}^* \times (-p)^{N-1} + \cdots + {a_{N-1}}^* \times (-p)^1 + {a_N}^* \times (-p)^0$, where ${a_r}^*$ is the normal conjugate operation or reflection about the real axis). Hence for a two port lossless passive and reciprocal filter network, the complete s-parameters matrix may be written as,

$$[S] = \begin{bmatrix} S_{11} & S_{12} \\ S_{21} & S_{22} \end{bmatrix} = \frac{1}{E_s}\begin{bmatrix} F_{11} & P_{12} \\ P_{21} & F_{22} \end{bmatrix} = \frac{1}{E_s}\begin{bmatrix} F_{11} & P_{21} \\ P_{21} & F_{11} \end{bmatrix} \tag{1.26}$$

1.1.2.2 S-parameter to ABCD-parameters

Utilising standard S-parameters to ABCD-parameters transformation in [6],

$$\begin{aligned} A &= \frac{(1+S_{11})(1-S_{22}) + S_{12}S_{21}}{2S_{21}} \\ B &= \frac{(1+S_{11})(1+S_{22}) - S_{12}S_{21}}{2S_{21}} \\ C &= \frac{(1-S_{11})(1-S_{22}) - S_{12}S_{21}}{2S_{21}} \\ D &= \frac{(1-S_{11})(1+S_{22}) + S_{12}S_{21}}{2S_{21}} \end{aligned} \tag{1.27}$$

Substituting (1.21) in (1.27) and re-writing yields

$$\begin{aligned} A &= \frac{E_s + F_{11} - F_{22} - \frac{F_{11}F_{22} - P_{12}P_{21}}{E_s}}{2P_{21}} \\ B &= \frac{E_s + F_{11} + F_{22} + \frac{F_{11}F_{22} - P_{12}P_{21}}{E_s}}{2P_{21}} \\ C &= \frac{E_s - F_{11} - F_{22} + \frac{F_{11}F_{22} - P_{12}P_{21}}{E_s}}{2P_{21}} \end{aligned} \tag{1.28}$$

$$D = \frac{E_s - F_{11} + F_{22} - \frac{F_{11}F_{22} - P_{12}P_{21}}{E_s}}{2P_{21}}$$

Since the ABCD polynomials must be rational polynomials with the degree of at most N, then it can be inferred from (1.28) that there exist a polynomial E_x such that

$$E_s E_x = F_{11}F_{22} - P_{12}P_{21}. \tag{1.29}$$

This is a general equation of conservation of energy [12]. It may be reduced to a more familiar unitary condition for a passive lossless filter network namely,

$$E_s E_s{}^* = F_{11}F_{11}{}^* + P_{21}P_{21}{}^* \tag{1.30}$$

By substituting (1.24) and (1.25) into (1.30) yields,

$$\begin{gathered} E_s E_s{}^* = \frac{F_{11}F_{22}}{(-1)^N} + \frac{P_{12}P_{21}}{(-1)^{N_{TZ}}} \\ E_s(-1)^N E_s{}^* = F_{11}F_{22} - (-1)^{N-N_{TZ}-1}P_{12}P_{21} \end{gathered} \tag{1.31}$$

which is equivalent to (1.29) if and only if two conditions are met,

$$\begin{gathered} P_{21} = P_{12} = (j)^{mod\left(\frac{N-N_{TZ}+1}{2}\right)}P_{21} \\ E_x = (-1)^N E_s{}^* \end{gathered} \tag{1.32}$$

(1.32) explains why the orthogonality condition is used in (1.23) before application of (1.29). If the transfer function has a half transmission zero as is the case with distributed filter networks such that

$$P_{21} = \sqrt{1-\rho^2}P_x \tag{1.33}$$

where P_x contains all non-half transmission zeros. This requires slight modification to the equation of conservation of energy (1.29).This is achieved by re-writing (1.25) as

$$P_{12} = P_{21} = (-1)^{N_{TZ}-1}P_{21}{}^* = \left(\sqrt{1-\rho^2}\right)(-1)^{N_{TZ}-1}P_x{}^* \tag{1.34}$$

Then substituting (1.24) and (1.34) into (1.30) gives

$$E_s E_s{}^* = \frac{F_{11}F_{22}}{(-1)^N} + \frac{P_{12}P_{21}}{(-1)^{N_{TZ}-1}}$$
$$E_s(-1)^N E_s{}^* = F_{11}F_{22} - (-1)^{N-N_{TZ}} P_{12}P_{21} \tag{1.35}$$

By substituting (1.33) into (1.35), it may be re-written as,

$$E_s(-1)^N E_s{}^* = F_{11}F_{22} - (-1)^{N-N_{TZ}}(1-\rho^2)P_x P_x \tag{1.36}$$

which again is equivalent to (1.29) if and only if

$$P_{21} = P_{12} = (j)^{mod\left(\frac{N-N_{TZ}}{2}\right)} P_{21} = (j)^{mod\left(\frac{N-N_{TZ}}{2}\right)} \left(\sqrt{1-\rho^2}\right) P_x$$
$$E_x = (-1)^N E_s{}^* \tag{1.37}$$

Therefore this is equivalent to multiplication of the transmission polynomial P_{21} (or P_x) by a j when $N - N_{TZ}$ is odd. Thus a similar conservation of energy formula may be written for the distributed filter network with a single half transmission zero pair from (1.36) as

$$E_s E_x = F_{11}F_{22} - (1-\rho^2)P_x P_x \tag{1.38}$$

The poles or roots of E_s and E_x may easily be determined from (1.29) or (1.38) by root assignment. Note that in application of (1.29) or (1.38), the P_{21} polynomial or the P_x polynomial is multiplied by a j when when $N - N_{TZ}$ is even and when $N - N_{TZ}$ is odd respectively to satisfy the orthogonality condition. For example, using (1.29) and for a two port passive lossless filter network, for which (1.24) and (1.25) apply then

$$E_s E_x = F_{11}F_{22} - P_{12}P_{21}$$
$$E_s E_x = F_{11}{}^2 - P_{21}{}^2$$
$$E_s E_x = (F_{11} - P_{21})(F_{11} + P_{21}) \tag{1.39}$$

E_s is the Hurwitz polynomial and hence may be formed from the left half plane (LHP) zeros of $F_{11} - P_{21}$ and $F_{11} + P_{21}$, while E_x may be formed from the right half plane (RHP) zeros of $F_{11} - P_{21}$ and $F_{11} + P_{21}$. Having determined the required polynomials E_s, E_x, F_{11} and P_{21} the complete ABCD parameters may now be determined. From (1.28) it is evident that the four ABCD polynomials share the same denominator P_{21} and their numerator polynomials are given by

$$
\begin{aligned}
A_n &= \frac{1}{2}[E_s - E_x + F_{11} - F_{22}] \\
B_n &= \frac{1}{2}[E_s + E_x + F_{11} + F_{22}] \\
C_n &= \frac{1}{2}[E_s + E_x - F_{11} - F_{22}] \\
D_n &= \frac{1}{2}[E_s - E_x - F_{11} + F_{22}]
\end{aligned}
\tag{1.40}
$$

which for a two port lossless reciprocal and symmetrical filter network, simplifies to

$$
\begin{aligned}
A_n &= \frac{1}{2}[E_s - E_x] \\
B_n &= \frac{1}{2}[E_s + E_x + 2F_{11}] \\
C_n &= \frac{1}{2}[E_s + E_x - 2F_{11}] \\
D_n &= \frac{1}{2}[E_s - E_x]
\end{aligned}
\tag{1.41}
$$

Clearly $A_n = D_n$ and the complete ABCD matrix may be written as

$$
[ABCD] = \frac{1}{P_{21}}\begin{bmatrix} A_n & B_n \\ C_n & D_n \end{bmatrix} \tag{1.42}
$$

1.1.2.3 S-parameters to Y-parameters

Utilising standard S-parameters to Y-parameters conversion formulae [6] in a similarly way as in section 1.1.2.2 and the equation of conservation of energy (1.29) gives

$$
\begin{aligned}
Y_{11} &= \frac{(1 - S_{11})(1 + S_{22}) + S_{12}S_{21}}{(1 + S_{11})(1 + S_{22}) - S_{12}S_{21}} = \frac{E_s - E_x - F_{11} + F_{22}}{E_s + E_x + F_{11} + F_{22}} \\
Y_{12} &= \frac{-2S_{12}}{(1 + S_{11})(1 + S_{22}) - S_{12}S_{21}} = \frac{-2P_{12}}{E_s + E_x + F_{11} + F_{22}} \\
Y_{21} &= \frac{-2S_{21}}{(1 + S_{11})(1 + S_{22}) - S_{12}S_{21}} = \frac{-2P_{21}}{E_s + E_x + F_{11} + F_{22}} \\
Y_{22} &= \frac{(1 + S_{11})(1 - S_{22}) + S_{12}S_{21}}{(1 + S_{11})(1 + S_{22}) - S_{12}S_{21}} = \frac{E_s - E_x + F_{11} - F_{22}}{E_s + E_x + F_{11} + F_{22}}
\end{aligned}
\tag{1.43}
$$

Hence in general the numerator polynomials of the Y-parameters are

$$
\begin{aligned}
Y_{11n} &= \frac{1}{2}[E_s - E_x - F_{11} + F_{22}] \\
Y_{12n} &= -P_{12} \\
Y_{21n} &= -P_{21} \\
Y_{22n} &= \frac{1}{2}[E_s - E_x + F_{11} - F_{22}]
\end{aligned}
\tag{1.44}
$$

and they all share the same denominator polynomial defined by,

$$
Y_{den} = \frac{1}{2}[E_s + E_x + F_{11} + F_{22}] \tag{1.45}
$$

Which for a two port lossless reciprocal and symmetrical filter network simplifies to

$$
\begin{aligned}
Y_{11n} &= \frac{1}{2}[E_s - E_x] \\
Y_{12n} &= -P_{12} \\
Y_{21n} &= -P_{21} \\
Y_{22n} &= \frac{1}{2}[E_s - E_x] \\
Y_{den} &= \frac{1}{2}[E_s + E_x + 2F_{11}]
\end{aligned}
\tag{1.46}
$$

Cleary $Y_{11n} = Y_{22n}$ and the complete Y-parameters matrix is given by

$$
[Y] = \frac{1}{Y_{den}}\begin{bmatrix} Y_{11n} & Y_{12n} \\ Y_{21n} & Y_{22n} \end{bmatrix} \tag{1.47}
$$

The S-parameters, ABCD parameters and Y-parameters are used extensively in modern analysis and synthesis of microwave filter networks. They thus form the basis of the synthesis methods described in the next two sections.

1.1.3 Coupling Matrix Synthesis Method

Among the modern filter synthesis methods, the Coupling Matrix (CM) method has been increasing in popularity ever since its introduction in the 1970's [13, 14]. With modern advances in computer aided design, designers often utilize software such as CMS [15] which computes the CM elements for a configurations suitable for a given application. Because the CM technique is amenable to computer manipulations, it allows designers to implement the filter in the topology of choice. Additionally, the CM technique offers a good relationship between the elements of

the physical network and the elements of the CM. In section 1.1.3.1, the CM for lowpass prototype filters is briefly reviewed. Detailed analysis and synthesis are well presented by Cameron in his papers [16, 17]. In section 1.1.3.2, the formulation of the CM for direct synthesis of single (or dual) bandpass filter used in Chapter 5 and Chapter 6 is derived.

Although it is possible to express any given filter circuit network (such as those obtained from section 1.1.3.3) in form of the CM, it is however, possible and often convenient to synthesise the CM directly from the Y matrix polynomials obtained in section 1.1.2.3. The concept is based on the transversal array network and the two methods are now examined.

1.1.3.1 Ideal Lowpass Prototype Filter Coupling Matrix

Any realisable lowpass filter network may be expressed in terms of the transversal array as shown in Fig. 1-3. Recall from (1.47) that the overall Y matrix for the lowpass prototype filter may be expressed as

$$[Y] = \frac{1}{Y_{den}} \begin{bmatrix} Y_{11n} & Y_{12n} \\ Y_{21n} & Y_{22n} \end{bmatrix}. \tag{1.48}$$

This may be expressed in terms of residues and poles a_i, z_i and p_i respectively as

$$[Y] = \begin{bmatrix} \sum_{i=1}^{N} \frac{a_i}{p - p_i} & jz_0 + \sum_{i=1}^{N} \frac{z_i}{p - p_i} \\ jz_0 + \sum_{i=1}^{N} \frac{z_i}{p - p_i} & \sum_{i=1}^{N} \frac{a_i}{p - p_i} \end{bmatrix} \tag{1.49}$$

It may be seen from the parallel-connected transversal array that the total admittance matrix is just the sum of the N array networks and the direct source-load coupling M_{sl}, where N is the degree of the lowpass filter network. Thus to obtain the elements of the $N + 2$ transversal CM, only the residues and poles are needed. Now, the total admittance Y matrix of the transversal array is

$$[Y] = \begin{bmatrix} \sum_{i=1}^{N} \frac{M^2{}_{si}}{c_i p + j b_i} & j M_{sl} + \sum_{i=1}^{N} \frac{M_{si} M_{il}}{c_i p + j b_i} \\ j M_{sl} + \sum_{i=1}^{N} \frac{M_{si} M_{il}}{c_i p + j b_i} & \sum_{i=1}^{N} \frac{M^2{}_{il}}{c_i p + j b_i} \end{bmatrix},$$

$$[Y] = \begin{bmatrix} \sum_{i=1}^{N} \frac{M^2{}_{si}}{p + j b_i} & j M_{sl} + \sum_{i=1}^{N} \frac{M_{si} M_{il}}{p + j b_i} \\ j M_{sl} + \sum_{i=1}^{N} \frac{M_{si} M_{il}}{p + j b_i} & \sum_{i=1}^{N} \frac{M^2{}_{il}}{p + j b_i} \end{bmatrix}, \quad (1.50)$$

where all the capacitor values in (1.50) have been normalised to unity. Comparing the two matrices in (1.49) and (1.50) yields the desired result for the transversal array CM values as

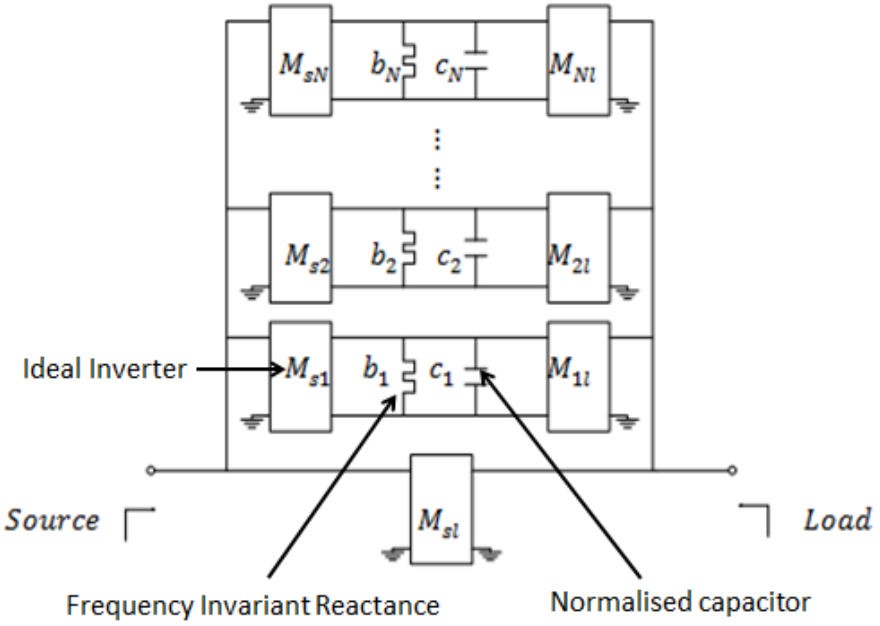

Fig. 1-3 Transversal array lowpass filter network

$$M_{sl} = z_0$$

$$M_{il} = \sqrt{a_i}$$

$$M_{si} = \frac{z_i}{M_{il}} \quad (1.51)$$

$$M_{ii} = b_i = -\frac{p_i}{j}$$

And using these values the $N+2$ fully canonical CM for the transversal array is formed as

$$M = \begin{array}{c|cccccccc} & S & 1 & 2 & \dots & k & \dots & N & L \\ \hline S & & M_{s1} & M_{s2} & \dots & M_{si} & \dots & M_{sN} & M_{sl} \\ 1 & M_{s1} & M_{11} & & & & & & M_{1l} \\ 2 & M_{s2} & & M_{22} & & & & & M_{2l} \\ \vdots & \vdots & & & \ddots & & & & \vdots \\ k & M_{si} & & & & M_{ii} & & & M_{il} \\ \vdots & \vdots & & & & & \ddots & & \vdots \\ N & M_{sN} & & & & & & M_{NN} & M_{Nl} \\ L & M_{sl} & M_{1l} & M_{2l} & \dots & M_{il} & \dots & M_{Nl} & \end{array} \quad (1.52)$$

where all other matrix entries for the above are zero. The leading diagonal elements, M_{ii}, are zero for symmetrical filter transfer function and if the number of transmission zeros is less than the degree of the network, then M_{sl} is zero. The M_{ii} elements represent frequency offsets from the centre frequency of individual resonators in the bandpass filter and define asymmetrical filter transfer functions [18].

1.1.3.1.1 Reconfiguration of the Lowpass Prototype Filter Transverse Coupling Matrix

The CM for the transversal array may be reduced to any desirable configuration or topology by performing some sequence of similarity transformations or rotations [14] that preserves the eigenvalues and eigenvectors of the original transversal array CM [17, 19]. The effect is to annihilate some undesired couplings and subsequently create new couplings forming different network configuration or topology which have exactly the same filter response of the origin filter network. Let the initial transverse coupling matrix M be written as

$$M = M_T + pI + jM_K \quad (1.53)$$

where I is an $(N+2)$ by $(N+2)$ matrix with all its initial elements zero except diagonal elements, $I(i,i) = 1,\ i = 2, 3, 4, \dots N+1,$

$$I = \begin{bmatrix} 0 & 0 & 0 & 0 & \dots & 0 & 0 & 0 & 0 \\ 0 & 1 & 0 & 0 & \dots & 0 & 0 & 0 & 0 \\ 0 & 0 & 1 & 0 & \dots & 0 & 0 & 0 & 0 \\ 0 & 0 & 0 & \ddots & \dots & 0 & 0 & 0 & 0 \\ \vdots & \vdots & \vdots & \vdots & 1 & \vdots & \vdots & \vdots & \vdots \\ 0 & 0 & 0 & 0 & \dots & \ddots & 0 & 0 & 0 \\ 0 & 0 & 0 & 0 & \dots & 0 & 1 & 0 & 0 \\ 0 & 0 & 0 & 0 & \dots & 0 & 0 & 1 & 0 \\ 0 & 0 & 0 & 0 & \dots & 0 & 0 & 0 & 0 \end{bmatrix} \tag{1.54}$$

M_T is an $(N+2)$ by $(N+2)$ matrix with all its initial elements zero except the first row and column and last row and column containing the transverse CM element values as defined below,

$$M_T = \begin{bmatrix} 0 & M_{s,1} & M_{s,2} & \dots & M_{s,N-1} & M_{s,N} & M_{s,l} \\ M_{s,1} & 0 & 0 & \dots & 0 & 0 & M_{1,l} \\ M_{s,2} & 0 & 0 & \dots & 0 & 0 & M_{2,l} \\ \vdots & \vdots & \vdots & \ddots & \vdots & \vdots & \vdots \\ M_{s,N-1} & 0 & 0 & \dots & 0 & 0 & M_{N-1,l} \\ M_{s,N} & 0 & 0 & \dots & 0 & 0 & M_{N,l} \\ M_{s,l} & M_{1,l} & M_{2,l} & \dots & M_{N-1,l} & M_{N,l} & 0 \end{bmatrix} \tag{1.55}$$

M_K is an $(N+2)$ by $(N+2)$ matrix containing frequency offsets with all its initial elements zero except diagonal elements, $M_K(i,i) = M_{ii},\ i = 2,3,4,\dots N+1$,

$$M_K = \begin{bmatrix} 0 & 0 & 0 & 0 & \dots & 0 & 0 & 0 & 0 \\ 0 & M_{11} & 0 & 0 & \dots & 0 & 0 & 0 & 0 \\ 0 & 0 & M_{22} & 0 & \dots & 0 & 0 & 0 & 0 \\ 0 & 0 & 0 & \ddots & \dots & 0 & 0 & 0 & 0 \\ \vdots & \vdots & \vdots & \vdots & M_{ii} & \vdots & \vdots & \vdots & \vdots \\ 0 & 0 & 0 & 0 & \dots & \ddots & 0 & 0 & 0 \\ 0 & 0 & 0 & 0 & \dots & 0 & M_{N-1,N-1} & 0 & 0 \\ 0 & 0 & 0 & 0 & \dots & 0 & 0 & M_{N,N} & 0 \\ 0 & 0 & 0 & 0 & \dots & 0 & 0 & 0 & 0 \end{bmatrix} \tag{1.56}$$

The matrix M may be reconfigured to a folded form in the conventional way described in [16] or an Arrow (Wheel) coupling matrix [20, 21] by a series of rotations. The rotations are performed such that the coupling matrix M' at the end of a single rotation is

$$M' = RMR^T = RM_TR^T + pI + jRM_KR^T \tag{1.57}$$

where R is a rotation matrix with its transpose matrix R^T. Note that I matrix is unaffected by the subsequent rotations where M_T and M_K matrices change accordingly as (1.57). Firstly, all couplings in M_T are reduced to zero except source to first resonator coupling $(M_T(1,2))$ and last resonator to load coupling $(M_T(N+1, N+2))$. Then some couplings in M_K are reduced to zero to give a canonical

folded topology or any other desired topology. A comprehensive description of coupling matrix reconfiguration is given in [3]. The final coupling matrix (Y) in canonical folded or arrow form may be expressed as

$$Y = M_T + pI + jM_K \tag{1.58}$$

1.1.3.2 Single (or Dual) Bandpass Filter Coupling Matrix

The existing method for obtaining the CM for bandpass filters uses the N by N coupling matrix constructed using the Gram-Schmidt orthornomalisation process or similar techniques [22, 23]. In this section a method for generating the transverse network coupling matrix for directly synthesised single or dual bandpass filter is now presented. The transverse network for directly synthesised single (or dual) bandpass filter is the same as that of Fig. 1-3 except that in each branch the shunt capacitor and frequency invariant reactance are replaced by a parallel LC resonator as shown in Fig. 1-4. Consider a single filter r, regardless of whether it is a single- or multi-bandpass filter, with the degree N_r and with highest degree of the filter characteristic polynomials being N ($N = 2N_r$). Note that the degree of the filter characteristic polynomials, N is always even and here it is assumed that the number of transmission zeros (N_{Zr}) is less than the degree of the filter characteristic polynomials ($N_{Zr} < N$) throughout this work. This implies that the filter has no direct source-load coupling as is often the practical case. Again here, the Y matrix is obtained using the methods developed in sections 1.1.1 and 1.1.2 and may be expressed in terms of residues a_i, z_i and poles p_i as follows,

$$[Y]_r = \begin{bmatrix} \sum_{i=1}^{N_r} \frac{a_i p}{p^2 - {p_i}^2} & \sum_{i=1}^{N_r} \frac{z_i p}{p^2 - {p_i}^2} \\ \sum_{i=1}^{N_r} \frac{z_i p}{p^2 - {p_i}^2} & \sum_{i=1}^{N_r} \frac{a_i p}{p^2 - {p_i}^2} \end{bmatrix}. \tag{1.59}$$

Note that the poles are purely imaginary and always occur in symmetrical pairs ($p = \pm p_i$) for directly realised bandpass filters. Thus two conjugate pairs are grouped together in the above formulation. Now consider an i^{th} branch of a transverse network between the source and load as shown in Fig. 1-4. As it was

done for the lowpass prototype filter network CM, the capacitance of the parallel LC resonant circuit is scaled to unity.

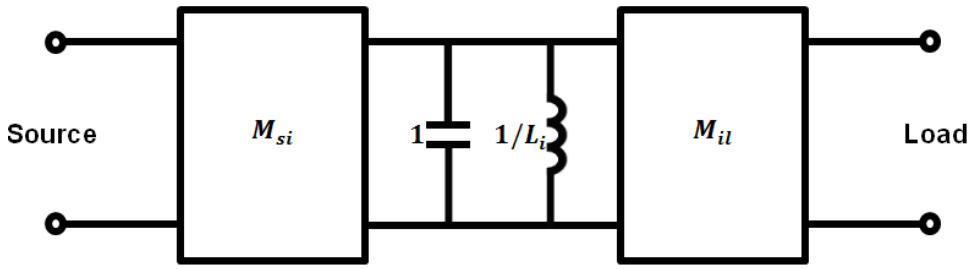

Fig. 1-4 An i^{th} branch of a transverse network

The $ABCD$ matrix may easily be computed as follows:

$$[ABCD]_i = \begin{bmatrix} 0 & j/M_{si} \\ jM_{si} & 0 \end{bmatrix}\begin{bmatrix} 1 & 0 \\ Y_i & 1 \end{bmatrix}\begin{bmatrix} 0 & j/M_{il} \\ jM_{il} & 0 \end{bmatrix}$$
$$[ABCD]_i = \begin{bmatrix} -M_{il}/M_{si} & -Y_i/(M_{si}M_{il}) \\ 0 & -M_{si}/M_{il} \end{bmatrix} \tag{1.60}$$

where

$$Y_i = p + \frac{1}{L_i p} = \frac{p^2 + 1/L_i}{p} \tag{1.61}$$

(1.60) may be converted to the admittance Y matrix as

$$[Y]_i = \frac{1}{Y_i}\begin{bmatrix} {M_{si}}^2 & M_{si}M_{il} \\ M_{si}M_{il} & {M_{il}}^2 \end{bmatrix} \tag{1.62}$$

Hence the total admittance Y matrix for N_r branches of Fig. 1-4 is

$$[Y]_r = \sum_{i=1}^{N_r}[Y]_i = \begin{bmatrix} \sum_{i=1}^{N_r}\frac{{M_{si}}^2 p}{p^2 + 1/L_i} & \sum_{i=1}^{N_r}\frac{M_{si}M_{il}p}{p^2 + 1/L_i} \\ \sum_{i=1}^{N_r}\frac{M_{si}M_{il}p}{p^2 + 1/L_i} & \sum_{i=1}^{N_r}\frac{{M_{il}}^2 p}{p^2 + 1/L_i} \end{bmatrix} \tag{1.63}$$

Comparing (1.59) and (1.63) yields,

$$\begin{aligned} {M_{il}}^2 &= a_i \\ M_{si}M_{il} &= z_i \\ 1/L_i &= -{p_i}^2 \end{aligned} \tag{1.64}$$

Thus the coupling elements of the transverse network consisting of N_r branches between source and load of Fig. 1-4 may be determined as

$$\begin{aligned} M_{il} &= \sqrt{a_i} \\ M_{si} &= z_i/\sqrt{a_i} \\ 1/L_i &= -{p_i}^2 \end{aligned} \tag{1.65}$$

1.1.3.2.1 Re-configuration of the Bandpass Filter Transverse Coupling Matrix

The transverse coupling matrix obtained using the previous description is not normally suitable for direct realisation of bandpass filters. Using similar technique as was done for lowpass prototype filter CM, a series of matrix rotations that preserves the frequency response may be used to convert the transverse CM to topological forms that are more suitable for implementation. Let the initial transverse coupling matrix M be written as

$$M = M_T + pI + \frac{1}{p}M_L \tag{1.66}$$

where I is an $(N_r + 2)$ by $(N_r + 2)$ matrix with all its initial elements zero except diagonal elements, $I(i,i) = 1,\ i = 2, 3, 4, \ldots N_r + 1,$

$$I = \begin{bmatrix} 0 & 0 & 0 & 0 & \ldots & 0 & 0 & 0 & 0 \\ 0 & 1 & 0 & 0 & \ldots & 0 & 0 & 0 & 0 \\ 0 & 0 & 1 & 0 & \ldots & 0 & 0 & 0 & 0 \\ 0 & 0 & 0 & \ddots & \ldots & 0 & 0 & 0 & 0 \\ \vdots & \vdots & \vdots & \vdots & 1 & \vdots & \vdots & \vdots & \vdots \\ 0 & 0 & 0 & 0 & \ldots & \ddots & 0 & 0 & 0 \\ 0 & 0 & 0 & 0 & \ldots & 0 & 1 & 0 & 0 \\ 0 & 0 & 0 & 0 & \ldots & 0 & 0 & 1 & 0 \\ 0 & 0 & 0 & 0 & \ldots & 0 & 0 & 0 & 0 \end{bmatrix} \tag{1.67}$$

M_T is an $(N_r + 2)$ by $(N_r + 2)$ matrix with all its initial elements zero except the first row and column and last row and column elements obtained from the transverse coupling matrix elements defined as,

$$M_T = \begin{bmatrix} 0 & M_{s,1} & M_{s,2} & \ldots & M_{s,N_r-1} & M_{s,N_r} & 0 \\ M_{s,1} & 0 & 0 & \ldots & 0 & 0 & M_{1,l} \\ M_{s,2} & 0 & 0 & \ldots & 0 & 0 & M_{2,l} \\ \vdots & \vdots & \vdots & \ddots & \vdots & \vdots & \vdots \\ M_{s,N_r-1} & 0 & 0 & \ldots & 0 & 0 & M_{N_r-1,l} \\ M_{s,N_r} & 0 & 0 & \ldots & 0 & 0 & M_{N_r,l} \\ 0 & M_{1,l} & M_{2,l} & \ldots & M_{N_r-1,l} & M_{N_r,l} & 0 \end{bmatrix} \tag{1.68}$$

M_L is an (N_r+2) by (N_r+2) all inductive matrix with all its initial elements zero except diagonal elements, $M_L(i,i) = 1/L_i,\ i = 2,3,4,\ldots N_r+1$,

$$M_L = \begin{bmatrix} 0 & 0 & 0 & 0 & \ldots & 0 & 0 & 0 & 0 \\ 0 & 1/L_1 & 0 & 0 & \ldots & 0 & 0 & 0 & 0 \\ 0 & 0 & 1/L_2 & 0 & \ldots & 0 & 0 & 0 & 0 \\ 0 & 0 & 0 & \ddots & \ldots & 0 & 0 & 0 & 0 \\ \vdots & \vdots & \vdots & \vdots & 1/L_i & \vdots & \vdots & \vdots & \vdots \\ 0 & 0 & 0 & 0 & \ldots & \ddots & 0 & 0 & 0 \\ 0 & 0 & 0 & 0 & \ldots & 0 & 1/L_{N_r-1} & 0 & 0 \\ 0 & 0 & 0 & 0 & \ldots & 0 & 0 & 1/L_{N_r} & 0 \\ 0 & 0 & 0 & 0 & \ldots & 0 & 0 & 0 & 0 \end{bmatrix} \tag{1.69}$$

Notice the subtle differences in the decomposition between the CM for lowpass and bandpass filters. Similarity transformations may be applied as described in section 1.1.3.1.1 to reduce the transverse coupling matrix to either folded or arrow canonical forms,

$$M = M_T + pI + \frac{1}{p}M_L. \tag{1.70}$$

The arrow coupling matrix may further be converted to cascaded n-tuplets or other in-line practical topologies. Since the rotation angles for reconfigurations of arrow matrix to cascaded n-tuplets are known for lowpass prototype filter CM [21], a similar approach is used to calculate the analytic formulae for the rotation angles required to convert the arrow matrix to cascaded n-tuplets topology for direct synthesised CM for bandpass filters. Consider a trisection for bandpass filter centred at node k in Fig. 1-5.

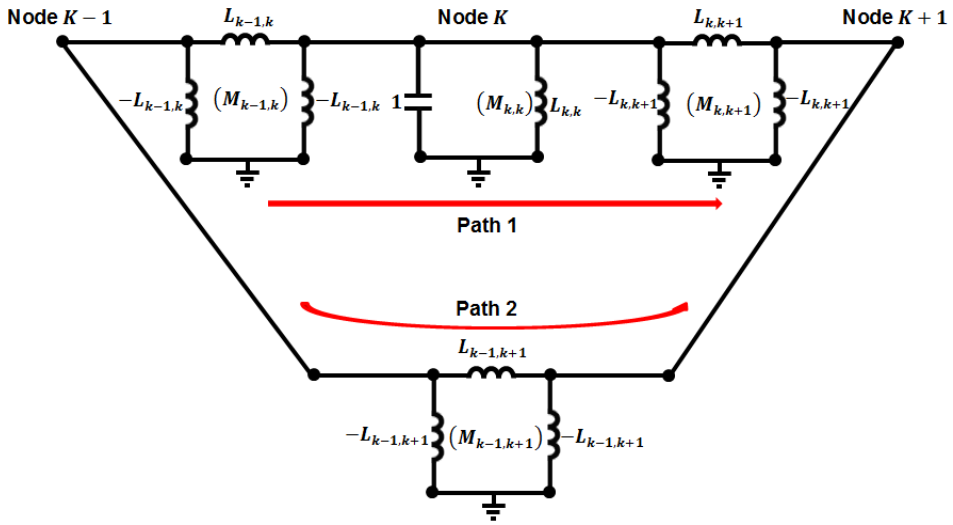

Fig. 1-5 A bandpass trisection with all inductive couplings centred at node k

Furthermore, consider two paths with $ABCD$ matrix as follows;

$$[ABCD]_1 = \begin{bmatrix} 0 & L_{k-1,k}p \\ -\dfrac{1}{L_{k-1,k}p} & 0 \end{bmatrix} \begin{bmatrix} 1 & 0 \\ Y_k & 1 \end{bmatrix} \begin{bmatrix} 0 & L_{k,k+1}p \\ -\dfrac{1}{L_{k,k+1}p} & 0 \end{bmatrix}$$
$$= \begin{bmatrix} -\dfrac{L_{k-1,k}}{L_{k,k+1}p} & L_{k-1,k}L_{k,k+1}p^2Y_k \\ 0 & -\dfrac{L_{k-1,k}}{L_{k,k+1}p} \end{bmatrix} \tag{1.71}$$

where

$$Y_k = p + \frac{1}{L_{k,k}p} = p + \frac{M_{k,k}}{p} = \frac{1}{p}\left(p^2 + M_{k,k}\right) \tag{1.72}$$

And for the second path,

$$[ABCD]_2 = \begin{bmatrix} 0 & L_{k-1,k+1}p \\ -\dfrac{1}{L_{k-1,k+1}p} & 0 \end{bmatrix}. \tag{1.73}$$

Converting the $ABCD$ matrices for the two paths to Y matrices and adding them yields,

$$[Y]_1 = \begin{bmatrix} \dfrac{1}{{L_{k,k+1}}^2p^2Y_k} & -\dfrac{1}{L_{k-1,k}L_{k,k+1}p^2Y_k} \\ -\dfrac{1}{L_{k-1,k}L_{k,k+1}p^2Y_k} & \dfrac{1}{{L_{k-1,k}}^2p^2Y_k} \end{bmatrix}$$
$$= \begin{bmatrix} \dfrac{{M_{k,k+1}}^2}{p^2Y_k} & -\dfrac{M_{k-1,k}M_{k,k+1}}{p^2Y_k} \\ -\dfrac{M_{k-1,k}M_{k,k+1}}{p^2Y_k} & \dfrac{{M_{k-1,k}}^2}{p^2Y_k} \end{bmatrix}, \tag{1.74}$$

and

$$[Y]_2 = \begin{bmatrix} 0 & -\dfrac{1}{L_{k-1,k+1}p} \\ -\dfrac{1}{L_{k-1,k+1}p} & 0 \end{bmatrix} = \begin{bmatrix} 0 & \dfrac{M_{k-1,k+1}}{p} \\ \dfrac{M_{k-1,k+1}}{p} & 0 \end{bmatrix}. \tag{1.75}$$

Hence,

$$[Y]_T = [Y]_1 + [Y]_2 \tag{1.76}$$

$$[Y]_T = \begin{bmatrix} \frac{{M_{k,k+1}}^2}{p^2 Y_k} & \frac{M_{k-1,k+1}}{p} - \frac{M_{k-1,k}M_{k,k+1}}{p^2 Y_k} \\ \frac{M_{k-1,k+1}}{p} - \frac{M_{k-1,k}M_{k,k+1}}{p^2 Y_k} & \frac{{M_{k-1,k}}^2}{p^2 Y_k} \end{bmatrix}$$

From (1.76) it is clear that the transmission zeros occur when

$$\left.\frac{M_{k-1,k+1}}{p} - \frac{M_{k-1,k}M_{k,k+1}}{p^2 Y_k}\right|_{p=j\omega_z} = 0 \tag{1.77}$$

Substituting for Y_k yields,

$$\left.\frac{M_{k-1,k+1}}{p} - \frac{M_{k-1,k}M_{k,k+1}}{p\left(p^2 + M_{k,k}\right)}\right|_{p=j\omega_z} = 0 \tag{1.78}$$

By ignoring the transmission zero at infinite ($p = \infty$) (1.78) can be alternatively expressed as,

$$\begin{gathered} \left(-{\omega_z}^2 + M_{k,k}\right)M_{k-1,k+1} - M_{k-1,k}M_{k,k+1} = 0 \\ det\begin{vmatrix} M_{k-1,k} & M_{k-1,k+1} \\ -{\omega_z}^2 + M_{k,k} & M_{k,k+1} \end{vmatrix} = 0 \end{gathered} \tag{1.79}$$

(1.79) is true whenever a trisection centred at node k (in the coupling matrix) with a pair of symmetrical transmission zeros at $p = \pm j\omega_z$ exists. Therefore, to create a trisection centred at node k, a rotation is performed pivoted at $[k, k+1]$ and the condition (1.79) is imposed forcing a trisection with a pair of transmission zeros at $p = \pm j\omega_z$. The element values [3] after this rotation are

$$\begin{gathered} M'_{k,k} = M_{k,k}\cos^2\theta - 2\,M_{k,k+1}\sin\theta\cos\theta + M_{k+1,k+1}\sin^2\theta \\ M'_{k-1,k+1} = M_{k-1,k}\sin\theta + M_{k-1,k+1}\cos\theta = M_{k-1,k}\sin\theta \\ M'_{k-1,k} = M_{k-1,k}\cos\theta - M_{k-1,k+1}\sin\theta = M_{k-1,k}\cos\theta \\ M'_{k,k+1} = (\cos^2\theta - \sin^2\theta)M_{k,k+1} + \sin\theta\cos\theta\left(M_{k,k} - M_{k+1,k+1}\right) \end{gathered} \tag{1.80}$$

where θ is the rotation angle. Notice that $M_{k-1,k+1}$ is assumed to be zero prior to the rotation. It is desired from (1.79) that

$$\left(-{\omega_z}^2 + M'_{k,k}\right)M'_{k-1,k+1} - M'_{k-1,k}M'_{k,k+1} = 0 \tag{1.81}$$

Substituting (1.80) in (1.81) yields,

$$\left(-{\omega_z}^2 + M_{k,k}\cos^2\theta - 2\,M_{k,k+1}\sin\theta\cos\theta + M_{k+1,k+1}\sin^2\theta\right)M_{k-1,k}\sin\theta = M_{k-1,k}\cos\theta\left[M_{k,k+1}(\cos^2\theta - \sin^2\theta) + \left(M_{k,k} - M_{k+1,k+1}\right)\sin\theta\cos\theta\right] \quad (1.82)$$

This simplifies to,

$$-{\omega_z}^2 + M_{k+1,k+1} = M_{k,k+1}\cot\theta \quad (1.83)$$

From which the required rotation angle for bandpass filter trisection may be obtained as

$$\theta = \cot^{-1}\left(\frac{M_{k,k+1}}{-{\omega_z}^2 + M_{k+1,k+1}}\right) \quad (1.84)$$

This is similar to the rotation angle used for lowpass prototype filter CM as [21]

$$\theta = \cot^{-1}\left(\frac{M_{k,k+1}}{\omega_z + M_{k+1,k+1}}\right) \quad (1.85)$$

The arrow coupling matrix may be reconfigured to cascaded trisections by first forming a first trisection centred at $k = N_r - 1$, with the first rotation pivoted at $[N_r - 1, N_r]$, and then moving this trisection to the required position towards the source. This is repeated for all the trisections. Then some trisections may be combined together to form higher order n-tuplets. Again well detailed analysis is given in [3].

1.1.3.2.2 Introduction of capacitive couplings in trisections and quadruplets

After reconfiguration the overall coupling matrix may still be expressed as in (1.70) with the definition given in section 1.1.3.2.1. This formulation assumes that the filter network has no capacitive coupling and as such all inter-resonator couplings are inductive. For some transfer functions, some of the element values in the inductive coupling matrix M_L may be negative. For narrow bandpass filters this does not present a challenge as the negative inductor may be replaced by a capacitor. For wideband filters, this will results in erroneous response. To avoid this, capacitive couplings may be incorporated in the formulation (1.70) by re-writing as

$$M = M_T + pM_C + \frac{1}{p}M_L \quad (1.86)$$

Where M_C is an (N_r+2) by (N_r+2) all capacitve coupling matrix with all its initial elements zero except diagonal elements, $M_C(i,i)=C_i=1,\ i=2,3,4,\ldots N_r+1$, defined as,

$$M_C=\begin{bmatrix}0&0&0&0&\ldots&0&0&0&0\\0&1&0&0&\ldots&0&0&0&0\\0&0&1&0&\ldots&0&0&0&0\\0&0&0&\ddots&\ldots&0&0&0&0\\\vdots&\vdots&\vdots&\vdots&1&\vdots&\vdots&\vdots&\vdots\\0&0&0&0&\ldots&\ddots&0&0&0\\0&0&0&0&\ldots&0&1&0&0\\0&0&0&0&\ldots&0&0&1&0\\0&0&0&0&\ldots&0&0&0&0\end{bmatrix} \tag{1.87}$$

Now, consider again the trisection in Fig. 1-5 centred at k and thus with index k. If any one of the three couplings is negative, a number of matrix operations are performed to introduce a capacitive coupling in its place. Let n and m be some indices for the row and column of the coupling matrix M. To eliminate the element $M_L(k-1,k)$ (where $n=k-1,m=k$) or $M_L(k,k+1)$ (where $n=k,m=k+1$), the following steps are carried out:

Step 1: Compute

$$\alpha=-\frac{M_L(n,m)}{M_L(m,m)} \tag{1.88}$$

Step 2: Compute new n^{th} row and column of M as

$$n^{th}\text{ row(column) of }M=n^{th}\text{ row(column) of }M+\alpha[m^{th}\text{ row(column) of }M] \tag{1.89}$$

This eliminates the $M_L(n,m)$ coupling element and introduces $M_C(n,m)$ coupling element.

Step 3: Compute the parameter,

$$\beta=-\frac{1}{\sqrt{M_C(n,n)}} \tag{1.90}$$

Step 4: Scale the n^{th} row and column of M as

$$n^{th}\text{ row (column) of }M=\beta[n^{th}\text{ row }(column)\text{ of }M] \tag{1.91}$$

This normalises the matrix M_C with all non-zero diagonal elements equal to unity and completes the procedure.

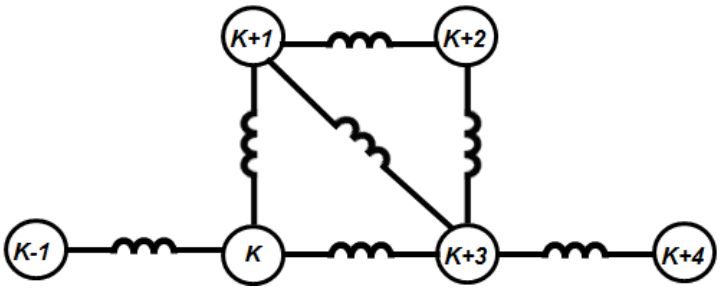

(a)

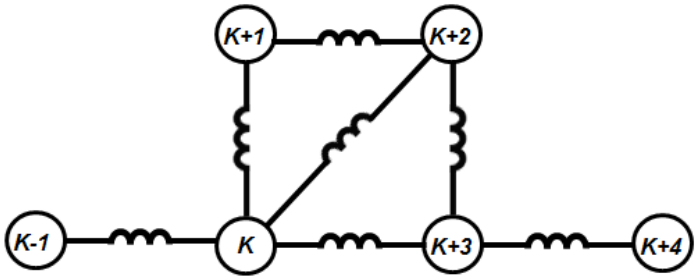

(b)

Fig. 1-6 Alternative forms of a quadruplet with all inductive couplings

If the element $M_L(k-1,k+1)$ is negative, it cannot be changed to capacitive coupling using this method and thus rescaling by a negative (-1) is necessary to make either $M_L(k-1,k)$ or $M_L(k,k+1)$ negative so that the above routine can be carried out to introduce a capacitive coupling. The above routine (1.88)-(1.91) may be applied to a quadruplet except that n and m take on different values as illustrated in Table 1-1. Here the index k is the first node in the quadruplet as depicted in Fig. 1-6. To enable elimination of two or more negative couplings elements in M_L in a quadruplet requires solving simultaneous equations for the scaling factors.

Table 1-1 Values of n and m for a Quadruplet

Element to Eliminate (Fig. 1-6 (a))	n	m	Element to Eliminate (Fig. 1-6 (b))	n	m
$M_L(k+1,k+2)$	$k+1$	$k+2$	$M_L(k,k+1)$	k	$k+1$
$M_L(k+2,k+3)$	$k+3$	$k+2$	$M_L(k+1,k+2)$	$k+2$	$k+1$
$M_L(k+1,k+3)$	$k+3$	$k+1$	$M_L(k,k+2)$	k	$k+2$

1.1.3.3 Coupling Matrix Analysis

Since most of the lowpass and bandpass filter sub-coupling matrices have elements in the first and last rows and columns equal to zero, then the $N_r + 2 \times N_r + 2$ final coupling matrix for lowpass filter and bandpass filter synthesis may be expressed in terms of $N_r \times N_r$ coupling matrix which is represented as follows:

$$Y_{LP} = M_{Ts} + pI + jM_{Ks} \tag{1.92}$$

for lowpass prototype filters and,

$$Y_{BP} = M_{Ts} + pM_{Cs} + \frac{1}{p}M_{Ls} \tag{1.93}$$

for single(multi) bandpass filters where I is an N_r by N_r identity matrix, M_{Ks} matrix is the remnant $N_r \times N_r$ coupling matrix with all possible coupling elements, M_{Ls} matrix is the remnant $N_r \times N_r$ inductive coupling matrix and M_{Cs} is the remnant normalised $N_r \times N_r$ capacitive coupling matrix with unit diagonal nodal elements. M_{Ts} is a $N_r \times N_r$ matrix with all its elements zero except $M_{Ts}(1,1)$ and $M_{Ts}(N_r, N_r)$ which are given by

$$\begin{aligned} M_{Ts}(1,1) &= G_1 \\ M_{Ts}(N_r, N_r) &= G_{N_r} \end{aligned} \tag{1.94}$$

where,

$$\begin{aligned} G_1 &= \left(M_T(1,2)\right)^2 \\ G_{N_r} &= \left(M_T(N_r+1, N_r+2)\right)^2 \end{aligned} \tag{1.95}$$

Finally the following analysis may be made to obtain the filter magnitude response

$$\begin{aligned} S_{11} &= 1 - 2 * G_1\left[{Y_{LP}}^{-1}\right]_{11} \\ S_{21} &= 2\sqrt{G_1 G_{N_r}}\left[{Y_{LP}}^{-1}\right]_{N_r,1} \end{aligned} \tag{1.96}$$

for lowpass filter and

$$\begin{aligned} S_{11} &= 1 - 2 * G_1\left[{Y_{BP}}^{-1}\right]_{11} \\ S_{21} &= 2\sqrt{G_1 G_{N_r}}\left[{Y_{BP}}^{-1}\right]_{N_r,1} \end{aligned} \tag{1.97}$$

for single(multi) bandpass filters [5]. Note that the dimension of the coupling matrix N_r is related to the degree of the filter's characteristic function N(highest degree of the characteristic polynomials) by,

$$N_r = N \text{ Lowpass Prototype Filter}$$
$$N_r = N/2 \text{ Single(Multi) Bandpass Filter} \tag{1.98}$$

The short hand representation of filter network elements shown in Fig. 1-7 to Fig. 1-9 will be adopted to show network topology derived from the CM. Each node of the form in Fig. 1-7 will be represented by a circle with an index inside of Fig. 1-8. The admittance inverters will be shown using the short hand representation shown in Fig. 1-9. The negative elements are usually absorbed at the surrounding nodes.

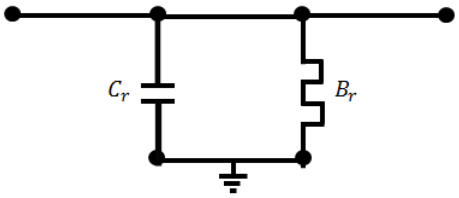

(a) Lumped Lowpass Resonator

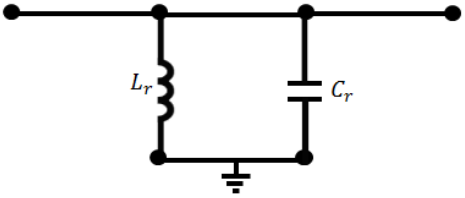

(b) Lumped Bandpass Resonator

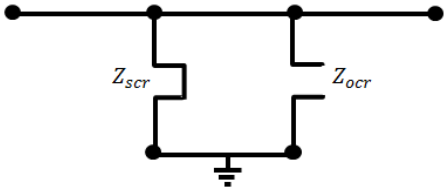

(c) Distributed Bandpass Resonator

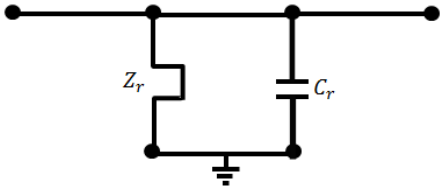

(d) Mixed Lumped-Distributed Resonator

Fig. 1-7 Resonators

Fig. 1-8 Nodal representation of filter networks

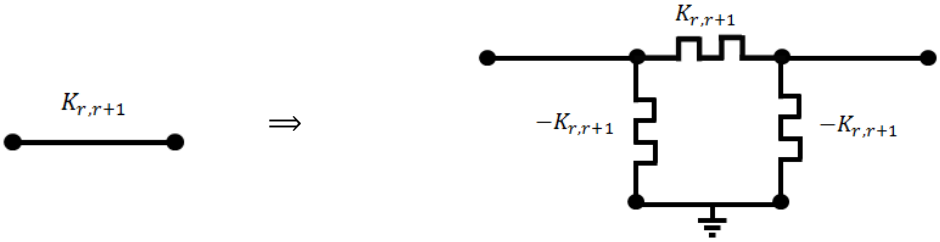

(a) Ideal Admittance Inverters ($M_K(r,r+1) = K_{r,r+1}$)

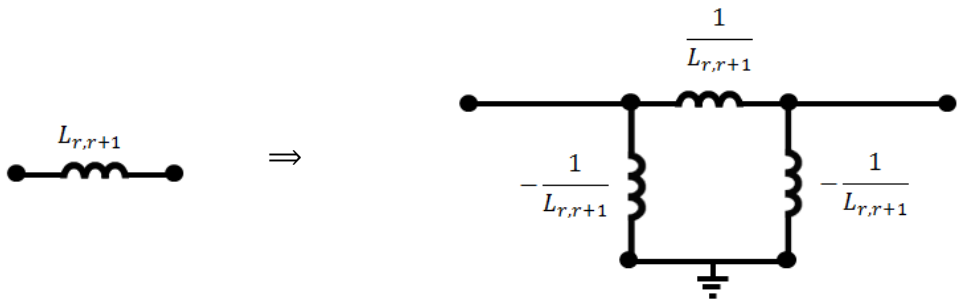

(b) Lumped Inductive Coupling Element ($M_L(r,r+1) = 1/L_{r,r+1}$)

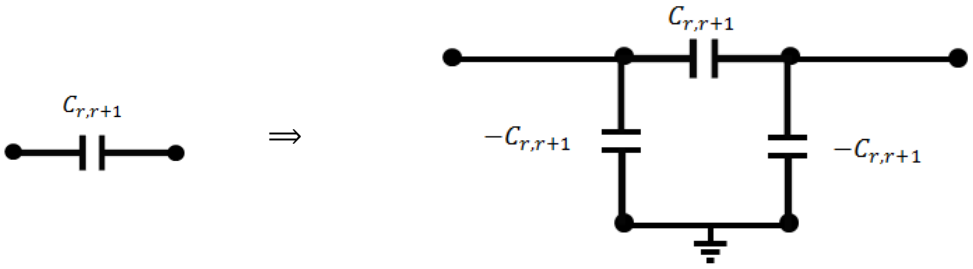

(c) Lumped Capacitive Coupling Element ($M_C(r,r+1) = C_{r,r+1}$)

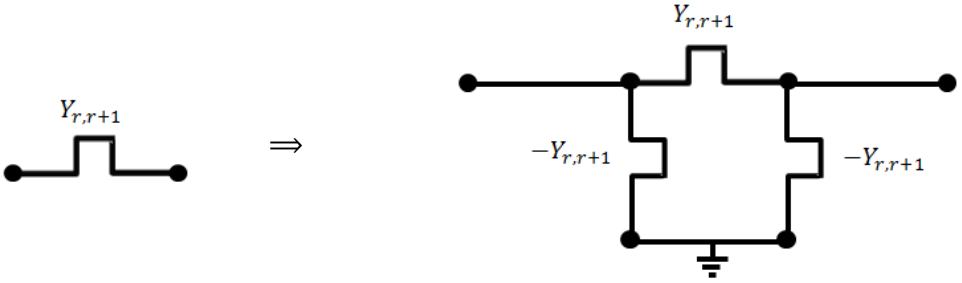

(d) Distributed Inductive Coupling Element ($M_L(r,r+1) = Y_{r,r+1}$))

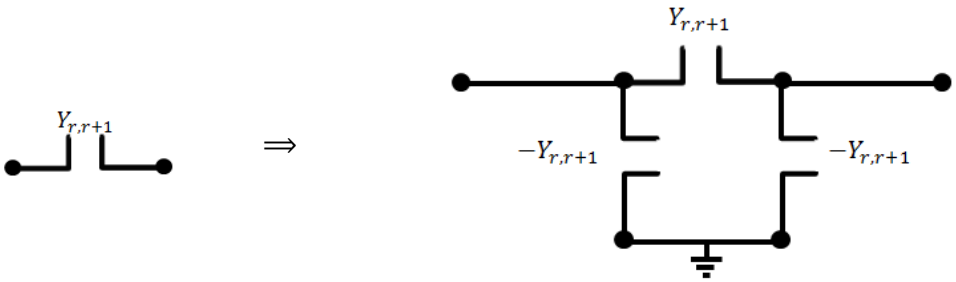

(e) Distributed Capacitive Coupling Element ($M_C(r, r+1) = Y_{r,r+1}$)

Fig. 1-9 Short hand representation of coupling elements between node r and $r+1$

1.1.4 Cascaded Synthesis Method

Most microwave filter networks are made up of cascaded elements in shunt and or series combinations. Sometimes, however, the cascaded network forms are impractical and some circuit transformations are then used to convert the cascaded network to a more practical network in which non-adjacent elements may interact in the so-called cross coupled networks [24]. Although somewhat becoming historical method, it is nonetheless a very suitable form of synthesis method at least for some microwave filter networks. Distributed low-pass filter synthesised using cascaded circuit synthesis is one such good example.

In this section, it is shown starting from the overall filter ABCD matrix, how the method may be used to extract the filter network elements through some matrix reduction or extraction procedures. From either source port or load port, the network elements are extracted one after another each time reducing the order of the ABCD matrix polynomials [3]. A similar technique may be applied using the driving point impedance [4]. In this work, however, the ABCD matrix method will be used which is more amenable to computer manipulations.

Sometimes this synthesis method does fail especially with high order networks or where the reflection zeros are clustered together as is the case in very narrow bandpass filters. In other words there are errors that are carried forward at each step of the process such that the polynomials do not retain their standard forms and extraction of correct and real valued elements becomes impossible. In such cases, appropriate scaling such as Norton transformation [25] at some stages during the synthesis process usually solves the problem. In [3], it is suggested to

extract elements alternatively from source and load. For most useful filter networks, this circuit approach works well as it will be seen in Chapter 3 and Chapter 4.

Furthermore, as will be evident later, this method presents advantages in filter networks where the use of the coupling matrix synthesis method (discussed in section 1.1.3) becomes an insurmountable task. Extraction procedures for some common elements pertinent to the research were derived and summarised in Table 1-2. The circuit synthesis approach is done by extraction of the individual elements that make up the filter network by reduction of the original ABCD matrix. The individual elements themselves are represented in matrix form and matrix inversion allows the elements to be extracted. The remainder of the ABCD matrix contains reduced order of some of the ABCD polynomials. The evaluation of the element value is done under certain conditions. Thus in the synthesis of the filter topologies such as trisection [26] or extracted pole [27, 28], the filter elements have to be extracted in a certain order that preserves the network behaviour and that the overall ABCD matrix reduces after each stage until all the polynomials are reduced to either zero or constants.

For example, suppose the origin ABCD matrix is denoted by T, and after extraction of a capacitor (c) with ABCD matrix, $\mathrm{T_C}$, the overall ABCD matrix reduces to $\mathrm{T_r}$, then

$$T_C T_r = T$$

$$\frac{1}{P_r}\begin{bmatrix} 1 & 0 \\ pc & 1 \end{bmatrix}\begin{bmatrix} A_r & B_r \\ C_r & D_r \end{bmatrix} = \frac{1}{P}\begin{bmatrix} A & B \\ C & D \end{bmatrix} \tag{1.99}$$

Multiplying by the inverse of T_C on both sides yields,

$$T_r = [T_C]^{-1} T$$

$$T_r = \frac{1}{P_r}\begin{bmatrix} A_r & B_r \\ C_r & D_r \end{bmatrix} = \frac{1}{P}\begin{bmatrix} 1 & 0 \\ -cp & 1 \end{bmatrix}\begin{bmatrix} A & B \\ C & D \end{bmatrix} = \frac{1}{P}\begin{bmatrix} A & B \\ C - cpA & D - cpB \end{bmatrix} \tag{1.100}$$

c may then be evaluated so that $D_{rem}(p = j\infty) = 0$

$$c = \left.\frac{D(p)}{pB(p)}\right|_{p=j\infty} \tag{1.101}$$

This is illustrated in Table 1-2. The only exception is for parallel connected networks. For example to extract a parallel inverter M_{ij} between two nodes (node i and j) the short-circuit admittance matrix parameters are used. For an inverter, the $[Y]$ matrix is

$$\begin{bmatrix} 0 & jM_{ij} \\ jM_{ij} & 0 \end{bmatrix}. \tag{1.102}$$

And for the remainder of the network after extraction of the parallel inverter, may be expressed as

$$[ABCD]_r = \frac{1}{P_r(p)}\begin{bmatrix} A_r(p) & B_r(p) \\ C_r(p) & D_r(p) \end{bmatrix}, \tag{1.103}$$

and its $[Y]$ matrix is

$$[Y]_r = \frac{1}{B_r(p)}\begin{bmatrix} -D_r(p) & -P_r(p) \\ -P_r(p) & -A_r(p) \end{bmatrix}. \tag{1.104}$$

The overall admittance for the original network is simply the addition of the two $[Y]$ matrices as,

$$[Y] = \frac{1}{B_r(p)}\begin{bmatrix} -D_r(p) & -P_r(p) + jM_{ij}B_r(p) \\ -P_r(p) + jM_{ij}B_r(p) & -A_r(p) \end{bmatrix}. \tag{1.105}$$

Converting this to the ABCD matrix yields,

$$\begin{aligned} [ABCD] &= \frac{1}{P(p)}\begin{bmatrix} A(p) & B(p) \\ C(p) & D(p) \end{bmatrix} \\ &= \frac{1}{P_r(p) - jM_{ij}B_r(p)}\begin{bmatrix} A_r(p) & B_r(p) \\ C_r(p) + j2M_{ij}P_r(p) - {M_{ij}}^2 B_r(p) & D_r(p) \end{bmatrix} \end{aligned} \tag{1.106}$$

Hence the polynomials $A(p)$, $B(p)$ and $D(p)$ remain unchanged after the extraction while $C(p)$ and $P(p)$ are reduced by 1 degree to

$$\begin{aligned} P_r(p) &= P(p) + jM_{ij}B_r(p) = P(p) + jM_{ij}B(p) \\ C_r(p) &= C(p) - j2M_{ij}P_r(p) + {M_{ij}}^2 B_r(p) = C(p) - j2M_{ij}P(p) - {M_{ij}}^2 B(p) \end{aligned} \tag{1.107}$$

Where M_{ij} is computed from equation (1.107) (a) as

$$M_{ij} = -\left.\frac{P(p)}{jB(p)}\right|_{p=j\infty} \tag{1.108}$$

Table 1-2 Cascaded Synthesis Using ABCD Matrices Extraction for Commonly Used Elements

Network Element	Element $[ABCD]$ matrix	Reduced $[ABCD]$ matrix
Shunt Capacitor (c) $c = \left.\frac{D(p)}{pB(p)}\right\|_{p=j\infty}$	$\begin{bmatrix} 1 & 0 \\ cp & 1 \end{bmatrix}$	$\frac{1}{P(p)}\begin{bmatrix} A(p) & B(p) \\ C(p)-cpA(p) & D(p)-cpB(p) \end{bmatrix}$
Condition for Extraction: Degree of $D(p)$ = Degree of $B(p)+1$		
Shunt Inductor (l) $l = \left.\frac{\left(\frac{B(p)}{p}\right)}{D(p)}\right\|_{p=0}$	$\begin{bmatrix} 1 & 0 \\ \frac{1}{lp} & 1 \end{bmatrix}$	$\frac{1}{P(p)}\begin{bmatrix} A(p) & B(p) \\ C(p)-\frac{\left(\frac{A(p)}{p}\right)}{l} & D(p)-\frac{\left(\frac{B(p)}{p}\right)}{l} \end{bmatrix}$
Condition for Extraction: $A(p)$ and $B(p)$ must be divisible by p		
Series Capacitor (c) $c = \left.\frac{\left(\frac{D(p)}{p}\right)}{B(p)}\right\|_{p=0}$	$\begin{bmatrix} 1 & \frac{1}{cp} \\ 0 & 1 \end{bmatrix}$	$\frac{1}{P(p)}\begin{bmatrix} A(p)-\frac{\left(\frac{C(p)}{p}\right)}{c} & B(p)-\frac{\left(\frac{D(p)}{p}\right)}{c} \\ C(p) & D(p) \end{bmatrix}$
Condition for Extraction: $C(p)$ and $D(p)$ must be divisible by p		

Series Inductor (l)

$$l = \left.\frac{B(p)}{pD(p)}\right|_{p=j\infty} \qquad \begin{bmatrix} 1 & lp \\ 0 & 1 \end{bmatrix} \qquad \frac{1}{P(p)}\begin{bmatrix} A(p) - lpC(p) & B(p) - lpD(p) \\ C(p) & D(p) \end{bmatrix}$$

Condition for Extraction: Degree of $B(p)$ = Degree of $D(p) + 1$

Unit Phase Shifter (θ)

$$\theta = atan\left(\frac{D(p)}{B(p)}\right)\Big|_{p=j\omega_z} \qquad \begin{bmatrix} cos(\theta) & jsin(\theta) \\ jsin(\theta) & cos(\theta) \end{bmatrix} \qquad \frac{1}{P(p)}\begin{bmatrix} A(p)\,cos(\theta) - jC(p)sin(\theta) & B(p)\,cos(\theta) - jD(p)sin(\theta) \\ C(p)cos(\theta) - jA(p)jsin(\theta) & D(p)cos(\theta) - jB(p)sin(\theta) \end{bmatrix}$$

Series unit inverter (J)

$$J = 1 \qquad \begin{bmatrix} 0 & j \\ j & 0 \end{bmatrix} \qquad \frac{1}{P(p)}\begin{bmatrix} -jC(p) & -jD(p) \\ -jA(p) & -jB(p) \end{bmatrix}$$

Shunt FIR (b)

$$b = \left.\frac{D(p)}{jB(p)}\right|_{p=j\infty} \qquad \begin{bmatrix} 1 & 0 \\ jb & 1 \end{bmatrix} \qquad \frac{1}{P(p)}\begin{bmatrix} A(p) & B(p) \\ C(p) - jbA(p) & D(p) - jbB(p) \end{bmatrix}$$

Condition for Extraction: Degree of $D(p)$= Degree of $B(p)$

Series FIR (x)

$$x = \left.\frac{B(p)}{jD(p)}\right|_{p=j\omega_z} \qquad \begin{bmatrix} 1 & jx \\ 0 & 1 \end{bmatrix} \qquad \frac{1}{P(p)}\begin{bmatrix} A(p) - jxC(p) & B(p) - jxD(p) \\ C(p) & D(p) \end{bmatrix}$$

Condition for Extraction: Degree of $D(p)$= Degree of $B(p)$

Shunt Series of Inductor and

FIR $\left(\frac{b_o}{p-j\omega_z}\right)$

$$b_o = \frac{D(p)}{[B(p)/(p-j\omega_z)]}\Big|_{p=j\omega_z}$$

$$\begin{bmatrix} 1 & 0 \\ \frac{b_o}{p-j\omega_z} & 1 \end{bmatrix}$$

$$\frac{1}{P(p)}\begin{bmatrix} A(p) & B(p) \\ C(p)-\frac{b_o}{p-j\omega_z}A(p) & D(p)-\frac{b_o}{p-j\omega_z}B(p) \end{bmatrix}$$

Condition for Extraction: Polynomials $A(p)$ and $B(p)$ have to be divisible by $p-j\omega_z$ or that one of the roots of $A(p)$ and $B(p)$ must be $p=j\omega_z$ where ω_z is the transmission zero

Parallel connected inverter

(M_{ij})

$$M_{ij} = \frac{jP(p)}{B(p)}\Big|_{p=j\infty}$$

$$\begin{bmatrix} 0 & j/M_{ij} \\ jM_{ij} & 0 \end{bmatrix}$$

$$\frac{1}{P(p)+jM_{ij}B(p)}\begin{bmatrix} A(p) & B(p) \\ C(p)+j2M_{ij}P(p)-{M_{ij}}^2B(p) & D(p) \end{bmatrix}$$

Condition for Extraction: Degree of $P(p)$= Degree of $B(p)$

Shunt Open Circuited Stub

(Z_{oc})

$$Z_{oc} = \frac{\rho B(\rho)}{D(\rho)}\Big|_{\rho=jt_z}$$

$$\begin{bmatrix} 1 & 0 \\ \frac{\rho}{Z_{oc}} & 1 \end{bmatrix}$$

$$\frac{1}{P(\rho)}\begin{bmatrix} A(\rho) & B(\rho) \\ C(\rho)-\frac{\rho A(\rho)}{Z_{oc}} & D(\rho)-\frac{\rho B(\rho)}{Z_{oc}} \end{bmatrix}$$

Condition for Extraction: Degree of $D(\rho)=$ Degree of $B(\rho)+1$

Series Short Circuited Stub

(Z_{sc})

$$Z_{sc} = \left.\frac{B(\rho)}{\rho D(\rho)}\right|_{\rho=jt_z}$$

$$\begin{bmatrix} 1 & Z_{sc}\rho \\ 0 & 1 \end{bmatrix}$$

$$\frac{1}{P(p)}\begin{bmatrix} A(p) - Z_{sc}\rho C(p) & B(p) - Z_{sc}\rho D(p) \\ C(p) & D(p) \end{bmatrix}$$

Condition for Extraction: Degree of $B(\rho)$ = Degree of $D(\rho) + 1$

Shunt Series of Short Circuited Stub (Z_{sc}) and Open Circuited Stub (Z_{oc})

$$Z_{sc} = \left.\frac{\rho\left(\frac{B(\rho)}{\rho^2 - {\rho_z}^2}\right)}{D(\rho)}\right|_{\rho=\rho_z}$$

$$Z_{oc} = -\left.\frac{\rho^3\left(\frac{B(\rho)}{\rho^2 - {\rho_z}^2}\right)}{D(\rho)}\right|_{\rho=\rho_z}$$

$$\begin{bmatrix} 1 & 0 \\ \frac{\rho}{Z_{sc}\left(\rho^2 + \frac{Z_{oc}}{Z_{sc}}\right)} & 1 \end{bmatrix}$$

where ${\rho_z}^2 = -{t_z}^2 = -\frac{Z_{oc}}{Z_{sc}}$

$$\frac{1}{\left(\frac{P(\rho)}{\rho^2 - {\rho_z}^2}\right)}\begin{bmatrix} \frac{A(\rho)}{\rho^2 - {\rho_z}^2} & \frac{B(\rho)}{\rho^2 - {\rho_z}^2} \\ \frac{\left(C(\rho) - \frac{\rho\left(\frac{A(\rho)}{\rho^2 - {\rho_z}^2}\right)}{Z_{sc}}\right)}{\rho^2 - {\rho_z}^2} & \frac{\left(D(\rho) - \frac{\rho\left(\frac{B(\rho)}{\rho^2 - {\rho_z}^2}\right)}{Z_{sc}}\right)}{\rho^2 - {\rho_z}^2} \end{bmatrix}$$

Condition for Extraction: $P(\rho)$, $A(p)$ and $B(p)$ must be divisible by ${\rho^2 - \rho_z}^2$

Unit Element (Z_{tx})

$$Z_{tx} = \left.\frac{B(\rho)}{D(\rho)}\right|_{\rho=jt=1} \qquad \frac{1}{\sqrt{1-\rho^2}}\begin{bmatrix} 1 & Z_{tx}\rho \\ \frac{\rho}{Z_{tx}} & 1 \end{bmatrix} \qquad \frac{1}{\left(\frac{P(\rho)}{1-\rho^2}\right)}\begin{bmatrix} \frac{A(\rho)-Z_{tx}\rho C(\rho)}{1-\rho^2} & \frac{B(\rho)-Z_{tx}\rho D(\rho)}{1-\rho^2} \\ \frac{C(\rho)-\left(\frac{\rho A(\rho)}{Z_{tx}}\right)}{1-\rho^2} & \frac{D(\rho)-\left(\frac{\rho B(\rho)}{Z_{tx}}\right)}{1-\rho^2} \end{bmatrix}$$

Condition for Extraction: Degree of $B(\rho)$ = Degree of $D(\rho)$

Double Unit Element (Z_{tx})

$$Z_{tx} = \left.\frac{B(\rho)}{D(\rho)}\right|_{\rho=jt=1} \qquad \frac{1}{\sqrt{1-\rho^2}}\begin{bmatrix} 1+\rho^2 & 2Z_{tx}\rho \\ \frac{2\rho}{Z_{tx}} & 1+\rho^2 \end{bmatrix} \qquad \frac{1}{\left(\frac{P(\rho)}{(1-\rho^2)^2}\right)}\begin{bmatrix} \frac{(1+\rho^2)A(\rho)-2Z_{tx}\rho C(\rho)}{(1-\rho^2)^2} & \frac{(1+\rho^2)B(\rho)-2Z_{tx}\rho D(\rho)}{(1-\rho^2)^2} \\ \frac{(1+\rho^2)C(\rho)-\left(\frac{2\rho A(\rho)}{Z_{tx}}\right)}{(1-\rho^2)^2} & \frac{(1+\rho^2)D(\rho)-\left(\frac{2\rho B(\rho)}{Z_{tx}}\right)}{(1-\rho^2)^2} \end{bmatrix}$$

Condition for Extraction: Degree of $B(\rho)$ = Degree of $D(\rho)$

Note that the above formulae apply both in lumped and distributed element filter networks with an appropriate change of variable. For example, the variable $p = j\omega$ in lumped element filters may be substituted by the variable $\rho = jt = jtan(\theta)$ for distributed filter networks. Consequently, the transmission zeros at the origin in lumped p-plane are mapped to the origin of the distributed ρ-plane and any of the transmission zeros at infinity $(p = \pm\infty)$ in lumped p-plane are mapped to $\theta = \pm 90^o$ of the distributed ρ-plane. The frequency invariant reactance (FIR) is a frequency independent ideal reactive component used solely for mathematical convenience.

1.2 Design of Microwave Filters

1.2.1 Lumped Lowpass Prototype Filters

Narrow and moderate bandwidth bandpass filters approximate synthesis is achieved by first synthesising a suitable lowpass prototype filter and then transforming the network to a bandpass domain by means of a simple frequency transformation [5]. Lowpass prototype filters are based on ideal immittance inverter models. The ideal immittance inverters are only fictitious elements. They are approximated in practice by real frequency dependent elements. Because of this, the designs using these prototypes are generally applicable for narrow band filters where the coupling element values are approximately constant over a narrow band of frequencies. However, it is this very fact that has allowed the development of simplified design techniques for many microwave filters [10]. Therefore many practical filter response such as bandpass and bandstop may be designed by means of the reactance/susceptance slope parameter approximation method [29].

Lumped lowpass prototype filters may be synthesised using either CM or cascaded synthesis method in lumped element domain. Frequency and element transformations are performed to convert to other filter network forms such as bandpass filters or distributed lowpass filters which are suitable for direct physical realisation.

In contrast, an alternative direct synthesis method as presented in this thesis both eliminates the need for such transformations and provides a direct and intuitive synthesis approach, based on reflection and transmission zero prescription on the basis function of Chebyshev characteristic functions. As a consequence, the immittance inverters associated with direct synthesised filter network are frequency dependant. This is the reason why this particular synthesis approach is valid for arbitrary filter bandwidths. It also provides better approximation to practical filter components which are frequency dependent.

No significant advantage is attained from using the lumped lowpass prototype filters apart from the benefit of using well established conventional techniques.

However, it will be clear in this thesis work that some directly synthesised filter transfer functions have no lumped lowpass filter equivalent. Thus transfer functions and resulting topologies from lumped lowpass prototype filters may not be realised by using the direct synthesis approach.

1.2.2 Frequency Transformation and Impedance Scaling

The process of synthesising filters from lumped lowpass prototype filters employs frequency transformations. Frequency mapping transforms a given lowpass prototype filter network to a form that enables practical realisation of microwave filters. Because the transformation is frequency dependent, it only changes reactive elements. Both the source (and load) resistive terminations and FIR elements for which ideal inverters are realised remain invariant under the transformation. The rudiments of various transformations have been covered in most important text books on filters [3-6].

The lowpass prototype filters have normalised element values so that both the cutoff frequency and the source resistance or conductance are normalised to unity (i.e. $R_s = 1\ \Omega$ and $\omega_c = 1$ rad/s). After the network synthesis, the element values are re-normalised to the system impedance (normally $50\ \Omega$) and the required cutoff frequencies. More often than not, the lowpass prototype filters obtained via coupling matrix or cascaded synthesis has impedance level unsuitable for direct physical realisation. Thus it may be necessary to scale the network to adjust element values to be within realisable values.

1.2.3 Distributed Elements Filters

Practical microwave filters are realised using distributed components. These are often made up components that are modelled as transmission line type components. At lower microwave frequency band (300 MHz to about 30 GHz with wavelength of 1 m to 10 mm), microwave filters are often realised using microstrip, striplines and coaxial cavity while at most of the upper (30 GHz to about 300 GHz with wavelength of 10 mm to 1 mm) microwave frequency band utilizes dielectric and waveguide resonators because of diminished waveguide dimensions at these frequencies. However, other factors such as unloaded quality factors, filter size and

power handling are important consideration in the choice of the technology of implementation [3]. Most of the filters discussed in this thesis were implemented in stripline or coaxial cavity realisation because of good compromise between size (loss) and power handling that they provide as well as the flexibility to realise different topologies.

Because microwave filters are primarily realised using transmission line type components, the direct synthesis in distributed domain has also been developed in this work. Even though, sometimes the use of lumped element synthesis simplifies the synthesis process, it has been shown throughout this thesis how lumped converts to the distributed network for practical realisations.

1.2.4 Numerical EM Techniques

It must be mentioned that to achieve equiripple Chebyshev response in the passband does require fractional adjustments in the physical dimensions. It is common to have up to a thousandth of a millimetre accuracy (0.0001 mm) on the tuning screws [30]! The time required to perform a full wave EM optimisation even on low degree cavity filters for example, is prohibitive. The solution is to use accurate EM based design techniques together with fast circuit simulation to reduce design time. Numerous methods are used today in the design and tuning of microwave filters and notably the paper by Ness [31] presented a useful method of tuning filter using reflected group delay for narrow bandpass filters.

Various pertinent techniques for physical dimensioning for microwave resonator filters are considered in this section. In conjunction with the coupling matrix synthesis method, it is shown first on how the initial course dimensions are obtained for the filter and how the needed fine tuning is achieved by means of space mapping techniques. The Cauchy method and the concept of EM port tuning are also reviewed as an alternative means of obtaining the fine-tuned dimensions required for equiripple tuned Chebyshev microwave filters.

1.2.4.1 Physical Dimensions

There are many physical realisations for microwave filters such as microstrip, stripe-lines, coaxial, waveguide and dielectric filters. The underlying synthesis,

however, is the same for all these filter realisations. There are many different ways of determining physical dimension for microwave filters. The mathematical models obtained through synthesis are only approximations of the full wave EM behaviour of distributed microwave circuits. Accurate dimensions are obtained through numerical EM techniques which take into account second order effects such as undesired couplings and high order waveguide modes. This requires reasonable appreciation of material properties and EM behaviour of microwave devices.

For simple physical structures like parallel coupled transmission lines, there exists empirical data that give very good approximation. For example in [4, 32] it is explained on how physical dimension for parallel coupled networks may be obtained under the assumption that the dominant propagation mode is the transverse electromagnetic (TEM) based on the data from Getsinger and Crystal [33, 34]. Rhodes [35] devised a technique that could be used for designing equal diameter rod bandpass filters under the TEM assumption. However, even in these evanescence mode filter designs, there is a need to account for parasitic couplings as well as high order non TEM waveguide modes that may exist in the structure especially for relatively large ground plane spacing for accurate physical dimensions.

Lumped element models based on lumped lowpass prototype filter circuit models do exist [3, 6] that could be used to determine the input (output) couplings as well inter-resonator couplings physical dimensions. The most comprehensive treatment of the calculation of the initial physical dimensions is made in [6] where formulae are presented for the lumped element models. These are more useful for narrowband filters.

A more accurate initial approximation is obtained by using mixed lumped-distributed models. In the following sections explicit formulae have been derived for computation of coupling coefficients required for determining the initial physical dimensions for lumped-distributed resonator models for microwave filters similar to the lumped resonator models presented in [36]. The measurements are obtained with the help of EM simulators which are mapped to the theoretical results enabling

the initial physical dimensions to be obtained. Fine tuning for equiripple response is achieved by applying the methods in sections 1.2.4.2 to 1.2.4.4.

1.2.4.1.1 Input (Output) 3 dB Coupling Bandwidth

Consider the circuit of Fig. 1-10 of the first (last) resonator connected to source or load by input coupling K_s and K is the loose coupling for the sniffer port to provide the transmission measurement. The EM model is set up as shown in Fig. 1-10 (a) The ABCD matrix of the equivalent circuit in Fig. 1-10 (b) may be computed as

$$\begin{aligned}[ABCD] &= \begin{bmatrix} 0 & j/K_s \\ jK_s & 0 \end{bmatrix}\begin{bmatrix} 1 & 0 \\ Y_{res} & 1 \end{bmatrix}\begin{bmatrix} 0 & j/K \\ jK & 0 \end{bmatrix} \\ &= \begin{bmatrix} -K/K_s & -Y_{res}/(KK_s) \\ 0 & -K_s/K \end{bmatrix}\end{aligned} \tag{1.109}$$

where

$$Y_{res} = j\frac{C_1\omega\tan\theta - Y_1}{\tan\theta} \tag{1.110}$$

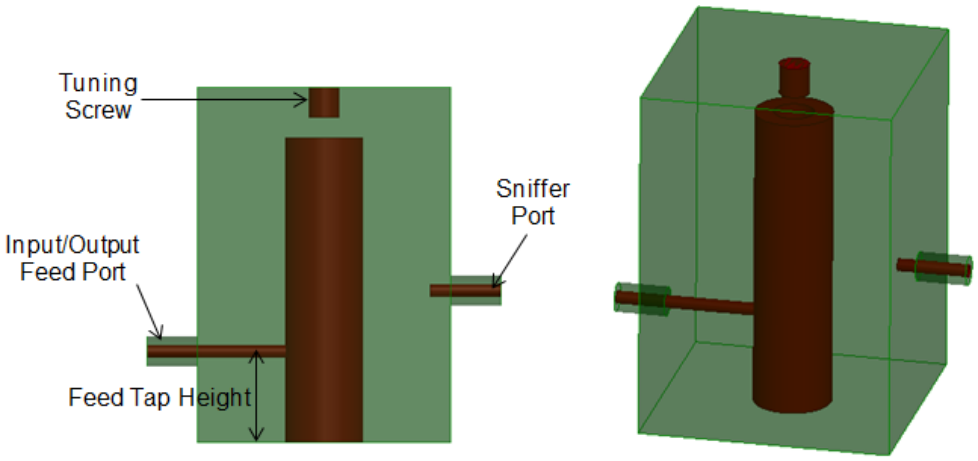

(a) EM model

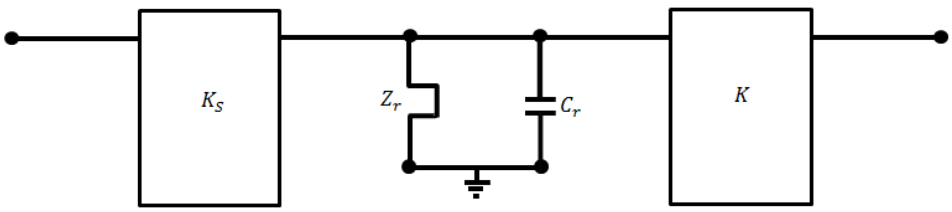

(b) Equivalent Circuit

Fig. 1-10 An example of 3D EM resonator model and its equivalent circuit for determining the input coupling 3 dB Bandwidth

Now the S_{21} may be obtained from the ABCD matrix elements as

$$S_{21} = \frac{2}{-\frac{K}{K_s} - \frac{K_s}{K} - \frac{Y_{res}}{KK_s}}$$

$$S_{21} = \frac{2KK_s \tan\theta}{-\left(K^2 + {K_s}^2\right)\tan\theta - j(C_1\omega\tan\theta - Y_1)} \tag{1.111}$$

Thus,

$$|S_{21}| = \frac{2KK_s|\tan\theta|}{\sqrt{\left(K^2 + {K_s}^2\right)^2\tan^2\theta + (C_1\omega\tan\theta - Y_1)^2}} \tag{1.112}$$

Now at the 3 dB frequency points, $\omega_{3\,dB}$,

$$|S_{21}(\omega_{3\,dB})| = \frac{1}{\sqrt{2}}|S_{21}(\omega_o)| = \frac{2KK_s}{\sqrt{2\left(K^2 + {K_s}^2\right)^2}} \tag{1.113}$$

where ω_o is the resonance frequency. Note that

$$C_1\omega_o\tan\theta_o - Y_1 = 0 \tag{1.114}$$

Hence from (1.113),

$$\frac{2KK_s}{\sqrt{2\left(K^2 + {K_s}^2\right)^2}} = \frac{2KK_s|\tan\theta_{3\,dB}|}{\sqrt{\left(K^2 + {K_s}^2\right)^2\tan^2\theta_{3\,dB} + (C_1\omega_{3\,dB}\tan\theta_{3\,dB} - Y_1)^2}} \tag{1.115}$$

which simplifies to

$$\left(K^2 + {K_s}^2\right)^2\tan^2\theta_{3\,dB} - (C_1\omega_{3\,dB}\tan\theta_{3\,dB} - Y_1)^2 = 0 \tag{1.116}$$

It is assumed here that the sniffer port only provides loose couplings,

$$K \ll K_s \tag{1.117}$$

so that,

$$K^2 + {K_s}^2 \cong {K_s}^2 \tag{1.118}$$

Hence (1.116) becomes

$${K_s}^4\tan^2\theta_{3\,dB} - (C_1\omega_{3\,dB}\tan\theta_{3\,dB} - Y_1)^2 = 0 \tag{1.119}$$

Solving (1.119) yields two solutions for the lower ($\omega_{3\ dBl}$) and upper ($\omega_{3\ dBu}$) 3 dB frequency point

$$\begin{aligned} {K_s}^2 \tan\theta_{3\ dBl} - (C_1\omega_{3\ dBl}\tan\theta_{3\ dBl} - Y_1) = 0 \\ {K_s}^2 \tan\theta_{3\ dBu} + (C_1\omega_{3\ dBu}\tan\theta_{3\ dBu} - Y_1) = 0 \end{aligned} \tag{1.120}$$

(1.120) may be solved iteratively using Newton – Raphson's method. The input (output) coupling may be determined from measurement data using

$$\begin{aligned} K_s = \pm\sqrt{\frac{C_1\omega_{3\ dBl}\tan\theta_{3\ dBl} - Y_1}{\tan\theta_{3\ dBl}}} = \pm\sqrt{imaginary\ Y_{res}(\omega_{3\ dBl})} \\ K_s = \pm\sqrt{\frac{C_1\omega_{3\ dBu}\tan\theta_{3\ dBu} - Y_1}{\tan\theta_{3\ dBu}}} = \pm\sqrt{-imaginary\ Y_{res}(\omega_{3\ dBu})} \end{aligned} \tag{1.121}$$

The theoretical or experimental 3 dB bandwidth is calculated from

$$f_{3\ dB} = \frac{\omega_{3\ dBu} - \omega_{3\ dBl}}{2\pi}, Hz \tag{1.122}$$

The measurement is done with an EM simulator as follows:

1. Set up the model as in Fig. 1-10 in an EM simulator. Choose a suitable initial tapping height for the input probe such as the middle of the inner conductor. The sniffer port should be set up so that the peak of $|S_{21}|$ in dB is at least below 30 dB.
2. Adjust the resonator tuning screw so that the required resonance frequency is attained. Note that the peak of $|S_{21}|$ occurs at the resonance frequency.
3. Measure the 3 dB bandwidth from the $|S_{21}|$ plot by measuring the frequency points where the peak drops to 3 dB. The 3 dB points may also be easily determined from the peaks of the real and imaginary of the S_{11} measurements.
4. Compare the measured 3 dB bandwidth to the theoretical one. If $(f_{3\ dB})_{experimental} \neq (f_{3\ dB})_{Theoretical}$, then change the tapping height to a new position.
5. Repeat the experimental procedure so that the correct resonance frequency and 3 dB bandwidth are attained. Alternatively the results for each tapping position and 3 dB bandwidth may be tabulated and plotted so that a good estimate of the tapping position and resonator tuning screw position are obtained by reading the graph.

1.2.4.1.2 Inter-resonator Coupling Coefficient – Magnetic Coupling

Here a two combline resonator model is used as in Fig. 1-11. The electric field is at its maximum near the open end top of the resonators and conversely the magnetic field is at its maximum near the bottom short circuited end of the resonators. It is assumed the magnetic coupling is a dominant form of coupling in the configuration shown in Fig. 1-11. Thus the equivalent circuit may be modelled as shown in Fig. 1-12. Resonance occurs when

$$Z_L + Z_R = 0 \tag{1.123}$$

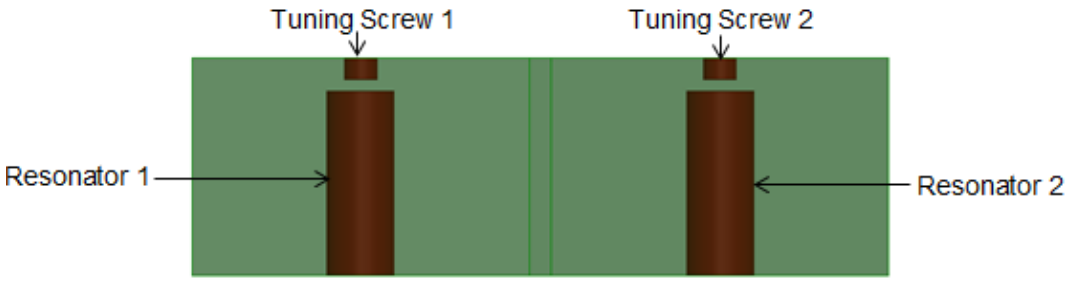

(a) Side view

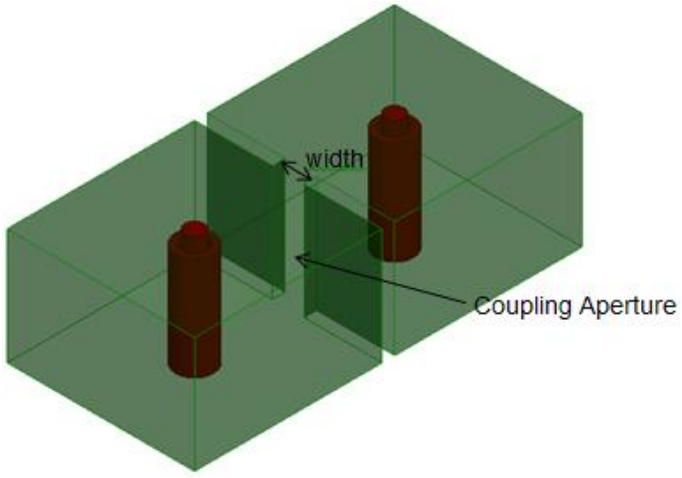

(b) Isometric view

Fig. 1-11 An example of a two resonator EM model used to compute magnetic inter-resonator couplings

Hence,

$$\frac{\rho}{2Y_{12}} + \frac{1}{\frac{Y_1 - Y_{12}}{\rho} + C_1 p} + \frac{\rho}{2Y_{12}} + \frac{1}{\frac{Y_2 - Y_{12}}{\rho} + C_2 p} = 0 \tag{1.124}$$

or

$$\frac{\tan\theta}{Y_{12}} + \frac{\tan\theta}{Y_1 - Y_{12} - \omega C_1 \tan\theta} + \frac{\tan\theta}{Y_2 - Y_{12} - \omega C_2 \tan\theta} = 0 \tag{1.125}$$

which simplifies to

$$(\omega \tan\theta)^2 - \left(\frac{Y_1}{C_1} + \frac{Y_2}{C_2}\right)\omega \tan\theta + \frac{Y_1 Y_2}{C_1 C_2} - \frac{{Y_{12}}^2}{C_1 C_2} = 0 \tag{1.126}$$

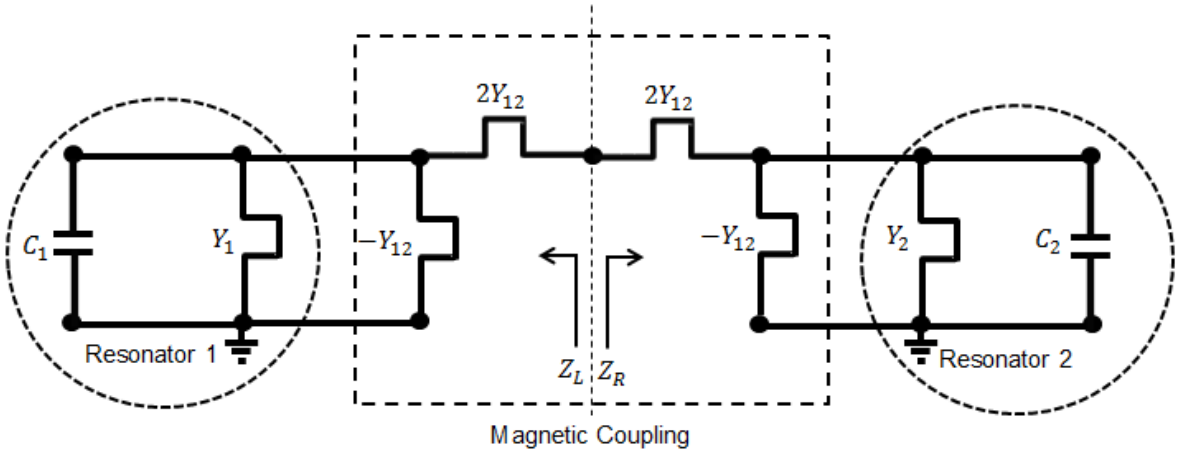

Fig. 1-12 Equivalent circuit of a two combline resonator EM model for computing magnetic inter-resonator couplings

Now for each resonator, resonance (ω_1 and ω_2) occurs when

$$\frac{Y_1}{C_1} = \omega_1 \tan\theta_1$$
$$\frac{Y_2}{C_2} = \omega_2 \tan\theta_2 \tag{1.127}$$

Define a new magnetic coupling coefficient K_m as

$${K_m}^2 = \frac{{Y_{12}}^2}{C_1 C_2} \tag{1.128}$$

Such that the theoretical magnetic coupling coefficient is determined from

$$d\omega_m = K_m = \frac{Y_{12}}{\sqrt{C_1 C_2}}\ rad/s \tag{1.129}$$

or

$$df_m = \frac{Y_{12}}{2\pi\sqrt{C_1 C_2}}\ Hz. \tag{1.130}$$

Hence (1.126) becomes,

$$(\omega \tan\theta)^2 - (\omega_1 \tan\theta_1 + \omega_2 \tan\theta_2)\omega \tan\theta + \omega_1\,\omega_2 \tan\theta_1 \tan\theta_2 - {K_m}^2 = 0 \quad (1.131)$$

which may be re-written as,

$$2\omega \tan\theta = \omega_1 \tan\theta_1 + \omega_2 \tan\theta_2 \pm \sqrt{(\omega_2 \tan\theta_2 - \omega_1 \tan\theta_1)^2 + 4{K_m}^2} \quad (1.132)$$

Define the even mode resonant frequency ω_{ev} as

$$2\omega_{ev}\ \tan\theta_{ev}\ = \omega_1 \tan\theta_1 + \omega_2 \tan\theta_2 - \sqrt{(\omega_2 \tan\theta_2 - \omega_1 \tan\theta_1)^2 + 4{K_m}^2} \quad (1.133)$$

And the odd mode resonant frequency ω_{od} as,

$$2\omega_{od}\ \tan\theta_{od}\ = \omega_1 \tan\theta_1 + \omega_2 \tan\theta_2 + \sqrt{(\omega_2 \tan\theta_2 - \omega_1 \tan\theta_1)^2 + 4{K_m}^2} \quad (1.134)$$

Thus, subtracting (1.133) from (1.134) yields

$$(\omega_{od}\ \tan\theta_{od} - \omega_{ev}\ \tan\theta_{ev}\ )^2 = (\omega_2 \tan\theta_2 - \omega_1 \tan\theta_1)^2 + 4{K_m}^2 \quad (1.135)$$

This may be solved for K_m as,

$$K_m = \pm\frac{1}{2}\sqrt{(\omega_{od}\ \tan\theta_{od} - \omega_{ev}\ \tan\theta_{ev}\ )^2 - (\omega_2 \tan\theta_2 - \omega_1 \tan\theta_1)^2} \quad (1.136)$$

Therefore the inter-resonator magnetic coupling coefficient is computed as

$$d\omega_m = K_m = \pm\frac{1}{2}\sqrt{(\omega_{od}\ \tan\theta_{od} - \omega_{ev}\ \tan\theta_{ev}\ )^2 - (\omega_2 \tan\theta_2 - \omega_1 \tan\theta_1)^2} \quad (1.137)$$

This coupling coefficient may be converted to more familiar frequency units as

$$df_m = \frac{d\omega_m}{2\pi} = \frac{K_m}{2\pi}\ Hz \quad (1.138)$$

so that the experimental coupling coefficient may be computed using

$$df_m = \pm\frac{1}{4\pi}\sqrt{(\omega_{od}\ \tan\theta_{od} - \omega_{ev}\ \tan\theta_{ev}\ )^2 - (\omega_2 \tan\theta_2 - \omega_1 \tan\theta_1)^2}\ Hz. \quad (1.139)$$

For synchronously tuned resonators, where $\omega_1 = \omega_2$ (1.139) simplifies to

$$df_m = \pm\frac{\omega_{od}\ \tan\theta_{od} - \omega_{ev}\ \tan\theta_{ev}}{4\pi}\ Hz. \quad (1.140)$$

After computing the required theoretical inter-resonator coupling bandwidths using (1.138), the following experiment procedure is carried out with an EM simulator with eigenvalue capability:

1. Set up the model as in Fig. 1-11 using an EM simulator

2. Tune each individual resonator to the required resonant frequency
3. For a range of inter-resonator spacings or aperture widths perform the eigen mode parametric analysis and obtain even mode resonant frequency f_{ev}(magnitude(Mode(1)) and odd mode resonant frequency f_{od}(magnitude(Mode(2)) for each parameter sweep
4. Obtain the experimental coupling bandwidth from (1.139)
5. Plot the graph of spacing/aperture width against $(df_m)_{Experimental}$
6. Obtain the required inter-resonator spacing/aperture width from the graph.

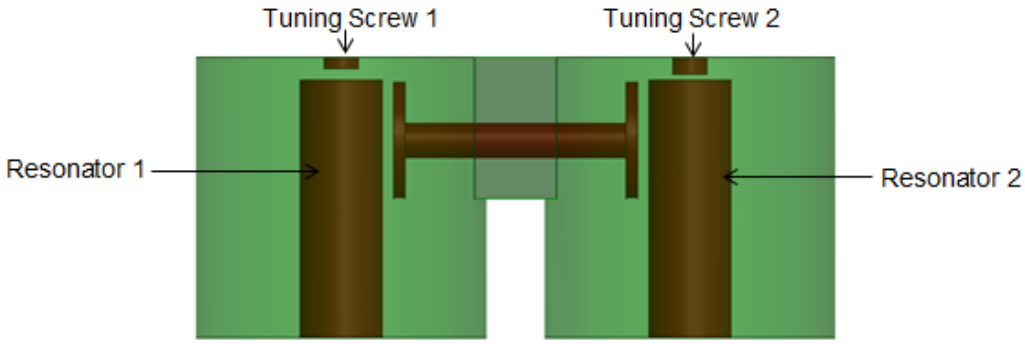

(a) Side view

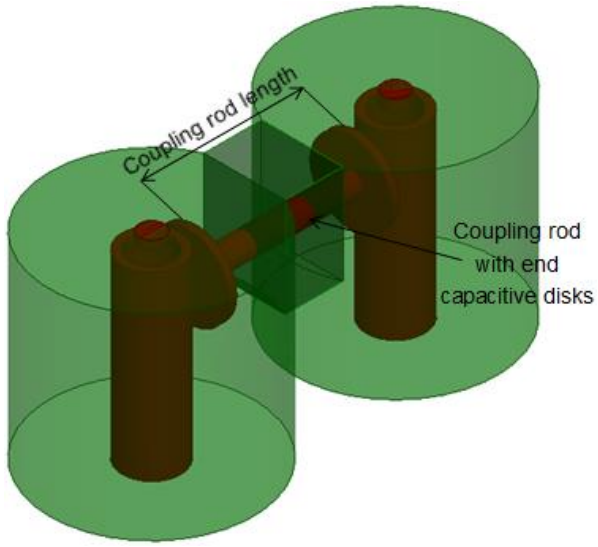

(b) Isometric view

Fig. 1-13 An example of a two resonator EM model used to compute electric inter-resonator couplings

1.2.4.1.3 Inter-resonator Coupling Coefficient – Electric Coupling

A similar analysis may be performed for electrical couplings which are modelled similar to magnetic couplings but with open circuited stubs for the coupling admittances. Fig. 1-13 shows the two resonator model for determining the electric

coupling dimensions in an EM simulator. Electric coupling is achieved by an aperture near the top of the resonator open ends where electric field is dominant and may be amplified by means of a suspended metal rod placed between the two resonators. Using Fig. 1-14, the electric coupling coefficient is defined just as for the magnetic coupling coefficient as

$$d\omega_e = K_e = \frac{Y_{12}}{\sqrt{C_1 C_2}}\ rad/s$$
$$df_m = \frac{Y_{12}}{2\pi\sqrt{C_1 C_2}}\ Hz \tag{1.141}$$

except in this case Y_{12} is the capacitive coupling admittance of the open circuited stub. The even mode resonant frequency ω_{ev} is obtained from the solution of,

$$2\omega_{ev}\tan\theta_{ev} = \omega_1\tan\theta_1 + \omega_2\tan\theta_2 - \sqrt{(\omega_2\tan\theta_2 - \omega_1\tan\theta_1)^2 + 4{K_e}^2(\tan\theta_{ev})^4} \tag{1.142}$$

and the odd mode resonant frequency ω_{od} is obtained from the solution of,

$$2\omega_{od}\tan\theta_{od} = \omega_1\tan\theta_1 + \omega_2\tan\theta_2 + \sqrt{(\omega_2\tan\theta_2 - \omega_1\tan\theta_1)^2 + 4{K_e}^2(\tan\theta_{ev})^4} \tag{1.143}$$

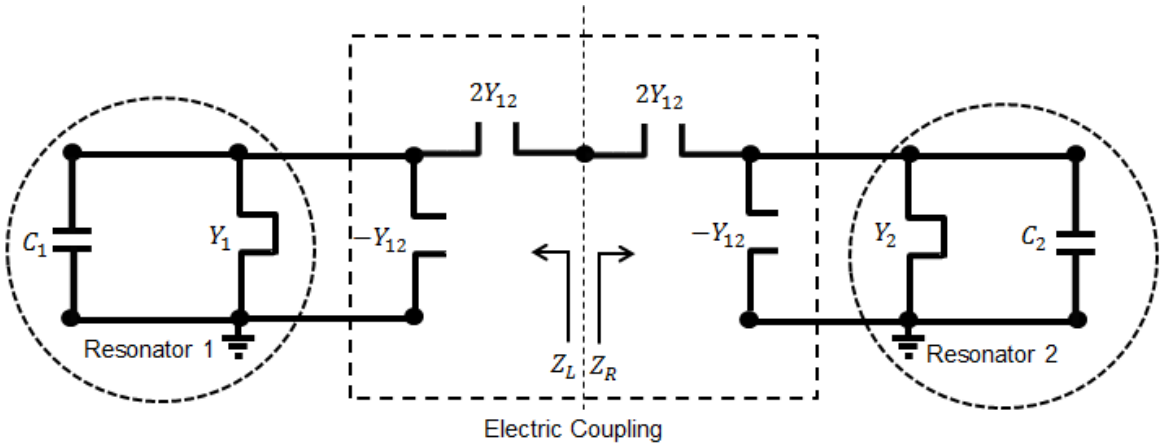

Fig. 1-14 Equivalent circuit of a two combline resonator EM model for computing electric inter-resonator couplings

Thus, K_e is determined by solving (1.142) and (1.143) simultaneously,

$$d\omega_e = K_e\ rad/s \tag{1.144}$$

$$d\omega_e = \pm\sqrt{\frac{(\omega_{od}\ \tan\theta_{od} - \omega_{ev}\ \tan\theta_{ev}\ )\left(\omega_{od}\ \tan\theta_{od} + \omega_{ev}\ \tan\theta_{ev} - \omega_1 \tan\theta_1 - \omega_2 \tan\theta_2\right)}{((\ \tan\theta_{od})^4 - (\ \tan\theta_{ev}\ )^4)}}$$

This coupling coefficient may be converted to more familiar frequency units as

$$df_e = \frac{d\omega_e}{2\pi} = \frac{K_e}{2\pi}\ Hz \tag{1.145}$$

Similar numerical technique as for magnetic coupling may be performed so that the even mode and odd mode resonance frequencies are obtained. The parametric analysis can be performed using an EM simulator with Eigen mode capability. Then experimental coupling coefficients may be computed using (1.144) and (1.145) which must be compared and made equal to the theoretical ones computed using (1.141) by varying some physical dimensions (usually the suspended coupling rod length or its capacitive disk or both for cavity resonator filters).

1.2.4.2 Space Mapping Technique

This is a technique used to reduce CPU time for computer aided designs. Bandler et el [37-42] were among the first pioneers in EM modelling techniques employing space mapping as applied to microwave filter design. The technique uses two models called (i) the fine model which is an accurate EM model and (ii) the coarse model which is a circuit simulator based model. Because the circuit model is fast, optimisation may quickly be made and results implemented in an accurate but time demanding EM simulator. The desired parameter mapping between the two parameter spaces, namely the coarse model space and fine model space, is achieved by means of the space mapping technique. Two corresponding parameter sets are defined for both the coarse model and fine model. The fine model parameters are used to obtain the full wave EM filter response. Then the coarse model parameters are found by optimisation techniques that make the coarse model response to be equal to the EM response. The resulting coarse model parameters are then compared to the ideal circuit model parameters so that the error magnitude and direction are established. The mapping is done to find the corresponding change in the fine model parameters space by using either the linear mapping called Space Mapping (SM) [43] or general non-linear mapping called Aggressive Space Mapping (ASM) [39, 40]. As a consequence of the

iterative application of SM or ASM accurate physical dimensions in the fine model are obtained. Sometimes the space mapping technique may be used together with Cauchy or EM port tuning methods briefly described in the next sections [44].

1.2.4.3 Cauchy Method

The Cauchy method is the curve fitting method of determining an approximate rational model from filter's response obtained from measurement or EM simulation [45-47]. The s-parameters are extracted from measurement or EM simulation at some sampled frequency points from which characteristic polynomials are determined by solving a determined or overdetermined linear system of equations [48]. The phase shift due to the input and output connections are removed by rationalisation. The characteristic polynomials are calculated from which the extracted coupling matrix may then be determined using the methods described above. The extracted CM can be compared to the synthesised (ideal) CM. The required fractional changes can then be applied to the EM model or physical filter to correct the filter response. Sometimes, parasitic couplings may be accounted for in the EM model by appropriate modelling of the transmission polynomial. When used in conjunction with the ASM, the Cauchy method is a useful method in designing and tuning of microwave filters [49].

1.2.4.4 EM Port Tuning Technique

This is a simple technique for fine tuning microwave filters that eliminates the need to fabricate and tune the physical filter hardware [50, 51]. The technique is achieved by adding internal ports called lumped ports between the open ends of each of resonator and top cover in the case of cavity filters. Then the complete EM model with extra lumped ports may be exported to the circuit simulator. In the circuit simulator, lumped capacitors are added to terminate the internal ports. Inter-resonator couplings may also be tuned by placing series capacitors or short circuited stubs between the internal ports. Because circuit simulators have much more efficient computation time as compared to EM simulators, the model may easily be optimised in the circuit simulator to fine tune it to the required filter response. After optimisation or manual tuning, the value of the capacitors (positive or negative) represents the magnitude and direction of the error vectors that must

be corrected in the EM model. By using EM port tuning in conjunction with space mapping techniques, a simple mapping between the lumped capacitors in the circuit simulator and the corresponding physical dimension (e.g. tuning screw position) may be established [44].

1.2.5 Other Design Considerations

Many of the important facets of filter designs have been highlighted in the previous sections. Synthesis method demonstrated in this thesis assumes a lossless filter network (i.e. infinite unloaded quality factor). However, practical microwave filters have finite unloaded quality factors. This means that they have at least some finite amount of dissipative losses.

Table 1-3 Summary of Synthesis and Design of Microwave Filters

1.	**Desired Filter Transfer Response** The filter specifications are the driving factor in determining the desired minimum degree transfer function.
2.	**Lossless Synthesis of Characteristic Polynomials** The characteristic function is obtained from the required reflection and transmission characteristic. Synthesis may be done in lumped or distributed domain.
3.	**Network Elements Synthesis** Coupling matrix or cascaded synthesis is used to obtain the filter network element values in the desired circuital topology. Lumped or distributed filter circuits.
4.	**Frequency Mapping, Frequency and Impedance Scaling** A vital step in ensuring physical realisability.
5.	**Physical Dimensions and EM Modelling** Initial physical dimensions obtained through use of empirical data or numerical EM techniques. Loss analysis and spurious control are important consideration at this point.
6.	**Fine Tuning, Fabrication and Testing** Use of both circuit and EM simulators is a cost effective way to achieve filter tuning before fabrication.

The approach is to synthesis a lossless filter network and depending on the required filter loss from the specifications, analyse the effect of losses via circuit or EM simulators. The filter is then dimensioned and materials (technology of

implementation) chosen to minimise the filter's passband loss. The effect of adding lossy components is degraded filter response. If relatively high unloaded quality factor is achieved, the overall filter response is only slightly perturbed (e.g. rounding of passband edges). It must be mentioned here that the quality factor requirement is the main criterion in deciding the technology of implementation [3]. This is also the limiting factor in terms of filter physical size (volume and weight) and cost as high unloaded quality factor generally requires large 3 dimensional filters size with high conductivity materials. The requirement to meet the unloaded quality factor by having large filter size is limited by the need to control out-of-band spurious resonances that are a direct result of the periodic nature of distributed elements and waveguide modes. This is because the filter dimensions become progressively cut-on at such frequencies with increased filter dimensions.

The important steps in conventional filter synthesis and design are summarised in Table 1-3. The bulk of the work done was concentrated on aspects of steps 1 to 4 of the synthesis and design procedure. However, in Chapter 3 to Chapter 6 various aspects of step 5 and 6 are considered with some measurement results shown from some fabricated filters.

1.3 Conclusion

In this chapter, a review of filter synthesis and design fundamentals has been made. The two methods normally used in filter synthesis have been described. However, a method of computing the characteristic polynomials used in the filter synthesis were not given. The next Chapter presents a method of generating the generalised Chebyshev characteristic function.

Chapter 2 Method for Generating Generalised Chebyshev Polynomials

2.1 Introduction

In this Chapter, an alternative method to synthesise different classes of Chebyshev microwave filters is presented. The principles and theories explained apply to a wide range of filter applications as will be evident later on. In particular, the general method for the generation of general Chebyshev polynomials is explained [52, 53]. A number of filter types including low-pass, bandpass and dual band filters are used to show the direct application of the synthesis method. The method is directly applicable for the synthesis of lumped and distributed filters. As alluded to in Chapter 1, Chebyshev filtering characteristic functions are used in most filter designs because they represent an optimum comprise between in-band return loss and out-of-band rejection. It will now be shown how this type of transfer characteristic function may generally be generated.

2.2 Generalised Chebyshev Characteristic Function

The characteristic function was defined in Chapter 1 as a rational function consisting of the reflection and transmission characteristic polynomials. For Chebyshev characteristic functions, it may be shown that the filter's overall characteristic function may be obtained from a linear combination of hyperbolic cosine of the sum of inverse hyperbolic cosines of low degree basis transfer functions defined by,

$$T_N(\omega) = cosh\left\{\sum_{r=1}^{m}[\alpha_r\, acosh\{X_r(\omega)\}]\right\} \tag{2.1}$$

where α_r (integer) is the corresponding weighting number to the basis characteristic function $X_r(\omega)$. Without loss of generality, the ω-plane variable is used for the lumped domain synthesis. However, the method described here is

applicable to distributed generalised Chebyshev filters were the variable t would be used instead. The proof (2.1) easily follows from solution of Chebyshev differential equations with appropriate boundary conditions as section 2.4 will show. $X_r(\omega)$ is a rational function expressed in terms of two polynomials $U_r(\omega)$ and $P_r(\omega)$ as

$$X_r(\omega) = \frac{U_r(\omega)}{P_r(\omega)} \tag{2.2}$$

Thus the problem of determining the higher degree rational polynomial $T_N(\omega)$ is reduced to determining some unique lower degree basis characteristic functions $X_r(\omega)$ which act as basic building blocks for higher degree polynomials. Each of the basis function is defined by the number and positions of both reflection and transmission zeros. The overall characteristic function given by (2.1) may further be expanded and after a bit of mathematical manipulations the final expression is presented below.

$$T_N(\omega) = \frac{1}{2}\left\{\prod_{r=1}^{m}\left[X_r(\omega) + \sqrt{{X_r}^2(\omega) - 1}\right]^{\alpha_r} + \prod_{r=1}^{m}\left[X_r(\omega) - \sqrt{{X_r}^2(\omega) - 1}\right]^{\alpha_r}\right\} \tag{2.3}$$

Table 2-1 Examples of Cutoff Polynomial V

Lumped Domain $V(\omega)$

Cutoff Points	V Polynomial	Application
$\pm\delta$	$(\omega^2 - \delta^2)$	Low-pass Filter
$\alpha, \beta, \pm\delta$	$(\omega - \alpha)(\omega - \beta)(\omega^2 - \delta^2)$	Bandpass/Dual Band Low-pass Filter
$\pm\alpha, \pm\beta, \pm\gamma, \pm\delta$	$(\omega^2 - \alpha^2)(\omega^2 - \beta^2)(\omega^2 - \gamma^2)(\omega^2 - \delta^2)$	Dual Bandpass Filter

Distributed Domain $V(t)$

Cutoff Points	V Polynomial	Application
$\pm t_c$	$(t^2 - {t_c}^2)$	Low-pass Filter
$\pm t_1, \pm t_2$	$(t^2 - {t_1}^2)(t^2 - {t_2}^2)$	Bandpass Filter
$\pm t_1, \pm t_2 \pm t_3, \pm t_4$	$(t^2 - {t_1}^2)(t^2 - {t_2}^2)(t^2 - {t_3}^2)(t^2 - {t_4}^2)$	Dual bandpass Filter

Now the zeros of $\left({X_r}^2(\omega)-1\right)$ are simply the zeros of $\left({U_r}^2-{P_r}^2\right)$ which are simply the tuning points and the bandedge points. Thus write

$$ {U_r}^2-{P_r}^2=\epsilon^2 V_T V \tag{2.4}$$

where ϵ is a constant, the polynomial V_T contains T number of in-band tuning points expressed as,

$$ V_T(\omega)=\prod_{t=1}^{T}(\omega^2-{\omega_t}^2)^2 \tag{2.5}$$

where ω_t is the radian frequency at the turning point. The monic polynomial V contains the cutoff (bandedge) frequency points is prescribed as depicted in Table 2-1. The numerator of $\sqrt{{X_r}^2(\omega)-1}$ in (2.3) may be written as

$$ \text{Numerator of } \left(\sqrt{{X_r}^2(\omega)-1}\right)=\sqrt{{U_r}^2-{P_r}^2}=\epsilon\sqrt{V_T}\sqrt{V} \tag{2.6}$$

Furthermore, define a new polynomial W_r as,

$$ W_r=\epsilon\sqrt{V_T}=\epsilon\prod_{t=1}^{T}(\omega^2-{\omega_t}^2) \tag{2.7}$$

Note that for lowest degree, (i.e. $N=1$, for low-pass, $N=2$ for bandpass and $N=4$, for dual bandpass) where no tuning point exist, $V_T(\omega)=1$ and thus $W_r=\epsilon$. In general the polynomial W_r may easily be found from the factorisation,

$$ W_r=\frac{\sqrt{{U_r}^2-{P_r}^2}}{\sqrt{V}} \tag{2.8}$$

Hence the following term in (2.3) is conveniently re-written as

$$ X_r(\omega)\pm\sqrt{{X_r}^2(\omega)-1}=\frac{U_r}{P_r}\pm\sqrt{\frac{{U_r}^2-{P_r}^2}{{P_r}^2}}=\frac{U_r\pm W_r\sqrt{V}}{P_r(\omega)} \tag{2.9}$$

Finally substituting (2.9) in (2.3) yields the final form of the characteristic function as

$$T_N(\omega) = k\frac{F(\omega)}{P(\omega)} = \frac{\prod_{r=1}^{m}\left[U_r + W_r\sqrt{V}\right]^{\alpha_r} + \prod_{r=1}^{m}\left[U_r - W_r\sqrt{V}\right]^{\alpha_r}}{2\prod_{r=1}^{m}[P_r]^{\alpha_r}} \tag{2.10}$$

The polynomials U_r, P_r, W_r and V will be considered as the canonical form of the basis function in any given Chebyshev characteristic function defined by (2.10). The numerator and denominator of the basis function given by (2.2) gives the polynomials U_r and P_r respectively. The polynomial W_r is given by (2.8) and the cutoff polynomial V is defined for a particular filter as given in Table 2-1. These polynomials completely characterises each of the basis functions. The next section shows how the characteristic polynomials $F(\omega)$ and $P(\omega)$ may be determined from (2.10).

2.3 General Recursive Technique - Determining the characteristic polynomials

Once the basis functions are determined, the computation of the overall characteristic function is fairly straight forward from (2.10). The weighting integer numbers α_r is the designer's choice depending on the number and positions of reflection and transmission zeros required from a given basis function. By expanding each of the numerator term in (2.10), two polynomial terms are obtained. The first polynomial X_N is independent of the radical polynomial $\sqrt{V}$, where the second polynomial Y_N contains the factor $\sqrt{V}$. At the end of the expansion, the term containing the radical term, Y_N is cancelled out so that the numerator term only contains X_N. Indeed that must be the case since the numerator contains the reflection zeros which must be real. Whereas the polynomial X_N contains the in-band reflection zeros, the polynomial Y_N contains the in-band turning points of the characteristic function. This is similar to conventional recursive technique as defined in [3].

The characteristic polynomials are computed by successive application of the general recursive technique with initial conditions $X_0 = 1$, $Y_0 = 0$ and $P_0 = 1$ and defined by

$$\begin{aligned} X_N &= U_r X_{N-1} + (W_r V) Y_{N-1} \\ Y_N &= W_r X_{N-1} + U_r Y_{N-1} \\ P_N &= P_r P_{N-1} \end{aligned} \tag{2.11}$$

where all the parameters are as defined above. (2.11) is used for m basis function and repeated α_r times for each basis function, each time using the previous results to compute the N^{th} polynomials in (2.11). As before, it does not matter whether the polynomials are in ω-plane or t-plane, the formulae apply. The particular formulation used here takes into account of (2.10) and the canonical representation of the basis functions in terms of the four polynomials U_r, P_r, W_r and V. It is written in a simple form using the already described nomenclature for computer aided synthesis. Finally

$$\begin{aligned} F(\omega) &= X_N \\ P(\omega) &= P_N \end{aligned} \tag{2.12}$$

The polynomials $F(\omega)$ and $P(\omega)$, are made monic by dividing each coefficient by the highest coefficient term. The normalisation is performed according to Chapter 1. From this point the conventional filter synthesis is performed as was described in Chapter 1. It is now left to determine the basis functions needed in the application of (2.11). The next section will show how the basis functions may be determined for different Chebyshev filtering functions.

2.4 Basis Characteristic Functions

It has been stated in section 2.2 that Chebyshev characteristic functions may be decomposed into their basis function using (2.1). Each basis function is unique and gives the number and position of the reflection and transmission zeros. Even though not all Chebyshev functions may be expressed in terms of elementary functions, for the most part synthesis of most single and multi-band filters is

simplified by using the suggested technique in which the filter is built up using basis functions. Most type of filters considered in this section may be decomposed into basis functions by solving a differential equation describing a particular characteristic function. However, it is often easier and more convenient to obtain the basis functions by solving a set of N non-linear simultaneous equations based on its known values at the critical points as,

$$X_r{}^2 - 1 = 0 \tag{2.13}$$

This imply that,

$$\left.\begin{matrix} U_r + P_r = 0 \\ U_r - P_r = 0 \end{matrix}\right|_{\omega = cutoff\ and\ Tuning\ points} \tag{2.14}$$

resulting in N non-linear systems of equations with N unknowns. For simple functions with no in-band turning points (i.e. $V_T = 1$), the numerator or the reflection function of the basis function may be obtained by completing the square (from (2.6)) as,

$$U_r = \sqrt{\epsilon^2 V_T V + P_r{}^2}, \tag{2.15}$$

assuming the transmission polynomial (P_r) is prescribed and ϵ is found so that (2.15) is a perfect square. The later method of determining the basis functions by solving a non-linear system of equation is completely general as long as the nature of each basis function is known. Since each basis function describes the number and position of transmission zeros, the basis function may be correctly modelled and solved for all possible transmission zeros. The following sections exemplify these two methods of determining the basis functions for Chebyshev characteristic functions in lumped and distributed domain.

Unless otherwise stated in this work, the nomenclature N-N_{FTZ}-N_{OTZ} is adopted to depict an N^{th} degree characteristic function with N_{FTZ} transmission zeros at some general complex frequencies, including purely real and imaginary (real frequency), and N_{OTZ} number of transmission zeros at the origin for transfer function in lumped domain. The remainder of the total number of transmission zeros, that is $N - N_{FTZ} - N_{OTZ}$, is assumed to be at infinity on the imaginary complex plane. A similar nomenclature is used for distributed low-pass filters where the function will be

designated as N-N_{FTZ}-N_{90^o}. In this case N and N_{FTZ} assumes the previous meaning and N_{90^o} is the number of transmission zeros at quarter-wave frequency (i.e. $\theta_z = \pm 90^o$) and $N - N_{FTZ} - N_{90^o}$ is the number of real axis half transmission zero pair at infinity (i.e. $\theta_z = \pm j\infty$). Where N_{FTZ} exists, these transmission zeros may either be symmetrically pure imaginary frequency pairs (i.e. $\theta_z = \pm\theta_t$), or in general paraconjugated pairs on the complex ρ-plane (i.e. $\theta_z = \theta_t \pm j\theta_\sigma$), such that N_{FTZ} is always even.

It is imperative to point out some advantages of using basis functions that it is possible to define any arbitrary transfer function based on transmission zeros and reflection zeros that satisfies Chebyshev characteristic. For example the transmission zeros at the origin or infinity may arbitrary be chosen corresponding to different coupling elements (electrical, magnetic couplings or both) by appropriate choice of the basis functions to give the required number of transmission zeros at the origin in ω domain (or at $\theta = 0^o$ in t domain).

2.4.1 Lumped Generalised Chebyshev Low-pass Filters

Consider the differential equation for Chebyshev low-pass filter in lumped domain defined as

$$\frac{dT_N(\omega)}{d\omega} = \frac{C_n \prod_{r=1}^{T} (\omega_r \omega - 1) \sqrt{{T_N}^2(\omega) - 1}}{\prod_{n=1}^{N} (1 - \omega/\omega_n) \sqrt{\omega^2 - 1}}, \qquad T < N \tag{2.16}$$

The term $\omega_r\omega - 1$ accounts for possible T out-of-band turning points. The other turning points are provided by the term $\sqrt{{T_N}^2(\omega) - 1}$ and the extra points provided by this expression are just the normalised cut-off points i.e. $\omega = -1 \text{ and } 1$, which are cancelled out by the denominator term $\sqrt{\omega^2 - 1}$. C_n is a possible constant and ω_n is general position for the transmission zero. (2.16) may be re-written as

$$\frac{dT_N(\omega)}{\sqrt{{T_N}^2(\omega)-1}} = \frac{C_n \prod_{r=1}^{T}(\omega_r\omega - 1)\, d\omega}{\prod_{n=1}^{N}(1-\omega/\omega_n)\sqrt{\omega^2-1}} \tag{2.17}$$

Then using partial fraction expansion on the right hand side,

$$\frac{dT_N(\omega)}{\sqrt{{T_N}^2(\omega)-1}} = \sum_{n=1}^{N} \frac{A_n d\omega}{(1-\omega/\omega_n)\sqrt{\omega^2-1}} \tag{2.18}$$

where,

$$A_n = \left(\frac{C_n(1-\omega/\omega_n)}{\prod_{n=1}^{N}(1-\omega/\omega_n)} \right)\Bigg|_{\omega=\omega_n} \tag{2.19}$$

Integrating both sides of (2.18),

$$\begin{aligned} \int \frac{dT_N(\omega)}{\sqrt{{T_N}^2(\omega)-1}} &= \sum_{n=1}^{N} \int \frac{A_n d\omega}{(1-\omega/\omega_n)\sqrt{\omega^2-1}} \\ acosh[T_N(\omega)] &= \sum_{n=1}^{N} \int \frac{A_n d\omega}{(1-\omega/\omega_n)\sqrt{\omega^2-1}} \end{aligned} \tag{2.20}$$

This right hand side integral may be solved by appropriate change of variable. Now let

$$X = \frac{\omega - 1/\omega_n}{1-\omega/\omega_n} \tag{2.21}$$

where X is the new variable dependant on ω so that,

$$\omega = \frac{X + 1/\omega_n}{1 + X/\omega_n} \tag{2.22}$$

Hence,

$$\begin{aligned} \frac{dX}{d\omega} &= \frac{1-1/{\omega_n}^2}{(1-\omega/\omega_n)^2} \\ dX\left(\frac{1-\omega/\omega_n}{1-1/{\omega_n}^2}\right) &= \frac{d\omega}{1-\omega/\omega_n} \end{aligned} \tag{2.23}$$

By substituting (2.22) in (2.23), (2.23) may be reduced to,

$$\frac{dX}{1+X/\omega_n} = \frac{d\omega}{1-\omega/\omega_n} \tag{2.24}$$

Substituting (2.22) and (2.24) in the right hand term of the integral (2.20) above yields,

$$acosh[T_N(\omega)] = \sum_{n=1}^{N} \int \frac{A_n dX}{(1+X/\omega_n)\sqrt{\left(\frac{X+1/\omega_n}{1+X/\omega_n}\right)^2 - 1}}$$

$$acosh[T_N(\omega)] = \sum_{n=1}^{N} \int \frac{A_n dX}{\sqrt{(X+1/\omega_n)^2 - (1+X/\omega_n)^2}} \tag{2.25}$$

$$acosh[T_N(\omega)] = \sum_{n=1}^{N} \frac{A_n}{\sqrt{1-1/{\omega_n}^2}} \int \frac{dX}{\sqrt{X^2-1}}$$

Solving the right hand side integral of (2.25) yields,

$$acosh[T_N(\omega)] = \sum_{n=1}^{N} \frac{A_n}{\sqrt{1-1/{\omega_n}^2}} acosh[X] + A_o \tag{2.26}$$

Hence the overall characteristic function may be expressed as,

$$T_N(\omega) = \cosh\left\{\sum_{n=1}^{N} \frac{A_n}{\sqrt{1-1/{\omega_n}^2}} acosh[X] + A_o\right\} \tag{2.27}$$

Now, A_n may be chosen so that $\frac{A_n}{\sqrt{1-1/{\omega_n}^2}} acosh[X]$ is a rational polynomial with highest degree 1. Hence

$$\frac{A_n}{\sqrt{1-1/{\omega_n}^2}} = 1$$

$$A_n = \sqrt{1-1/{\omega_n}^2} \tag{2.28}$$

Also since at the cutoff frequency point $\omega = 1$, $T_N(1) = 1$, then from (2.27),

$$A_o = 0 \tag{2.29}$$

Thus the final form for the characteristic function is

$$T_N(\omega) = \cosh\left\{\sum_{n=1}^{N} acosh[X]\right\} \tag{2.30}$$

The proof of (2.1) is clearly evident from (2.30) with,

$$X(\omega) = X_{1-1-0}(\omega) = \frac{\omega - 1/\omega_n}{1 - \omega/\omega_n} \tag{2.31}$$

as the basis function. Note that this happens to be the substitution (2.21) required to solve the differential equation (2.16). A special class of Chebyshev low-pass filter is obtained if all the transmission zeros are at infinity (i.e. $\omega_n = \infty$), then the basis function becomes,

$$X(\omega) = X_{1-0-0}(\omega) = \omega \tag{2.32}$$

Thus the differential equation (2.16) yields a solution,

$$T_N(\omega) = \cosh\left\{\sum_{n=1}^{N} acosh[X]\right\} = \cosh\{Nacosh(\omega)\} \tag{2.33}$$

This is called all pole Chebyshev low-pass filter transfer function [4]. The two basis functions (2.31) and (2.32) may easily be obtained using the second method by formulating a rational function (2.13) such that,

$$X(\omega) = k_o \frac{\omega + a_0}{1 - \omega/\omega_n} \tag{2.34}$$

And since the values at the cutoff are known as $X(1) = 1$ and $X(-1) = -1$ then the constants, k_o and a_0 can easily be determined simultaneously as,

$$k_o = -1/\omega_n \; and \; a_0 = -\omega_n \tag{2.35}$$

Thus as before the two basis functions are,

$$X_{1-0-0}(\omega) = \omega$$
$$X_{1-1-0}(\omega) = \frac{\omega - 1/\omega_n}{1 - \omega/\omega_n} \tag{2.36}$$

Note that each basis function has a particular position for the transmission zero. As pointed out earlier, to generate an overall transfer function using (2.1), appropriate weighting integers are used which indicate how many of those transmission zeros in each basis function are used and where they are located. This will be made much clearer with an example. A more general Chebyshev low-pass filter transfer

function may also include half transmission zero pair (or simply 'half-zero'). One way of obtaining the required basis functions is by solving the differential equation below.

$$\frac{dT_N(\omega)}{d\omega} = \frac{C_n \prod_{r=1}^{T} (\omega_r \omega - 1) \sqrt{{T_N}^2(\omega) - 1}}{\prod_{h=1}^{N_{Half}} \sqrt{{\omega_n}^2 - \omega^2} \prod_{n=1}^{N_{FTZ}} (1 - \omega/\omega_n) \sqrt{\omega^2 - 1}}, T < N \tag{2.37}$$

where N_{Half} is the number of half transmission zero pairs and N_{FTZ} is the number of the non-half-zero transmission zeros. However, using the theory developed above, only one more basis function is required in addition to the two already found for Chebyshev low-pass filters (2.36) to completely characterise such a transfer function using (2.1). The required basis function may be modelled as

$$X_{1-1/2-0}(\omega) = k_o \frac{\omega + a_0}{\sqrt{{\omega_n}^2 - \omega^2}} \tag{2.38}$$

Using the boundary conditions, $X(\pm 1) = \pm 1$, yields,

$$X_{1-1/2-0}(\omega) = \frac{\omega \sqrt{{\omega_n}^2 - 1}}{\sqrt{{\omega_n}^2 - \omega^2}} \tag{2.39}$$

Now, the solution to generalised Chebyshev low-pass filter characteristic function may be written as

$$T_N(\omega) = cosh \left\{ \begin{array}{c} \alpha_1 \, acosh\{X_{1-0-0}(\omega)\} \\ +\alpha_2 \, acosh\{X_{1-1/2-0}(\omega)\} \\ +\alpha_3 \, acosh\{X_{1-1-0}(\omega)\} \end{array} \right\} \tag{2.40}$$

The Chebyshev characteristic functions with at least a pair of half transmission zero are called Chebyshev of second kind [54, 55]. In order to generate the characteristic polynomials, the three basis function are expressed in their canonical form using polynomials described in section 2.2 as shown in Table 2-2. Calculating the characteristic polynomials is fairly straight forward using generalised recursive technique described in section 2.3.

Table 2-2: Normalised Basis Function Polynomials for Synthesis of Common Chebyshev Low-pass Filters

$V(\omega) = \omega^2 - 1$

N-N_{FTZ}-N_{OTZ}	$U_r(\omega)$	$W_r(\omega)$	$P_r(\omega)$
$1-0-0$	ω	1	1
$1-1/2-0$	$\omega\sqrt{{\omega_n}^2-1}$	ω_n	$\sqrt{{\omega_n}^2-\omega^2}$
$1-1-0$	$-\omega_n\omega+1$	$\sqrt{{\omega_n}^2-1}$	$\omega-\omega_n$

2.4.2 Distributed Generalised Chebyshev Low-pass Filters

Similar basis functions for direct synthesis of distributed low-pass filters may be derived. Although differential equations may be written in distributed domain and the characteristic function decomposed into its basis functions, it is intuitive and easier to simply mathematically model the basis function based on different transmission zero positions as was done for the lumped domain.

Table 2-3 Basis Function Polynomials for Synthesis of Distributed Chebyshev Low-pass Filters

$V(t) = t^2 - {t_c}^2 \qquad t = tan\,\theta \qquad t_c = tan\,\theta_c \qquad t_z = tan\,\theta_z$

N-N_{FTZ}-N_{90^o}	$U_r(t)$	$W_r(t)$	$P_r(t)$
$1-0-0^*$	$\left(\sqrt{1+{t_c}^2}\right)t$	1	$t_c\sqrt{1+t^2}$
$1-0-1$	t	1	t_c
$2-2-0$	$({t_c}^2-2{t_z}^2)t^2+{t_c}^2{t_z}^2$	$2t_z\left(\sqrt{{t_z}^2-{t_c}^2}\right)t$	${t_c}^2(t^2-{t_z}^2)$

* A pair of half transmission zeros at infinity on the real axis of the ρ complex plane (i.e. $\theta_z = \pm j\infty$))

The advantage of using the proposed synthesis technique is that arbitrary low-pass transfer functions may be synthesised as opposed to only those which may be derived from lumped element prototype filters by lumped to distributed transformations such as Richard's transformation [9]. The synthesis is carried out directly in the distributed domain without any reference to the lumped domain. The

synthesis of meander-like distributed low-pass filters in Chapter 3 is one example where it was not possible to synthesise certain transfer functions from a lumped domain via some forms of lumped to distributed transformations. This is because, inherently, the unity element of a transmission line does not have a lumped element equivalent [4]. However, it is hereby shown in this case that the generalised synthesis method outline in this Chapter is applicable.

Three different basis functions were determined which may be used to design any distributed low-pass filters with unit length transmission line elements.

The first basis function in Table 2-3 is a $X_{1-0-0}(t)$ distributed basis function with a single real axis half transmission zero pair at infinity ($\theta_z = \pm j\infty$) on the complex ρ plane. This is realised using a series connected unit element (transmission line).

The second basis function in Table 2-3 is a $X_{1-0-1}(t)$ distributed basis function with a single transmission zero at $\theta_z = \pm 90^o$ on the complex ρ plane. This is referred to as a quarter-wave frequency transmission zero. Hence, it is realised either as a shunt open-circuited stub or series short circuited stub.

The third basis function in Table 2-3 is a $X_{2-2-0}(t)$ distributed basis function with a symmetrical pair of transmission zeros. These transmission zeros could be any symmetrical pairs on the real or imaginary axis of the complex ρ plane or exist as complex paraconjugated pairs (i.e. $\theta_z = \pm\theta_\tau + j\theta_t$) to ensure physical realisability. This basis function is realised using shunt series LC or series shunt LC foster realisation in case of a pair of imaginary axis transmission zeros.

The general recursive technique is then applied to generate the overall distributed Chebyshev low-pass filter characteristic function as outlined in section 2.3. The distributed low-pass filters described in Chapter 3 employ these basis functions.

2.4.3 Lumped Generalised Chebyshev Bandpass Filters

Direct synthesis of lumped bandpass filter requires the use of bandpass basis functions. The analysis begins with a consideration of a minimum phase lumped bandpass filter network where all the transmission zeros are either at infinity or at

the origin. The characteristic function satisfies the general differential equation of the form,

$$\frac{dT_N(\omega)}{d\omega} = \frac{C_n(\omega^2 + {\omega_m}^2)\sqrt{{T_N}^2(\omega) - 1}}{\omega\sqrt{\omega^4 - (1 + {\omega_c}^2)\omega^2 + {\omega_c}^2}} \tag{2.41}$$

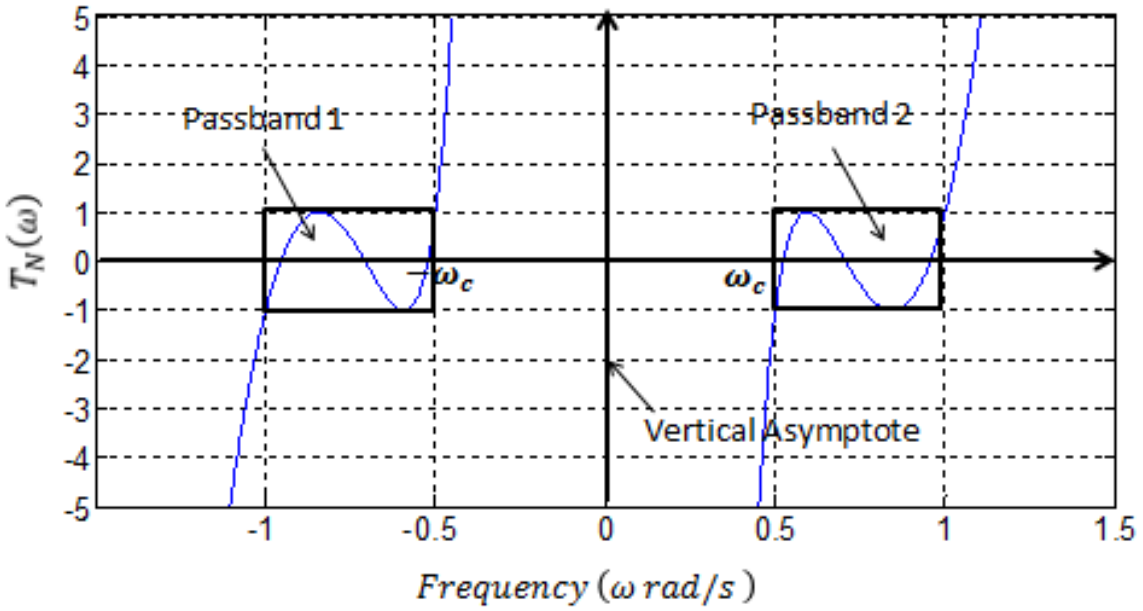

Fig. 2-1 Normalised minimum phase bandpass network characteristic function plot for $N = 6$ and $\omega_c = 0.5$

The term $\omega^2 + {\omega_m}^2$ accounts for a pair of imaginary turning points. The other turning points are provided by the term $\sqrt{{T_N}^2(\omega) - 1}$ and the extra points provided by this expression are just the normalised cut-off points i.e. $\omega = -1, -\omega_c, \omega_c,$ and 1, which are cancelled out by the denominator term $\sqrt{\omega^4 - (1 + {\omega_c}^2)\omega^2 + {\omega_c}^2}$. C_n is a possible constant. Fig. 2-1 shows the example plot of $T_N(\omega)$ for $N = 6$ and $\omega_c = 0.5$. By solving this differential equation, the general solution of the characteristic function for minimum phase filter networks is obtained. Re-writing (2.41) as,

$$\frac{dT_N(\omega)}{\sqrt{{T_N}^2(\omega) - 1}} = \frac{C_n(\omega^2 + {\omega_m}^2)d\omega}{\omega\sqrt{\omega^4 - (1 + {\omega_c}^2)\omega^2 + {\omega_c}^2}} \tag{2.42}$$

and integrating both side for $|\omega| > 1$ and $acosh\left(T_N(\omega)\right) > 0$ yields,

$$\int \frac{dT_N(\omega)}{\sqrt{{T_N}^2(\omega)-1}} = \int \frac{C_n(\omega^2+{\omega_m}^2)d\omega}{\omega\sqrt{\omega^4-(1+{\omega_c}^2)\omega^2+{\omega_c}^2}} \tag{2.43}$$

where the left integral in (2.43) is known and the right integral may be expanded as,

$$\begin{aligned}\operatorname{acosh} T_N(\omega) = C_n \int \frac{\omega d\omega}{\sqrt{\omega^4-(1+{\omega_c}^2)\omega^2+{\omega_c}^2}} \\ + C_n{\omega_m}^2 \int \frac{d\omega}{\omega\sqrt{\omega^4-(1+{\omega_c}^2)\omega^2+{\omega_c}^2}}\end{aligned} \tag{2.44}$$

The right integral may be integrated using change of variable. Let

$$u = \omega^2 \tag{2.45}$$

Then,

$$\frac{du}{2} = \omega d\omega \text{ and } \frac{du}{2u} = \frac{d\omega}{\omega} \tag{2.46}$$

Changing the variable to u, integrating [56] and substituting back for u gives,

$$\begin{aligned}\operatorname{acosh} T_N(\omega) = \frac{C_n}{2} \int \frac{du}{\sqrt{u^2-(1+{\omega_c}^2)u^2+{\omega_c}^2}} \\ + \frac{C_n{\omega_m}^2}{2\omega_c} \int \frac{du}{u\sqrt{u^2-(1+{\omega_c}^2)u^2+{\omega_c}^2}}\end{aligned} \tag{2.47}$$

$$\begin{aligned}\operatorname{acosh} T_N(\omega) = \frac{C_n}{2} log\left(2\omega^2-(1+{\omega_c}^2)+2\sqrt{V}\right) \\ - \frac{C_n{\omega_m}^2}{2\omega_c} log\left(\frac{-(1+{\omega_c}^2)\omega^2+2{\omega_c}^2+2\omega_c\sqrt{V}}{\omega^2}\right)+C\end{aligned} \tag{2.48}$$

where

$$V = \omega^4-(1+{\omega_c}^2)\omega^2+{\omega_c}^2 \tag{2.49}$$

is the cutoff polynomial and C is the constant of integration. Let $m = \frac{{\omega_m}^2}{\omega_c} > 0$. (2.48) may further be expressed as,

$$\begin{aligned}\operatorname{acosh} T_N(\omega) = log\left\{\frac{\left(2\omega^2-(1+{\omega_c}^2)+2\sqrt{V}\right)^{\frac{C_n}{2}}}{(-1)^{\frac{C_nm}{2}}\omega^{-C_nm}\left((1+{\omega_c}^2)\omega^2-2{\omega_c}^2-2\omega_c\sqrt{V}\right)^{\frac{C_nm}{2}}}\right\} \\ + C\end{aligned} \tag{2.50}$$

Since $T_N(1) = 1$, then the constant C may be evaluated as

$$log\left\{\frac{\left(2\omega^2 - (1+{\omega_c}^2) + 2\sqrt{V}\right)^{\frac{C_n}{2}}}{(-1)^{\frac{C_n m}{2}}\omega^{-C_n m}\left((1+{\omega_c}^2)\omega^2 - 2{\omega_c}^2 - 2\omega_c\sqrt{V}\right)^{\frac{C_n m}{2}}}\right\}\Bigg|_{\omega=1} + C = 0 \tag{2.51}$$

yielding

$$log\left\{\frac{(1-{\omega_c}^2)^{\frac{C_n}{2}}}{(-1)^{\frac{C_n m}{2}}(1-{\omega_c}^2)^{\frac{C_n m}{2}}}\right\} + C = 0 \tag{2.52}$$

$$\mathrm{C} = -log\left\{\frac{(1-{\omega_c}^2)^{\frac{C_n}{2}(1-m)}}{(-1)^{\frac{C_n m}{2}}}\right\} = log\left\{\frac{(-1)^{\frac{C_n m}{2}}}{(1-{\omega_c}^2)^{\frac{C_n}{2}(1-m)}}\right\} \tag{2.53}$$

Substituting this into (12) yields,

$$\begin{aligned}\operatorname{acosh} T_N(\omega) = log&\left\{\frac{\left(2\omega^2 - (1+{\omega_c}^2) + 2\sqrt{V}\right)^{\frac{C_n}{2}}}{(-1)^{\frac{C_n m}{2}}\omega^{-C_n m}\left((1+{\omega_c}^2)\omega^2 - 2{\omega_c}^2 - 2\omega_c\sqrt{V}\right)^{\frac{C_n m}{2}}}\right\} \\ &+ log\left\{\frac{(-1)^{\frac{C_n m}{2}}}{(1-{\omega_c}^2)^{\frac{C_n}{2}(1-m)}}\right\}\end{aligned} \tag{2.54}$$

which may be written as,

$$\operatorname{acosh} T_N(\omega) = log\left\{\frac{\left(2\omega^2 - (1+{\omega_c}^2) + 2\sqrt{V}\right)^{\frac{C_n}{2}}}{(1-{\omega_c}^2)^{\frac{C_n}{2}(1-m)}\omega^{-C_n m}\left((1+{\omega_c}^2)\omega^2 - 2{\omega_c}^2 - 2\omega_c\sqrt{V}\right)^{\frac{C_n m}{2}}}\right\} \tag{2.55}$$

Now write,

$$\operatorname{acosh} T_N(\omega) = log\left\{\frac{R^{\frac{C_n}{2}}}{(1-{\omega_c}^2)^{\frac{C_n}{2}(1-m)}\omega^{-C_n m}(S^*)^{\frac{C_n m}{2}}}\right\} \tag{2.56}$$

So that,

$$R = 2\omega^2 - (1 + {\omega_c}^2) + 2\sqrt{V}$$

$$S = (1 + {\omega_c}^2)\omega^2 - 2{\omega_c}^2 + 2\omega_c\sqrt{V} \tag{2.57}$$

$$S^* = (1 + {\omega_c}^2)\omega^2 - 2{\omega_c}^2 - 2\omega_c\sqrt{V}$$

(2.56) may therefore be re-written by multiplying both the numerator and denominator of the argument of the natural logarithm function by $S^{\frac{C_n m}{2}}$ as

$$\operatorname{acosh} T_N(\omega) = log\left\{\frac{R^{\frac{C_n}{2}}(S)^{\frac{C_n m}{2}}}{(1 - {\omega_c}^2)^{\frac{C_n}{2}(1-m)}\omega^{-C_n m}(S^*)^{\frac{C_n m}{2}}(S)^{\frac{C_n m}{2}}}\right\} \tag{2.58}$$

$$\operatorname{acosh} T_N(\omega) = log\left\{\frac{R^{\frac{C_n}{2}}(S)^{\frac{C_n m}{2}}}{(1 - {\omega_c}^2)^{\frac{C_n}{2}(1-m)}\omega^{-C_n m}(SS^*)^{\frac{C_n m}{2}}}\right\} \tag{2.59}$$

Furthermore, introduce new indices in (2.59) and re-write as,

$$\operatorname{acosh} T_N(\omega) = log\left\{\frac{R^{\alpha}(RS)^{\frac{\beta}{2}}(S)^{\gamma}}{(1 - {\omega_c}^2)^{\alpha-\gamma}\omega^{-(\beta+2\gamma)}(SS^*)^{\frac{\beta}{2}+\gamma}}\right\} \tag{2.60}$$

such that from (2.59) and (2.60) the index of polynomial R is,

$$\frac{C_n}{2} = \alpha + \frac{\beta}{2} \tag{2.61}$$

and also from (2.59) and (2.60) the index of polynomial S is,

$$\frac{C_n m}{2} = \frac{\beta}{2} + \gamma \tag{2.62}$$

where α, β and γ are scalars related to C_n and m by (2.61) and (2.62). Now, the following identities hold for R and S:

$$RS = (1 + \omega_c)^2\left(\omega^2 - \omega_c + \sqrt{V}\right)^2 \tag{2.63}$$

and

$$SS^* = (1 - {\omega_c}^2)^2\omega^4 \tag{2.64}$$

At this point R and S may be substituted back into (2.60) and using identity (2.63)-(2.64) to substitute for RS and SS^* into (2.60) yields,

$$\operatorname{acosh} T_N(\omega) = log\left\{\frac{\left(2\omega^2-(1+{\omega_c}^2)+2\sqrt{V}\right)^{\alpha}\left((1+\omega_c)^2\left(\omega^2-\omega_c+\sqrt{V}\right)^2\right)^{\frac{\beta}{2}}\left((1+{\omega_c}^2)\omega^2-2{\omega_c}^2+2\omega_c\sqrt{V}\right)^{\gamma}}{(1-{\omega_c}^2)^{\alpha-\gamma}\omega^{-(\beta+2\gamma)}((1-{\omega_c}^2)^2\omega^4)^{\frac{\beta}{2}+\gamma}}\right\} \tag{2.65}$$

$$\operatorname{acosh} T_N(\omega) = log\left\{\frac{\left(2\omega^2-(1+{\omega_c}^2)+2\sqrt{V}\right)^{\alpha}\left(\omega^2-\omega_c+\sqrt{V}\right)^{\beta}\left((1+{\omega_c}^2)\omega^2-2{\omega_c}^2+2\omega_c\sqrt{V}\right)^{\gamma}}{(1+\omega_c)^{-\beta}(1-{\omega_c}^2)^{\alpha+\beta+\gamma}\omega^{\beta+2\gamma}}\right\} \tag{2.66}$$

$$\operatorname{acosh} T_N(\omega) = log\left\{\frac{\left(2\omega^2-(1+{\omega_c}^2)+2\sqrt{V}\right)^{\alpha}\left(\omega^2-\omega_c+\sqrt{V}\right)^{\beta}\left((1+{\omega_c}^2)\omega^2-2{\omega_c}^2+2\omega_c\sqrt{V}\right)^{\gamma}}{(1-\omega_c)^{\beta}(1-{\omega_c}^2)^{\alpha+\gamma}\omega^{\beta+2\gamma}}\right\} \tag{2.67}$$

With further algebra, (2.67) may be expanded as follows:

$$\operatorname{acosh} T_N(\omega) = log\left\{\left(\frac{2\omega^2-(1+{\omega_c}^2)+2\sqrt{V}}{(1-{\omega_c}^2)}\right)^{\alpha}\left(\frac{\omega^2-\omega_c+\sqrt{V}}{(1-\omega_c)\omega}\right)^{\beta}\left(\frac{(1+{\omega_c}^2)\omega^2-2{\omega_c}^2+2\omega_c\sqrt{V}}{(1-{\omega_c}^2)\omega^2}\right)^{\gamma}\right\} \tag{2.68}$$

$$\operatorname{acosh} T_N(\omega) = \alpha log\left(\frac{2\omega^2-(1+{\omega_c}^2)+2\sqrt{V}}{(1-{\omega_c}^2)}\right)+\beta log\left(\frac{\omega^2-\omega_c+\sqrt{V}}{(1-\omega_c)\omega}\right)+\gamma log\left(\frac{(1+{\omega_c}^2)\omega^2-2{\omega_c}^2+2\omega_c\sqrt{V}}{(1-{\omega_c}^2)\omega^2}\right) \tag{2.69}$$

After further decomposition, (2.69) becomes,

$$\operatorname{acosh} T_N(\omega) = \alpha log\left(\frac{2\omega^2 - (1+{\omega_c}^2)}{(1-{\omega_c}^2)} + \sqrt{\left(\frac{2\omega^2 - (1+{\omega_c}^2)}{(1-{\omega_c}^2)}\right)^2 - 1}\right) + \beta log\left(\frac{\omega^2 - \omega_c}{(1-\omega_c)\omega} + \sqrt{\left(\frac{\omega^2 - \omega_c}{(1-\omega_c)\omega}\right)^2 - 1}\right)$$
$$+ \gamma log\left(\frac{(1+{\omega_c}^2)\omega^2 - 2{\omega_c}^2}{(1-{\omega_c}^2)\omega^2} + \sqrt{\left(\frac{(1+{\omega_c}^2)\omega^2 - 2{\omega_c}^2}{(1-{\omega_c}^2)\omega^2}\right)^2 - 1}\right) \tag{2.70}$$

Now, let

$$X_{2-0-0}(\omega) = \frac{2\omega^2 - (1+{\omega_c}^2)}{(1-{\omega_c}^2)}, \tag{2.71}$$

$$X_{2-0-1}(\omega) = \frac{\omega^2 - \omega_c}{(1-\omega_c)\omega} \tag{2.72}$$

and

$$X_{2-0-2}(\omega) = \frac{(1+{\omega_c}^2)\omega^2 - 2{\omega_c}^2}{(1-{\omega_c}^2)\omega^2}. \tag{2.73}$$

Substituting (2.71)-(2.73) into (2.70) gives,

$$\operatorname{acosh} T_N(\omega) = \alpha log\left(X_{2-0-0} + \sqrt{{X_{2-0-0}}^2 - 1}\right) + \beta log\left(X_{2-0-1} + \sqrt{{X_{2-0-1}}^2 - 1}\right) + \gamma log\left(X_{2-0-2} + \sqrt{{X_{2-0-2}}^2 - 1}\right) \tag{2.74}$$

Using the identity:

$$\operatorname{acosh} X_n(\omega) = log\left(X_n(\omega) + \sqrt{{X_n}^2(\omega) - 1}\right) \tag{2.75}$$

and substituting in (2.74) yields,

$$\operatorname{acosh} T_N(\omega) = \alpha \operatorname{acosh}\{X_{2-0-0}\} + \beta \operatorname{acosh}\{X_{2-0-1}\} + \gamma \operatorname{acosh}\{X_{2-0-2}\} \quad (2.76)$$

Finally, the general solution to the differential equation (2.41) may be written as,

$$T_N(\omega) = \cosh\{\alpha \operatorname{acosh}\{X_{2-0-0}\} + \beta \operatorname{acosh}\{X_{2-0-1}\} + \gamma \operatorname{acosh}\{X_{2-0-2}\}\} \quad (2.77)$$

Clearly then, $X_{2-0-0}(\omega)$ is a basis function with two transmission zeros at infinity, $X_{2-0-1}(\omega)$ is a basis function with a single transmission zero at infinity and a single transmission zero at the origin, and $X_{2-0-2}(\omega)$ is a basis function with all two transmission zeros at the origin. The following observations are made from equation (2.68) and (2.77). From (2.77) for $T_N(\omega)$ to be an even N^{th} degree rational polynomial in ω, $2\alpha + 2\beta + 2\gamma = N$ i.e.

$$\alpha + \beta + \gamma = N/2 \quad (2.78)$$

Thus α, β and γ must be either zero or positive integers. From (2.68), the number of transmission zeros at the origin for $T_N(\omega)$ is

$$N_{TZ} = \beta + 2\gamma \quad (2.79)$$

By assigning different integer values including zero to α, β and γ, different linear combinations of functions in $X_{2-0-0}(\omega)$, $X_{2-0-1}(\omega)$ and $X_{2-0-2}(\omega)$ in (2.77) may be obtained as unique solutions to the differential equation (2.41). $T_N(\omega)$ given by (2.77) is thus the general solution to the differential equation defined by (2.41). There are only two equations in α, β and γ i.e. (2.78) and (2.79). Thus one of the three scalars may be chosen and the other two may be determined from (2.78) and (2.79). One suitable choice is as follows: For $N_{OTZ} \leq N/2, \text{choose } \gamma = 0$, then from (2.78) and (2.79),

$$\alpha = N/2 - N_{OTZ} \quad (2.80)$$

$$\beta = N_{OTZ} \quad (2.81)$$

For $N_{OTZ} \geq N/2, \text{choose } \alpha = 0$, then (2.78) and (2.79) becomes,

$$\beta + \gamma = N/2 \quad (2.82)$$

$$\beta + 2\gamma = N_{OTZ} \quad (2.83)$$

Solving (2.82) and (2.83) simultaneously yields,

$$\beta = N - N_{OTZ} \quad (2.84)$$

$$\gamma = N_{OTZ} - N/2 \quad (2.85)$$

Table 2-4 Possible Values for Weighting Numbers α, β and γ

Condition	α	β	γ
$N_{OTZ} \leq N/2$	$N/2 - N_{OTZ}$	N_{OTZ}	0
$N_{OTZ} \geq N/2$	0	$N - N_{OTZ}$	$N_{OTZ} - N/2$

Table 2-5 Minimum Phase Bandpass Filter Family of Solutions

$(N - 0 - N_{OTZ})$	α	β	γ
$N - 0 - 0$	$N/2$	0	0
$N - 0 - 1$	$N/2 - 1$	1	0
$N - 0 - 2$	$N/2 - 2$	2	0
$\vdots$	$\vdots$	$\vdots$	$\vdots$
$N - 0 - (N/2 - 1)$	1	$N/2 - 1$	0
$N - N/2$	0	$N/2$	0
$N - 0 - (N/2 - 1)$	0	$N/2 - 1$	1
$\vdots$	$\vdots$	$\vdots$	$\vdots$
$N - 0 - (N - 2)$	0	2	$N/2 - 2$
$N - 0 - (N - 1)$	0	1	$N/2 - 1$
$N - 0 - N$	0	0	$N/2$

The different weighting numbers are summarized in Table 2-4. This yields a family of solutions based on the number of transmission zeros at the origin (N_{OTZ}) as illustrated in Table 2-5. It is interesting to note from Table 2-5 that the first family of solution (N-0-0) are simply the even degree Achieser-Zolotarev characteristic function [29]. These are characterised by (2.71). The well-known even degree Chebyshev low-pass characteristic functions as discussed in section 2.4.1 may be obtained from this class by simply setting the parameter $\omega_c = 0$. Also N-0-$N/2$ family in the middle of Table 2-5 characterised by a characteristic function defined by (2.72) is a well-known function in the design of dual passband filters e.g. used in [2] or as a transform from low-pass to bandpass filter [4]. Therefore, Table 2-5 gives all possible transmission zeros at the origin (N_{OTZ}) for any given minimum phase bandpass filter degree (N).

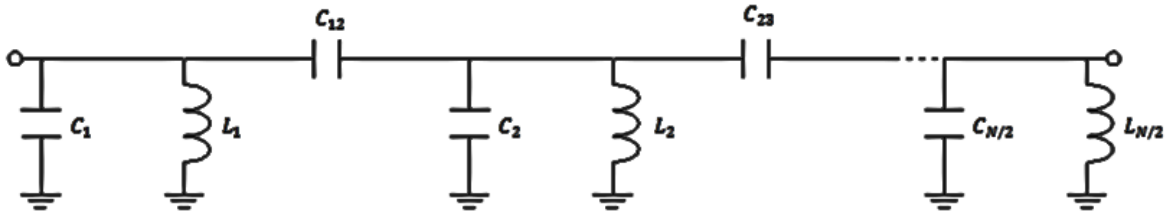

Fig. 2-2 Lumped element low-pass prototype filter used for design of bandpass filters with $N_{TZ} = N - 1$

As an illustrative example, Fig. 2-2 shows the realisation of a bandpass filter characterised by an N-0-$(N-1)$ transfer function. The filter network contains $N-1$ transmission zeros at the origin which are the result of the series capacitors and shunt inductors as in Fig. 2-2. Table 2-5 above shows that the weighting numbers for each of the basis function are $\alpha = 0$, $\beta = 1$ and $\gamma = N/2 - 1$ in order to provide the required transmission zeros at the origin.

The basis functions derived above may be used in the direct synthesis of other bandpass filters. For example distributed combline bandpass filters may be synthesised using the N-0-1 family of solutions, with $N_{TZ} = 1$ transmission zeros at the origin in Table 2-5 by means of a suitable lumped to distributed transformation. This will be considered in detail in Chapter 5. With the known required number of transmission zeros at the origin corresponding to weighting numbers α, β and γ as in Table 2-5, other types of bandpass filters may easily be synthesised.

A more complete general solution for lumped bandpass filters include arbitrary placed transmission zeros on the complex plane. This might be achieved by solving a differential equation of the form

$$\frac{dT_N(\omega)}{d\omega} = \frac{C_n \prod_{r=1}^{T} (\omega^2 - {\omega_r}^2) \sqrt{{T_N}^2(\omega) - 1}}{\omega^q \prod_{n=1}^{N_{FTZ}} (\omega^2 - {\omega_n}^2) \sqrt{\omega^4 - (1 + {\omega_c}^2)\omega^2 + {\omega_c}^2}} \tag{2.86}$$

All terms are defined as before. Note that the T out-of-band turning point may be complex in nature. However, to avoid elaborate mathematical manipulations as was the case for a simple minimum phase network, it is intuitive to realise that (2.1) is true for this case and that the basis function may be independently determined

by mathematically modelling simple lowest degree characteristic functions based on the number and position of the transmission zeros. The second method for determining the basis function becomes handy in this case. Now since the three basis functions already give the different combinations of transmission zeros, the only required basis function is the one with arbitrary placed symmetrical pairs of transmission zeros. This symmetrical basis function may be computed by solving a set of two non-linear simultaneous equations based on its known values at the critical points, (i.e. $\pm\alpha, \pm\beta$ for bandpass filter) as depicted in Fig. 2-3. Using (2.13) and the known values at the cutoff points, the basis function with a symmetrical pair of transmission zeros prescribed at $\pm\omega_n$ and unknown coefficients p, q and d may be determined as,

$$X_{2-2-0}(\omega) = \frac{U_r(\omega)}{P_r(\omega)} = \frac{p\omega^2 + q}{d(\omega^2 - {\omega_n}^2)} =$$

$$X_{2-2-0}(\omega) = \pm\frac{(2{\omega_n}^2 - 1 - {\omega_c}^2)\omega^2 + 2{\omega_c}^2 - {\omega_n}^2(1 + {\omega_c}^2)}{(1 - {\omega_c}^2)(\omega^2 - {\omega_n}^2)}. \quad (2.87)$$

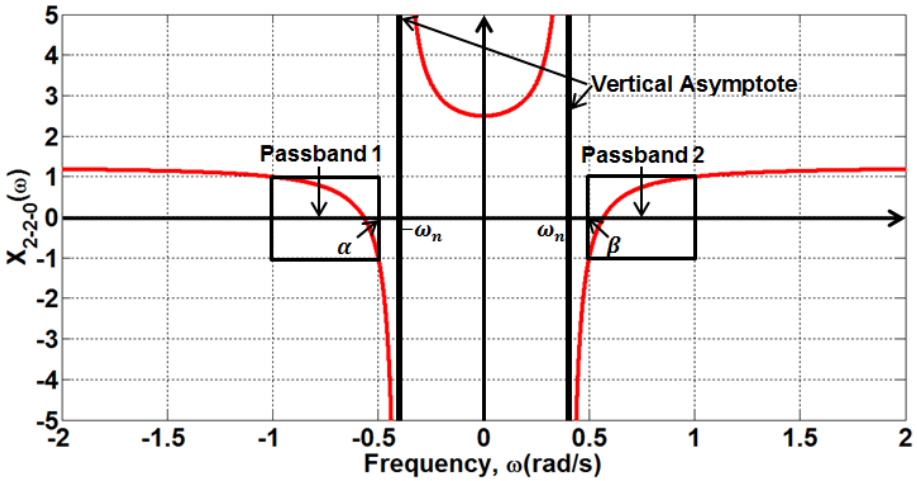

Fig. 2-3 Example of a plot of normalised (with $\delta = 1$) $X_{2-2-0}(\omega)$ basis characteristic function

Additionally, ω_n is in general the position of any arbitrary located complex transmission zero. In fact all the other three basis functions above may be found in this way. For symmetrical networks, all the cutoff points are symmetrical (i.e. $\beta = -\alpha = \omega_c$).

Table 2-6 Basis Functions for Direct Synthesis of Lumped Bandpass Filters or Symmetrical Low-pass Prototype Filter for Dual Bandpass Filter

$$V(\omega) = (\omega^2 - \beta^2)(\omega^2 - \delta^2)$$

$2-0-0$ $U_r(\omega) = \pm(2\omega^2 - \alpha^2 - \delta^2)$ $W_r(\omega) = 2$ $P_r(\omega) = \alpha^2 - \delta^2$
$2-0-1$ $U_r(\omega) = \pm(\omega^2 - \alpha\delta)$ $W_r(\omega) = 1$ $P_r(\omega) = (\alpha - \delta)\omega$
$2-0-2$ $U_r(\omega) = \pm\left((\alpha^2 + \delta^2)\omega^2 - 2\alpha^2\delta^2\right)$ $W_r(\omega) = 2\alpha\delta$ $P_r(\omega) = (\alpha^2 - \delta^2)\omega^2$
$2-2-0$ $U_r(\omega) = \pm\{(2{\omega_n}^2 - \alpha^2 - \delta^2)\omega^2 + 2\alpha^2\delta^2 - {\omega_n}^2(\alpha^2 + \delta^2)\}$ $W_r(\omega) = \begin{cases} +2\sqrt{({\omega_n}^2 - \alpha^2)({\omega_n}^2 - \delta^2)}, \text{for } \lvert\omega_n\rvert > \delta \\ -2\sqrt{({\omega_n}^2 - \alpha^2)({\omega_n}^2 - \delta^2)}, \text{for } \alpha < \omega_n < \beta \end{cases}$ $P_r(\omega) = (\alpha^2 - \delta^2)(\omega^2 - {\omega_n}^2)$

Now the general solution to the differential equation (2.86) may be written as,

$$T_N(\omega) = cosh\begin{Bmatrix} \alpha_1\, acosh\{X_{2-0-0}(\omega)\} \\ +\alpha_2\, acosh\{X_{2-0-1}(\omega)\} \\ +\alpha_3\, acosh\{X_{2-0-2}(\omega)\} \\ +\alpha_4\, acosh\{X_{2-2-0}(\omega)\} \end{Bmatrix} \tag{2.88}$$

where,

$$X_{2-0-0}(\omega) = \frac{2\omega^2 - (1 + {\omega_c}^2)}{(1 - {\omega_c}^2)}$$

$$X_{2-0-1}(\omega) = \frac{\omega^2 - \omega_c}{(1 - \omega_c)\omega} \tag{2.89}$$

$$X_{2-0-2}(\omega) = \frac{(1+{\omega_c}^2)\omega^2 - 2{\omega_c}^2}{(1-{\omega_c}^2)\omega^2}$$

$$X_{2-2-0}(\omega) = \frac{(2{\omega_n}^2 - 1 - {\omega_c}^2)\omega^2 + 2{\omega_c}^2 - {\omega_n}^2(1+{\omega_c}^2)}{(1-{\omega_c}^2)(\omega^2 - {\omega_n}^2)}$$

and α_1, α_2, α_3 and α_4 are integer scalars which determine the number of the transmission zeros that each basis function provide. The four (4) basis functions above completely characterises any bandpass filter network.

Not only are these basis functions used for direct synthesis of bandpass filters but they may also be used for synthesis of symmetrical narrow dual bandpass filters. All the computed basis functions were expressed in terms of the required polynomials and are tabulated in Table 2-6. Notice that the inner cutoff points $\beta = -\alpha$ and the outer cutoff points $\pm\delta$ in Table 2-6 may be arbitrarily chosen and have been denormalised (i.e. $\delta \neq 1$). These basis function are completely identical to the normalised form in (2.89) when $\beta = -\alpha = \omega_c$ and $\delta = 1$. For the $X_{2-2-0}(\omega)$ basis function calculated above, $W_r > 0$ for $|\omega_n| > \delta$ and $W_r < 0$ for $\alpha < \omega_n < \beta$.

2.4.4 Lumped Chebyshev Low-pass Prototype Filter for Interdigital Bandpass Filter

An approach to the exact synthesis of interdigital bandpass filters is now examined. Fig. 2-4 shows the realisation of an interdigital bandpass filter consisting of shunt short circuited stubs separated by unit length transmission lines. The goal is now to obtain characteristic polynomials which may be used to exactly synthesise the network of Fig. 2-4. It is clear from Fig. 2-4 that even degree interdigital bandpass filters have a single pair of half transmission zeros at infinity on the real ρ complex plane due to an old number of unit elements. Old degree interdigital bandpass filters on the other hand have an even number of unit elements. Firstly, synthesis of even degree case will be outlined as these are directly obtained from the basis functions of section 2.4.3.

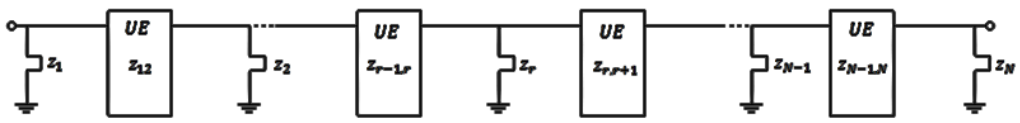

Fig. 2-4 General distributed equivalent circuit for interdigital bandpass filter

2.4.4.1 Even degree Interdigital bandpass filter characteristic polynomials

Even degree interdigital bandpass filters may be synthesised using the basis function in Table 2-5 corresponding to the second family of solution, N-0-1, with $\alpha = N/2 - 1$, $\beta = 1$ and $\gamma = 0$. For this family, the lumped domain s-parameters take the following form:

$$S_{11}(\omega) = \frac{F(\omega)/\mu}{E(\omega)}, \; S_{21}(\omega) = \frac{\omega/\varepsilon}{E(\omega)} \tag{2.90}$$

This characteristic function has a single transmission zero at the origin, i.e. $N_{TZ} = 1$. Using the above weighting numbers and the general recursive technique, the bandpass filter characteristic polynomials are first obtained in the lumped domain. Then using the following lumped-to-distributed transformation,

$$p = \frac{\rho}{\sqrt{1-\rho^2}} \text{ or } \omega = \frac{t}{\sqrt{1+t^2}} \tag{2.91}$$

and its inverse transform defined by

$$\rho = \frac{\pm p}{\sqrt{1+p^2}} \; or \; t = \frac{\pm \omega}{\sqrt{1-\omega^2}}, \tag{2.92}$$

the distributed characteristic polynomials are obtained. The critical points are mapped from the ω – plane to θ – plane as follows:

$$\begin{gathered} 0 \to 0 \\ \omega_c \to \theta_1 \\ 1 \to 90^0 (= \theta_o) \end{gathered} \tag{2.93}$$

where $\theta_1$and θ_o are the electrical lengths at the lower bandedge and centre frequency in degrees of the bandpass filter respectively. In fact the transformation maps a portion $-1 \le \omega \le 1$ in ω – plane to the fundamental period $-90^o \le \theta \le 90^o$ in θ – plane (or $-\infty \le t \le \infty$ in t plane) which is concatenated throughout the entire θ axis. Thus the s-parameters of (2.90) becomes

$$S_{11}(t) = \frac{F(t)/\mu'}{E(t)}, \tag{2.94}$$

$$S_{21}(t) = \frac{P(t)/\varepsilon'}{E(t)} = \frac{t(1+t^2)^{\frac{N-1}{2}}/\varepsilon'}{E(t)}$$

The transmission polynomial $P(t)$ is known following through the transformation. The network is fully canonical since $S_{21}(t)$ has N transmission zeros i.e. a single transmission zero at the origin and $N-1$ pairs of transmission half-zeros at infinity on the real ρ complex plane (i.e. $t = \pm 1$). The polynomials $F(t)$ and $E(t)$ may be obtained from $F(\omega)$ and $E(\omega)$ by transforming the singularities of $F(\omega)$ and $E(\omega)$ using (2.92). The normalising parameters μ' and ε' are computed at points in the $t-$ domain where both $S_{11}(t)$ and $S_{21}(t)$ are known (e.g. $t = t_c$) so that the unitary condition and the prescribed return loss level are satisfied as explained in Chapter 1. Because all the polynomials $P(t)$, $F(t)$ and $E(t)$ are assumed to be monic and of degree N (N even), then appropriate formulae for the normalising parameters ε' and μ' must be used. Here negative signs are taken for both ε' and μ'.

2.4.4.2 Odd degree Interdigital bandpass filter characteristic polynomial

For odd degree interdigital bandpass filters the lumped low-pass characteristic function in ω domain has the form

$$T_N(\omega) = \frac{d_n}{\omega}\left(\sqrt{1-\omega^2}\right)\prod_{n=1}^{N-1}(\omega^2 - \omega_n^2)$$
$$T_N(\omega) = \frac{d_n}{\omega}\left(\sqrt{1-\omega^2}\right)H(\omega) \qquad (2.95)$$

where ω_n is the n^{th} reflection zero position and d_n is a constant. The function is characterised by a symmetrical pair of reflection half-zero at $\omega = \pm 1$ with the polynomial $H(\omega)$ containing the remaining $N-1$ reflection zeros. The characteristic polynomial satisfies the differential equation of the form,

$$\frac{dT_N(\omega)}{d\omega} = \frac{C_n(\omega^2 + {\omega_m}^2)\sqrt{{T_N}^2(\omega) - 1}}{\omega\sqrt{1-\omega^2}\sqrt{\omega^2 - {\omega_c}^2}} \qquad (2.96)$$

with all the parameters as defined above in (2.41). The solution takes the same form as in (2.50) where,

$$\operatorname{acosh} T_N(\omega) = log\left\{\frac{\left(2\omega^2 - (1+{\omega_c}^2) + 2\sqrt{V}\right)^{\frac{C_n}{2}}}{(-1)^{\frac{C_n m}{2}}\omega^{-C_n m}\left((1+{\omega_c}^2)\omega^2 - 2{\omega_c}^2 - 2\omega_c\sqrt{V}\right)^{\frac{C_n m}{2}}}\right\}\Bigg|_{\omega=1} + C_o, \tag{2.97}$$

except that the constant of integration C_o is computed for $T_N(\omega = 1) = 0$ as follows

$$\operatorname{acosh}(0) = log\left\{\frac{\left(2\omega^2 - (1+{\omega_c}^2) + 2\sqrt{V}\right)^{\frac{C_n}{2}}}{(-1)^{\frac{C_n m}{2}}\omega^{-C_n m}\left((1+{\omega_c}^2)\omega^2 - 2{\omega_c}^2 - 2\omega_c\sqrt{V}\right)^{\frac{C_n m}{2}}}\right\}\Bigg|_{\omega=1} + C_o \tag{2.98}$$

yielding

$$C_o = log\left\{\frac{j(-1)^{\frac{C_n m}{2}}}{(1-{\omega_c}^2)^{\frac{C_n}{2}(1-m)}}\right\}. \tag{2.99}$$

Substituting this into (2.97) yields,

$$T_N(\omega) = cosh\left[log\left\{\frac{j\left(2\omega^2 - (1+{\omega_c}^2) + 2\sqrt{V}\right)^{\frac{C_n}{2}}}{(1-{\omega_c}^2)^{\frac{C_n}{2}(1-m)}\omega^{-C_n m}\left((1+{\omega_c}^2)\omega^2 - 2{\omega_c}^2 - 2\omega_c\sqrt{V}\right)^{\frac{C_n m}{2}}}\right\}\right] \tag{2.100}$$

By multiplying the numerator and denominator of the natural logarithm argument by $(\omega^2-1)^{\frac{C_n m}{2}}$ and using the identities

$$\begin{aligned}(\omega^2-1)\left((1+{\omega_c}^2)\omega^2 - 2{\omega_c}^2 - 2\omega_c\sqrt{V}\right) &= \left(\omega_c\omega^2 - \omega_c - \sqrt{V}\right)\\ \left(\omega_c\omega^2 - \omega_c + \sqrt{V}\right)\left(\omega_c\omega^2 - \omega_c - \sqrt{V}\right) &= ({\omega_c}^2-1)(\omega^2-1)\omega^2\end{aligned} \tag{2.101}$$

The solution may be shown to be

$$T_N(\omega) = cosh\left[log\left\{\frac{j(\omega^2-1)^{\frac{C_n m}{2}}\left(2\omega^2 - (1+{\omega_c}^2) + 2\sqrt{V}\right)^{\frac{C_n}{2}}\left(\omega_c\omega^2 - \omega_c + \sqrt{V}\right)^{C_n m}}{(1-{\omega_c}^2)^{\frac{C_n}{2}(1-m)}\omega^{C_n m}\left(({\omega_c}^2-1)(\omega^2-1)\right)^{C_n m}}\right\}\right] \tag{2.102}$$

Clearly, for a single transmission zero at the origin,

$$C_n m = 1 \tag{2.103}$$

and for N^{th} degree characteristic polynomial,

$$C_n = N - 1 \tag{2.104}$$

Thus, $C_n m$ and C_n may be substituted for in (2.102) and the solution becomes,

$$T_N(\omega) = cosh\left[log\left\{\frac{j(\omega^2-1)^{\frac{1}{2}}\left(2\omega^2-(1+{\omega_c}^2)+2\sqrt{V}\right)^{\frac{N-1}{2}}\left(\omega_c\omega^2-\omega_c+\sqrt{V}\right)}{(1-{\omega_c}^2)^{(N-2)/2}\omega({\omega_c}^2-1)(\omega^2-1)}\right\}\right] \tag{2.105}$$

With little manipulation, this equation may be expressed in its final form as,

$$T_N(\omega) =$$

$$cosh\left[log\left\{\left(\frac{\sqrt{1-\omega^2}}{1-\omega^2}\right)\left(\frac{2\omega^2-(1+{\omega_c}^2)+2\sqrt{V}}{1-{\omega_c}^2}\right)^{\frac{N-1}{2}}\left(\frac{\omega_c\omega^2-\omega_c+\sqrt{V}}{\left(1-{\omega_c}^2\right)\omega}\right)\right\}\right] \tag{2.106}$$

As before, the general recursive technique may be applied to obtain $F(\omega)$. Writing,

$$\frac{F(\omega)}{\sqrt{1-\omega^2}} = H(\omega) = \frac{X_N}{\omega^2-1} \tag{2.107}$$

The polynomial X_N is obtained by applying the general recursive technique defined in section 2.3 with initial conditions

$$X_0 = \omega_c\omega^2 - \omega_c \text{ and } Y_0 = 1 \tag{2.108}$$

and using the following basis function

$$\begin{gathered} U_n = 2\omega^2 - (1+{\omega_c}^2) \\ W_n = 2 \\ V = (\omega^2-1)(\omega^2-\omega_c) \end{gathered} \tag{2.109}$$

where the weighting number is

$$\alpha = (N-1)/2 \tag{2.110}$$

At the end of the routine, the $(N-1)^{\text{th}}$ degree polynomial $H(\omega)$ and hence $F(\omega)$ is determined from (2.107). The transformation (2.91)-(2.92) may then be applied as for the even degree case. The monic transmission polynomial $P(\omega)$ is directly obtained from (2.106) as,

$$P(\omega) = \omega \tag{2.111}$$

It follows therefore, directly from the transformation that the transmission polynomial $P(t)$, takes the same form as for the even degree case as

$$P(t)/\varepsilon' = t(1+t^2)^{\frac{N-1}{2}}/\varepsilon' \tag{2.112}$$

The $N-1$ reflection zeros of $H(\omega)$ in $\omega-$domain are then transformed to $t-$domain by application of (2.92) to give the zeros of $F(t)$. Notice that the radical sign on the reflection polynomial (2.107) disappears after the transformation. Appropriate formulae in section 1.1.1.2 of Chapter 1 must be used for the normalizing parameters μ' and ε' since in this case, the polynomials $P(t)$ and $E(t)$ are both of degree N except for $F(t)$ which is of degree $N-1$. Note too that the radical on the $P(t)$ polynomial disappears after the transformation as N is odd. Therefore the more accurate method of determining polynomial $E(t)$ as described in Chapter 1 is used. The rest of the synthesis process is as described in Chapter 1.

The question is whether it would be possible to synthesise combline and interdigital bandpass filters directly in the distributed domain without using the lumped to distributed transformation? It will be reviewed in section 2.4.5 that the basis functions may directly be obtained in the distributed domain enabling direct synthesis of generalised distributed bandpass filters.

2.4.5 Distributed Generalised Chebyshev Bandpass Filters

Since most bandpass filters are implemented using distributed elements it is often convenient to directly synthesise the filter in the distributed domain. Therefore, for direct synthesis of distributed bandpass filters, the basis functions were also determined and are shown in Table 2-7. These basis functions are the distributed domain equivalence of the lumped basis function computed in Table 2-6. Note that the first basis function 2-0-0 has two quarter-wave frequency transmission zeros ($\theta_z = 90^o$). The 2-0-1 basis function has a single quarter-wave frequency transmission zero ($\theta_z = 90^o$) and a single transmission zero at the origin ($\theta_z = 0^o$). The 2-0-2 basis function has all its transmission zeros at the origin ($\theta_z = 0^o$) and finally the 2-2-0 basis function provides a pair of generally located transmissions zeros on the complex ρ plane ($\theta_z = \theta_\omega \pm j\theta_\delta$). Note that the fundamental period is

$0^o \leq \theta \leq 90^o$ which is concatenated throughout the entire θ-plane due to the periodic nature of the tangent function.

Table 2-7 Basis Functions for Direct Synthesis of Distributed Bandpass Filters or Symmetrical Low-pass Prototype Filter for Dual Bandpass Filter (N-N_{FTZ}-N_{0^o})

$$V(t) = (t^2 - {t_1}^2)(t^2 - {t_2}^2) \quad t = tan\,\theta$$

Cutoff points θ_1 and θ_2 rad/s ($t_1 = tan\,\theta_1$ and $t_2 = tan\,\theta_2$)

Transmission zero position θ_z rad/s ($t_z = tan\,\theta_z$)

$2-0-0$ $U_r(t) = \pm(2t^2 - {t_2}^2 - {t_1}^2)$ $W_r(t) = 2$ $P_r(t) = {t_2}^2 - {t_1}^2$
$2-0-1$ $U_r(t) = \pm(t^2 - t_1 t_2)$ $W_r(t) = 1$ $P_r(t) = (t_2 - t_1)t$
$2-0-2$ $U_r(t) = \pm\left((t_1^2 + t_2^2)t^2 - 2{t_1}^2{t_2}^2\right)$ $W_r(t) = 2t_1 t_2$ $P_r(t) = ({t_2}^2 - {t_1}^2)t^2$
$2-2-0$ $U_r(t) = \pm\left\{({t_1}^2 + {t_2}^2 - 2{t_z}^2)t^2 + {t_z}^2({t_1}^2 + {t_2}^2) - 2{t_1}^2{t_2}^2\right\}$ $W_r(t) = \begin{cases} 2\sqrt{({t_z}^2 - {t_1}^2)({t_z}^2 - {t_2}^2)}, & \text{for } \lvert\theta_z\rvert > \theta_2 \\ -2\sqrt{({t_z}^2 - {t_1}^2)({t_z}^2 - {t_2}^2)}, & \text{for } -\theta_1 < \theta_z < \theta_1 \end{cases}$ $P_r(t) = ({t_2}^2 - {t_1}^2)(t^2 - {t_z}^2)$

Another class of distributed bandpass filter may be defined which is made up of unit length of transmission lines of quarter-wave electrical length at the centre frequency. Classical interdigital bandpass filter falls in this category. This class of

filters may also be synthesised using the synthesis technique developed thus far by directly determining the basis functions. In section 2.4.4, the interdigital bandpass filter is synthesised from the lumped domain by making use of lumped distributed transformation (2.91) or (2.92). To demonstrate the power of this technique, the same transfer function may be obtained using direct quarter wavelength bandpass filter basis functions. Without solving any differential equation, these basis functions are given in Table 2-8.

Table 2-8 Quarter-wavelength Bandpass Filter Basis Functions (N-N_{FTZ}-N_{0^o})

$$V(t) = (t^2 - {t_1}^2) \quad t = tan\,\theta$$

Cutoff points θ_1 and θ_2 rad/s ($t_1 = tan\,\theta_1$ and $t_2 = tan\,\theta_2 = -tan\,\theta_1$)

N-N_{FTZ}-N_{0^o}	$U_r(t)$	$W_r(t)$	$P_r(t)$
$1-0-0^*$	$\pm\sqrt{1+{t_1}^2}$	j	$\sqrt{1+t^2}$
$1-0-1$	$\pm t_1$	j	t
$2-2-0$	$\pm\left(t^2+{t_z}^2-2{t_1}^2\right)$	$2\sqrt{{t_z}^2-{t_1}^2}$	$t^2-{t_z}^2$

* A pair of half transmission zeros at infinity on the real axis of the ρ complex plane (i.e. $\theta_z = \pm j\infty$)

In general interdigital bandpass filters of this form have the weighting numbers $\alpha_{1-0-0} = N-1$, $\alpha_{1-0-1} = 1$ and $\alpha_{2-2-0} = 0$ (since no finite frequency transmission zeros) for the basis functions in Table 2-8. They are characterised by $N-1$ half transmission zeros pairs at infinity on the real axis of the ρ complex plane and a single transmission zero at $\theta_z = 0^o$ (and $\theta_z = 180^o$). As opposed to the earlier method of section 2.4.4, it is clear, using direct distributed basis functions, on the transmission zeros that each basis function provides and how the entire characteristic function is built up. It will be proved in Chapter 5 that these basis functions yields the same transfer functions. Because this is a quarter wavelength bandpass filter, it is centred around $\theta_o = 90^o$ and the bandedge is chosen such that $\theta_1 < \theta_o$. Sometimes there might be a requirement to increase selectivity by

finite transmission zeros placement and the 2-2-0 basis function provides a symmetrical pair of transmission zeros. Note that for this basis function the finite frequency transmission zeros must be in the region $0 < \theta_z < \theta_1$.

Other distributed bandpass filters utilizing cascades of unit length transmission lines may easily be synthesised using the 1-0-0 basis function in Table 2-8. This is especially true of microwave filters implemented using waveguides.

2.4.6 Lumped Chebyshev Narrow Dual Bandpass Filters

To synthesise symmetrical narrow band dual bandpass filters in the lumped domain, the same basis functions as for direct synthesis of bandpass filters in Table 2-6 may be used. Asymmetrical functions require different basis function and these may be determined in similar ways as demonstrated above. For these basis functions, $\alpha \neq -\beta$. Because of the asymmetric nature of these functions, some of the transmission zeros of the basis function may be dependent so that the function is constrained to pass through all its cutoff points. Even though these transmission zeros are not controlled, the basis function may be mathematically modelled such that these transmission zeros occur in the specified stopband regions. For this lumped prototype filter, there are three stopband regions namely, lower stopband (LSB), inner stopband (ISB) and upper stopband (USB). Ideally this further entails that frequency invariant reactances are used in the lumped element synthesis and because the filter is assumed to be narrow band, these fictitious elements may be approximated by real elements using reactance slope approximation [29]. Some of the low ordered basis functions were calculated and are shown in Table 2-9 in terms of the required polynomials.

Table 2-9 Asymmetrical Narrow Dual Bandpass Prototype Filter Basis Functions

$$V = (\omega^2 - 1)(\omega - \alpha)(\omega - \beta)$$

Basis Function (N -N_{FTZ}-N_{OTZ}) and Position of Dependent Transmission Zero (ω_z) ISB = Inner Stopband, LSB = Lower Stopband, USB = Upper Stopband
$2-2-0$ $(\omega_z - \omega_n \Rightarrow LSB - ISB$ or $ISB - USB)$ $\omega_z = [(2\alpha\beta + \beta - \alpha)/\omega_n - \alpha - \beta]/[(\alpha + \beta)/\omega_n - \alpha + \beta - 2]$ $\varepsilon = (\alpha + 1)/[(\omega_z - \alpha)/\omega_n + \omega_z + 1]$ $U_r(\omega) = \omega^2 - \varepsilon(\omega_z + 1/\omega_n)\omega + \varepsilon(1 + \omega_z/\omega_n) - 1$ $P_r(\omega) = \varepsilon\left((\omega_z/\omega_n)\omega^2 - (\omega_z + 1/\omega_n)\omega - \omega_z\right)$ $W_r(\omega) = 1$ if ω_n is infinite $W_r(\omega) = \sqrt{1 - \varepsilon^2}$ if ω_n is finite
$2-2-0$ $(\omega_z - \omega_n \Rightarrow LSB - USB$ or $ISB - ISB)$
$\varepsilon = [\alpha\beta + 1 - (\alpha + \beta)\omega_n]/[1 - \alpha\beta + (a + b - 2\omega_n)\omega_n]$ $\omega_z = (\alpha\beta + 1 + (\alpha\beta - 1)\varepsilon)/(2\varepsilon\omega_n)$ $U_r(\omega) = \omega^2 - (1 + \varepsilon)(\alpha + \beta)\omega/2 + (\alpha\beta - 1)/2 + \varepsilon(\alpha\beta + 1)/2$ $P_r(\omega) = \varepsilon(\omega^2 - (\omega_z + \omega_n)\omega + \omega_z\omega_n)$ $W_r(\omega) = \sqrt{1 - \varepsilon^2}$
$3-1-0$ $(1 - \beta > \alpha + 1)$ $(\omega_z\ ISB)$
$\omega_m = (\alpha + \beta + 2)/2$ $\varepsilon = ({\omega_m}^2 - 2\omega_m - \alpha - \beta - \alpha\beta)/2$ $\omega_z = -({\omega_m}^2 + \alpha\beta)/(2\varepsilon)$ $U_r(\omega) = \omega^3 - (2\omega_m + \alpha + \beta)\omega^2/2 + ({\omega_m}^2 - 2\omega_m + \alpha + \beta + \alpha\beta)\omega/2$ $+ ({\omega_m}^2 - \alpha\beta)/2$ $P_r(\omega) = \varepsilon(\omega - \omega_z)$ $W_r(\omega) = \omega - \omega_m$
$3-1-0$ $(1 - \beta > \alpha + 1)$ $(\omega_z - \omega_n \Rightarrow LSB$ or $USB)$
$\omega_m = (\beta - \alpha)/2$ $\varepsilon = ({\omega_m}^2 + 2\alpha\omega_m + 1)/2$ $\omega_z = (\alpha{\omega_m}^2 + \beta)/(2\varepsilon)$ $U_r(\omega) = \omega^3 - (2\omega_m + \alpha + \beta)\omega^2/2 + ({\omega_m}^2 + 2\alpha\omega_m - 1)\omega/2$ $+ (-\alpha{\omega_m}^2 + \beta)/2$ $P_r(\omega) = \varepsilon(\omega - \omega_z)$ $W_r(\omega) = \omega - \omega_m$
$3-1-0$ $(1 - \beta < \alpha + 1)$ $(\omega_z\ ISB)$
$\omega_m = (\alpha + \beta - 2)/2$ $\varepsilon = -({\omega_m}^2 + 2\omega_m + \alpha + \beta - \alpha\beta)/2$ $\omega_z = -({\omega_m}^2 + \alpha\beta)/(2\varepsilon)$ $U_r(\omega) = \omega^3 - (2\omega_m + \alpha + \beta)\omega^2/2 + ({\omega_m}^2 + 2\omega_m - \alpha - \beta + \alpha\beta)\omega/2$ $+ (-{\omega_m}^2 + \alpha\beta)/2$ $P_r(\omega) = \varepsilon(\omega - \omega_z)$ $W_r(\omega) = \omega - \omega_m$

$3-1-0\ (1-\beta>\alpha+1)\ (\omega_z\ ISB)$
$\omega_m=(\alpha+\beta+2)/2$ $\varepsilon=({\omega_m}^2-2\omega_m-\alpha-\beta-\alpha\beta)/2$ $\omega_z=-({\omega_m}^2+\alpha\beta)/(2\varepsilon)$ $U_r(\omega)=\omega^3-(2\omega_m+\alpha+\beta)\omega^2/2+({\omega_m}^2-2\omega_m+\alpha+\beta+\alpha\beta)\omega/2$ $+({\omega_m}^2-\alpha\beta)/2$ $P_r(\omega)=\varepsilon(\omega-\omega_z)$ $W_r(\omega)=\omega-\omega_m$
$3-1-0\ (1-\beta>\alpha+1)\ (\omega_z-\omega_n\ \Rightarrow\ LSB\ \text{or}\ USB)$
$\omega_m=(\beta-\alpha)/2$ $\varepsilon=({\omega_m}^2+2\alpha\omega_m+1)/2$ $\omega_z=(\alpha{\omega_m}^2+\beta)/(2\varepsilon)$ $U_r(\omega)=\omega^3-(2\omega_m+\alpha+\beta)\omega^2/2+({\omega_m}^2+2\alpha\omega_m-1)\omega/2$ $+(-\alpha{\omega_m}^2+\beta)/2$ $P_r(\omega)=\varepsilon(\omega-\omega_z)$ $W_r(\omega)=\omega-\omega_m$
$3-1-0\ (1-\beta<\alpha+1)\ (\omega_z\ ISB)$
$\omega_m=(\alpha+\beta-2)/2$ $\varepsilon=-({\omega_m}^2+2\omega_m+\alpha+\beta-\alpha\beta)/2$ $\omega_z=-({\omega_m}^2+\alpha\beta)/(2\varepsilon)$ $U_r(\omega)=\omega^3-(2\omega_m+\alpha+\beta)\omega^2/2+({\omega_m}^2+2\omega_m-\alpha-\beta+\alpha\beta)\omega/2$ $+(-{\omega_m}^2+\alpha\beta)/2$ $P_r(\omega)=\varepsilon(\omega-\omega_z)$ $W_r(\omega)=\omega-\omega_m$
$3-1-0\ (1-\beta<\alpha+1)\ (\omega_z\ LSB\ \text{or}\ USB)$
$\omega_m=(\alpha-\beta)/2$ $\varepsilon=({\omega_m}^2+2\beta\omega_m+1)/2$ $\omega_z=\left(\beta{\omega_m}^2+\alpha\right)/(2\varepsilon)$ $U_r(\omega)=\omega^3-(2\omega_m+\alpha+\beta)\omega^2/2+({\omega_m}^2+2\beta\omega_m-1)\omega/2$ $+(-\beta{\omega_m}^2+\alpha)/2$ $P_r(\omega)=\varepsilon(\omega-\omega_z)$ $W_r(\omega)=\omega-\omega_m$
$4-1-0\ (\omega_z\ ISB)$
$p=(-\alpha+\beta+2)/2$ $\omega_{m1}=[\alpha+\beta-p^2-2p(\alpha-1)]/[2(\alpha-\beta+p-2)]$ $\omega_{m2}=\omega_{m1}+p$ $\varepsilon=(2\beta\omega_{m1}+2\alpha\omega_{m2}+(\beta+1){\omega_{m1}}^2-(\alpha-1){\omega_{m2}}^2)/2$ $\omega_z=\left(\beta{\omega_{m1}}^2+\alpha{\omega_{m2}}^2\right)/(2\varepsilon)$ $U_r(\omega)=\omega^4-(2\omega_{m1}+2\omega_{m2}+\alpha+\beta)\omega^3/2+$ $({\omega_{m1}}^2+{\omega_{m2}}^2+2(\beta+1)\omega_{m1}+2(\alpha-1)\omega_{m2}-\alpha+\beta)\omega^2/2-$ $\left((\beta+1){\omega_{m1}}^2+(\alpha-1){\omega_{m2}}^2+2\beta\omega_{m1}-2\alpha\omega_{m2}\right)\omega/2+$ $(\beta{\omega_{m1}}^2-\alpha{\omega_{m2}}^2)/2$ $P_r(\omega)=\varepsilon(\omega-\omega_z)$

$$W_r(\omega) = \omega^2 - (\omega_{m1} + \omega_{m2})\omega + \omega_{m1}\omega_{m2}$$

2.4.7 Lumped Generalised Chebyshev Dual Bandpass Filters

For direct synthesis of dual bandpass, the same method is used in computing the basis functions. The differential equation may take up the following form with normalised cutoff frequency points at $\pm\alpha$, $\pm\beta$, $\pm\gamma$ and $\pm 1(\delta)$,

$$\frac{dT_N(\omega)}{d\omega} = \frac{C_n \prod_{r=1}^{T} (\omega^2 - {\omega_r}^2) \sqrt{{T_N}^2(\omega) - 1}}{\omega^{OTZ}(\omega^2 - {\omega_z}^2) \prod_{n=1}^{N_{FTZ}} (\omega^2 - {\omega_n}^2) \sqrt{(\omega^2 - \alpha^2)(\omega^2 - \beta^2)(\omega^2 - \gamma^2)(\omega^2 - 1)}} \quad (2.113)$$

with the usual variable definitions as given above. The characteristic function has prescribed transmission zeros ω_n as other functions considered thus far. Unfortunately, for direct dual bandpass synthesis some transmission zeros, ω_z, are inevitably and inherently dependent due to the very nature of the mathematical function. Because the number of passbands and stopband regions are increased in the dual bandpass, there is also increased permutation for the reflection and transmission zeros. The trade-off for this is the decreased freedom for transmission zeros placement. Even though, from a mathematical point of view, all the prescribed transmission zeros may be arbitrarily placed in any of the stopband regions, in reality the transmission zeros are constrained in certain stopband regions for certain dual bandpass characteristic functions. It is important to note that the degree of the cutoff polynomial, V is now increased to 8th degree. The dependent transmission zeros are also unknown prior to solving the problem (2.113). Furthermore, because there are four passbands including the ones at negative frequencies, the number of reflection zeros in each band must be specified.

All the above factors make the differential equation (2.113) harder to solve. Fortunately the method described in sections 2.2 to 2.3 may be applied to solving this problem by only solving for low degree basis functions based on different transmission zeros permutations. It can be observed in section 2.4 that increasing the number of stopbands also increases the permutation of transmission zeros for the basis functions and hence increases the number of basis functions. To

completely characterise any dual bandpass filter requires basis functions to incorporate all different possible positions of transmission zeros and the number of reflection zeros in each band of the dual bandpass filter. The most useful lowest order basis functions are shown in the Table 2-10, Table 2-11 and Table 2-12. In Table 2-10 and Table 2-11, the possible region of stopband for the dependent transmission zero position is indicated.

Because the function is broken down into discrete independent basis functions, it follows that any given N^{th} basis characteristic function would have at least a symmetrical pair of dependent transmission zero. Using individual basis functions as explained in this work to build the overall characteristic function means that the number of the dependent transmission zeros are increased each time a given basis function is used. Fortunately, these dependent transmission zeros normally depend on the relative bandwidths and position of the prescribed transmission zeros so that they appear to be in synchronously controlled positions and often close to the band-edges. As explained above for asymmetrical narrow dual passband low-pass basis functions, the dependent transmission zeros may be constrained to be in a particular stopband region.

Table 2-10 Normalized 4th Degree Basis Functions for Direct Synthesis of Dual

Bandpass Filters

$$V(\omega) = (\omega^2 - \alpha^2)(\omega^2 - \beta^2)(\omega^2 - \gamma^2)(\omega^2 - 1)$$

Basis Function $(N - N_{FTZ} - N_{OTZ})$	Parametric Equations	
$4 - 0 - 1$ $N_1 = 2, \quad N_2 = 2$ Symmetrical i.e. $\alpha - \beta - \gamma + 1 = 0$	$p = -1 - \alpha\beta - \alpha\gamma + \beta\gamma$ $q = \alpha\beta\gamma$ $\varepsilon_r = \alpha\beta\gamma - \alpha\beta - \alpha\gamma + \beta\gamma$ $U_r(\omega) = \omega^4 + p\omega^2 + q$ $P_r(\omega) = \varepsilon_r\, \omega$ $W_r(\omega) = 1$	
$4 - 2 - 0$ $N_1 = 2, \quad N_2 = 2$ $\pm\omega_z$ ISB Dependent Transmission Zeros	$k = \alpha^2 + \beta^2 + \gamma^2 + 1$ $l = \alpha^2 - \beta^2 + \gamma^2 - 1$ $m = \alpha^2\gamma^2 + \beta^2$ $n = \alpha^2\gamma^2 - \beta^2$ $U_r(\omega) = \omega^4 + p\omega^2 + q$ $P_r(\omega) = \varepsilon_r(\omega^2 - {\omega_z}^2)$ $W_r(\omega) = 1$	$p = -k/2$ $q = m/2$ $\varepsilon_r = -l/2$ $\omega_z = \sqrt{n/l}$
$4 - 2 - 0$ $N_1 = 2,\ N_2 = 2$ $\pm\omega_z$ LSB/Imaginary/USB Dependent Transmission Zeros	$k = \alpha^2 + \beta^2 + \gamma^2 + 1$ $l = \alpha^2 - \beta^2 - \gamma^2 + 1$ $m = \alpha^2 + \beta^2\gamma^2$ $n = \alpha^2 - \beta^2\gamma^2$ $U_r(\omega) = \omega^4 + p\omega^2 + q$ $P_r(\omega) = \varepsilon_r(\omega^2 - {\omega_z}^2)$ $W_r(\omega) = 1$	$p = -k/l$ $q = m/2$ $\varepsilon_r = l/2$ $\omega_z = \sqrt{\frac{n}{l}}$

Table 2-10 (Continued.)

$4-2-1$ $N_1 = 2,\ N_2 = 2$ $\pm\omega_z$ ISB Dependent Transmission Zeros	$p = -\alpha + \beta - \gamma - \alpha\beta + \alpha\gamma - \beta\gamma$ $q = \alpha\beta\gamma$ $\varepsilon_r = -\alpha + \beta - \gamma + 1$ $\omega_z = \sqrt{\frac{\alpha\beta - \alpha\gamma + \beta\gamma - \alpha\beta\gamma}{\varepsilon_r}}$ $U_r(\omega) = \omega^4 + p\omega^2 + q$ $P_r(\omega) = \varepsilon_r\omega(\omega^2 - {\omega_z}^2)$ $W_r(\omega) = 1$	
$4-4-0$ $N_1 = 2,\ N_2 = 2$ $\pm\omega_z$ ISB Dependent Transmission Zeros $\pm\omega_r$ Prescribed LSB/USB Transmission Zeros	$k = \alpha^2 + \beta^2 + \gamma^2 + 1$ $l = \alpha^2 - \beta^2 + \gamma^2 - 1$ $m = \alpha^2\gamma^2 + \beta^2$ $n = \alpha^2\gamma^2 - \beta^2$ $U_r(\omega) = \omega^4 + p\omega^2 + q$ $P_r(\omega) = \varepsilon_r(\omega^2 - {\omega_z}^2)(\omega^2 - {\omega_r}^2)$ $W_r(\omega) = \sqrt{1 - {\varepsilon_r}^2}$	$\varepsilon_r = \frac{{\omega_r}^2 l - n}{2{\omega_r}^4 - k{\omega_r}^2 + m}$ $p = -(k + \varepsilon_r l)/2$ $q = (m + \varepsilon_r n)/2$ $\omega_z = \sqrt{\frac{n + \varepsilon_r m}{2\varepsilon_r {\omega_r}^2}}$
$4-4-0$ $N_1 = 2,\ N_2 = 2$ $\pm\omega_z$ ISB (LSB) Dependent Transmission zeros $\pm\omega_r$ ISB (LSB) Prescribed Transmission Zeros	$k = \alpha^2 + \beta^2 + \gamma^2 + 1$ $l = \alpha^2 - \beta^2 - \gamma^2 + 1$ $m = \alpha^2 + \beta^2\gamma^2$ $n = \alpha^2 - \beta^2\gamma^2$ $U_r(\omega) = \omega^4 + p\omega^2 + q$ $P_r(\omega) = \varepsilon_r(\omega^2 - {\omega_z}^2)(\omega^2 - {\omega_r}^2)$ $W_r(\omega) = \sqrt{1 - {\varepsilon_r}^2}$	$\varepsilon_r = \frac{n - {\omega_r}^2 l}{2{\omega_r}^4 - k{\omega_r}^2 + m}$ $p = -(k - \varepsilon_r l)/2$ $q = (m - \varepsilon_r n)/2$ $\omega_z = \sqrt{-\frac{n - \varepsilon_r m}{2\varepsilon_r {\omega_r}^2}}$

Table 2-11 Normalized 6th Degree Basis Functions for Direct Synthesis of Dual Bandpass Filters

$$V(\omega) = (\omega^2 - \alpha^2)(\omega^2 - \beta^2)(\omega^2 - \gamma^2)(\omega^2 - 1)$$

Basis Function $(N - N_{FTZ} - N_{OTZ})$	Parametric Equations
$6 - 2 - 0$ $N_1 = 2, \quad N_2 = 4$ $1 - \gamma > \beta - \alpha$ $\pm\omega_z$ ISB Dependent Transmission zeros	$k = -(\alpha^2 + \gamma^2 + 1)$ $l = \alpha^2\gamma^2 + \alpha^2 + \gamma^2$ $m = -\alpha^2\gamma^2$ $\omega_m = \sqrt{\frac{-\beta^2 - p}{2}}$ $p = k$ $q = \frac{{\omega_m}^4 + 2\beta^2{\omega_m}^2 + l}{2}$ $r = \frac{m - \beta^2{\omega_m}^4}{2}$ $\varepsilon_r = \frac{{\omega_m}^4 + 2\beta^2{\omega_m}^2 - l}{2}$ $\omega_z = \sqrt{\frac{m + \beta^2{\omega_m}^4}{2\varepsilon_r}}$ $U_r(\omega) = \omega^6 + p\omega^4 + q\omega^2 + r$ $P_r(\omega) = \varepsilon_r(\omega^2 - {\omega_z}^2)$ $W_r(\omega) = \omega^2 - {\omega_m}^2$
$6 - 2 - 0$ $N_1 = 4, \quad N_2 = 2$ $\beta - \alpha > 1 - \gamma$ $\pm\omega_z$ ISB Dependent Transmission Zeros	$l = \alpha^2\beta^2 + \alpha^2 + \beta^2$ $m = -\alpha^2\beta^2$ $p = -(\alpha^2 + \beta^2 + 1)$ $\omega_m = \sqrt{\frac{-\gamma^2 - p}{2}}$ $q = \frac{{\omega_m}^4 + 2\gamma^2{\omega_m}^2 + l}{2}$ $r = \frac{m - \gamma^2{\omega_m}^4}{2}$ $\varepsilon_r = \frac{{\omega_m}^4 + 2\gamma^2{\omega_m}^2 - l}{2}$ $\omega_z = \sqrt{\frac{m + \gamma^2{\omega_m}^4}{2\varepsilon_r}}$ $U_r(\omega) = \omega^6 + p\omega^4 + q\omega^2 + r$ $P_r(\omega) = \varepsilon_r(\omega^2 - {\omega_z}^2)$ $W_r(\omega) = \omega^2 - {\omega_m}^2$

Table 2-11 (Continued.)

$6-2-1$ $N_1 = 2, \quad N_2 = 4$ $1-\gamma > \beta-\alpha$ $\pm\omega_z$ ISB Dependent Transmission Zeros	$k = -\alpha+\beta-\gamma-1$ $l = \alpha-\beta+\gamma-\alpha\beta+\alpha\gamma - \beta\gamma$ $m = \alpha\beta\gamma+\alpha\beta-\alpha\gamma + \beta\gamma$ $n = -\alpha\beta\gamma$ $\omega_m = -k/2$ $U_r(\omega) = \omega^6 + p\omega^4 + q\omega^2 + r$ $P_r(\omega) = \varepsilon_r\omega(\omega^2 - {\omega_z}^2)$ $W_r(\omega) = \omega^2 - {\omega_m}^2$	$p = {\omega_m}^2 + 2k\omega_m + l$ $q = l{\omega_m}^2 + 2m\omega_m + n$ $r = n{\omega_m}^2$ $\varepsilon_r = -(k{\omega_m}^2 + 2l\omega_m + m)$ $\omega_z = \sqrt{\frac{m{\omega_m}^2 + 2n\omega_m}{\varepsilon_r}}$
$6-2-1$ $N_1 = 4, N_2 = 2$ $\beta-\alpha > 1-\gamma$ $\pm\omega_z$ ISB Dependent Transmission Zeros	$k = -\alpha-\beta+\gamma-1$ $l = \alpha+\beta-\gamma+\alpha\beta-\alpha\gamma - \beta\gamma$ $m = \alpha\beta\gamma+\alpha\beta-\alpha\gamma + \beta\gamma$ $n = -\alpha\beta\gamma$ $\omega_m = -k/2$ $U_r(\omega) = \omega^6 + p\omega^4 + q\omega^2 + r$ $P_r(\omega) = \varepsilon_r\omega(\omega^2 - {\omega_z}^2)$ $W_r(\omega) = \omega^2 - {\omega_m}^2$	$p = {\omega_m}^2 + 2k\omega_m + l$ $q = l{\omega_m}^2 + 2m\omega_m + n$ $r = n{\omega_m}^2$ $\varepsilon_r = -(k{\omega_m}^2 + 2l\omega_m + m)$ $\omega_z = \sqrt{\frac{m{\omega_m}^2 + 2n\omega_m}{\varepsilon_r}}$

Table 2-11 (Continued.)

	$P_{rem}(\omega) = (\omega^2 - {\omega_{r1}}^2)(\omega^2 - {\omega_{r2}}^2)$
	$p = \dfrac{\alpha^2 - \beta^2}{2P_{rem}(\alpha)}$
	$q = \dfrac{(\beta^2 - \alpha^2)(\beta^2 - \gamma^2)(\beta^2 - 1)^2}{2P_{rem}(\beta)}$
	$r = \dfrac{\gamma^2 - \beta^2}{2P_{rem}(\gamma)}$
$6 - 6 - 0$	$s = \dfrac{1 - \beta^2}{2P_{rem}(1)}$
$N_1 = 2, \quad N_2 = 4$	
$1 - \gamma > \beta - \alpha$	$m = 0, N_{TZ} < 6$ else $m = 1, N_{TZ} = 6$
$\pm\omega_z$ ISB Dependent Transmission Zeros	$A = (\alpha^2 - \beta^2 + 2qm)(s - r) + p(\gamma^2 - 1)$
	$B = 2(\alpha^2 - \beta^2 + 2qm)(r\gamma^2 - s) - 2\alpha^2 p(\gamma^2 - 1)$
$\pm\omega_{r1}, \pm\omega_{r2},$	$C = (\alpha^2 - \beta^2 + 2qm)(s - r\gamma^4) + (\gamma^2 - 1)(q + p\alpha^4)$
Prescribed	$\omega_m = \sqrt{-C/B},\ P_{rem}(\omega) = 1$
LSB(USB)/USB(LSB) Transmission Zeros	$\omega_m = \sqrt{\dfrac{-B + \sqrt{B^2 - 4AC}}{2A}}, \omega_{r1}, \omega_{r2} > 1$
	In general
	$\omega_m = \sqrt{\frac{-B \pm \sqrt{B^2 - 4AC}}{2A}}$, where, $\gamma < \omega_m < 1$
	$\varepsilon_r = \dfrac{q + p(\alpha^2 - {\omega_m}^2)^2}{\alpha^2 - \beta^2 + qm - pm(\alpha^2 - {\omega_m}^2)^2}$
	$\omega_z = \sqrt{\beta^2 + q(1/\varepsilon_r - m)}$
	$V_1(\omega) = (1/\varepsilon_r - m)(\omega^2 - \alpha^2)(\omega^2 - \gamma^2)(\omega^2 - 1)$
	$V_{-1}(\omega) = (1/\varepsilon_r + m)(\omega^2 - \beta^2)(\omega^2 - {\omega_m}^2)^2$
	$U_r(\omega) = \dfrac{\varepsilon_r}{2}[V_1(\omega) + V_{-1}(\omega)]$
	$P_r(\omega) = \varepsilon_r(\omega^2 - {\omega_z}^2)P_{rem}(\omega)$
	$W_r(\omega) = \omega^2 - {\omega_m}^2, N_{TZ} < 6$
	$W_r(\omega) = \sqrt{1 - {\varepsilon_r}^2}(\omega^2 - {\omega_m}^2), N_{TZ} = 6$

Table 2-11 (Continued.)

$6-6-0$

$N_1 = 2, \qquad N_2 = 4$

$1-\gamma > \beta-\alpha$

$\pm\omega_z$ ISB Dependent Transmission Zeros

$\pm\omega_{r1}, \pm\omega_{r2},$ Prescribed ISB Transmission Zeros

$$P_{rem}(\omega) = (\omega^2 - {\omega_{r1}}^2)(\omega^2 - {\omega_{r2}}^2)$$

$$p = \frac{(\alpha^2-\beta^2)(\alpha^2-\gamma^2)(\alpha^2-1)}{2P_{rem}(\alpha)}$$

$$q = \frac{\beta^2-\alpha^2}{2P_{rem}(\beta)}$$

$$r = \frac{\gamma^2-\alpha^2}{2P_{rem}(\gamma)}$$

$$s = \frac{1-\alpha^2}{2P_{rem}(1)}$$

$$m = 0, N_{TZ} < 6 \text{ else } m = 1, N_{TZ} = 6$$

$$A = (\beta^2 - \alpha^2 + 2pm)(s-r) + q(\gamma^2-1)$$

$$B = 2(\beta^2 - \alpha^2 + 2pm)(r\gamma^2 - s) - 2\beta^2 q(\gamma^2-1)$$

$$C = (\beta^2 - \alpha^2 + 2pm)(s - r\gamma^4) + (\gamma^2-1)(p + q\beta^4)$$

$$\omega_m = \sqrt{-C/B},\ P_{rem}(\omega) = 1$$

$$\omega_m = \sqrt{\frac{-B+\sqrt{B^2-4AC}}{2A}}, \beta < \omega_{r1}, \omega_{r2} < \gamma$$

In general

$$\omega_m = \sqrt{\frac{-B\pm\sqrt{B^2-4AC}}{2A}}, \text{ where, } \gamma < \omega_m < 1$$

$$\varepsilon_r = \frac{p + q(\beta^2 - {\omega_m}^2)^2}{\beta^2 - \alpha^2 + pm - qm(\beta^2 - {\omega_m}^2)^2}$$

$$\omega_z = \sqrt{\alpha^2 + p(1/\varepsilon_r - m)}$$

$$V_1(\omega) = (1/\varepsilon_r - m)(\omega^2-\beta^2)(\omega^2-\gamma^2)(\omega^2-1)$$

$$V_{-1}(\omega) = (1/\varepsilon_r + m)(\omega^2-\alpha^2)(\omega^2 - {\omega_m}^2)^2$$

$$U_r(\omega) = \frac{\varepsilon_r}{2}[V_1(\omega) + V_{-1}(\omega)]$$

$$P_r(\omega) = \varepsilon_r(\omega^2 - {\omega_z}^2)P_{rem}(\omega)$$

$$W_r(\omega) = \omega^2 - {\omega_m}^2, N_{TZ} < 6$$

$$W_r(\omega) = \sqrt{1-{\varepsilon_r}^2}(\omega^2 - {\omega_m}^2), N_{TZ} = 6$$

Table 2-12 Normalized 8th Degree Basis Functions for Direct Synthesis of Dual Bandpass Filters

$$V(\omega) = (\omega^2 - \alpha^2)(\omega^2 - \beta^2)(\omega^2 - \gamma^2)(\omega^2 - 1)$$

Basis Function $(\mathrm{N} - \mathrm{N_{FTZ}} - \mathrm{N_{OTZ}})$	Parametric Equations
$8 - \mathrm{N_{FTZ}} - 0$ $N_1 = 4, \quad N_2 = 4$ max-min tuning points single dependent transmission zeros $\pm\omega_z$ m general prescribed transmission zeros $\pm\omega_n$	If $\omega_n = \infty \; \forall \; n$ $P_{rem}(\omega) = 1$ else $P_{rem}(\omega) = \prod_{n=1}^{m}(\omega^2 - {\omega_n}^2)$ $p = \left.\frac{(\omega^2 - \gamma^2)(\omega^2 - 1^2)}{2P_{rem}(\omega)}\right\|_{\omega=\alpha}$ $q = \left.\frac{(\omega^2 - \gamma^2)(\omega^2 - 1^2)}{2P_{rem}(\omega)}\right\|_{\omega=\beta}$ $s = \left.\frac{(\omega^2 - \alpha^2)(\omega^2 - \beta^2)}{2P_{rem}(\omega)}\right\|_{\omega=\gamma}$ $t = \left.\frac{(\omega^2 - \alpha^2)(\omega^2 - \beta^2)}{2P_{rem}(\omega)}\right\|_{\omega=1}$ $p\left(\frac{1}{\varepsilon_r} - 1\right)(\alpha^2 - {\omega_1}^2)^2 + \alpha^2 - {\omega_z}^2 = 0$ $q\left(\frac{1}{\varepsilon_r} - 1\right)(\beta^2 - {\omega_1}^2)^2 + \beta^2 - {\omega_z}^2 = 0$ $s\left(\frac{1}{\varepsilon_r} + 1\right)(\gamma^2 - {\omega_2}^2)^2 - \gamma^2 + {\omega_z}^2 = 0$ $t\left(\frac{1}{\varepsilon_r} + 1\right)(1^2 - {\omega_2}^2)^2 - 1^2 + {\omega_z}^2 = 0$

$$U_r(\omega) = \frac{1}{2}(1 - \varepsilon_r)(\omega^2 - {\omega_1}^2)(\omega^2 - {\omega_1}^2)(\omega^2 - \gamma^2)(\omega^2 - 1^2) + \frac{1}{2}(1 + \varepsilon_r)(\omega^2 - {\omega_2}^2)(\omega^2 - {\omega_2}^2)(\omega^2 - \alpha^2)(\omega^2 - \beta^2)$$

$$P_r(\omega) = \varepsilon_r(\omega^2 - {\omega_z}^2)P_{rem}(\omega)$$

$$W_r(\omega) = (\omega^2 - {\omega_1}^2)(\omega^2 - {\omega_2}^2)$$

Table 2-12 (Continued.)

Basis Function $(\mathrm{N}-\mathrm{N_{FTZ}}-\mathrm{N_{OTZ}})$	Parametric Equations
$8-\mathrm{N_{FTZ}}-0$ $N_1=4, \quad N_2=4$ min-min tuning points single dependent transmission zeros $\pm\omega_z$ m general prescribed transmission zeros $\pm\omega_n$	If $\omega_n=\infty\ \forall\ n$ $P_{rem}(\omega)=1$ else $P_{rem}(\omega)=\prod_{n=1}^{m}(\omega^2-{\omega_n}^2)$ $p=\left.\frac{1}{2P_{rem}(\omega)}\right\|_{\omega=\alpha}$ $q=\left.\frac{1}{2P_{rem}(\omega)}\right\|_{\omega=\beta}$ $s=\left.\frac{1}{2P_{rem}(\omega)}\right\|_{\omega=\gamma}$ $t=\left.\frac{1}{2P_{rem}(\omega)}\right\|_{\omega=1}$ $p\left(\frac{1}{\varepsilon_r}+1\right)(\alpha^2-{\omega_1}^2)^2(\alpha^2-{\omega_2}^2)^2-\alpha^2+{\omega_z}^2=0$ $q\left(\frac{1}{\varepsilon_r}+1\right)(\beta^2-{\omega_1}^2)^2(\beta^2-{\omega_2}^2)^2-\beta^2+{\omega_z}^2=0$ $s\left(\frac{1}{\varepsilon_r}+1\right)(\gamma^2-{\omega_1}^2)^2(\gamma^2-{\omega_2}^2)^2-\gamma^2+{\omega_z}^2=0$ $t\left(\frac{1}{\varepsilon_r}+1\right)(1^2-{\omega_1}^2)^2(1^2-{\omega_2}^2)^2-1^2+{\omega_z}^2=0$
$U_r(\omega)=\frac{1}{2}(1-\varepsilon_r)(\omega^2-\alpha^2)(\omega^2-\beta^2)(\omega^2-\gamma^2)(\omega^2-1^2)$ $+\frac{1}{2}(1+\varepsilon_r)(\omega^2-{\omega_1}^2)(\omega^2-{\omega_1}^2)(\omega^2-{\omega_2}^2)(\omega^2-{\omega_2}^2)$ $P_r(\omega)=\varepsilon_r(\omega^2-{\omega_z}^2)P_{rem}(\omega)$ $W_r(\omega)=(\omega^2-{\omega_1}^2)(\omega^2-{\omega_2}^2)$	

Table 2-12 (Continued.)

Basis Function $(\mathrm{N}-\mathrm{N}_{\mathrm{FTZ}}-\mathrm{N}_{\mathrm{OTZ}})$	Parametric Equations
$8-\mathrm{N}_{\mathrm{FTZ}}-1$ $N_1=4, \quad N_2=4$ max-min tuning points single dependent transmission zeros $\pm\omega_{\mathrm{z}}$ m general prescribed transmission zeros $\pm\omega_n$	If $\omega_n=\infty\ \forall\ n$ $P_{rem}(\omega)=1$ else $P_{rem}(\omega)=\prod_{n=1}^{m}(\omega^2-{\omega_n}^2)$ $p=\left.\frac{(\omega+\alpha)(\omega+\beta)(\omega-\gamma)(\omega-1)}{2P_{rem}(\omega)}\right\|_{\omega=\alpha}$ $q=\left.\frac{(\omega+\alpha)(\omega+\beta)(\omega-\gamma)(\omega-1)}{2P_{rem}(\omega)}\right\|_{\omega=\beta}$ $s=\left.\frac{(\omega-\alpha)(\omega-\beta)(\omega+\gamma)(\omega+1)}{2P_{rem}(\omega)}\right\|_{\omega=\gamma}$ $t=\left.\frac{(\omega-\alpha)(\omega-\beta)(\omega+\gamma)(\omega+1)}{2P_{rem}(\omega)}\right\|_{\omega=1}$ $p(\alpha-\omega_1)^2(\alpha+\omega_2)^2+\alpha\varepsilon_r(\alpha^2-{\omega_z}^2)=0$ $q(\beta-\omega_1)^2(\beta+\omega_2)^2+\beta\varepsilon_r(\beta^2-{\omega_z}^2)=0$ $s(\gamma+\omega_1)^2(\gamma-\omega_2)^2-\gamma\varepsilon_r(\gamma^2-{\omega_z}^2)=0$ $t(1+\omega_1)^2(1-\omega_2)^2-\varepsilon_r(1^2-{\omega_z}^2)=0$ $U_r(\omega)=\frac{1}{2}(\omega-\alpha)(\omega-\beta)(\omega+\gamma)(\omega+1)(\omega+\omega_1)^2(\omega-\omega_2)^2$ $+\frac{1}{2}(\omega+\alpha)(\omega+\beta)(\omega-\gamma)(\omega-1)(\omega-\omega_1)^2(\omega+\omega_2)^2$ $P_r(\omega)=\varepsilon_r(\omega^2-{\omega_z}^2)P_{rem}(\omega)$ $W_r(\omega)=(\omega^2-{\omega_1}^2)(\omega^2-{\omega_2}^2)$

Table 2-12 (Continued.)

Basis Function $(\mathrm{N}-\mathrm{N_{FTZ}}-\mathrm{N_{OTZ}})$	Parametric Equations
$8-\mathrm{N_{FTZ}}-1$ $N_1=4, \quad N_2=4$ min-min tuning points single dependent transmission zeros $\pm\omega_z$ m general prescribed transmission zeros $\pm\omega_n$	If $\omega_n=\infty\ \forall\ n$ $P_{rem}(\omega)=1$ else $P_{rem}(\omega)=\prod_{n=1}^{m}(\omega^2-{\omega_n}^2)$ $p=\left.\frac{(\omega+\alpha)(\omega+\beta)(\omega+\gamma)(\omega+1)}{2P_{rem}(\omega)}\right\vert_{\omega=\alpha}$ $q=\left.\frac{(\omega+\alpha)(\omega+\beta)(\omega+\gamma)(\omega+1)}{2P_{rem}(\omega)}\right\vert_{\omega=\beta}$ $s=\left.\frac{(\omega+\alpha)(\omega+\beta)(\omega+\gamma)(\omega+1)}{2P_{rem}(\omega)}\right\vert_{\omega=\gamma}$ $t=\left.\frac{(\omega+\alpha)(\omega+\beta)(\omega+\gamma)(\omega+1)}{2P_{rem}(\omega)}\right\vert_{\omega=1}$ $p(\alpha-\omega_1)^2(\alpha-\omega_2)^2-\alpha\varepsilon_r(\alpha^2-{\omega_z}^2)=0$ $q(\beta-\omega_1)^2(\beta-\omega_2)^2-\beta\varepsilon_r(\beta^2-{\omega_z}^2)=0$ $s(\gamma-\omega_1)^2(\gamma-\omega_2)^2-\gamma\varepsilon_r(\gamma^2-{\omega_z}^2)=0$ $t(1-\omega_1)^2(1-\omega_2)^2-\varepsilon_r(1^2-{\omega_z}^2)=0$ $U_r(\omega)=\frac{1}{2}(\omega-\alpha)(\omega-\beta)(\omega-\gamma)(\omega-1)(\omega+\omega_1)^2(\omega+\omega_2)^2$ $+\frac{1}{2}(\omega+\alpha)(\omega+\beta)(\omega+\gamma)(\omega+1)(\omega-\omega_1)^2(\omega-\omega_2)^2$ $P_r(\omega)=\varepsilon_r(\omega^2-{\omega_z}^2)P_{rem}(\omega)$ $W_r(\omega)=(\omega^2-{\omega_1}^2)(\omega^2-{\omega_2}^2)$

The requirement to have at least a single pair of dependent transmission zeros is evident when a lowest degree basis function is considered. A 4th degree general (symmetric/asymmetric) basis function can only be constrained to pass through all the prescribed cutoff points ($\pm\alpha$, $\pm\beta$, $\pm\gamma$ and $\pm1(\delta)$) if and only if there is a single

pair of symmetrical transmission zeros for real reflection zeros. In general this applies to all the basis functions. The only exception to this is in the case of some symmetrical basis functions, only because symmetry provides some redundancy as the 4-0-1 basis function shows in Table 2-10.

2.5 Procedure for Generating the Filter Characteristic Polynomials

The following procedure may be adopted for computing Chebyshev characteristic functions for microwave filter synthesis.

1. Pre-Calculated Basis Functions Use the calculated basis functions as tabulated in section 2.4.1 to 2.4.7
2. Desired Transfer Function Given the filter specifications and required topology, determine the basis functions required and their weighting integers based on the number and position of reflection and transmission zeros.
3. Characteristic Polynomials Apply general recursive technique of section 2.3 to determine the characteristic polynomials F and P. Use suitable V polynomial for each filtering function.
4. CM Synthesis or Cascaded Synthesis Proceed with filter synthesis as described in Chapter 1

The whole procedure can easily be programmed using MATLAB or any similar software. The examples in the next section will illustrate this procedure and show how the principles described earlier may be applied for different filtering functions. Further applied examples are given in Chapter 3 to Chapter 6.

2.6 Examples

Two examples are given to demonstrate the synthesis method presented above. The first one is on direct synthesis of a distributed Chebyshev low-pass filter and the second one is direct synthesis of a distributed bandpass filter. The same principles apply to other filtering functions as will be demonstrated in later Chapters.

2.6.1 Direct Synthesis of Generalised Distributed Chebyshev Low-pass Filter

Consider a distributed low-pass filter with the specification as shown in Table 2-13 below. In order to achieve the above specifications a single real axis half transmission zero pair at infinity ($\theta_z = \pm j\infty$), six transmission zeros at quarter-wave frequency ($\theta_z = \pm 90^o$) and a pair of symmetrical transmission zeros where placed at $\theta_z = \pm 58.23^o$ to yield a 9th degree distributed low-pass filter as shown in Fig. 2-5. The basis functions choice is shown in Table 2-14. This gives an overall 9-2-6 characteristic function. A real axis half transmission zero pair at infinity was included to enable realisation in a meander-like circuit topology explained in Chapter 3.

Table 2-13 Specification for a Distributed Low-pass Filter Example 2.6.1

Cutoff frequency (f_c)	1 GHz
Electrical Length at Cutoff Frequency (θ_c)	$\pm 45^o$
Passband Return Loss (RL)	20 dB
Stopband Insertion loss (ILs) at 1.3 GHz	70 dB

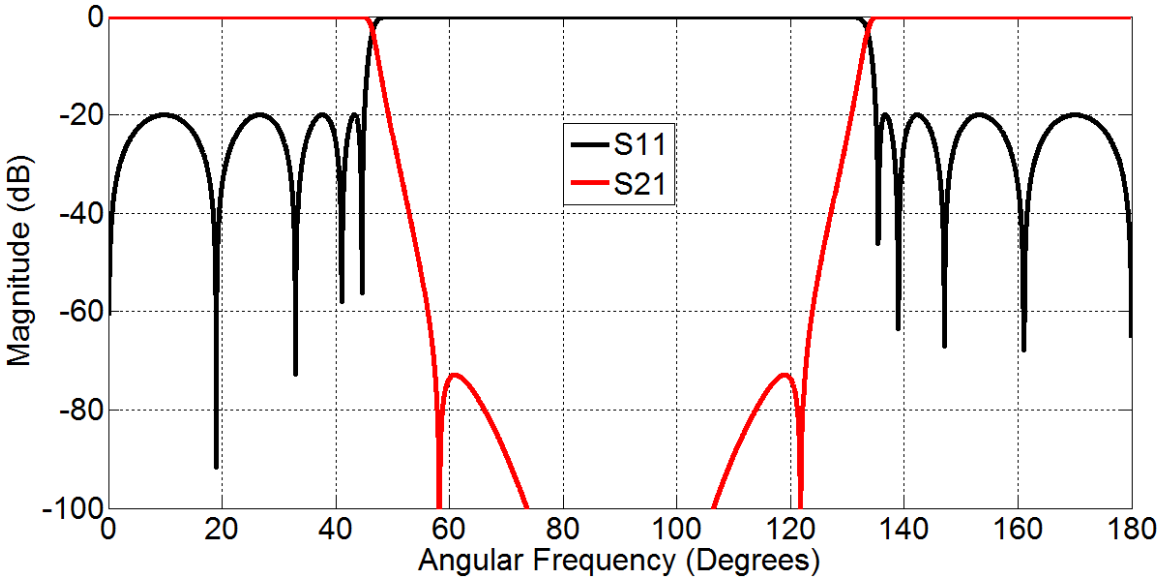

Fig. 2-5 Simulated response of design example 2.6.1

The characteristic polynomials were then computed using the general recursive technique of section 2.3 with the basis functions of Table 2-14. The ABCD matrix polynomials may be obtained as described in Chapter 1. Table 2-15 gives the characteristic polynomials and ABCD matrix polynomials. Synthesis of network elements easily follows from the ABCD matrix using cascaded synthesis described in Chapter 1.

Table 2-14 Basis Functions for a Distributed Chebyshev Low-pass Filter

α_r	N-N_{FTZ}-N_{90^o}	Purpose
1	$1-0-0$	Provide a single real axis half transmission zero pair at infinity ($\theta_z = \pm j\infty$)
6	$1-0-1$	Provide six transmission zeros at quarter-wave frequency ($\theta_z = \pm 90^o$)
1	$2-2-0$	Provide a pair of symmetrical transmission zeros at $\theta_z = \pm 58.23^o$ (1.294 GHz)

Table 2-15 $9-2-6$ Distributed Low-pass Filter Polynomials

Characteristic Polynomials

($\varepsilon = 64.5141,\ \mu = 1$)

$$P(\rho) = (\rho^2 + 2.6073)\sqrt{1-\rho^2}$$

$$F(\rho) = \rho^9 + 2.2673\rho^7 + 1.7161\rho^5 + 0.4817\rho^3 + 0.0365\rho$$

$$E(\rho) = \rho^9 + 1.9478\rho^8 + 4.1643\rho^7 + 4.9683\rho^6 + 5.2931\rho^5 + 3.9665\rho^4 + 2.3988\rho^3 + 1.0161\rho^2 + 0.2896\rho + 0.0404$$

ABCD Matrix Polynomials

$$A(\rho) = 1.9478\rho^8 + 4.9683\rho^6 + 3.9665\rho^4 + 1.0161\rho^2 + 0.0404$$

$$B(\rho) = 2\rho^9 + 6.4316\rho^7 + 7.0091\rho^5 + 2.8806\rho^3 + 0.3260\rho$$

$$C(\rho) = 1.8971\rho^7 + 3.5770\rho^5 + 1.9171\rho^3 + 0.2531\rho$$

$$D(\rho) = 1.9478\rho^8 + 4.9683\rho^6 + 3.9665\rho^4 + 1.0161\rho^2 + 0.0404$$

2.6.2 Direct Synthesis of Generalised Distributed Bandpass Filter

In this example, a distributed bandpass filter is considered with specifications as shown in Table 2-16. A six degree ($N_r = N/2 = 6$) bandpass filter was synthesised by placing transmission zeros according to the basis functions in Table 2-17. For realisation using combline bandpass filter resonators, a single transmission zero at the origin ($\theta_z = 0^o$) is required which is provided for by the 2-0-1 basis function. Two transmission zeros were placed at finite frequencies to increase close-to-band rejection and the rest of the transmission zeros were placed at a quarter-wave frequency ($\theta_z = 90^o$). Because transmission zeros are asymmetrically located at $\theta_z = 0^o$ and $\theta_z = 90^o$, the distributed bandpass filter is asymmetrical in nature with more selectivity on the upper stopband.

Table 2-16 Distributed Bandpass Filter Specifications

Centre frequency (f_o)	2 GHz
Electrical Length at Centre Frequency (θ_o)	45^o
Filter Bandwidth	50 MHz
Passband Return Loss (RL)	$\geq 20\ dB$
Stopband Insertion loss (ILs) $DC - 1.964\ GHz$ and $2.036 - 3\ GHz$	$\geq 40\ dB$

Table 2-17 Basis Functions for a Distributed Chebyshev Bandpass Filter

α_r	N-N_{FTZ}-N_{0^o}	Purpose
3	$2-0-0$	Provide six quarter-wave frequency transmission zeros ($\theta_z = 90^o$)
1	$2-0-1$	Provide a single quarter-wave frequency transmission zero ($\theta_z = 90^o$) and a single transmission zero at the origin ($\theta_z = 0^o$)
2	$2-2-0$	Provide two pairs of symmetrical transmission zeros at $\theta_z = \pm 44.155^o$ and $\pm 45.825^o$

As before, once the basis functions are determined the characteristic polynomials are determined using the general recursive technique of section 2.3. Table 2-18

shows the characteristic polynomials and the Y matrix polynomials. Using the methods described in Chapter 1, the transverse coupling matrix is obtained from the Y matrix polynomials of Table 2-18 and first converted to an arrow coupling matrix and then to two cascaded trisections. Table 2-19 shows a $N_r \times N_r$ final coupling matrix in distributed domain.

Table 2-18 12-4-1 Distributed Bandpass Filter Polynomials

Characteristic Polynomials

($\varepsilon = 2.2487 \times 10^6,\ \mu = 1$)

$$P(\rho) = \rho^5 + 2.0020\rho^3 + 0.9986\rho$$

$$F(\rho) = \rho^{12} + 6.0041\rho^{10} + 15.0180\rho^8 + 20.0311\rho^6 + 15.0262\rho^4 + 6.0107\rho^2 + 1.0017$$

$$E(\rho) = \rho^{12} + 0.0779\rho^{11} + 6.0071\rho^{10} + 0.3899\rho^9 + 15.0301\rho^8 + 0.7802\rho^7 + 20.0493\rho^6 + 0.7805\rho^5 + 15.0384\rho^4 + 0.3903\rho^3 + 6.0137\rho^2 + 0.0780\rho + 1.0017$$

Y Matrix Polynomials

$$Y_{11n}(\rho) = 0.0779\rho^{11} + 0.3899\rho^9 + 0.7802\rho^7 + 0.7805\rho^5 + 0.3903\rho^3 + 0.0780\rho = Y_{22n}(\rho)$$

$$Y_{21n}(\rho) = Y_{12n}(\rho) = -(\rho^5 + 2.0020\rho^3 + 0.9986\rho)/\varepsilon$$

$$Y_{den}(\rho) = 2\rho^{12} + 12.0112\rho^{10} + 30.0481\rho^8 + 40.0804\rho^6 + 30.0646\rho^4 + 12.0244\rho^2 + 2.0033$$

An approximation method by Wenzel [57] was used to convert the distributed bandpass filter network with coupling matrix given in Table 2-19 to a capacitively loaded combline distributed bandpass filter. The resulting filter topology is shown in Fig. 2-6. The final scaled bandpass filter circuit elements in 50 Ohm system are shown in Table 2-20. The circuit elements in Table 2-20 were simulated in circuit simulator as shown in Fig. 2-7. To complete the filter design requires the computation of the coupling bandwidths, resonance frequencies of each resonator as well as the external quality factor and from these the physical dimensions may be determined using experimental EM modelling and simulations techniques as described in Chapter 1.

Table 2-19 $N_r \times N_r$ Coupling Matrix of a 12-4-1 Distributed Bandpass Filter

$$Y_{BP} = M_{Ts} + \rho M_{Ls} + \frac{1}{\rho} M_{Ls}, \qquad \rho = jt = jtan(a\omega), \qquad a = \frac{T_o}{\omega_o}$$

$$M_{Ts} = \begin{bmatrix} 0.0389 & 0 & 0 & 0 & 0 & 0 \\ 0 & 0.0000 & 0 & 0 & 0 & 0 \\ 0 & 0 & 0.0000 & 0 & 0 & 0 \\ 0 & 0 & 0 & 0.0000 & 0 & 0 \\ 0 & 0 & 0 & 0 & 0.0000 & 0 \\ 0 & 0 & 0 & 0 & 0 & 0.0389 \end{bmatrix}$$

$$M_{Cs} = \begin{bmatrix} 1 & -0.0292 & 0 & 0 & 0 & 0 \\ -0.0292 & 1 & 0.0000 & 0 & 0 & 0 \\ 0 & 0.0000 & 1 & 0.0000 & 0 & 0 \\ 0 & 0 & 0.0000 & 1 & 0.0000 & 0 \\ 0 & 0 & 0 & 0.0000 & 1 & 0.0000 \\ 0 & 0 & 0 & 0 & 0.0000 & 1 \end{bmatrix}$$

$$M_{Ls} = \begin{bmatrix} +0.9993 & 0.0000 & -0.0153 & 0 & 0 & 0 \\ 0.0000 & +0.9784 & -0.0199 & 0 & 0 & 0 \\ -0.0153 & -0.0199 & +1.0026 & -0.0228 & 0 & 0 \\ 0 & 0 & -0.0228 & +0.9991 & -0.0198 & -0.0157 \\ 0 & 0 & 0 & -0.0198 & +1.0234 & -0.0286 \\ 0 & 0 & 0 & -0.0157 & -0.0286 & +1.0010 \end{bmatrix}$$

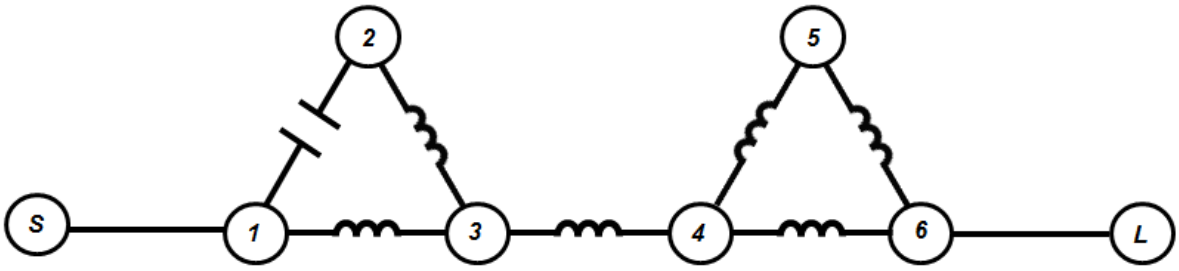

Fig. 2-6 Illustration of a 6th degree bandpass filter example 2.6.2 implemented using two cascaded trisections showing inductively and capacitively coupled shunt LC resonator nodes (circled)

2.7 Conclusion

Chapter 2 has demonstrated a method of generating the generalised Chebyshev characteristic function. This method was described in section 2.2, from which an algorithm for computing the overall characteristic function may be determined as it

was described in section 2.3. The basis functions for different filtering functions may be determined as was explained in section 2.4. Tables of these basis functions for typical filtering functions were also given. Two illustrative examples were then given in section 2.6 to demonstrate the synthesis technique. In Chapters 3 to 6, numerous other synthesis examples are given using this synthesis approach. In Chapter 3, a new class of low-pass filter realisation is explained.

Table 2-20 Final Element Values of a Capacitively Loaded Distributed Bandpass Filter

Capacitors	Inductive Inter-resonator Coupling Impedances	Short-Circuited Stubs Impedance $Z_r = 75\ \Omega$
$C_1 = 1.0618\ pF$ $C_2 = 1.0803\ pF$ $C_3 = 1.0589\ pF$ $C_4 = 1.0620\ pF$	$Z_{13} = 5995.0\ \Omega$ $Z_{23} = 4574.2\ \Omega$ $Z_{34} = 4019.2\ \Omega$ $Z_{45} = 4679.9\ \Omega$	Input/Output Coupling Impedance (Ω) $K_{input} = 343.0421$ $K_{output} = 343.1379$
$C_5 = 1.0413\ pF$ $C_6 = 1.0604\ pF$	$Z_{46} = 5820.8\ \Omega$ $Z_{56} = 3234.8\ \Omega$	Capacitive Inter-resonator Coupling Impedance $Z_{12} = 3114.9\ \Omega$

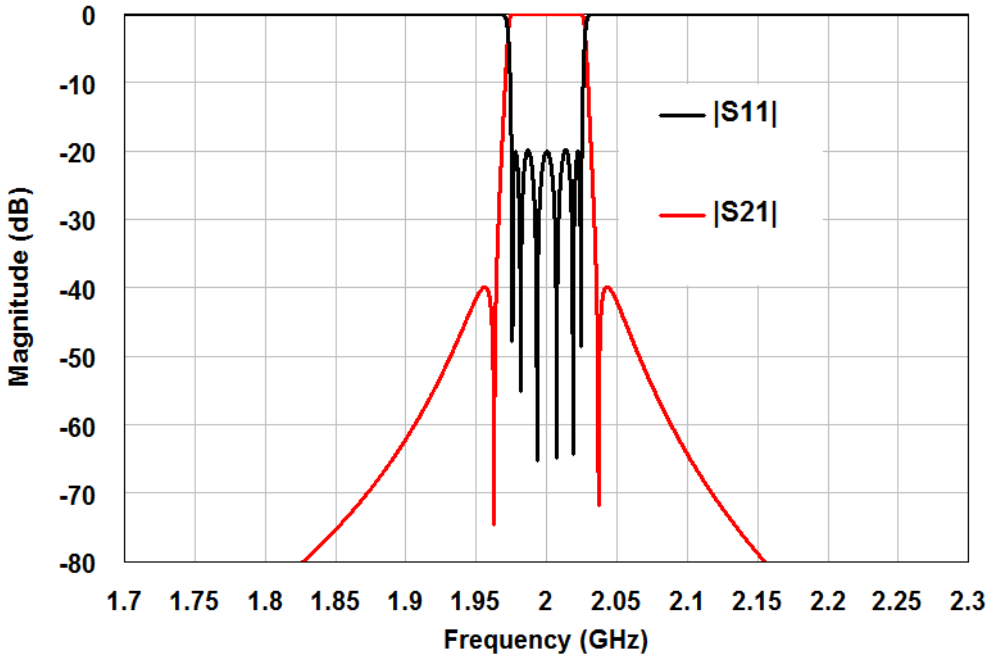

Fig. 2-7 Simulated response of the distributed bandpass example 2.6.2

Chapter 3 Synthesis and Realisation of a New Class of Distributed Low-pass Filters

3.1 Introduction

Low-pass filters are often needed in microwave systems to ‘clean up’ spurious responses in the stopband of coaxial and dielectric resonator filters. The most important driving factors in their design are compact size, sharp roll-off and wide stopband. Some of the recent works have addressed some of these problems [58, 59]. Although it is relatively easy to obtain theoretical circuit models, the challenge in practical low-pass filters lies in achieving good approximation using real transmission line components.

There exist many realisations for low-pass filters. One popular type is the stepped impedance low-pass filter consisting of interconnections of commensurate lengths of transmission lines of alternating low and high impedance [4]. This type of filter has low selectivity for a given network order because the transmission zeros are all at infinity on the real axis in the complex plane.

In order to increase selectivity, transmission zeros may be placed at finite frequencies using distributed generalised Chebyshev low-pass prototype filters [11]. The problem is that there is no direct realisation of the series short circuited stubs associated with this low-pass prototype filter. In the existing physical realisation [60] the series short circuited stubs are approximated by short lengths of high impedance transmission line (forcing those transmission zeros at a quarter-wave frequency to move to infinity on the real axis), while the shunt series foster is realised exactly as an open circuited stub of double unit length. The approximation involved results in relatively poor stopband rejection.

This Chapter presents two original solutions [61, 62] in which the series short circuited stubs are exactly realised within the equivalent circuit of the low-pass filter. In section 3.2, the synthesis technique for the two physical realisations has

been developed. Furthermore, the synthesis for the general realisation for the proposed structure is developed and presented together with the required canonical low-pass circuit forms and corresponding transmission zeros that the transfer functions may realise. The procedure for different low-pass filter degrees is included with the required circuit transformations. Design examples are included to illustrate the synthesis and design technique. Analytical comparisons with state-of-the-art were also given in section 3.2.3.

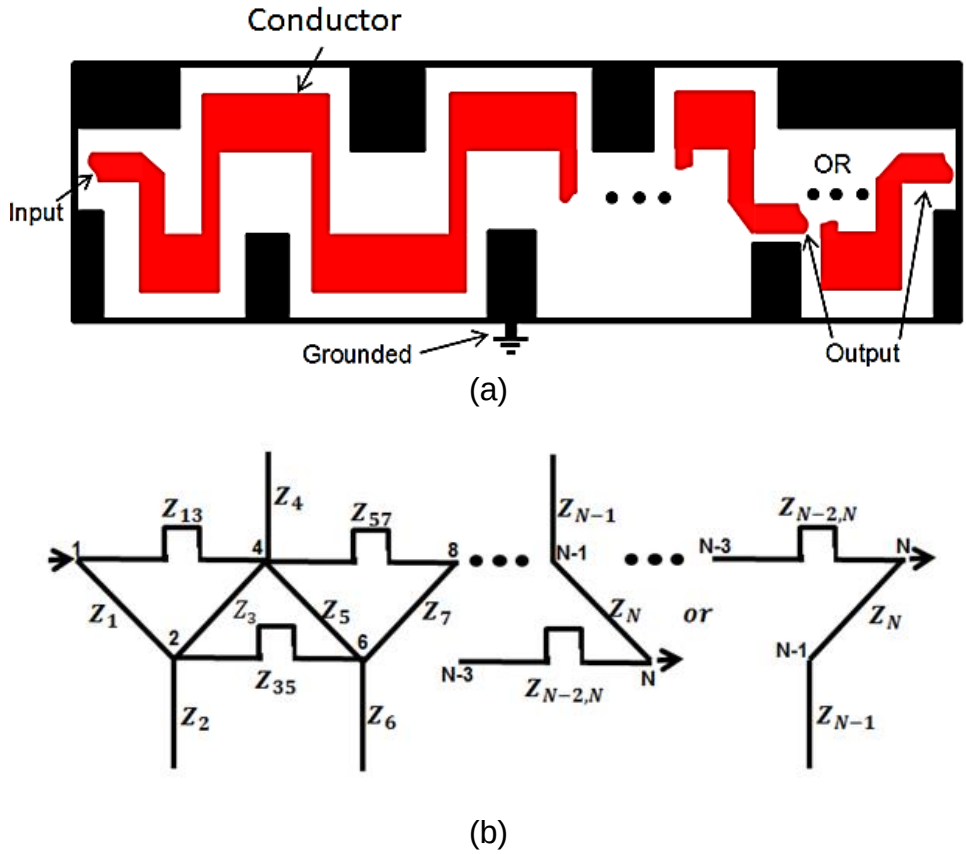

Fig. 3-1 Proposed layout of meander-like low-pass filter (a) composed of a section of high impedance parallel coupled lines short circuited by a low impedance open circuited stub at alternate ends (b) graphical line equivalent circuit

3.2 Design Theory

In Fig. 3-1, the general physical layout is given for the proposed method. The structure consists of a middle section of high impedance coupled transmission lines terminated at every alternate end in a low impedance open-circuit stub forming a ‘meander-like’ structure as in Fig. 3-1. All the transmission lines are of

commensurate length. Grounded decoupling walls must be utilised to eliminate coupling between the open-circuited stubs.

In this work it is shown how a general Chebyshev transfer function may be used to implement two alternative realisations arising from Fig. 3-1 via a series of derived circuit transformations and one of the earlier transformation derived by Sato in Table I of [63]. The synthesis of distributed low-pass filter networks is based on work done in [52, 53]. Fig. 3-2 shows the derived equivalent circuit transformations and the required admittance relationships.

Transformation I

$$y_0 = y_2(y_1 + y_3 + y_4) + y_3(y_1 + y_4)$$

$$y_a = \frac{y_1 y_2 y_3}{y_0}$$

$$y_b = \frac{{y_3}^2(y_1 + y_2 + y_4)}{y_0}$$

$$y_c = \frac{y_2 y_3 y_4}{y_0}$$

$$y_{ab} = \frac{y_1 y_4 (y_2 + y_3)}{y_0}$$

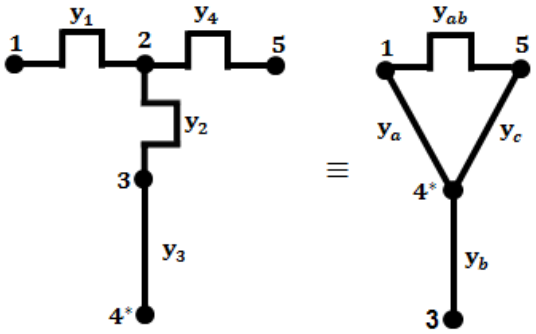

Transformation II

$$y_0 = y_1 + y_2 + y_3$$

$$y_a = \frac{y_1 y_2}{y_0}$$

$$y_c = \frac{y_2 y_3}{y_0}$$

$$y_b = \frac{{y_2}^2}{y_0}$$

$$y_{ab} = \frac{y_1 y_3}{y_0}$$

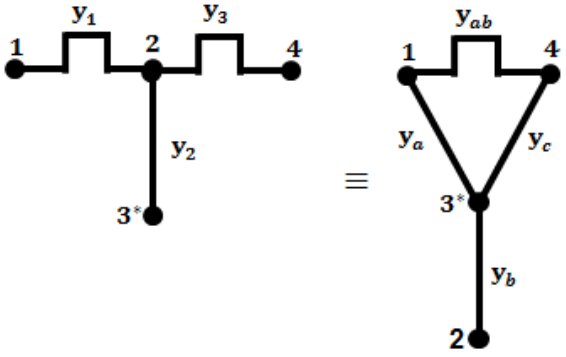

Fig. 3-2 Derived equivalent circuit transformations (*May be a hanging node)

Transformation III

Choose y_b

$$y_a = y_1 + y_2 - y_b$$

$$y_{ab} = \frac{y_a(y_2 - y_b)}{y_1}$$

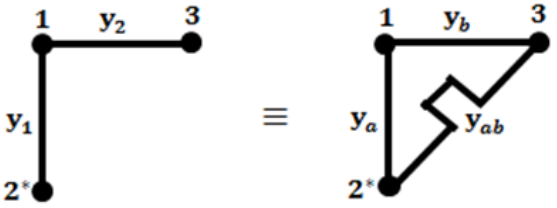

Transformation IV

$$A = \frac{4{y_1}^2 y_4(y_3 + y_4 + y_5)}{{y_2}^2 y_3 y_5}$$

$$B = \frac{4y_1 y_4(2y_3 y_5 + 2y_4 y_5 + {y_5}^2)}{y_2 y_3 y_5}$$

$$C = \frac{y_5({y_3}^2 + 4{y_4}^2 + 4y_3 y_4)}{y_3}$$

$$y_a = \frac{-B \pm \sqrt{B - 4AC}}{2A}$$

$$y_b = \sqrt{y_a\left(y_5 - \frac{y_a y_1}{y_2}\right)}$$

$$y_c = \frac{y_3 y_5 y_a}{2y_4 y_b}$$

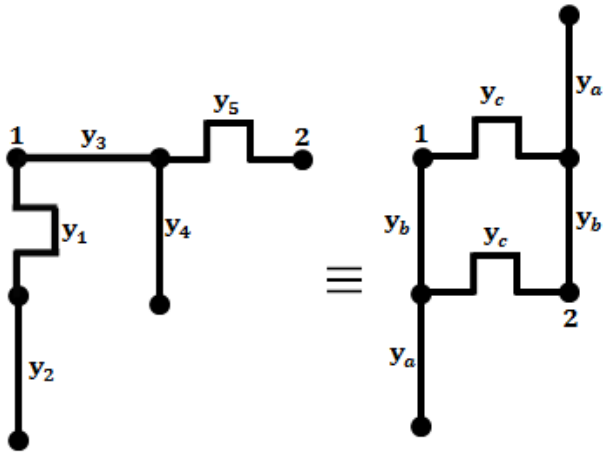

Transformation V

$$y_{ab} = y_{bc}$$

$$y_b = y_2 + 2\sqrt{y_2 y_{12}}$$

$$y_{ab} = 2y_{12} + \sqrt{y_2 y_{12}}$$

$$y_o = y_b + 2y_{ab}$$

$$y_a = y_1 - \frac{y_b y_{ab}}{y_o}$$

$$y_c = y_3 - \frac{y_b y_{ab}}{y_o}$$

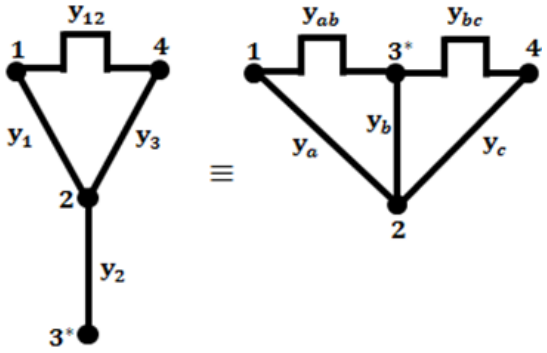

Fig. 3-2 (Continued.) Derived equivalent circuit transformations (*May be a hanging node)

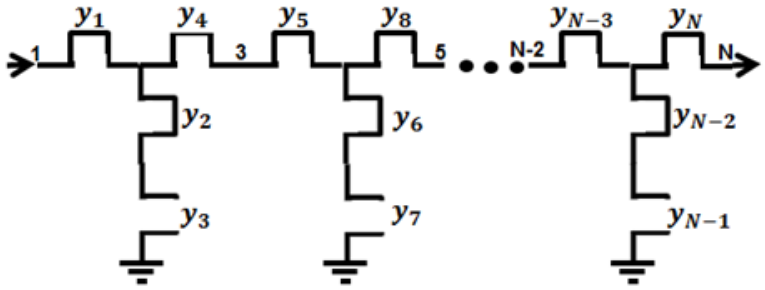

Fig. 3-3 Generalised Chebyshev distributed low-pass prototype filter

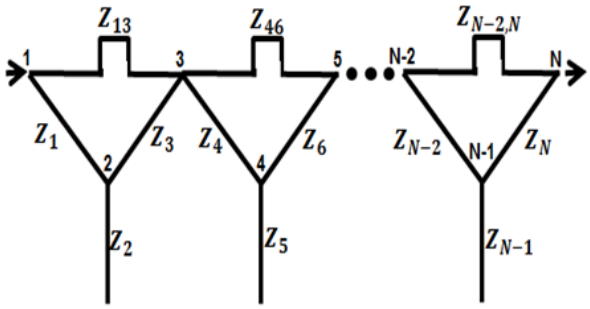

Fig. 3-4 Graphical representation of the equivalent circuit of Fig. 3-3 after transformation of the 3rd degree basic sections

The next two sections describe how these transformations were used to derive the equivalent circuit for the two possible physical realisations from their canonical low-pass filter derivatives.

Physical Realisation I

The first physical realisation realises the equivalent circuit for the general Chebyshev distributed network given in Fig. 3-3. By using the synthesis technique given in Chapter 1 and Chapter 2, the network of Fig. 3-3 may be synthesized directly in distributed domain from an N^{th} (N odd) degree Chebyshev transfer function with $(N-1)/2$ pairs of symmetrically located transmission zeros ($\pm\theta_z$) and a single transmission zero at a quarter-wave frequency ($\theta_z = \pm 90^o$). In general, therefore, the distributed network of Fig. 3-3 is of the form N-$(N-1)/2$-1. Using circuit transformation I on each of the 3rd degree section, Fig. 3-3 may be transformed into Fig. 3-4. It is then clear from Fig. 3-4 that each of the 3rd degree sections is just the equivalent circuit of a pair of two parallel coupled lines with one end terminated in an open circuited stub as depicted in Fig. 3-5. The overall network after the transformation is illustrated in Fig. 3-6. This is equivalent to Fig. 3-1 but with every second coupling between the parallel coupled lines section

removed (i.e. couplings Z_{35}, Z_{79}, … removed in Fig. 3-1(b)), such that the structure is composed of cascaded 3rd degree basic sections of Fig. 3-5 as shown in Fig. 3-6.

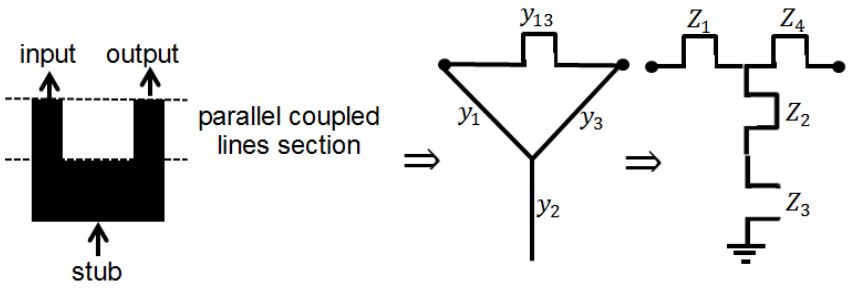

Fig. 3-5 A basic section containing a pair of coupled line and a stub and its equivalent circuits

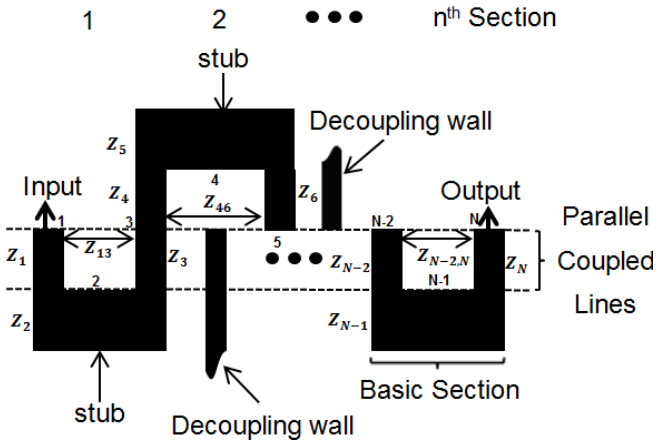

Fig. 3-6 Physical layout for generalised Chebyshev distributed low-pass filter

3.2.1.1 Design Example

To demonstrate the physical realisation I, a 7th degree low-pass filter was designed using the techniques described above with cutoff frequency at 1 GHz, 20 dB minimum passband return loss with pairs of finite transmission zeros at $\theta_z = \pm 54.44^o$, $\pm 43.00^o$ and $\pm 54.44^o$ (2.18, 1.72 and 2.18 GHz) and a single quarter-wave transmission zero ($\theta_z = \pm 90^o$) and electrical length at the cutoff frequency, $\theta_c = 25^o$.The element values are shown in Table 3-1 corresponding to the circuit of Fig. 3-3 Generalised Chebyshev distributed low-pass prototype filter where symmetry is assumed for the element values. Using the circuit transformation I, the circuit was transformed to the final form of Fig. 3-4 with the element values shown

in Table 3-2. All the element values are clearly realizable. Fig. 3-7 shows the circuit simulation of the design example.

Table 3-1 7^{th} Degree Low-pass Filter Synthesised Admittance Values $(\mho)$

Section I	Section II	Section III
$y_1 = 0.4983$	$y_5 = 0.5830$	$y_9 = 0.4983$
$y_2 = 5.5807$	$y_6 = 2.5671$	$y_{10} = 5.5807$
$y_3 = 2.8517$	$y_7 = 2.9514$	$y_{11} = 2.8517$
$y_4 = 0.4983$	$y_8 = 0.5830$	$y_{12} = 0.4983$

Table 3-2 7^{th} Degree Low-pass Filter Impedance Values (Ω) After Transformation II (A)-(C) in $50\ \Omega$ system

Section I	Section II	Section III
$Z_1 = 153.3$	$Z_4 = 158.6$	$Z_7 = 153.3$
$Z_2 = 22.73$	$Z_5 = 21.54$	$Z_8 = 22.73$
$Z_3 = 153.3$	$Z_6 = 158.6$	$Z_9 = 153.3$
$Z_{13} = 580.7$	$Z_{46} = 373.5$	$Z_{79} = 580.7$

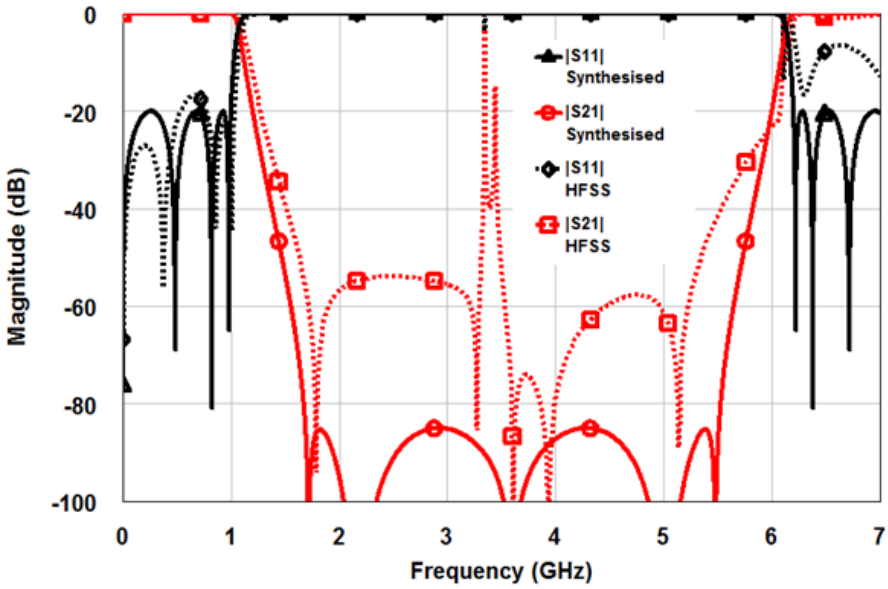

Fig. 3-7 Circuit and HFSS simulation response for design example 3.2.1.1

In this realisation I, $\theta_c = 25^o$ is approaching the practical limits for realisable element values. Reducing the electrical length at the cutoff frequency further causes the impedance values of the high and low impedance lines to become unrealisably high and low respectively. However, in reality the practical stopband bandwidth is perturbed due to high order modes and spurious couplings between the basic sections as shown by the HFSS simulation in Fig. 3-7 with small resonance peaks around $\theta = 90^o$. The decoupling walls do not give exact circuit realisation for realisation I. In the second physical realisation, however, some of the couplings are allowed between the basic sections.

3.2.2 Physical Realisation II – 'Meander-like' Low-pass Filter

A more general realisation is achieved by using the layout of Fig. 3-1. The only difference with the previous physical realisation I is that, in the general case (physical realisation II) all the couplings between high impedance coupled lines of Fig. 3-1 are allowed. The structure is built from the basic 3rd degree section of Fig. 3-5 by adding a parallel line to the parallel coupled lines section and an open circuited stub at one end to form an interconnect each time to increase the network degree by 2.

The stripline layout for physical realisation II is given in Fig. 3-8 and its derived equivalent circuit is shown below in Fig. 3-9 with the unit element impedance values named sequentially from input to output. This realisation is optimal since an N^{th} degree filter requires N commensurate length transmission lines. At the quarter-wave frequency, all the series short circuited stubs become open circuited while all the open circuited stubs become short circuited so that the alternate ends of the parallel coupled lines are shorted to ground. Thus the meander-like low-pass filter of Fig. 3-8 has at least one transmission zero at the quarter-wave frequency. The other transmission zero pairs may exist at infinity on the real axis or as symmetrical pure imaginary frequency pair or in general as paraconjugated pairs on the complex plane due to multipath in the structure.

It is now shown how the meander-like low-pass filter network of Fig. 3-8 and Fig. 3-9 may be synthesized from suitable low-pass filter networks and then using

appropriate circuit transformation to transform the canonical low-pass filter network forms to a meander-like low-pass filter. The canonical low-pass filter network forms were obtained by the synthesis method in Chapter 1 and Chapter 2 and then applying cascaded synthesis. The 3rd, 5th, 7th and 9th degree meander-like low-pass filter are examined next as depicted in Fig. 3-10.

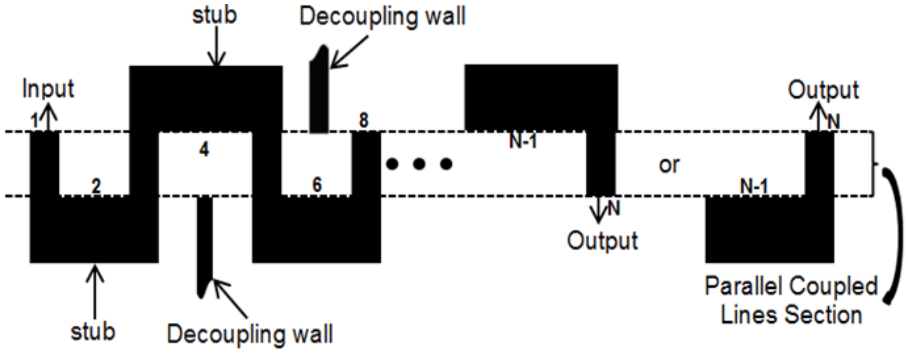

Fig. 3-8 Physical layout of the striplines for the general meander-like low-pass filter

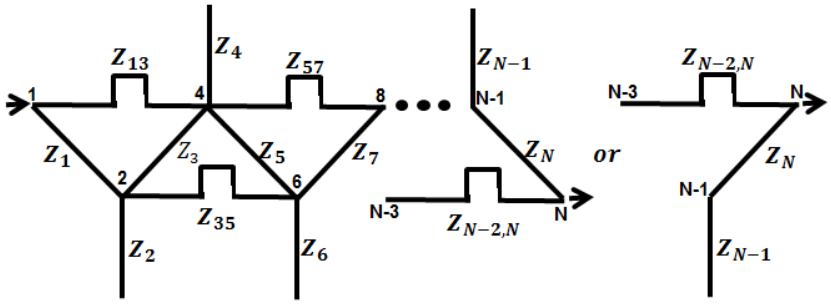

Fig. 3-9 Graphical representation of the equivalent circuit of Fig. 3-8 for a meander-like low-pass filter

The 3rd degree filter is simply a trivial case corresponding to circuit transformation I as shown in Fig. 3-10(I). In this case a 3-0-3 or 3-2-1 low-pass filter may be realised.

There are two possible cases for 5th degree filter, namely 5-0-4 and 5-2-2 low-pass filters. For the first case of Fig. 3-10 (II), a 5-0-4 low-pass filter has a single real axis half transmission zero pair at infinity ($\theta_z = \pm j\infty$) and four transmission zeros are at a quarter-wave frequency ($\theta_z = \pm 90^o$). Beginning with the canonical network form, step 1 is to split the transmission lines into two equal parts between port 2 and 4. In step 2, transformation III is carried out on each of the branch 3,2,4 and 2,4,5 respectively. Finally in step 3, two separate transformations II are carried out on each of the three port subnetworks of 1,3,5 and 3,5,6 to derive the final equivalent circuit as illustrated in Fig. 3-10 (II).

Transformation I

N=3 (3-2-1)

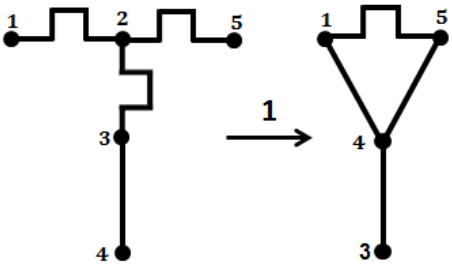

Transformation II

N=5 (5-0-4)

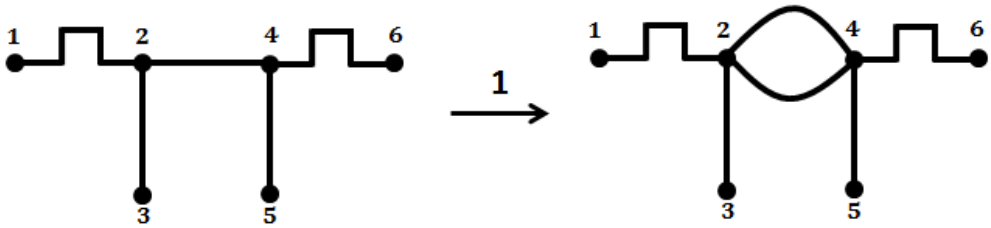

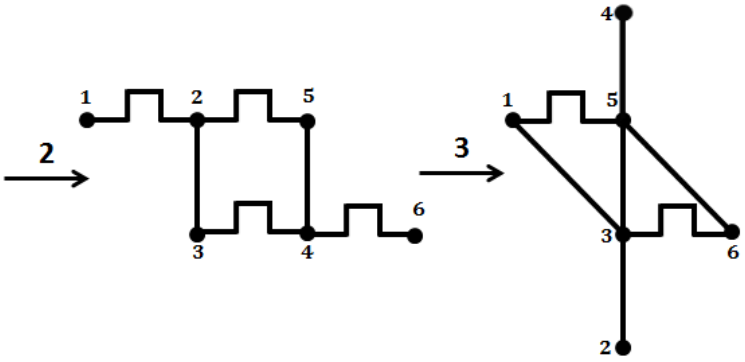

Transformation III

N=5 (5-2-2)

Asymmetrical

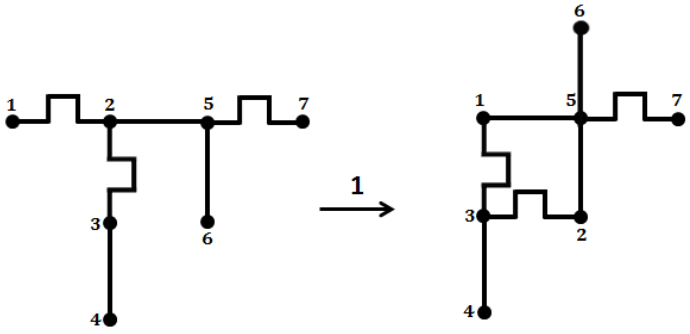

Fig. 3-10 Derived network transformation for $N = 3,5,7$ and 9 meander-like low-pass filters

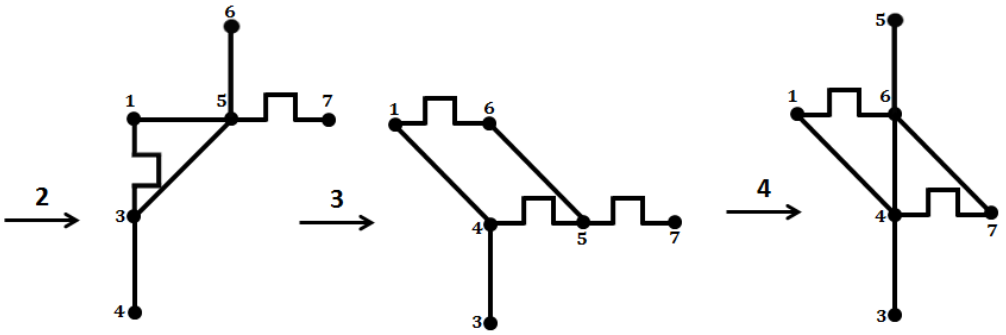

Transformation IV

N=5 (5-2-2)

Symmetrical

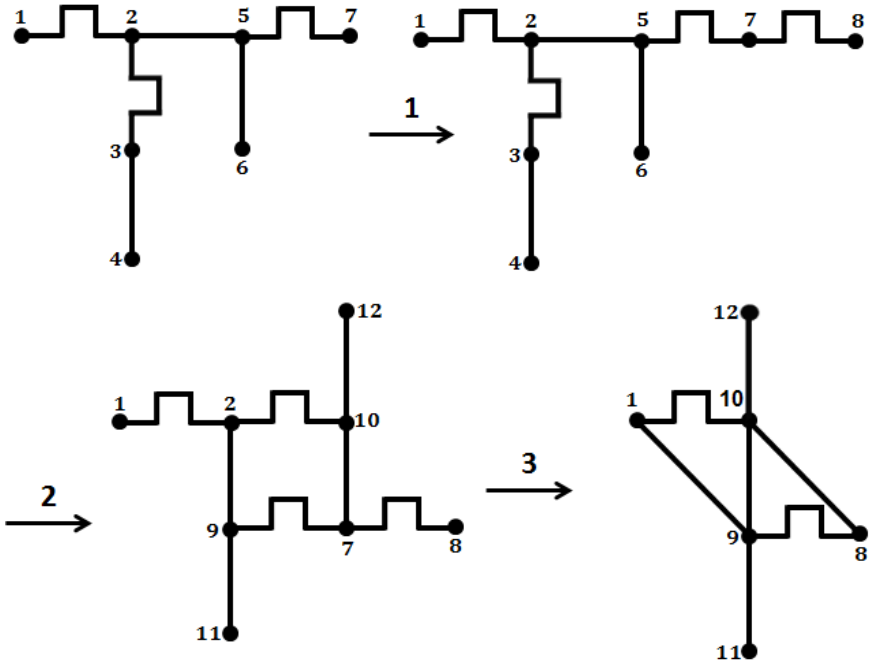

Transformation V

N=7 (7-2-5)

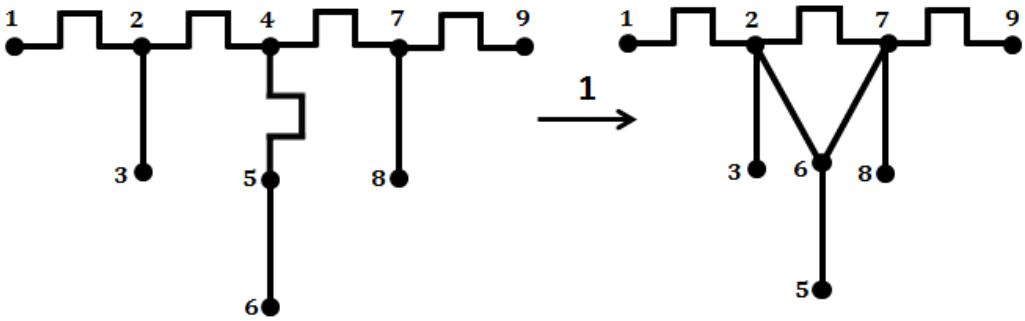

Fig. 3-10 (Continued.) Derived network transformation for $N = 3,5,7$ and 9 meander-like low-pass filters

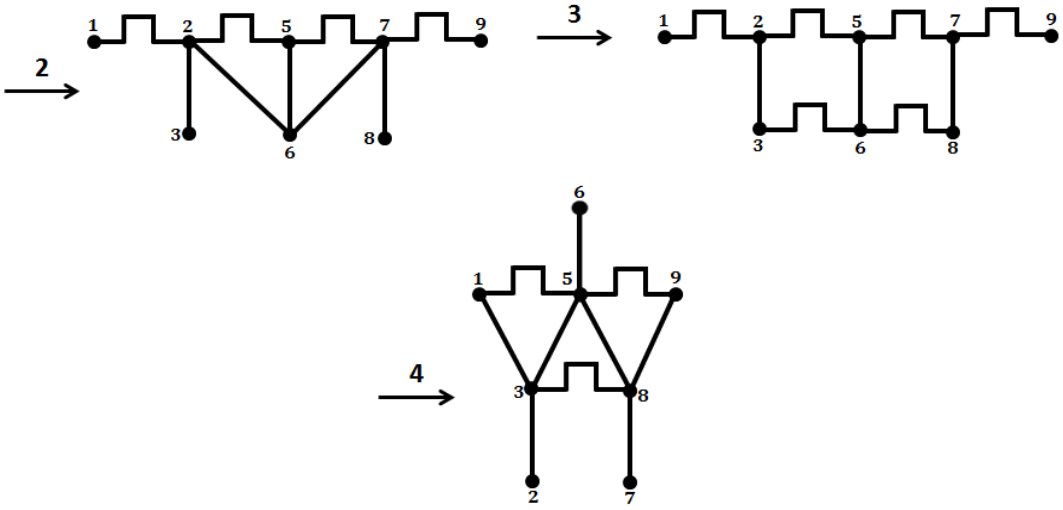

Transformation VI

N=9 (9-0-8)

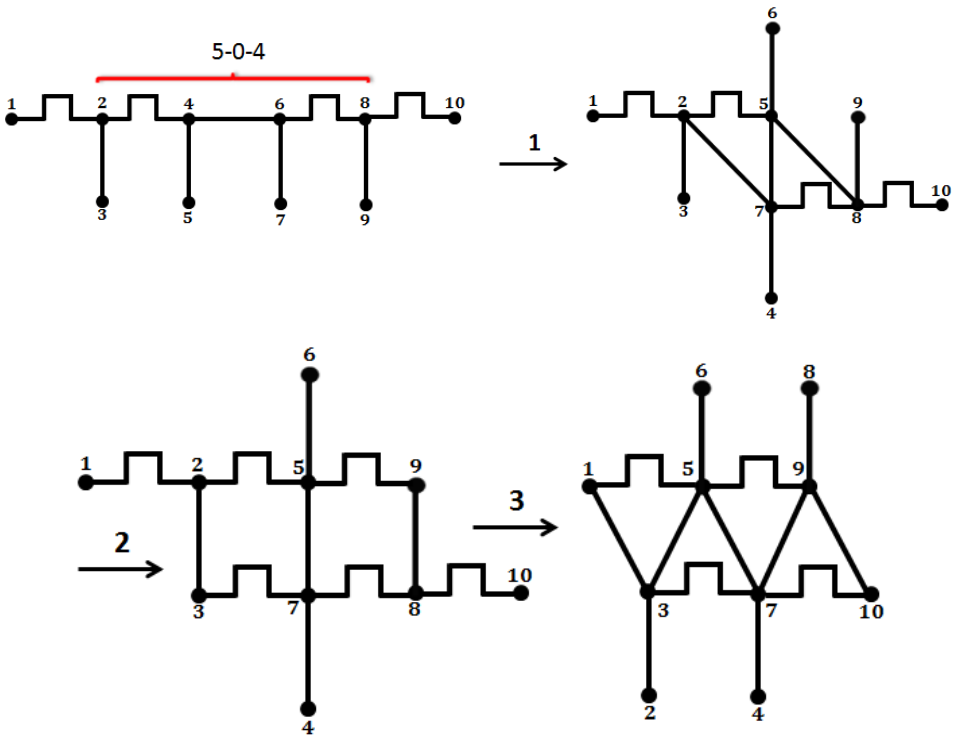

Fig. 3-10 (Continued.) Derived network transformation for $N = 3,5,7$ and 9 meander-like low-pass filters

Transformation VII

N=9 (9-2-6)

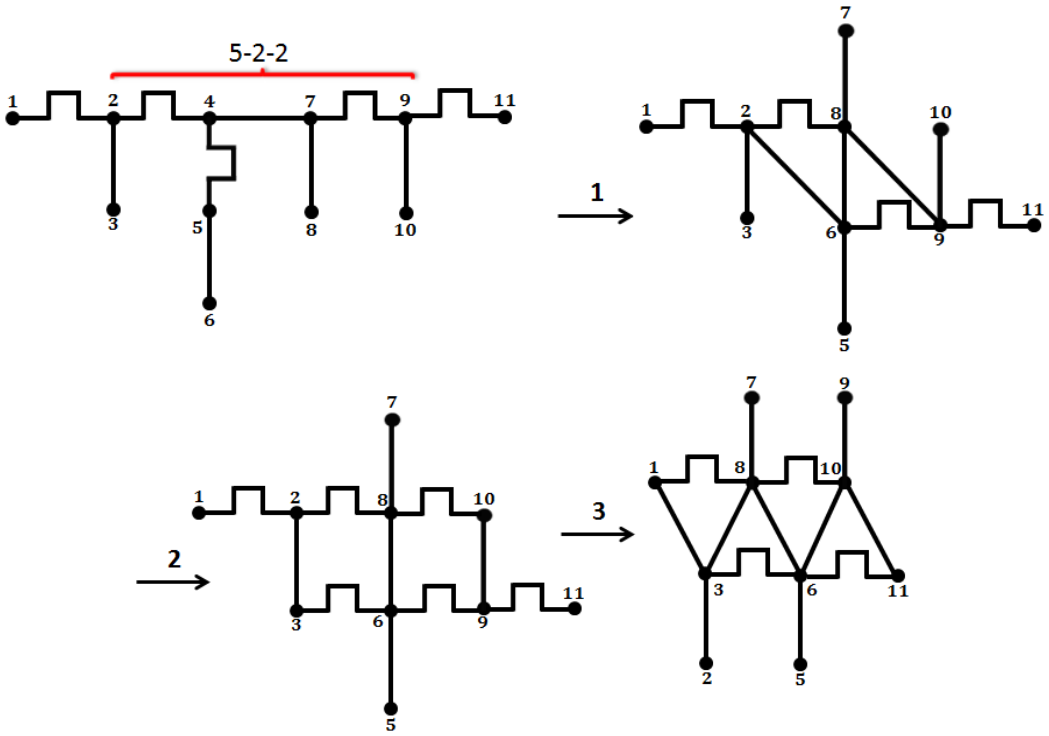

Fig. 3-10 (Continued.) Derived network transformation for $N = 3,5,7$ and 9 meander-like low-pass filters

The second meander-like low-pass filters, the 5-2-2 low-pass filter in Fig. 3-10 (III and IV), have a single pair of symmetrical finite frequency transmission zeros ($\theta_z = \pm\theta_\omega$), a single real axis half transmission zero pair at infinity ($\theta_z = \pm j\infty$) and two transmission zeros at the quarter-wave frequency ($\theta_z = \pm 90^o$). For an asymmetrical 5-2-2 case of Fig. 3-10 (III), step 1 utilises Sato's transformation (Table I of [63]) to eliminate branch 1,2 and in turn creates branch 1,3 and 1,5. In Step 2, Sato's transformation is used again to eliminate branch 2,3 and creates branch 3,5. In step 3, transformation III is applied on branch 1,5,6 and two sequential transformations III are applied on branch 1,3,5. The final equivalent circuit is obtained by application of transformation II on a three port subnetwork of 4,6,7 as illustrated in Fig. 3-10 (III).

For the symmetrical 5-2-2 low-pass filter of Fig. 3-10 (IV), step 1 splits the series short circuited stub between node 5 and 7 such that the admittances of the outermost series short circuited stubs in branch 1,2 and 7,8 are identical. In step 2,

transformation IV is carried out on the two port network between node 2 and 7 and finally two separate transformations II are carried out on three port subnetworks 1,9,10 and 9,8,10 respectively to obtain the final symmetrical form as illustrated in Fig. 3-10 (IV). Note that a negative sign on y_a in transformation IV should be taken for realizable impedance values.

For a 7th degree filter, one possible realisation derived is a 7-2-5 low-pass filter of Fig. 3-10 (V) with a single pair of symmetrical finite frequency transmission zero pair ($\theta_z = \pm\theta_\omega$) and all the remaining five transmission zeros at the quarter-wave frequency ($\theta_z = \pm 90^o$) which is now illustrated. From the canonical low-pass filter form, transformation I is applied on the two port network between node 2 and 7 in step 1. This is followed by transformation V again on the same two port network between nodes 2 and 7 in step 2. Then in step 3, two separate transformations III are applied on branch 3,2,6 and 8,7,9 and finally, in step 4, three separate transformation II are applied on the three port subnetworks of 1,3,5, 3,5,8 and 5,8,9 respectively to obtain the final form of the meander-like low-pass filter of Fig. 3-10 (V).

For a 9th degree filter, two derivative low-pass filter networks were examined whose core subnetworks were derived from a 5th degree network discussed above.

The first one is a 9-0-8 filter, with a single real axis half transmission zero pair at infinity ($\theta_z = \pm j\infty$) and all remaining eight transmission zeros at a quarter-wavelength frequency ($\theta_z = \pm 90^o$). Beginning with the canonical low-pass filter in Fig. 3-10 (VI) in step 1, a two port network between node 2 and 8 is replaced by a derived circuit for a 5-0-4 circuit as explained above (Fig. 3-10 (II)). Then in step 2, two separate transformations III are applied to branch 3,2,7 and 5,8,9. This is followed by two separate transformations II which are applied on three port subnetworks of 1,3,5 and 7,9,10 respectively to give the final equivalent circuit as illustrated in Fig. 3-10 (VI).

The second 9th degree low-pass filter is a 9-2-6 low-pass filter with a single symmetrical pair of finite frequency transmission zeros ($\theta_z = \pm\theta_\omega$), a single real axis half transmission zero pair at infinity ($\theta_z = \pm j\infty$) and all remaining six

transmission zeros at a quarter-wave frequency ($\theta_z = \pm 90^o$). Beginning with the canonical low-pass filter form in Fig. 3-10 (VII) in step 1, a two port network between node 2 and 9 is replaced by a derived circuit for a 5-2-2 circuit as explained above (Fig. 3-10 (III or IV)). Then in step 2, two separate transformations III are applied to branch 3,2,6 and 8,9,10 respectively. This is followed by two separate transformations II which are applied on three port subnetworks of 1,3,8 and 6,10,11 respectively to give the final equivalent circuit shown in Fig. 3-10 (VII). Note that a positive sign on y_a in transformation IV should be taken for realisable impedance values.

Multiple solutions do exist depending on the transformations used. Impedance levels are within positive realisable values as long as the electrical length at the cutoff is chosen to be around $\theta_c = \pm 45^o$ as the two examples will show. Moving further away from $\theta_c = \pm 45^o$ in either direction tends to lead to extreme element impedance values some of which may assume negative values arising from the formulae used in some of the cases of Fig. 3-2. As its canonical circuit form, the meander-like low-pass filter is relatively unaffected by small changes in the impedances values because it requires an optimal number of elements (N). Thus a small mismatch in the impedance values only slightly degrades the passband return loss.

Table 3-3 7th Degree Canonical Low-pass Filter Impedance Values (Ω)

$Z1 = 60.2932$	$Z2 = 29.1279$	$Z3 = 110.2028$	$Z4 = 6.2196$	$Z5 = 28.6033$

Table 3-4 7th Degree Meander-Like Low-pass Filter Impedance Values (Ω)

$Z1$	$Z2$	$Z3$	$Z4$	$Z13$	$Z35$
108.2319	53.7139	215.9667	25.8734	362.2136	44439.57

3.2.2.1 Design Example I

A 7th degree (7-2-5) meander-like low-pass was designed with a symmetrical pair of finite frequency transmission zeros at $\theta_z = \pm 65^o$(1.625 GHz) and five

transmission zeros at a quarter-wave frequency ($\theta_Z = \pm 90^o$), 20 dB minimum passband return loss and electrical length of $\theta_c = \pm 40^o$at cutoff frequency of 1 GHz. The synthesised element values for the canonical low-pass filter is shown in Table 3-3 (assuming symmetry with impedance values assigned sequentially from left to right of Fig. 3-10 (V)). Then using the technique as explained in section 3.2.2 and Fig. 3-10 (V) by a sequence of circuit transformations, the meander-like element values were obtained as shown in Table 3-4. The circuit simulation shown in Fig. 3-11 validates the synthesis process.

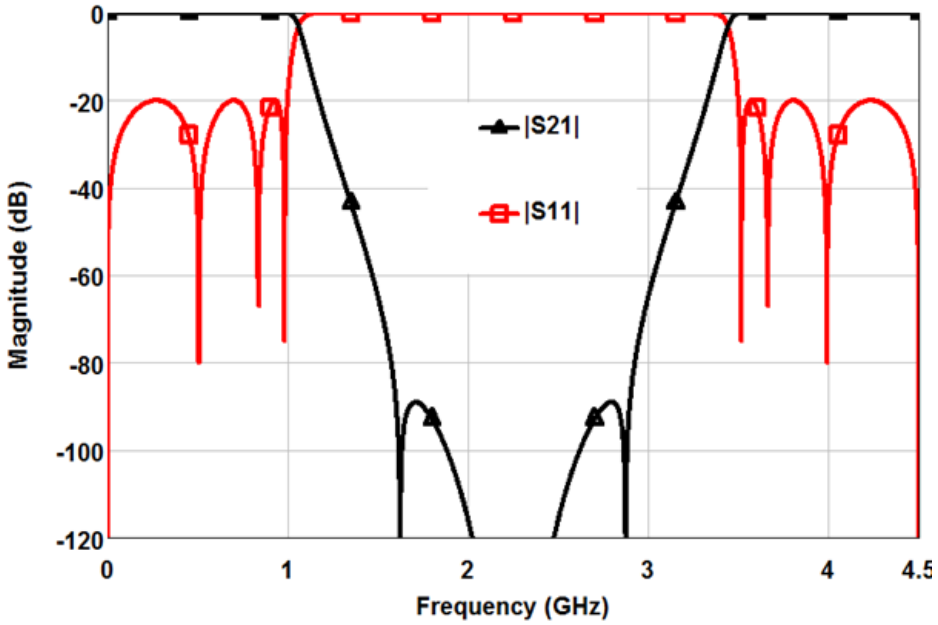

Fig. 3-11 Circuit simulation of a 7-2-5 meander-like low-pass filter in example 0

3.2.2.2 Design Example II

An experimental 9th degree meander-like low-pass filter was designed with cutoff frequency at 1 GHz, 20 dB minimum return loss and $\theta_c = \pm 45^o$. The stopband insertion loss was defined to be above $70\,dB$ between $1.3\,GHz$ and $2.7\,GHz$ and this was achieved by placing a symmetrical transmission zero pair at $\theta_z = \pm 58.23^o$(1.294 GHz), a single real axis half transmission zero pair at infinity ($\theta_z = \pm j\infty$) and six transmission zeros at quarter-wave frequency ($\theta_z = \pm 90^o$) yielding a 9-2-6 low-pass filter of Fig. 3-10 (VII). The characteristic polynomials and ABCD matrix polynomials were synthesised in section 2.6.1 (Chapter 2). Using cascaded synthesis, the synthesised element values for the canonical 9th degree

low-pass filter are shown in Table 3-5. These values were transformed to the meander-like circuit with the element values shown in Table 3-6.

Table 3-5 Synthesised 9th Degree Canonical Low-pass Filter Impedance Values

$Z1 = 51.3388\ \Omega$	$Z6 = 114.8003\ \Omega$
$Z2 = 34.1469\ \Omega$	$Z7 = 30.5252\ \Omega$
$Z3 = 86.4301\ \Omega$	$Z8 = 99.4671\ \Omega$
$Z4 = 15.2258\ \Omega$	$Z9 = 34.1469\ \Omega$
$Z5 = 39.6987\ \Omega$	$Z10 = 51.3388\ \Omega$

Table 3-6 Synthesised 9th Degree Meander-Like Low-pass Filter Impedance Values

$Z1 = 101.2065\ \Omega$	$Z13 = 317.8744\ \Omega$
$Z2 = 66.08394\ \Omega$	$Z35 = 1798.938\ \Omega$
$Z3 = 207.5597\ \Omega$	
$Z4 = 34.02597\ \Omega$	
$Z5 = 147.2685\ \Omega$	

Table 3-7 9th Degree Low-pass Filter optimised Dimensions (mm)

$w1 = 9.04$	$sw1 = 12.5$	$s12 = 6.75$	$dL1 = 2.5$
$w2 = 1.85$	$sw2 = 3.00$	$s23 = 23.25$	$dL2 = 8.5$
$w3 = 2.33$	$sw3 = 7.25$	$b = 25$	$dL3 = 6.5$
$w4 = 17.64$	$sw4 = 3.00$	$t = 5$	$wt = 13.0$
$w5 = 27.44$		L =37.5	

The low-pass filter is then realised using rectangular bars or striplines. The technique by Getsinger [32, 33] was used to determine the initial physical dimensions. The final optimised dimensions are given in Table 3-7. The nomenclature used in Table 3-7 corresponds to Fig. 3-12 and Fig. 3-13. The filter

measurements were performed with an Agilent Technologies E5071C ENA series network analyser. Fig. 3-14 shows good correspondence between the measured and theoretical simulation using HFSS.

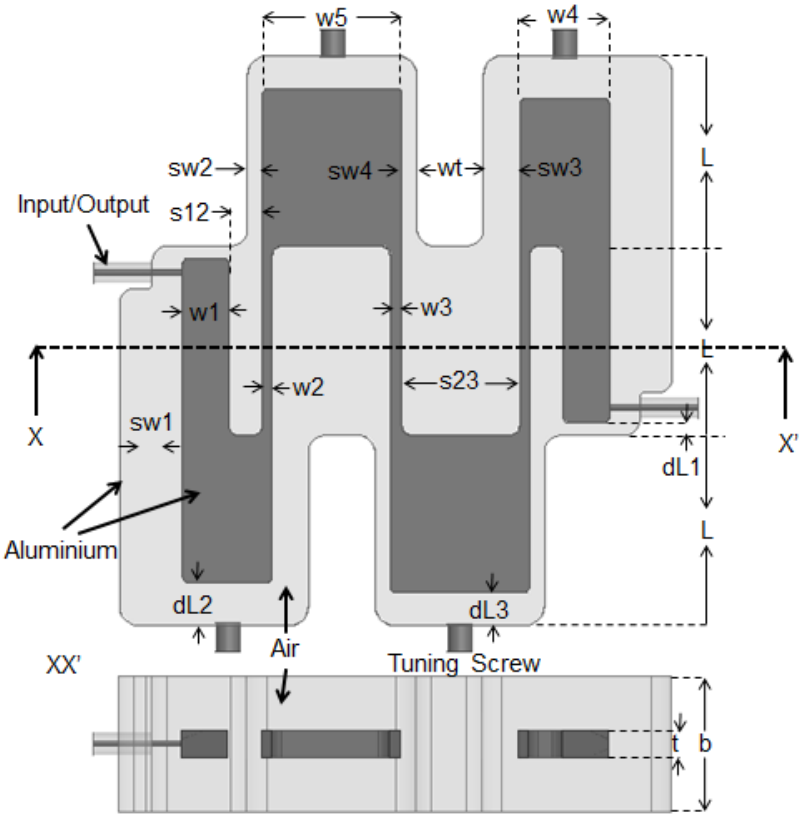

Fig. 3-12 Diagram showing the layout of the fabricated 9th degree meander-like low-pass filter. Dimensions shown are as given in Table 3-7

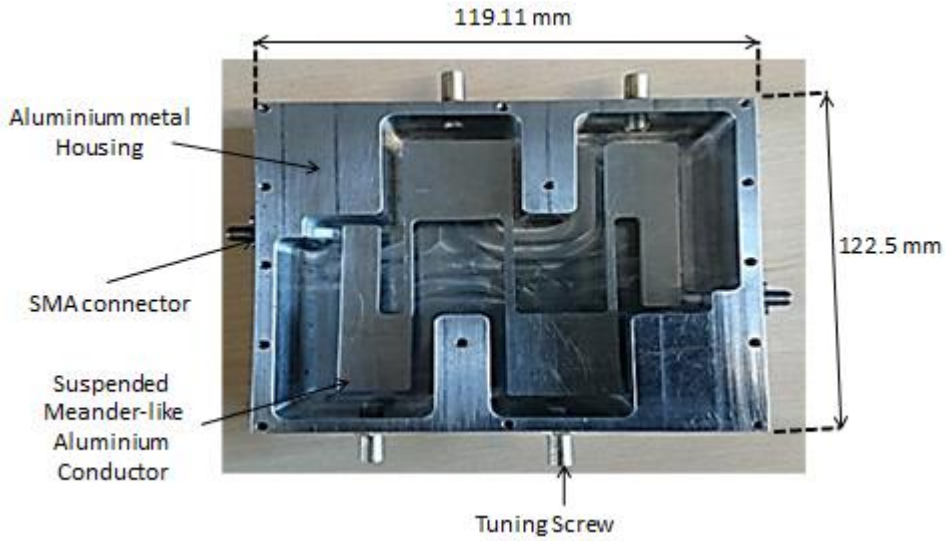

Fig. 3-13 Physical hardware of the fabricated 9th degree 'meander-like' low-pass Filter (top cover removed)

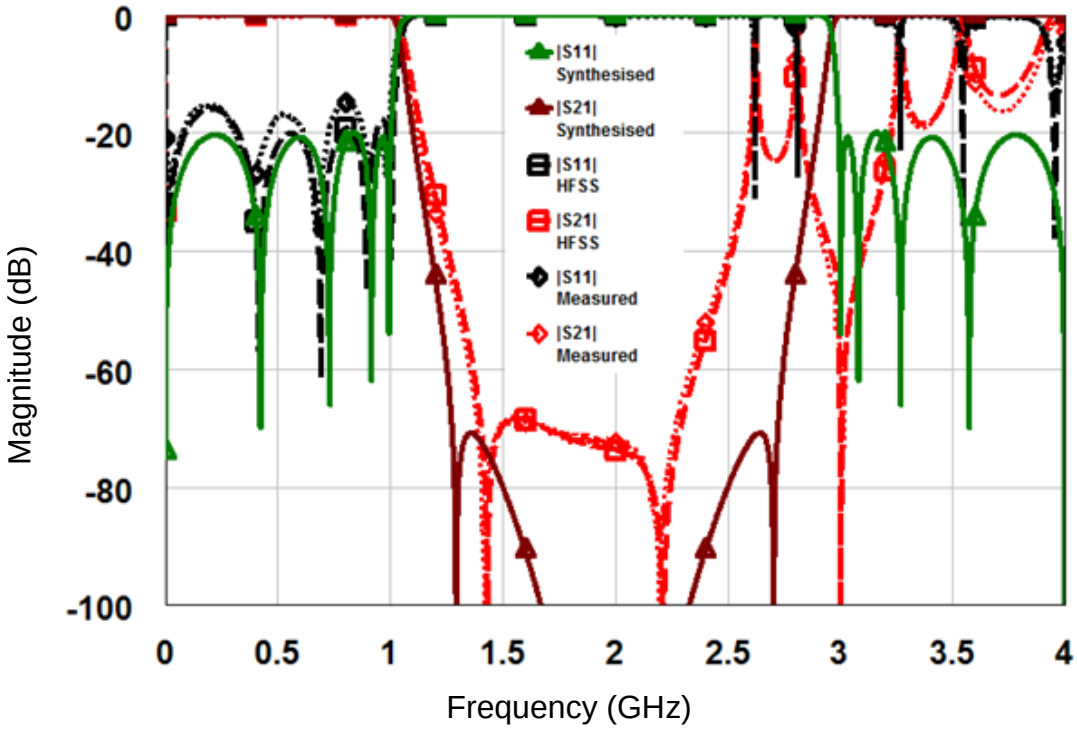

Fig. 3-14 Comparison of simulated response of the synthesized, HFSS and measurement of meander-like low-pass filter

The overall length of the low-pass filter realisation is three times the electrical length at the cutoff frequency. High order modes do exist in the structure that potentially could worsen the stopband response especially with relatively larger ground plane spacing. The effect is to shorten the effective stopband frequency window as the design example shows in Fig. 3-14. The choice of the ground plane spacing affects the spurious resonances within the filter structure which in this case appeared above $2.6\,GHz$. Since the low-pass filter is implemented using high Q stripline with individual theoretical Q factor of transmission lines ranging from about 1200 – 3300 (ground plane spacing of 25 mm). Thus the insertion loss is fairly low across the passband with a peak at 0.3476 dB at the cutoff frequency in the measured response as depicted in Fig. 3-15. The slight discrepancy in the insertion loss between the simulated and measurement results in Fig. 3-15 is due to slight mismatched response as evident from the return loss plot in Fig. 3-14 and Fig. 3-16.

Improvement in the stopband response may be achieved by reducing the ground plane spacing from 25 mm to 15 mm at expense of slightly increased insertion loss

(Fig. 3-15). Fig. 3-16 shows HFSS simulations for different ground plane spacing versus the ideal circuit response. Clearly the stopband performance matches very well with the prediction for $b = 15$ mm. Table 3-8 shows the corresponding optimized physical dimensions. Notice that much smaller ground plane spacing is limited by realisability of the physical dimensions as the dimensions of the low-pass filter are proportional to the ground plane spacing.

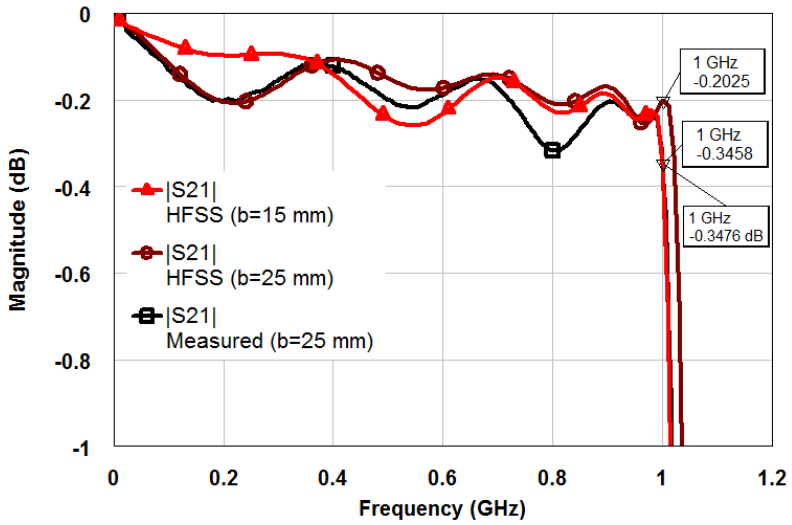

Fig. 3-15 Comparison of insertion losses between HFSS simulations for b=15 mm and b=25 mm and measured response with b=25 mm

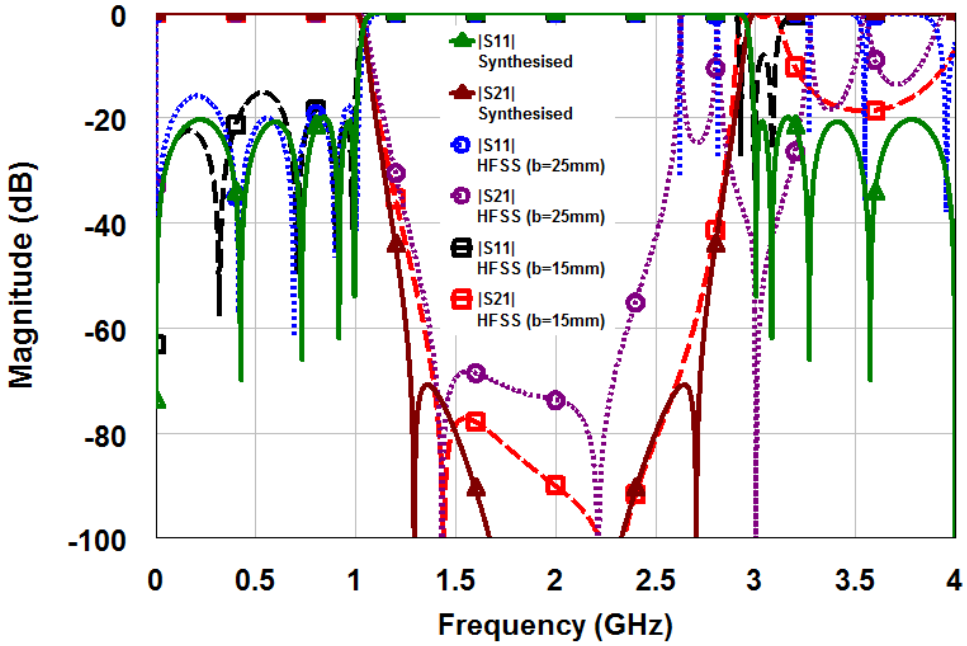

Fig. 3-16 Comparison of optimised equivalent circuit simulation and HFSS simulations of meander-like low-pass filter with ground plane spacing of 15 mm and 25 mm

Another way to improve the stopband width could be achieved by shortening the open circuited stubs length and capacitively loading the ends of the open circuited stubs. This is illustrated in Fig. 3-17. The stub length (L_s) may be fixed and the lumped capacitor (C_s) for loading the ends may be theoretically calculated from

$$C_s = \frac{tan(\theta_c - \theta_s)}{Z_s \omega_c} \tag{3.1}$$

where θ_s is the new electrical length of the shortened stub at the cutoff frequency point ω_c and Z_s is the characteristic impedance of the stub. Using the previous example and choosing $\theta_s = 5^o$ then $C_2 = 2.0209\,pF$ and $C_4 = 3.9249\,pF$ can be calculated from (3.1). At least on the circuit level, improved stopband is clearly evident from the circuit simulation in Fig. 3-18.

Table 3-8 Improved 9th Degree Low-pass Filter optimised Dimensions (mm)

$w1 = 5.42$	$sw1 = 7.5$	$s12 = 4.80$	$dL1 = 3$
$w2 = 1.11$	$sw2 = 1.8$	$s23 = 13.95$	$dL2 = 5.1$
$w3 = 1.40$	$sw3 = 7.5$	$b = 15$	$dL3 = 3.9$
$w4 = 11.33$	$sw4 = 1.8$	$t = 3$	$wt = 4.65$
$w5 = 16.46$		L =37.5	

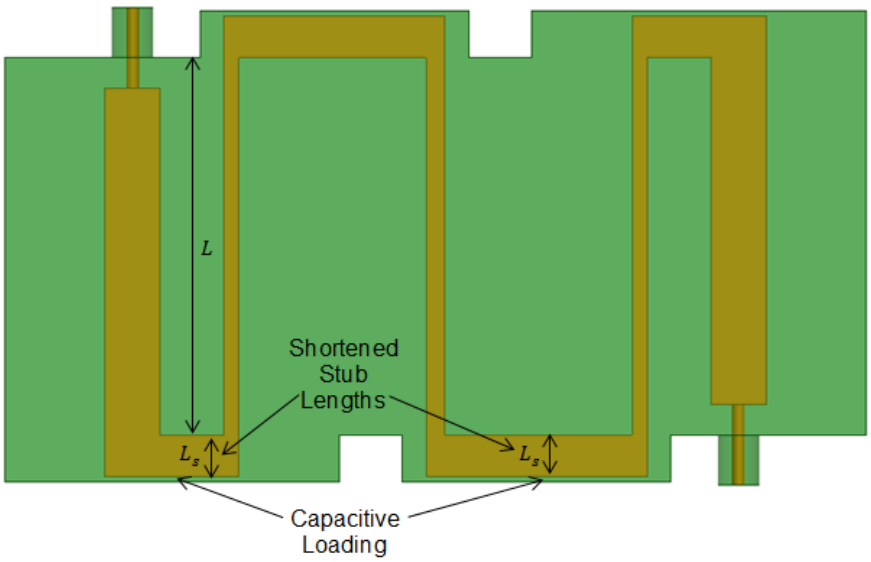

Fig. 3-17 Modified Meander-like structure obtained from Fig. 3-12 by shortening the open ends of the open circuited stubs

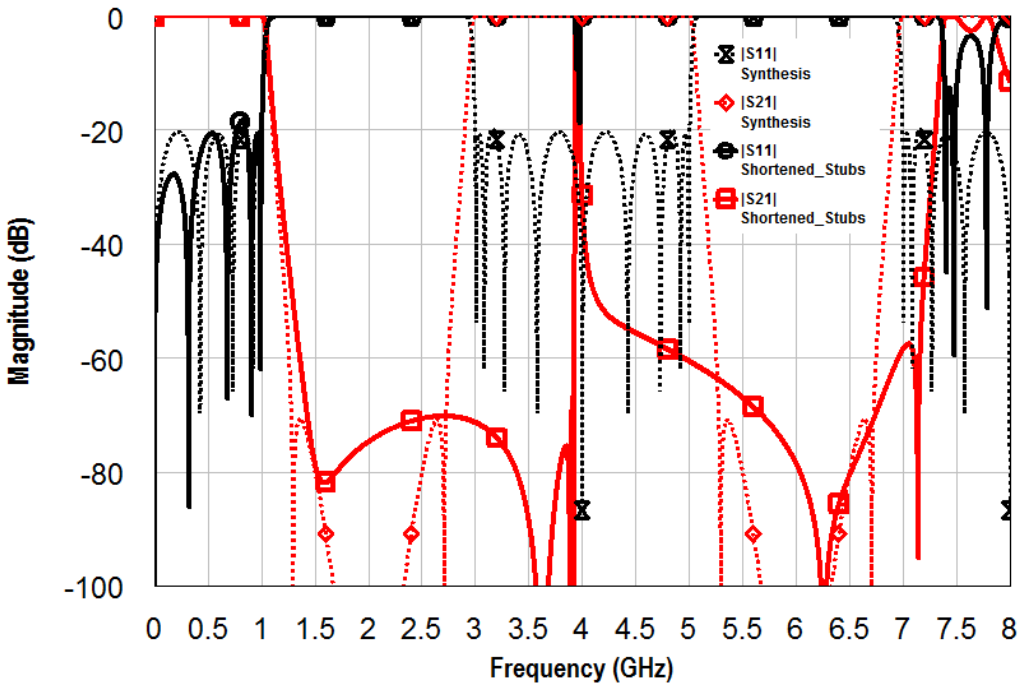

Fig. 3-18 Improvement in stopband performance of the meander-like low-pass filter by shortening the open ends of the open circuited stubs

3.2.3 Comparison based on theory and simulations

A 9th degree meander-like low-pass filter was compared to other low-pass filter realisations. To achieve the same selectivity, a 9th degree generalised Chebyshev low-pass filter would be required while a 15th degree stepped impedance low-pass filter would be required as depicted in Fig. 3-19 with $\pi/4$ electrical length at the cutoff frequency of 1 GHz. Thus for the same selectivity, the proposed structure requires a much lower filter elements than the stepped impedance low-pass filter. Although the generalised Chebyshev low-pass filter may be designed with the same degree as the meander-like low-pass filter, its stopband performance is much poorer in its physical realisation as shown in Fig. 3-19 because the series short circuited stubs are approximated by high impedance transmission lines [4]. Furthermore, both the generalised Chebyshev and stepped impedance low-pass filters' effective stopband response is much worse in practice because it is difficult to realise ideal commensurate transmission line elements and often discontinuities, high order modes and mode conversion occur within the filter structure [3]. These

reduce the effective stopband width of practical low-pass filters to as much as half of the predicted width! Even though effective stopband width may be widened by using a lower electrical length at cutoff frequency, it is often limited by element realisation as the variations in element values tend to be extreme. By utilizing relatively smaller ground plane spacing as described in section 0 the proposed low-pass structure offers superior stopband performance.

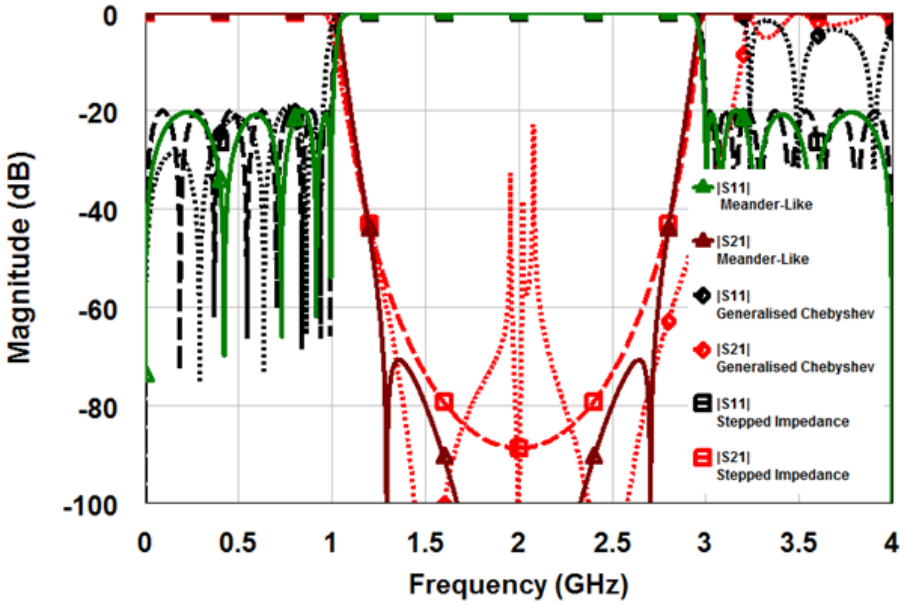

Fig. 3-19 Circuit simulation comparison of 9th degree meander-like low-pass filter with a 9th degree generalised Chebyshev low-pass filter and 15th degree stepped impedance low-pass filter

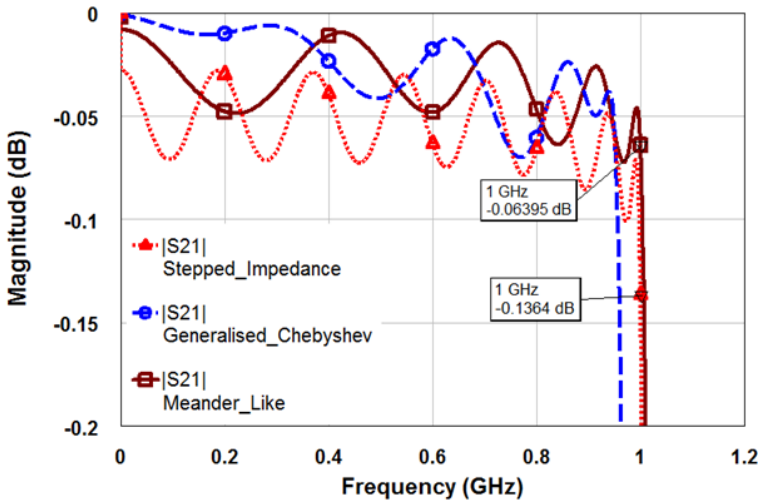

Fig. 3-20 Circuit insertion loss simulation comparison of 9th degree meander-like low-pass filter with a 9th degree generalised Chebyshev low-pass filter and 15th degree stepped impedance low-pass filter

Fig. 3-20 shows the circuit level insertion loss analysis of the three low-pass filters being compared above with the same ground plane spacing of 25 mm assuming copper conductors in air. It is quite obvious the stepped impedance low-pass filter fairs worse because of the high number of unit elements required to achieve the selectivity. The generalised Chebyshev low-pass filter passband insertion compares well with the proposed meander-like low-pass filter with the losses increasing towards the cutoff frequency. The proposed structure has an optimal number of unit elements equal to the degree of the network regardless of the number of finite frequency transmission zeros. The generalised Chebyshev low-pass filter on the other hand requires 12 unit elements to achieve the selectivity requirements. Thus the proposed meander-like low-pass filter is much more compact with lower insertion loss than the other two low-pass filters. The meander-like low-pass filter has a high achievable roll-off rate of 246.7 dB/GHz with an achievable relative stopband bandwidth of 0.883 [64] and could be advantageous where a much deeper out-of-band rejection is required.

3.3 Conclusion

A new class of low-pass filter realisation called the meander-like low-pass filter has been demonstrated. The design theory was given in section 3.2 with the two proposed physical realisation distinguished. These physical realisations enable exact realisation of the generalised Chebyshev low-pass filter. The required transfer functions as well as the necessary circuit transformations were given together with a complete design procedure. Both of these low-pass filter realisations have relatively higher roll-off rate and a deeper effective stopband. In the next Chapter, a method of achieving finite frequency transmission using re-entrant resonators is presented.

Chapter 4 Synthesis and Design of Bandpass Filters with 'Integrated' Transmission Zeros Using Re-entrant Transmission Lines

4.1 Introduction

In this Chapter, the re-entrant line is used in the design of small percentage bandwidth bandpass filters to create a bandpass resonance with an integrated finite frequency transmission zero thus realizing finite frequency transmission zeros without the need for complicated cross couplings [65]. A re-entrant bandpass filter with transmission zeros above the passband is demonstrated. Transmission zeros below the passband are also theoretically possible using this approach but impractical to realize in real systems.

The proposed design offers a simple and easy implementation for pseudo-elliptic filters where a higher level of attenuation is required on the high side of the passband than can be provided by conventional coaxial filters. This type of filter is useful for interference rejection in cellular base stations.

At the outset, the available methods of generating transmission zeros are described in section 4.2. The re-entrant bandpass filter is designed from pseudo-elliptic lowpass prototype filter whose synthesis is presented in section 4.3. The concept of a re-entrant line resonator is developed in section 4.4, while in section 4.5, development of the design technique for bandpass filters with transmission zeros above the passband is presented. Comparisons of the re-entrant resonator to the coaxial resonator and their merits in terms of size, loss and stopband responses are also discussed. Some design examples are given in section 4.6 and a prototype re-entrant bandpass filter was built and laboratory tested as discussed in section 4.7.

4.2 Transmission Zeros Generation Methods

Finite transmission zeros are routinely used to increase the selectivity of bandpass filters. There are two known basic methods for generating transmission zeros in the filter network [66].

The first one uses multi-paths in the filter structure to produce destructive interference at the desired transmission zero frequencies [67, 68]. The well-known cross-coupled resonator cavity filters typically employ this method. Transmission zeros are introduced in the filter network by means of some cross-coupling between non-adjacent nodes in the network with suitable positive (magnetic) or negative (electric) couplings. Cross-coupling produces alternative signal paths resulting in multipath signal propagation between the input and the output or between two nodes in the filter network. Understanding the phase changes that a signal undergoes as it travel through these multipath is key to grasping how these transmission zeros are generated. In fact in [68], the formulation of transmission zeros by different coupling positions and coupling elements is well explained. However, these methods often lead to bulky filters due to high number of elements required and sometimes inconvenient topologies.

The second method involves the use of transmission zero generating elements [27, 28]. The filter may be designed entirely of these elements [27, 69] or it may be mixed with the non-transmission zero generating elements or ordinary resonators [66, 70]. In fact the use of non-resonating nodes as a realisation for pseudo-elliptic filters has been gaining ground in fairly recent research [66, 71, 72]. The design of bandpass filters using re-entrant transmission lines described in this Chapter utilises this later method of generating transmission zeros and will be dealt with in more details in later sections. The next section describes a method for synthesising a lowpass prototype filter suitable for re-entrant bandpass filters.

4.3 Lowpass Prototype Filter Circuits for Pseudo-elliptic Bandpass Filters

Different synthesis methods exist for a lowpass prototype filter used in design of the so called elliptic in-line topologies [27, 70, 73, 74]. The limitations on some of them is that only one or two transmission zeros may be extracted. The other existing methods employ extracted pole techniques then followed by circuital transformation. In this section, two novel, unique and simple synthesis techniques are introduced.

The first one employs an asymmetrical frequency transformation on a well-known all pole Chebyshev transfer function. While this provides a simplified method of design, it is limited by the fact that it realises all finite frequency transmission zeros at a single frequency. It is also fully asymmetric meaning that the transmission zeros position can only be on one side of the passband.

The second method allows arbitrary transmission zero placements and thus represents the most general pseudo-elliptic lowpass prototype filter. In both synthesis methods, the lowpass prototype use frequency-invariant-reactance (FIR) elements (here generalised as FIR but may also be frequency-invariant-susceptance) [18] which may physically be realised as non-resonating-nodes (NRN) [69]. Because the transfer function is asymmetric, all the resonator nodes are asynchronously tuned by the presence of FIR elements. The application of these lowpass prototype filters to bandpass filters design is outlined in section 4.5.

4.3.1 Asymmetrical-Frequency-Transformed Pseudo-elliptic Lowpass Prototype Filter

Consider a well-known traditional Chebyshev with all its transmission zeros at infinity. From Chapter 2, it is evident that the general Chebyshev characteristic function may be expressed as,

$$T_N = cosh \sum_{n=1}^{N} cosh^{-1}(x_n) \tag{4.1}$$

where the basis function is given by,

$$x_n = \frac{1 - \omega_n \omega}{\omega - \omega_n} \tag{4.2}$$

Alternatively,

$$x_n = \frac{1/\omega_n - \omega}{\omega/\omega_n - 1} \tag{4.3}$$

to accommodate $\omega_n = \infty$ where ω_n is the location of the n^{th} transmission zero. Now consider what happens when a frequency transformation of the form of (4.4) is used in the transfer function. The transformation is defined from (4.2) as

$$\omega \rightarrow \frac{1 - \omega_o \omega}{\omega - \omega_o} \tag{4.4}$$

where ω_o is the location of the new transmission zeros. Substituting the transformation (4.4) into (4.3) yields

$$x_n = \frac{1 - \left(\frac{1 + \omega_o \omega_n}{\omega_o + \omega_n}\right)\omega}{\omega - \left(\frac{1 + \omega_o \omega_n}{\omega_o + \omega_n}\right)} = \frac{1 - \omega_n{}'\omega}{\omega - \omega_n{}'} \tag{4.5}$$

where,

$$\omega_n{}' = \frac{1 + \omega_o \omega_n}{\omega_o + \omega_n} = \frac{1/\omega_n + \omega_o}{1 + \omega_o/\omega_n} \tag{4.6}$$

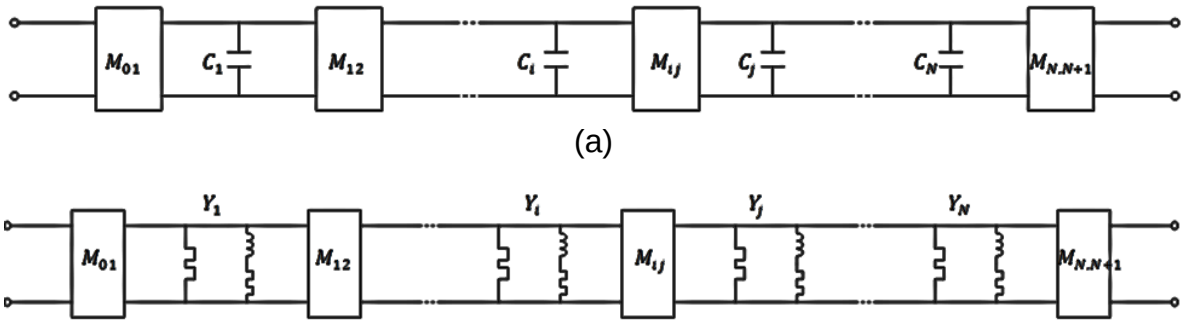

Fig. 4-1 Asymmetrical-frequency-transformed elliptic lowpass prototype filter (a) all-pole Chebyshev lowpass prototype filter (b) asymmetrical-frequency-transformed pseudo elliptical lowpass prototype filter where $Y_r = j\left(\frac{1-\omega_o\omega}{\omega-\omega_o}\right)C_r,\ r = 1,2,\ldots,N$

Thus if all the transmission zeros are placed at a single frequency ω_o, it is possible to transform the well-known all-pole ladder network for which $\omega_n = \infty$ by

application of a simple transformation defined by (4.4) above. All the transmission zeros at infinity ($\omega_n = \infty$) are transformed to a single finite frequency (ω_o), i.e. $\infty \rightarrow \omega_o$. The circuit is transformed as in Fig. 4-1.

It can be concluded from the foregoing proof that the transformation given in (4.4) transforms a traditional Chebyshev lowpass prototype filter with all its transmission zeros at infinity to a pseudo-elliptic lowpass filter response where all the transmission zeros are at a single finite frequency ω_o. The position of the transmission zeros can either be below or above the passband and remains purely a designer's choice by taking appropriate sign of ω_o. Fig. 4-1 above illustrates this transformation. The ideal admittance inverters remain invariant under this transformation. Since all transmission zeros are at a single frequency ω_o, then S_{21} is finite at infinity. Let

$$|S_{21}(\infty)|^T = ILo \tag{4.7}$$

be defined as the rejection level (in dB) in the stopband after the transformation. Thus for the transformed filter network, ILo is obtained from

$$|S_{21}(\pm\omega_o)| = ILo \tag{4.8}$$

Thus ILo is the horizontal asymptote for the insertion loss function. As ω_o tends to ± 1 rad/s, $|S_{21}(\pm\omega_o)|$ tends to $0\ dB$ at infinity. This intuitively leads to a fundamental behaviour of filter networks which means that as the selectivity increases, the overall rejection reduces. In practice though it is imperative that the transmission zeros be distributed over some range of frequency to improve the overall rejection as opposed to being on a single frequency. Despite this drawback, this class of lowpass filter offers a basic synthesis procedure for pseudo-elliptic lowpass filters synthesis from which a more general synthesis procedure may be built. The synthesis is fairly straight forward. The single frequency transmission zero ω_o needs to be determined from the required rejection level (ILo). Since for an all pole transfer function, i.e. $\omega_n = \infty$, (4.1) the denormalised characteristic function becomes,

$$\frac{T_N}{k} = cosh \sum_{n=1}^{N} cosh^{-1}(x_n) = \cosh[N cosh^{-1}(\omega)]. \tag{4.9}$$

Conversely,

$$\omega = \cosh\left[\frac{cosh^{-1}\left(\frac{T_N}{k}\right)}{N}\right]. \tag{4.10}$$

Also from Chapter 1,

$$|S_{21}(\omega)|^2 = \frac{1}{1+(T_N)^2} = \frac{1}{1+\left(\frac{F(\omega)/\mu}{P(\omega)/\varepsilon}\right)^2}$$

$$ILo = -10\log_{10}|S_{21}(\omega_o)|^2 = -10\log_{10}\left[\frac{1}{1+\left(\frac{F(\omega)/\mu}{P(\omega)/\varepsilon}\right)^2}\right] \tag{4.11}$$

where for the un-normalised characteristic function,

$$\varepsilon = k = \pm\frac{1}{\sqrt{10^{(RL/10)}-1}}\left|\frac{P(\omega)}{F(\omega)}\right|_{\omega=\pm1} = \pm\frac{1}{\sqrt{10^{(RL/10)}-1}} \tag{4.12}$$

$$\mu = \pm 1$$

is the specified ripple level in the passband for a given return loss (RL). Note also that $\left|\frac{P(\omega)}{F(\omega)}\right|_{\omega=\pm1} = 1$ for all-pole Chebyshev transfer function. Hence (4.11) becomes,

$$\frac{T_N(\omega_o)}{k} = \frac{\sqrt{10^{(ILo/10)}-1}}{k} = \frac{\sqrt{10^{(ILo/10)}-1}}{\frac{1}{\sqrt{10^{(RL/10)}-1}}} \tag{4.13}$$

$$\frac{T_N(\omega_o)}{k} = \sqrt{10^{((RL+ILo)/10)} - 10^{(ILo/10)} - 10^{(RL/10)} + 1}$$

From substituting (4.13) in (4.10) becomes,

$$\omega_o = \cosh\left[\frac{cosh^{-1}\left(\frac{T_N(\omega_o)}{k}\right)}{N}\right]$$

$$\omega_o = \cosh\left[\frac{cosh^{-1}\left(\sqrt{10^{((RL+ILo)/10)} - 10^{(ILo/10)} - 10^{(RL/10)} + 1}\right)}{N}\right] \tag{4.14}$$

For example if $RL = 20\,dB$, $ILo = 20\,dB$, and $N = 4$ then ω_o may be determined from equation (4.14) as $\omega_o \cong 2$. Alternatively N may be determined for a given ω_o. First using an all-pole transfer function, a Chebyshev lowpass prototype is synthesised. Then each capacitor (or inductor) is transformed according to equation (4.4) as,

$$Y(j\omega) = j\omega C = j\left(\frac{1 - \omega_o\omega}{\omega - \omega_o}\right)C$$

$$Y(j\omega) = -j\omega_o C + \frac{1}{j\omega\left(\frac{1}{C({\omega_o}^2 - 1)}\right) + j\left(\frac{-\omega_o}{C({\omega_o}^2 - 1)}\right)} = jB + \frac{1}{j\omega L + jX} \tag{4.15}$$

where,

$$B = -\omega_o C$$

$$L = \frac{1}{C({\omega_o}^2 - 1)} \tag{4.16}$$

$$X = -\frac{\omega_o}{C({\omega_o}^2 - 1)}$$

The elements values may be obtained from (4.16). Similar equations may be obtained in the case of an inductor as depicted in Fig. 4-2 (b). At this point the common physical filter realisation using coaxial cavity or waveguide filter may apply. The only exception is FIR elements which may be approximated by non-resonating-nodes (NRN). The advantage of this method is that because it is derived from the all pole transfer function which is a symmetrical function, the resulting transformed circuit has also symmetrical element values for the otherwise asymmetrical transfer characteristic they represent. This is ideal because the physical structure will also be symmetrical about the physical centre and only half

of the values are required to completely characterise and design the filter. Although the transformation offers a simplified synthesis approach for elliptic lowpass filters, its limitation lies in the fact that only finite single frequency transmission zeros can be realised. A more general method where the transmission zeros are distributed in the stopband is required.

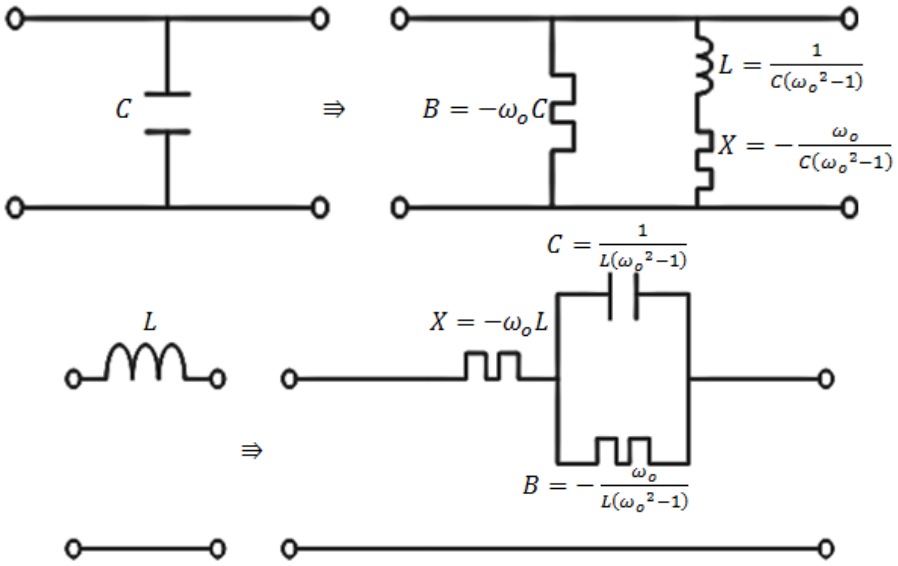

Fig. 4-2 The dual circuit transformation of a capacitor (a) and an inductor (b)

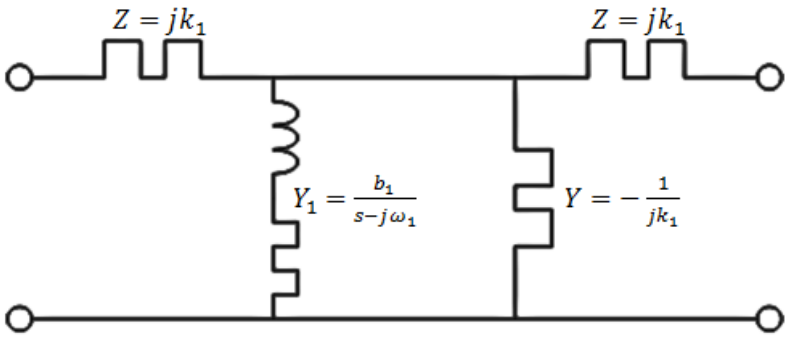

Fig. 4-3 TZG element

4.3.2 General Synthesis for Pseudo-elliptic Lowpass Prototype Filter

In this section a general synthesis method that involves arbitrary placed transmission zeros is presented. The synthesis begins by extracting transmission-zero-generating (TZG) elements as shown in Fig. 4-3. It is assumed that the filter network is of order N and has N transmission zeros. Thus N TZG's are extracted that are separated by admittance inverters. A section of TZG consists of a series

FIR, a shunt series of inductor with an FIR, a shunt FIR and a series FIR as is shown in Fig. 4-3.

The element values were extracted as described in Chapter 1 and given in Table 1-2 from the synthesised lowpass filter ABCD matrix given as

$$ABCD = \frac{1}{P(p)}\begin{bmatrix} A(p) & B(p) \\ C(p) & D(p) \end{bmatrix} \tag{4.17}$$

Firstly two elements are extracted that make $A(p)$ and $B(p)$ polynomials have a zero at $p = j\omega_1$, where ω_1 is the first transmission zero. And since $P(p)$ already contain a zero at $p = j\omega_1$, then the transmission zero is completely extracted from the network by dividing all the polynomials by $p - j\omega_1$ after extraction of these first two elements. Thus the series frequency invariant reactance (FIR),

$$Z = jk_1, \tag{4.18}$$

is extracted first so that the remaining polynomials,

$$\begin{aligned} A_r(p) &= A(p) - jk_1C(p) \\ B_r(p) &= B(p) - jk_1D(p) \end{aligned} \tag{4.19}$$

both possess a transmission zero at $p = j\omega_1$. The element value k_1 is computed (Table 1-2) as

$$k_1 = \left.\frac{B(p)}{jD(p)}\right|_{p=j\omega_1}. \tag{4.20}$$

Secondly, the residue b_o is found so that the transmission zero generating shunt admittance

$$Y_1 = \frac{b_1}{p - j\omega_1}, \tag{4.21}$$

is extracted to make the remaining two polynomials, $C_r(p)$ and $D_r(p)$, have a zero at $p = j\omega_1$. This is realised as a shunt series of inductor, with value $L = 1/b_1$, and FIR with value $x = -\omega_1/b_1$ .The value of the residue is obtained from

$$b_1 = \left.\frac{D(p)}{[B(p)/(p - j\omega_1)]}\right|_{p=j\omega_1}, \tag{4.22}$$

so that the new polynomials,

$$C_r(p) = C(p) - Y_1 A(p)$$
$$D_r(p) = D(p) - Y_1 B(p) \quad (4.23)$$

have a zero at $p = j\omega_1$. Since all the new ABCD polynomials are zero at $p = j\omega_1$. Then they can be divided by $p - j\omega_1$ to effectively remove the transmission zero so that all the ABCD polynomials including $P(p)$ reduces by 1 degree. To complete the synthesis cycle two other elements are extracted i.e. a shunt FIR of value

$$Y = -\frac{1}{jk_1}, \quad (4.24)$$

is extracted followed by a series FIR of value,

$$Z = jk_1. \quad (4.25)$$

A unit inverter is then extracted and the whole process is repeated until all transmission zeros are extracted. To avoid extreme values for the residues, the TGZ elements are extracted alternatively from the input and output of the network until all the transmission zeros have been extracted. To do this the network is turned after extraction of the first TZG element. This is achieved by swapping the two leading diagonal polynomials i.e. $A(p)$ and $D(p)$. The other polynomials remain unchanged. The last TZG is extracted and the network is turned back to the input so that extraction of a unit inverter followed by second TZG element is done from the input side. The network is turned again so that extraction continues from the output side. A unit inverter is extracted followed by second from last TZG. The network is again turned back to the input and the whole process is repeated until the last TZG element is extracted. Finally, a parallel connected inverter is extracted between the last two TZG's in the middle of the network. The formulae for the element extraction were given in Chapter 1(Table 1-2). The initial circuit then undergoes three more circuit transformations to produce the ultimate circuit form. Fig. 4-4 to Fig. 4-6 below shows the circuit transformations and the associated transformation formulae.

4.3.2.1 Circuit Transformations

1st circuit transformation (Fig. 4-4): Series FIR and inverters

$$N_{ij} = \frac{M_{ij}}{1 - k_i k_j {M_{ij}}^2} \tag{4.26}$$

$$k_i^{ij} = \frac{k_j {M_{ij}}^2}{1 - k_i k_j {M_{ij}}^2} \tag{4.27}$$

$$k_j^{ij} = \frac{k_i {M_{ij}}^2}{1 - k_i k_j {M_{ij}}^2} \tag{4.28}$$

where $j = i + 1$.

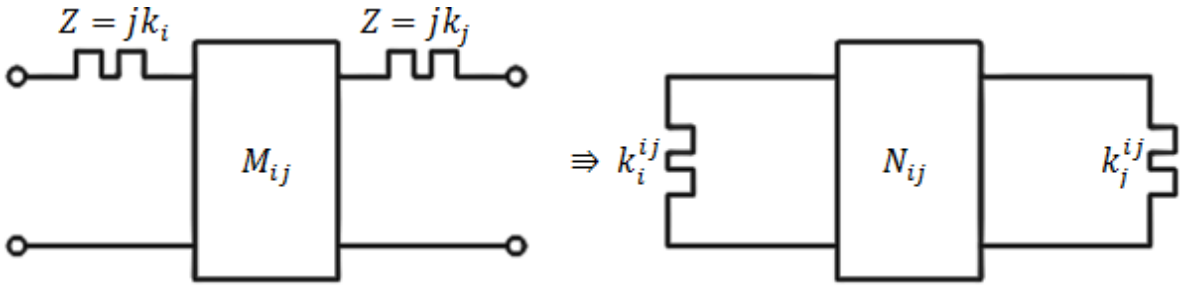

Fig. 4-4 Circuit transformation for the series FIRs and inverters

2nd circuit transformation (Fig. 4-5):

For the input (or output), the series FIR (jk_1) and Shunt FIR ($-\frac{1}{jk_1}$) are transformed to a shunt FIR followed by an inverter of values

$$Y = \frac{1}{jk_1} \tag{4.29}$$

$$M_{01} = \frac{1}{k_1} \tag{4.30}$$

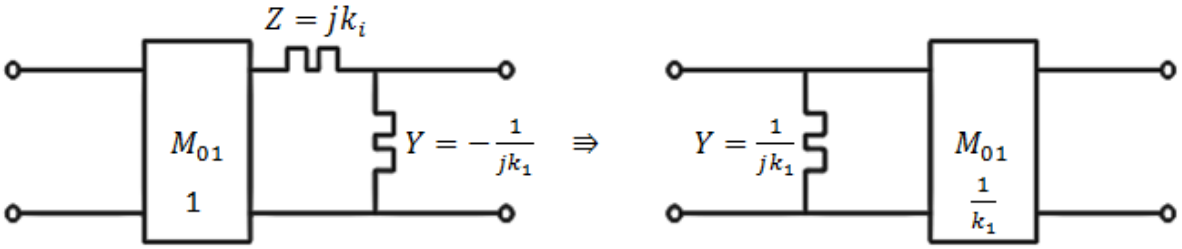

Fig. 4-5 Circuit transformation for the input series FIRs

3rd circuit transformation (Fig. 4-6):

The shunt FIR followed by an inverter at the input of the network from the second circuit transformation are then transformed further into series circuit of a unit phase shifter, an inverter and shunt FIR in that order with the values

$$\theta_{01} = acos\left(\frac{1}{\sqrt{(1+{k_1}^2)}}\right) \tag{4.31}$$

$$N_{01} = \frac{1}{\sqrt{(1+{k_1}^2)}} \tag{4.32}$$

$$k_1^{01} = \frac{1}{k_1(1+{k_1}^2)} \tag{4.33}$$

The output part undergoes similar transformations. The final circuit element may then be computed as follows

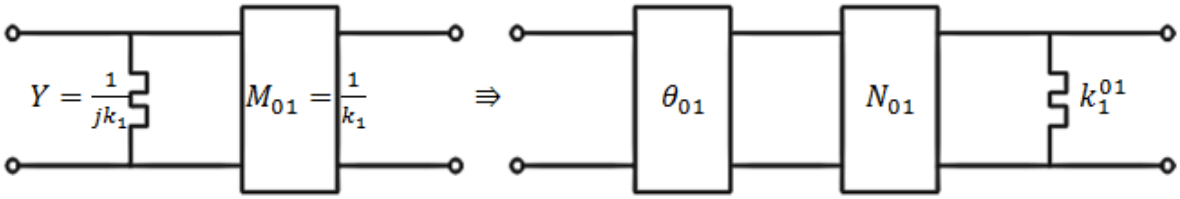

Fig. 4-6 Further circuit transformation at the input (output) of the network

Input:

$$\theta_{01} = acos\left(\frac{k_1}{\sqrt{1+{k_1}^2}}\right) \tag{4.34}$$

$$N_{01} = \frac{1}{\sqrt{1+{k_1}^2}} \tag{4.35}$$

1^{st} node:

$$Y_1 = jNRN_1 + \frac{b_1}{p - j\omega_1} \tag{4.36}$$

where

$$NRN_1 = k_1^{01} + k_1^{12} = \frac{1}{k_1(1+{k_1}^2)} + \frac{k_2{M_{12}}^2}{1 - k_1k_2{M_{12}}^2} \tag{4.37}$$

i^{th} node:

$$N_{ij} = \frac{M_{ij}}{1 - k_i k_j {M_{ij}}^2} \tag{4.38}$$

$$Y_i = jNRN_i + \frac{b_i}{p - j\omega_i} \tag{4.39}$$

where

$$NRN_i = k_i^{i-1,i} + \frac{1}{k_i} + k_i^{i,i+1} = \frac{k_{i-1}{M_{i-1,i}}^2}{1 - k_{i-1}k_i{M_{i-1,i}}^2} + \frac{1}{k_i} + \frac{k_{i+1}{M_{i,i+1}}^2}{1 - k_i k_{i+1}{M_{i,i+1}}^2} \tag{4.40}$$

N^{th} node:

$$Y_N = jNRN_N + \frac{b_N}{p - j\omega_N} \tag{4.41}$$

where

$$NRN_N = k_N^{N-1,N} + k_N^{N,N+1} = \frac{k_{N-1}{M_{N-1,N}}^2}{1 - k_{N-1}k_N{M_{N-1,N}}^2} + \frac{1}{k_N(1 + {k_N}^2)} \tag{4.42}$$

And the output would be:

$$N_{N,N+1} = \frac{1}{\sqrt{(1 + {k_N}^2)}} \tag{4.43}$$

$$\theta_{N,N+1} = acos\left(\frac{1}{\sqrt{(1 + {k_N}^2)}}\right) \tag{4.44}$$

This concept is best illustrated using the example shown in the next section.

Table 4-1 ABCD Polynomials Of The Synthesis Example 0

Term	$A(s)$	$B(s)$	$C(s)$	$D(s)$	$P(s)$
3		1.9933	0.0067		-0.1154
2	2.7036	$-1.2428i$	$-0.1161i$	2.7036	$1.0388i$
1	$-2.9389i$	4.0578	2.8368	$-2.9389i$	3.0009
0	0.3553	$-3.0087i$	$-2.5085i$	0.3553	$-2.7701i$

4.3.3 Synthesis Illustrative Example

To demonstrate the general synthesis technique for pseudo-elliptic lowpass prototype filter, a hypothetical 3^{rd} degree elliptic lowpass filter with transmission zeros at $\omega = 2, 3, 4\ rad/s$ and 20 dB return loss is synthesised. The Chebyshev lowpass prototype filter ABCD matrix polynomials are derived using the methods described in Chapter 1 and Chapter 2 as shown in Table 4-1 below.

The TZG elements are then extracted as shown below. For the first TZG element with a transmission zero, $p = j2$ is extracted to give

$$k_1 = 1.2810$$
$$b_1 = 0.9539 \tag{4.45}$$

Table 4-2 Element Values Of The General Pseudo-elliptic Lowpass Prototype Filter

Input Coupling	$\theta_{01} = 37.9771^o$ $N_{01} = 0.6153$
TZG 1	$NRN_1 = -0.6102$ $Y_1 = -j0.6102 + \dfrac{0.9539}{p - j2}$
Inter Resonator Coupling	$N_{12} = 0.1603$
TZG 2	$NRN_2 = -0.2238$ $Y_2 = -j0.2238 + \dfrac{0.5973}{p - j3}$
Inter Resonator Coupling	$N_{23} = 0.0819$
TZG 3	$NRN_3 = -0.3317$ $Y_3 = -j0.3317 + \dfrac{1.2461}{p - j4}$
Output Coupling	$N_{34} = 0.3131$ $\theta_{34} = 18.2479^o$

The network is turned to start the extraction from the output and the last TZG element with a transmission zero at $p = j4$ is extracted to give,

$$k_3 = 3.0330$$
$$b_3 = 1.2461 \tag{4.46}$$

The network is turned back and a unit inverter is extracted

$$M_{12} = 1 \tag{4.47}$$

Then the middle TZG element is extracted with a transmission zero at $p = j3$ to give

$$k_2 = 5.6508$$
$$b_2 = 0.5973 \tag{4.48}$$

Finally the last element to be extracted is parallel connected inverter with a value

$$M_{23} = 0.7866 \tag{4.49}$$

The next step is to transform the network to the desired form of Fig. 4-8. Applying the formulae above, the circuit transformations were done. The final element values after the transformation are shown below in Table 4-2. The circuit simulation response is shown in Fig. 4-7.

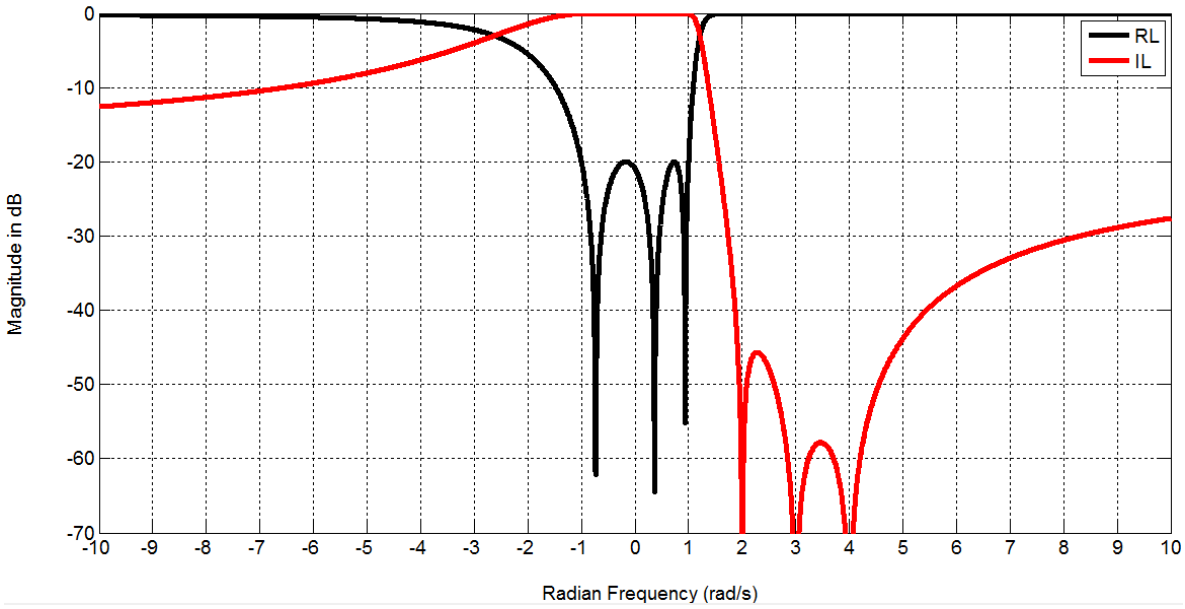

Fig. 4-7 Simulated response of the 3rd degree general elliptic lowpass prototype filter

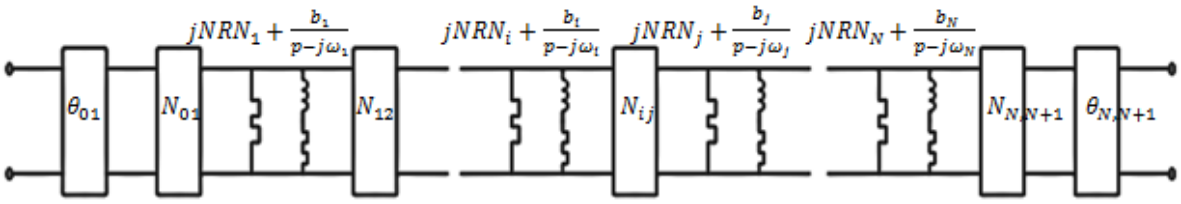

Fig. 4-8 General pseudo-elliptic lowpass prototype filter circuit after the 3 circuit transformations

Finally, the unity phase shifters at the input and output of the network only alter the phase response of the filter network and may thus be removed from the network to produce the final circuit form as in Fig. 4-9.

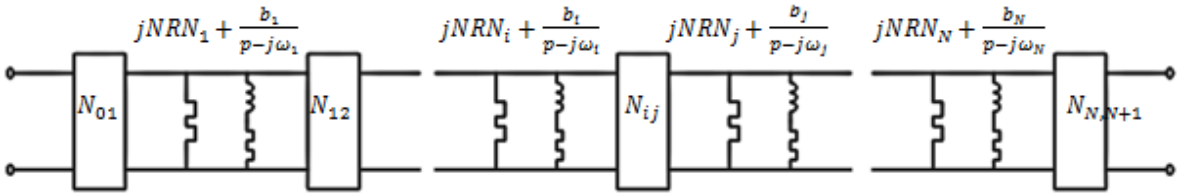

Fig. 4-9 General pseudo-elliptic lowpass prototype filter in its final circuit form

Filters with NRN represent the modern filter methods and the techniques to find the coupling coefficients for physical realisation have been a focal point in fairly recent research [71, 72]. With modern accuracy in computers, the accuracy lost in performing the transformations in a moderate order filters is negligible. Thus the foregoing synthesis method of elliptic lowpass prototype filters could prove a very useful arsenal in modern filter synthesis providing a starting point for physical realisation of pseudo-elliptic filter in the desirable technology of implementation such as coaxial cavity or waveguide filters.

4.4 Re-entrant Resonators

The concept of the re-entrant line was first introduced by Cohn in the design of couplers [75] and similar configurations were further applied in [76] for the design of wide bandpass and bandstop filters. The re-entrant cross section has also been used in [77] where the dual resonance and finite frequency transmission zero produced by a single resonator was exploited for dual bandpass applications.

The basic concept of a re-entrant transmission line is that it is a form of triaxial transmission line with three concentric conductors, one of which is grounded. Fig.

4-10 shows an example of an air filled re-entrant resonator. Because the inner conductor has zero admittance to ground, a re-entrant transmission line makes for practical and convenient realization as a microwave filter element. In fact this unique property alone makes the re-entrant line very useful as opposed to conventional two conductor transmission lines.

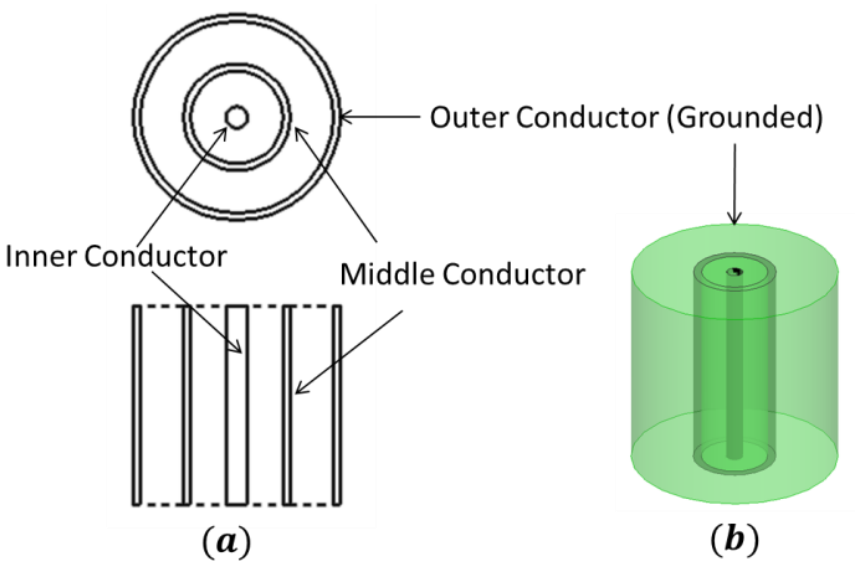

Fig. 4-10 A physical re-entrant transmission line: (a) top and cross section view (b) isometric view

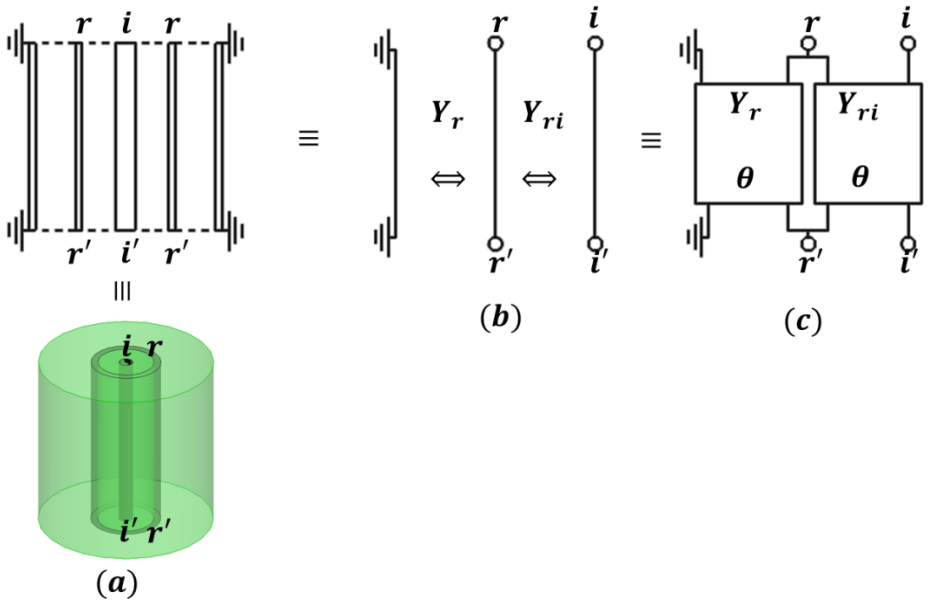

Fig. 4-11 A re-entrant line equivalent circuit (a) Physical transmission line (b) Graph representation (c) two series-connected transmission lines

Although, the conductors used in Fig. 4-10 are of cylindrical profile, other profiles such as square or rectangular coaxial may be employed where convenient. Furthermore, Fig. 4-10 also shows that a basic re-entrant transmission line is a four port transmission line. It is also readily seen from Fig. 4-10 that the equivalent circuit for the re-entrant line is a two series connected transmission line networks of commensurate length (θ) as depicted in Fig. 4-11. Here Y_r is the admittance to ground of the middle conductor, Y_{ri} is the admittance between the middle conductor and the inner center conductor and r indicates r^{th} resonator in the filter.

This equivalent circuit may be used to derive useful filtering elements by appropriately terminating two of the four ports in either short or open circuits. The choice of the termination depends on the physical realisability and required transmission and reflection characteristics.

A more useful and convenient equivalent circuit is obtained from Sato's two-wire equivalent circuit of coupled-lines [78] consisting of short circuited series stubs and transmission lines as depicted in Fig. 4-12. The four port numbers in [78] are replaced by variables (i.e. r, i, r' and i' as in Fig. 4-11). In this case, the only condition imposed on the inner conductor is that it has no admittance to ground i.e. $Y_{ii} = Y_{ri}$.

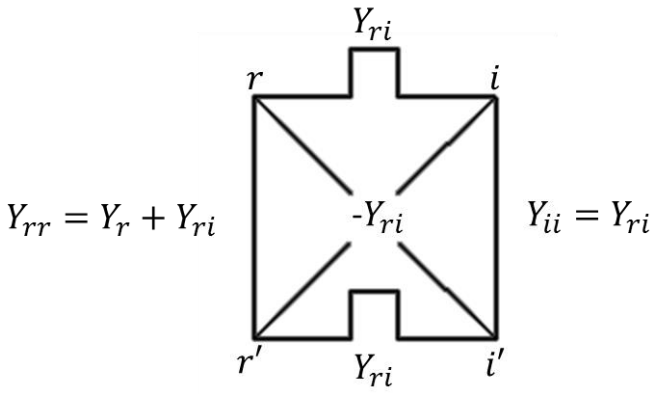

Fig. 4-12 Graph representation of the equivalent circuit of re-entrant line using Sato's equivalent circuit of two coupled lines

To realise useful filtering function for the re-entrant line, several equivalent circuits have been derived from the re-entrant line with their corresponding termination at two of the four ports. Clearly, there are 24 such permutations of a two port network

that may be derived from a four port network with appropriate short and open circuit termination at the two ports – since if any two ports are randomly picked, then there are 4 different possible ways of terminating the other two ports with either a short or open circuit and there are 6 unique combinations ($\binom{4}{2} = 6$) for each choice of any two terminals. Some of the equivalents circuits were listed in Table 4-3. However, not all of those equivalent circuit and termination in Table 4-3 are realisable for generating transmission zeros. The next section considers in detail three possible candidate solutions for producing transmission zeros in filter networks.

Table 4-3 Equivalent Circuits Under Different Terminations Of Re-Entrant Transmission Line

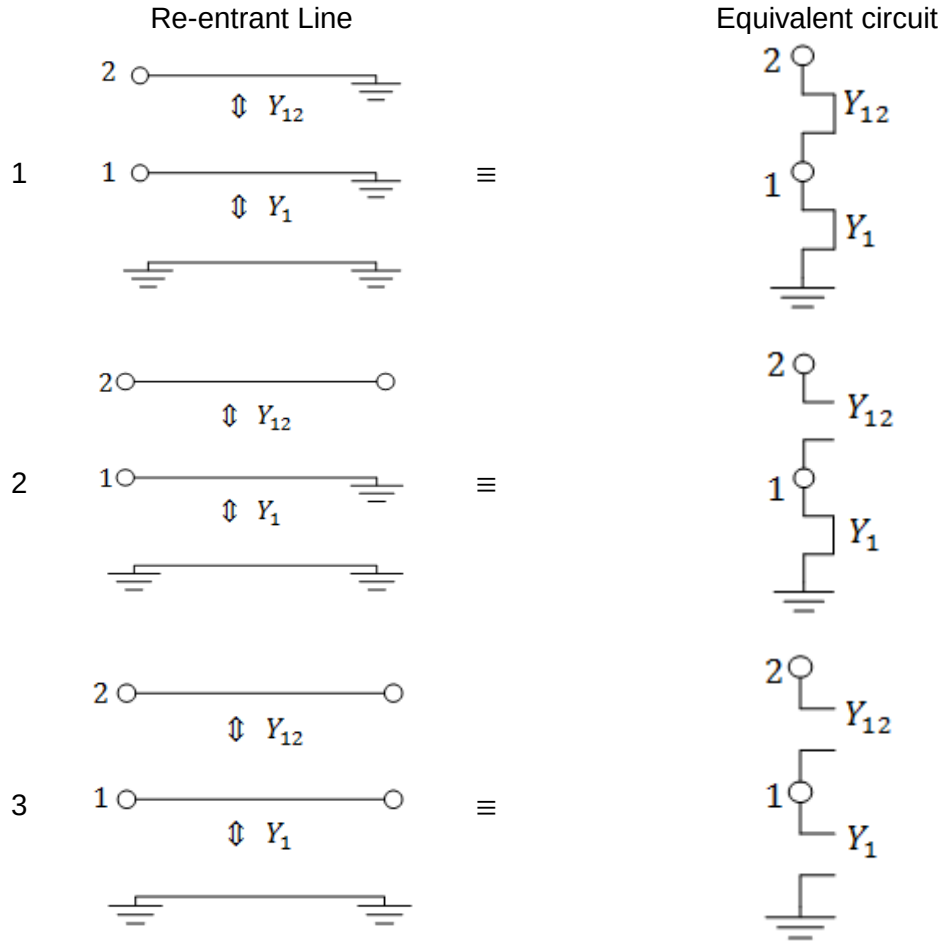

4

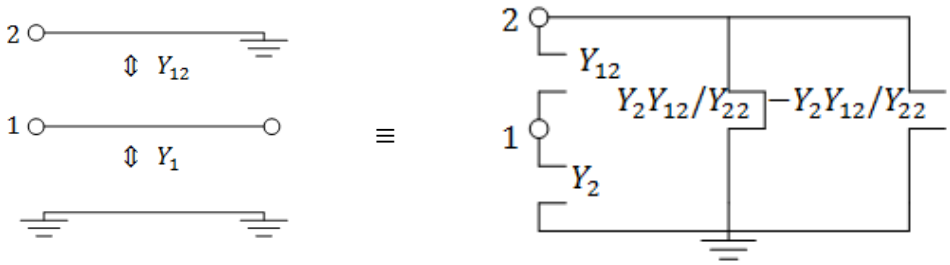
2
Y_{12}
1
Y_1
≡
2
Y_{12}
Y_2Y_{12}/Y_{22}
$-Y_2Y_{12}/Y_{22}$
1
Y_2

5

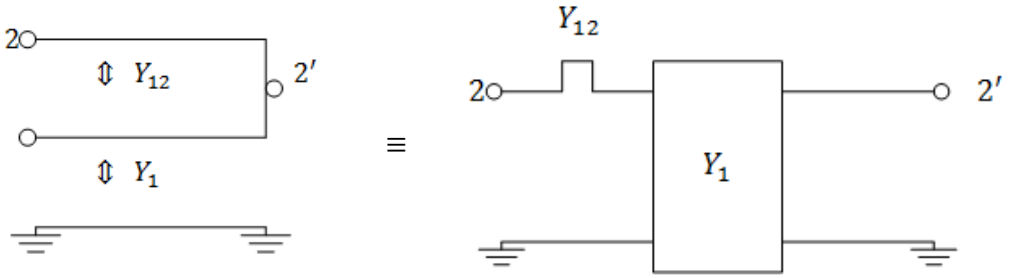
2
Y_{12}
2′
Y_1
≡
Y_{12}
2
2′
Y_1

6

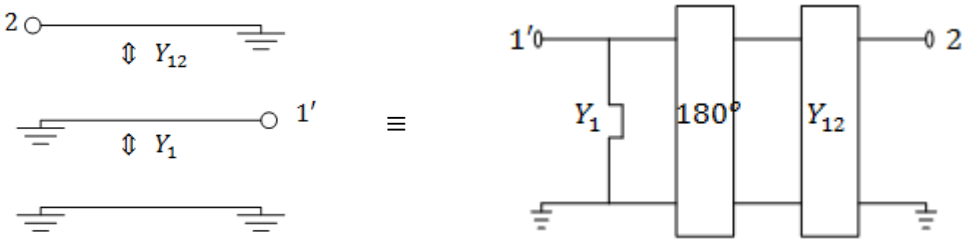
2
Y_{12}
1′
Y_1
≡
1′
2
Y_1
180°
Y_{12}

7

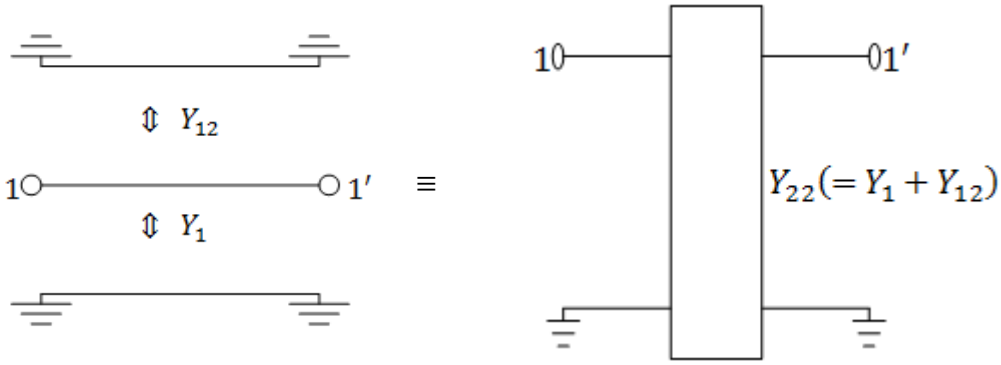
Y_{12}
1
1′
Y_1
≡
1
1′
$Y_{22}(=Y_1+Y_{12})$

8

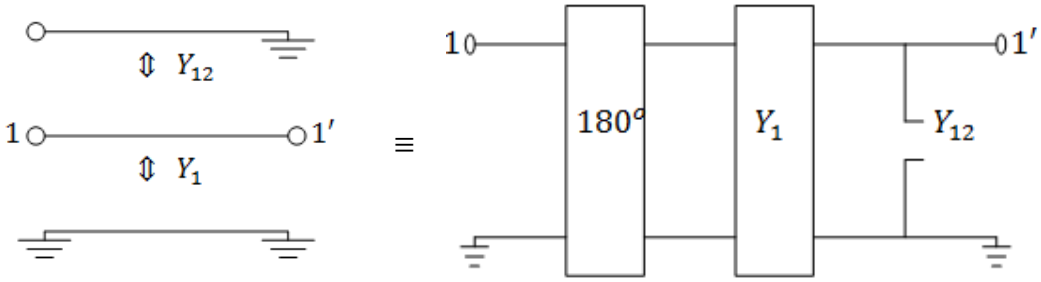
Y_{12}
1
1′
Y_1
≡
1
180°
Y_1
1′
Y_{12}

4.4.1 Re-entrant Resonator producing a transmission zero above the passband

To realize a transmission zero above the passband, two convenient re-entrant structures may be used. For case 1, the two ports on one end of the re-entrant line in Fig. 4-12 i.e. port r' and i', are short-circuited to the ground yielding the equivalent circuit as shown in Fig. 4-13(a) consisting of short-circuited stubs. This can be verified by inspection of the equivalent circuit shown in Fig. 4-11(c). Resonance is achieved by capacitively loading port i as shown in Fig. 4-13(b) and Fig. 4-14.

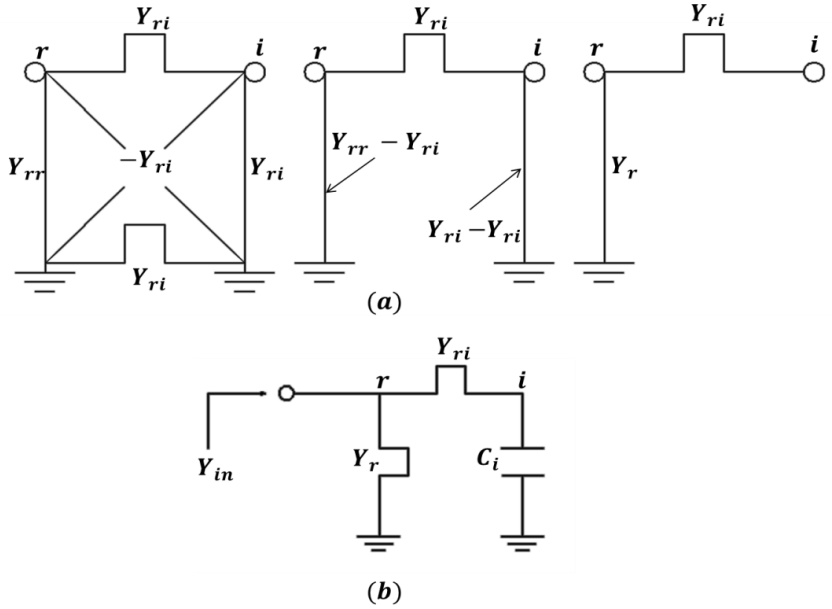

Fig. 4-13 Case 1 - Re-entrant resonator realizing a transmission zero above the passband (a) derivation of the equivalent circuit (b) resonance circuit.

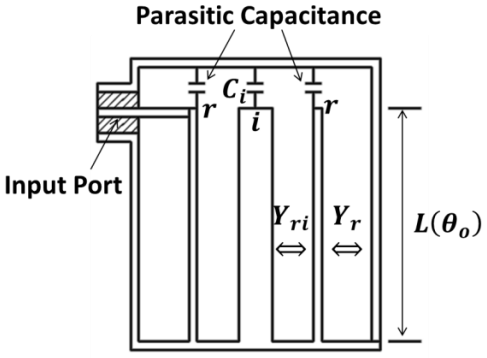

Fig. 4-14 Cross section of a physical realization of circuit of Fig. 4-13(b)

The input impedance of circuit of Fig. 4-13(b) may be computed as

$$Z_{in}(j\omega) = j\frac{Z_r \tan(a\omega)\,(\omega C_r Z_{ri} \tan(a\omega) - 1)}{1 - \omega C_r (Z_r + Z_{ri}) \tan(a\omega)} \tag{4.50}$$

where

$$a = \frac{\theta_o}{\omega_o} \tag{4.51}$$

and

$$C_r = \frac{1}{\omega_z Z_{ri}\, tan(a\omega_z)}$$
$$Z_r = Z_{ri}\left(\frac{\omega_o\, tan(a\omega_o)}{\omega_z\, tan(a\omega_z)} - 1\right) \tag{4.52}$$

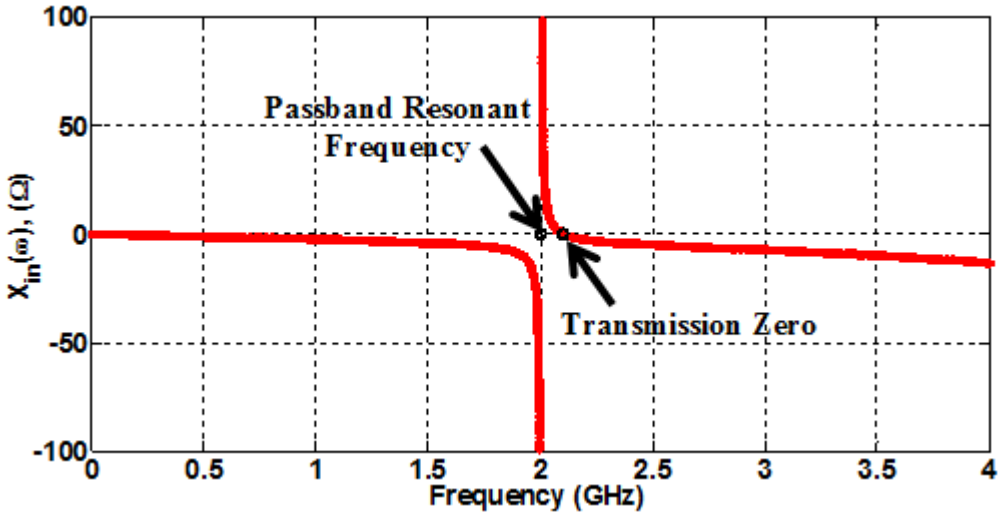

Fig. 4-15 Reactance function $X_{in}(\omega)$ plot corresponding to circuit of Fig. 4-13

Where, $\omega_o = 2\pi f_o$, $\omega_z = 2\pi f_z$, and θ_o are the centre frequency, the position of the transmission zero frequency and the electrical length at the centre frequency respectively. Circuit element values are obtained for example if $f_o = 2\ GHz$, $f_z = 2.2\ GHz$, $\theta_o = \pi/6\ rad$, and $Z_{ri} = 77\ \Omega$, then using (4.51) - (4.52), $C_i = 1.45\ pF$ and $Z_r = 18.27\ \Omega$. A plot of a reactance $X_{in}(\omega)$ of $Z_{in}(j\omega)$ against frequency is shown in Fig. 4-15. The presence of the parasitic capacitance in Fig. 4-14 results in the second passband very close to the first passband.

Although case 1 offers the easiest form of realization, it does present a challenge in the filter to control the lumped capacitance at port i as well as the shortening of

the open-circuit end of port r (parasitic capacitance). This may easily be solved in case 2 by short-circuiting the alternate ends of the inner and middle conductor of Fig. 4-11 i.e. port r' and i. The equivalent circuit for case 2 is found from the two-wire admittance matrix for coupled lines as [4],

$$\begin{bmatrix} I_r \\ I_i \\ I_{r'} \\ I_{i'} \end{bmatrix} = \frac{1}{t}\begin{bmatrix} Y_{rr} & -Y_{ri} & Y_{rr}{}' & -Y_{ri}{}' \\ -Y_{ir} & Y_{ii} & -Y_{ir}{}' & Y_{ii}{}' \\ Y_{rr}{}' & -Y_{ri}{}' & Y_{rr} & -Y_{ri} \\ -Y_{ir}{}' & Y_{ii}{}' & -Y_{ir} & Y_{ii} \end{bmatrix}\begin{bmatrix} V_r \\ V_i \\ V_{r'} \\ V_{i'} \end{bmatrix}, \tag{4.53}$$

where,

$$Y'_{nm} = -\left(\sqrt{1-t^2}\right)Y_{nm},\ n \text{ and } m \text{ are indices as in [4]} \tag{4.54}$$

$t = jtanh(ap)$, p is the complex frequency variable, and I and V are port current and voltage. Now, for case 2 port $r'$and i are short-circuited to ground so that $V_i = V_{r'} = 0$ in (4.53). Thus (4.53) may be re-written for a two-port as

$$\begin{bmatrix} I_r \\ I_{i'} \end{bmatrix} = \begin{bmatrix} \dfrac{Y_r + Y_{ri}}{t} & \dfrac{\left(\sqrt{1-t^2}\right)Y_{ri}}{t} \\ \dfrac{\left(\sqrt{1-t^2}\right)Y_{ri}}{t} & \dfrac{Y_{ri}}{t} \end{bmatrix}\begin{bmatrix} V_r \\ V_{i'} \end{bmatrix}. \tag{4.55}$$

Where the substitution

$$\begin{aligned} Y_{rr} &= Y_r + Y_{ri} \\ Y_{ii} &= Y_{ri} \\ Y_{ri} &= Y_{ir} \end{aligned} \tag{4.56}$$

was made to arrive at (4.55). The two-port admittance matrix between port r and i' from (4.55) is

$$[Y] = \begin{bmatrix} \dfrac{Y_r + Y_{ri}}{t} & \dfrac{\left(\sqrt{1-t^2}\right)Y_{ri}}{t} \\ \dfrac{\left(\sqrt{1-t^2}\right)Y_{ri}}{t} & \dfrac{Y_{ri}}{t} \end{bmatrix}. \tag{4.57}$$

This may be converted to ABCD matrix as

$$[ABCD] = \frac{1}{\sqrt{1-t^2}}\begin{bmatrix} -1 & -\frac{t}{Y_{ri}} \\ -\left(\frac{Y_r}{t} + Y_{ri}t\right) & -\left(\frac{Y_r}{Y_{ri}} + 1\right) \end{bmatrix}. \tag{4.58}$$

This may further be decomposed into

$$[ABCD] = \begin{bmatrix} 1 & 0 \\ \frac{Y_r}{t} & 1 \end{bmatrix}\begin{bmatrix} -1 & 0 \\ 0 & -1 \end{bmatrix}\frac{1}{\sqrt{1-t^2}}\begin{bmatrix} 1 & \frac{t}{Y_{ri}} \\ Y_{ri}t & 1 \end{bmatrix}. \tag{4.59}$$

This ABCD matrix represents the series connection of a shunt short-circuited stub of characteristic admittance Y_r, a unit admittance 180^o phase shifter and a transmission line of characteristic admittance Y_{ri}. Thus the equivalent circuit of case 2 is as shown in Fig. 4-16(a). Resonance is achieved at node r by capacitively loading port i' as shown in Fig. 4-16(b) and Fig. 4-17. This is a convenient form of realization because the lumped fringing capacitance at the bottom end of the inner line (port i') and the open-circuit end of the middle line (port r) may be independently controlled allowing independent tuning of the resonant frequency and the transmission zero location associated with each resonator. The input impedance of circuit of Fig. 4-16(b) may be computed as

$$Z_{in}(j\omega) = j\frac{Z_r Z_{ri}(\omega C_r Z_{ri}\tan(a\omega) - 1)\tan(a\omega)}{Z_r\tan^2(a\omega) - Z_{ri} + \omega C_r Z_{ri}(Z_r + Z_{ri})\tan(a\omega)} \tag{4.60}$$

where

$$a = \frac{\theta_o}{\omega_o} \tag{4.61}$$

and

$$\begin{aligned} C_r &= \frac{1}{\omega_z Z_{ri}\, tan(a\omega_z)} \\ Z_r &= \frac{Z_{ri}(1 - \omega_o C_r Z_{ri}\tan(a\omega))}{tan(a\omega_o)\,(tan(a\omega_o) + \omega_o C_r Z_{ri})} \end{aligned} \tag{4.62}$$

Similarly, circuit element values are obtained for example if $f_o = 2\,GHz$, $f_z = 2.2\,GHz$, $\theta_o = \pi/6\ rad$, and $Z_{ri} = 77\,\Omega$, then using (4.61) - (4.62), $C_r = 1.45\,pF$ and $Z_r = 12.94\ \Omega$. The plot of the reactance function $X_{in}(\omega)$ of $Z_{in}(j\omega)$ against frequency is shown in Fig. 4-18 for the above example.

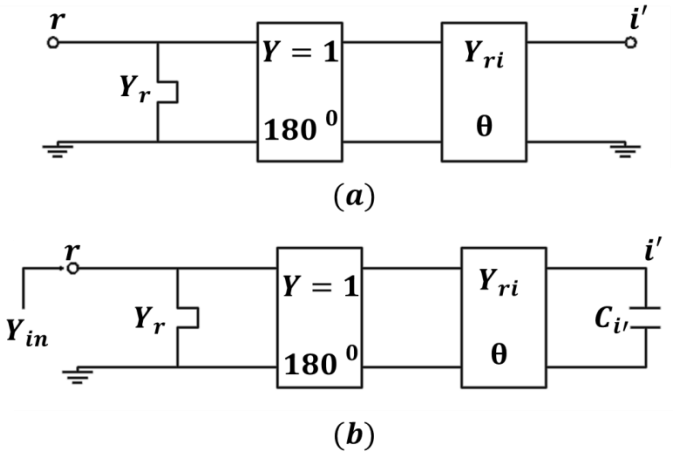

Fig. 4-16 Case 2 - Re-entrant resonator circuit realizing a transmission zero above passband (a) equivalent circuit (b) resonance circuit

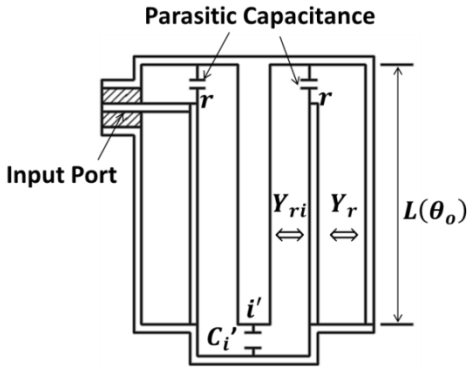

Fig. 4-17 Cross section of a physical realization of circuit of Fig. 4-16(b)

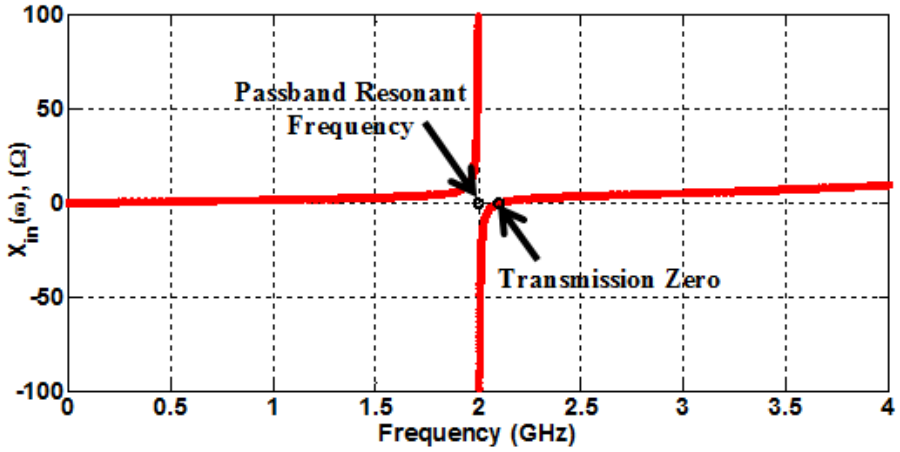

Fig. 4-18 Reactance function $X_{in}(\omega)$ plot corresponding to circuit of Fig. 4-16(b)

4.4.2 Re-entrant Resonator producing a transmission zero below the passband

A transmission zero below the passband may be achieved by terminating port r' and port i' of the re-entrant line in Fig. 4-11 with an open-circuit and short-circuit respectively. The equivalent circuit of the resulting two port network is found by reducing the four port admittance matrix of the re-entrant line to a two-port admittance matrix as was done for case 2 of section 0. The equivalent circuit between port r and i may then be obtained directly from the 2-port admittance matrix or conversion into ABCD matrix as shown in Fig. 4-19(a). Capacitively loading port i produces the resonant circuit as shown in Fig. 4-19(b) and Fig. 4-20. The input impedance of circuit of Fig. 4-19(b) may be computed as

$$Z_{in}(j\omega) = j\frac{Z_r Z_{ri} - {Z_r}^2 \tan^2(a\omega) - \omega Z_r Z_{ri} C_i (Z_r + Z_{ri}) \tan(a\omega)}{(Z_r + Z_{ri}) \tan(a\omega)\,(\omega C_i (Z_r + Z_{ri}) \tan(a\omega) - 1)} \tag{4.63}$$

Where

$$a = \frac{\theta_o}{\omega_o} \tag{4.64}$$

and

$$Z_r = \frac{(\omega_o \tan(a\omega_o) - \omega_z \tan(a\omega_z))}{\omega_o \tan(a\omega_o)\, tan^2(a\omega_z)} Z_{ri}$$

$$C_i = \frac{1}{\omega_o (Z_r + Z_{ri}) \tan(a\omega_o)} \tag{4.65}$$

Circuit element values are obtained for example if $f_o = 2\,GHz$, $f_z = 1.95\,GHz$, $\theta_o = \pi/6\ rad$, and $Z_{ri} = 77\,\Omega$, then using (15) - (16), $Z_r = 13.32\,\Omega$ and $C_i = 1.53\ pF$. Finally, the plot of the reactance function $X_{in}(\omega)$ of $Z_{in}(j\omega)$ against frequency is shown in Fig. 4-21. Though, it is theoretically possible to realize transmission zeros below the passband using the re-entrant structure of Fig. 4-20, its physical construction is impractical for real applications as it requires the suspension of the middle conductor. For this reason, design theory has only been fully developed for case 2 of section II (A) for re-entrant bandpass filters with transmission zeroes above the passband.

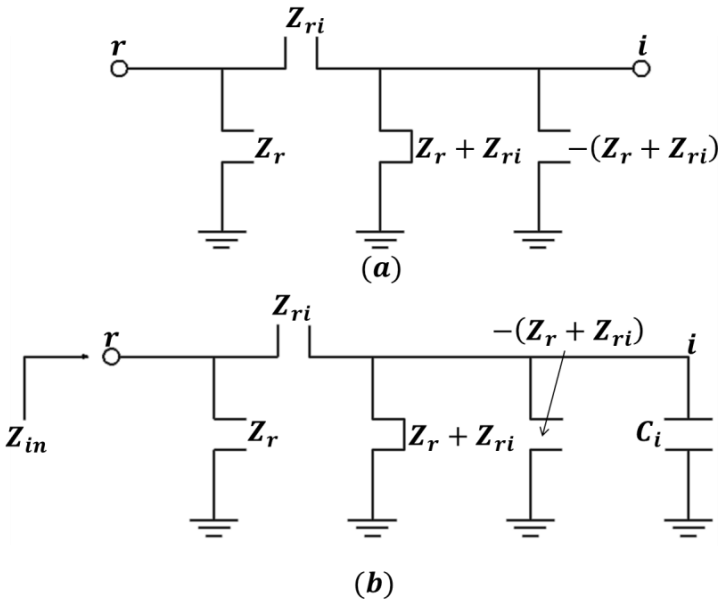

Fig. 4-19 Re-entrant resonator circuit that realizes transmission zero below the passband (a) equivalent circuit (b) resonance circuit

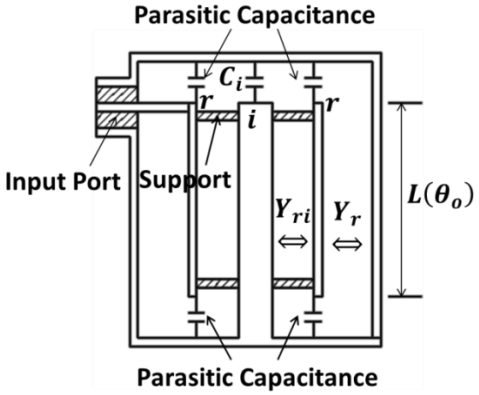

Fig. 4-20 Cross section of a physical realization of circuit of Fig. 4-19(b)

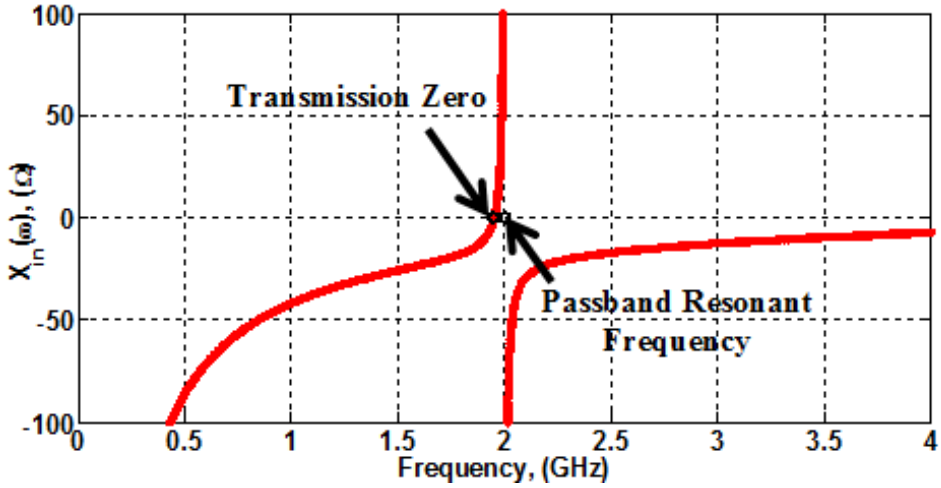

Fig. 4-21 Reactance function $X_{in}(\omega)$ plot corresponding to circuit of Fig. 4-19 (b)

4.5 Design Theory for Re-entrant Bandpass Filter

Having obtained the equivalent circuit of a re-entrant resonator, design theory to obtain the re-entrant line element values for bandpass filter design is now derived.

4.5.1 Re-entrant Bandpass Filter Equivalent Circuit

The equivalent circuit of two coupled nodes in the re-entrant bandpass filter with case 2 resonators may easily be obtained from [78] by considering two middle transmission lines of the re-entrant resonators, short-circuited at one end and then superimposing the equivalent circuit towards the inner transmission lines at node r and $r+1$. This is similar to a combline bandpass filter except for the inner transmission lines. Therefore, the equivalent circuit of the N^{th} re-entrant bandpass filter is simply the interconnection of N re-entrant resonator circuits of Fig. 4-16(b) in section 0 by coupling series short-circuited stubs.

Fig. 4-22 shows the equivalent circuit of the N^{th} degree re-entrant bandpass filter. Note that the 180^o phase shifters in Fig. 4-16(b) may be ignored as they only account for the phase and have no effect on the magnitude response. Admittance inverters may be formed by adding shunt short-circuited stubs at r^{th} and $(r+1)^{th}$ nodes as in Fig. 4-23 where,

$$K_{r,r+1} = \frac{Y_{r,r+1}}{\tan(\theta)}. \tag{4.66}$$

The positive shunt short-circuited stub admittances in circuit of Fig. 4-23 are absorbed at the surrounding nodes leading to the final equivalent circuit as shown in Fig. 4-24 where,

$$\begin{aligned} Y_{11} &= Y_1 + Y_{12} \\ Y_{rr} &= Y_r + Y_{r-1,r} + Y_{r,r+1} \\ Y_{NN} &= Y_N + Y_{N-1,N} \end{aligned} \tag{4.67}$$

It is now left to derive the frequency transformation from a pseudo-elliptic lowpass prototype filter of section 4.3 that preserves the frequency response so that the bandpass elements in (4.66) and (4.67) may be determined.

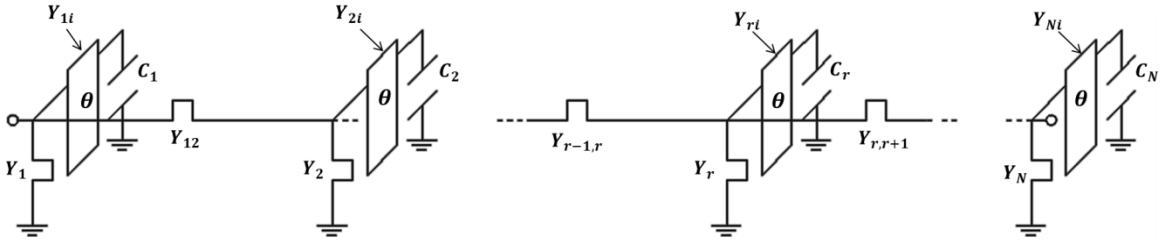

Fig. 4-22 Equivalent circuit of an N^{th} degree re-entrant bandpass filter

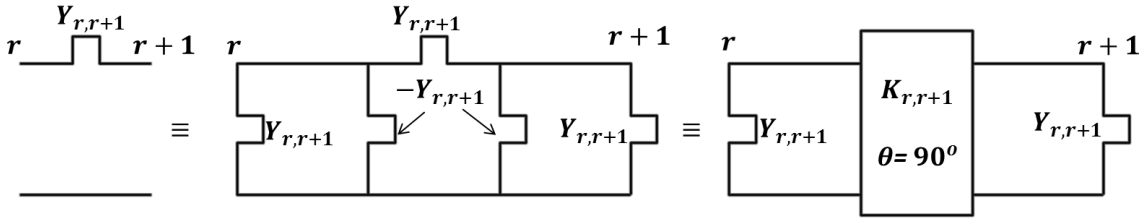

Fig. 4-23 Formation of admittance inverters between node r and $r+1$

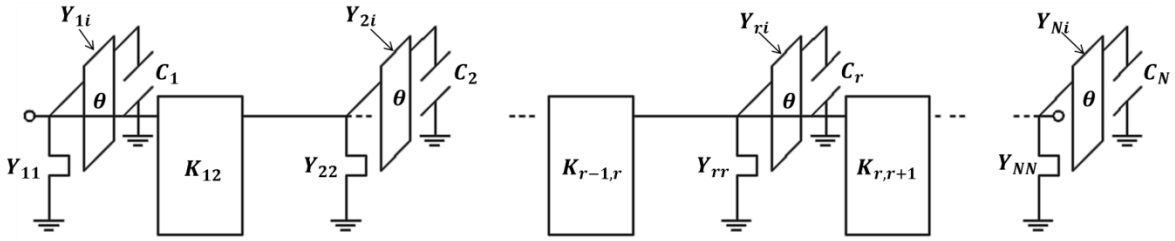

Fig. 4-24 Final equivalent circuit of an N^{th} degree re-entrant bandpass filter with admittance inverters

4.5.2 Pseudo-elliptic Lowpass Prototype filter to Bandpass filter Frequency Transformation

In section 4.3 a suitable lowpass prototype filter was derived as shown in Fig. 4-25 consisting of a shunt frequency invariant reactance (B_r) in parallel with a shunt series of an inductor ($1/b_r$) with frequency invariant reactance ($-\omega_r/b_r$) separated by frequency invariant admittance inverters $K'_{r-1,r}$ and $K'_{r,r+1}$. Thus at each network node r, the r^{th} input admittance may be expressed as,

$$Y'_{in}(j\omega) = jB_r + \frac{b_r}{p - j\omega_r} = j\left(\frac{1 - \omega_r\omega}{\omega - \omega_r}\right)C_r. \tag{4.68}$$

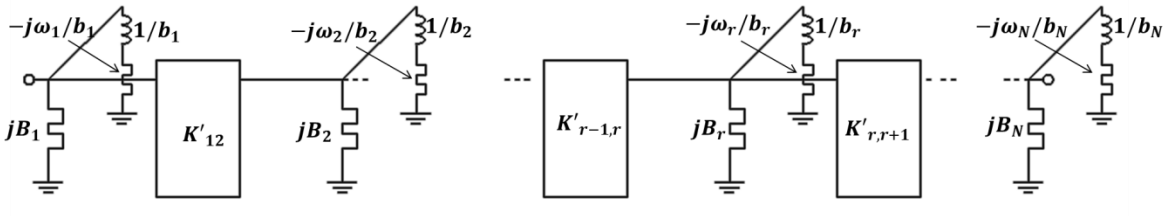

Fig. 4-25 N^{th} degree all-pole pseudo-elliptic lowpass prototype filter with admittance inverters (input and output inverters not shown)

Recall that for the first lowpass filter of section 4.3.1 where all the transmission zeros are at a single finite frequency ω_r rad/s ($\omega_r = \omega_0, r = 1,2,\dots,N$) in the lowpass domain, an all-pole Chebyshev lowpass filter network shown in Fig. 4-26 needs to be synthesised first.

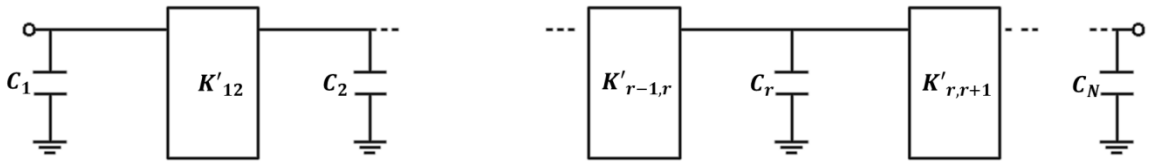

Fig. 4-26 N^{th} degree all-pole Chebyshev lowpass filter

Then using transformation (4.4), the all-pole Chebyshev lowpass filter network of shunt capacitors C_r separated by admittance inverters $K'_{r,r+1}$ may be transformed to the required lowpass prototype filter of Fig. 4-25 as

$$Y'_{in}(j\omega) = j\omega C_r = j\left(\frac{1-\omega_r\omega}{\omega-\omega_r}\right)C_r. \tag{4.69}$$

Which may be re-written as in (4.68) as,

$$Y'_{in}(j\omega) = -j\omega_r C_r + \frac{C_r({\omega_r}^2-1)}{j\omega - j\omega_r} = jB_r + \frac{b_r}{s-j\omega_r}. \tag{4.70}$$

Where,

$$\begin{aligned} B_r &= -\omega_r C_r \\ b_r &= C_r({\omega_r}^2-1) \end{aligned} \tag{4.71}$$

Again the frequency invariant admittance inverters $K'_{r,r+1}$ between the nodes in the all-pole Chebyshev lowpass prototype filter remain unchanged by this transformation. In order to make the admittance inverters frequency invariant in the re-entrant bandpass equivalent circuit, the admittance of the entire network is

scaled by $tan(\theta)/tan(\theta_o)$, where θ_o is the electrical length of the re-entrant resonator at the center frequency. The source and load admittances are also scaled by $tan(\theta)/tan(\theta_o)$ but the variations of $tan(\theta)/tan(\theta_o)$ is small for narrow bandwidth filters. Thus the frequency invariant admittance inverters are mapped as

$$K_{r,r+1} = \frac{Y_{r,r+1}}{tan(\theta_o)} = K'_{r,r+1}. \tag{4.72}$$

Hence,

$$Y_{r,r+1} = K'_{r,r+1} tan(\theta_o). \tag{4.73}$$

Furthermore, the frequency variant admittance at r^{th} node of the re-entrant bandpass, (4.60), maps onto the admittance at r^{th} node of the lowpass. For example utilising the lowpass prototype filter from section 4.3.1, the mapping may be achieved as follows:

$$\left(\frac{1-\omega_r\omega}{\omega-\omega_r}\right) C_r \Rightarrow$$

$$\frac{\alpha_r - \alpha_r\beta_r\omega\tan(\theta) - \tan^2(\theta) - \beta_r\omega\tan(\theta)}{\gamma_r\tan(\theta_o) * [\beta_r\omega\tan(\theta) - 1]} \tag{4.74}$$

where,

$$\alpha_r = \frac{Y_{rr}}{Y_{ri}},\ \beta_r = \frac{C_r}{Y_{ri}} \text{ and } \gamma_r = \frac{1}{Y_{ri}} \tag{4.75}$$

Fig. 4-27 illustrates the frequency mapping defined using (4.74) above. The parameters α_r, β_r and γ_r may be determined by mapping the centre frequency, $\omega = 0$ and the two bandedge frequencies at $\omega = \pm 1$ of the lowpass prototype onto the centre frequency ω_o, lower cut-off frequency ω_1 and upper cut-off frequency ω_2 respectively of the re-entrant bandpass filter using (4.74) and solving the resulting non-linear equations for the variables α_r, β_r and γ_r at each node r. The re-entrant bandpass element values are then obtained as follows:

$$Y_{ri} = \frac{1}{\gamma_r},\ Y_r = \frac{\alpha_r}{\gamma_r} \text{ and } C_r = \frac{\beta_r}{\gamma_r} \tag{4.76}$$

The same mapping may be achieved for the general pseudo-elliptic lowpass filter as demonstrated above. Finally the entire network nodal admittance matrix may be scaled at the nodes to yield realisable impedance values. The input and output

connections are made by direct tap onto the first and last middle conductors. Redundant coupled lines at the input and output may also be added if desired.

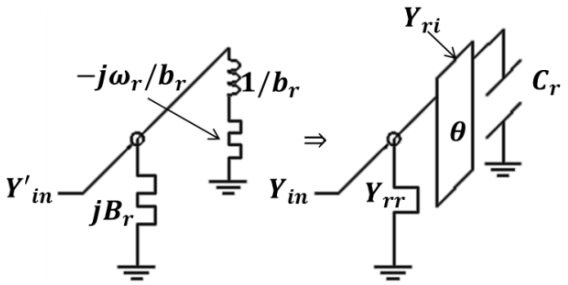

Fig. 4-27 Frequency mapping of the admittances at r^{th} node

4.5.3 Close-to-Band Transmission Zeroes

In this section, the limitation of the transmission zero locations is discussed with respect to the element realisations. For example for the transmission zero above the passband re-entrant structure of Fig. 4-17, consider a single resonator where the bandwidth is controlled by the input and output couplings, then using (4.62) of section 0 for $f_o = 1\,GHz$ and $Z_{ri} = 77\,\Omega$, the ratio of Z_{ri}/Z_r and C_r were plotted against the transmission zero locations as depicted in Fig. 4-28. It is clear from Fig. 4-28 that the ratio Z_{ri}/Z_r increases as the transmission zero location gets closer to the upper passband edge. As the transmission zeros get very close to the passband, clearly Z_r becomes unrealisably small. Increasing θ_o from $\theta_o = 30^o$ in Fig. 4-28(a) to $\theta_o = 45^o$ in Fig. 4-28(b) increases the ratio Z_{ri}/Z_r while the capacitance loading C_r decreases. This means Z_r decreases for a fixed Z_{ri}. By using a different θ_o a similar analysis may be done to determine the location of the transmission zeros that will give realizable Z_r given Z_{ri}. For a given bandwidth and centre frequency, the closest transmission zero to the passband the structure can support would be determined by the realisability of Z_r for a fixed Z_{ri} by using an appropriate electrical length (θ_o). Thus the structure can realize transmission zeros as close as one passband bandwidth away from the passband edge. More specific design examples and impedance levels for the elements will be given later.

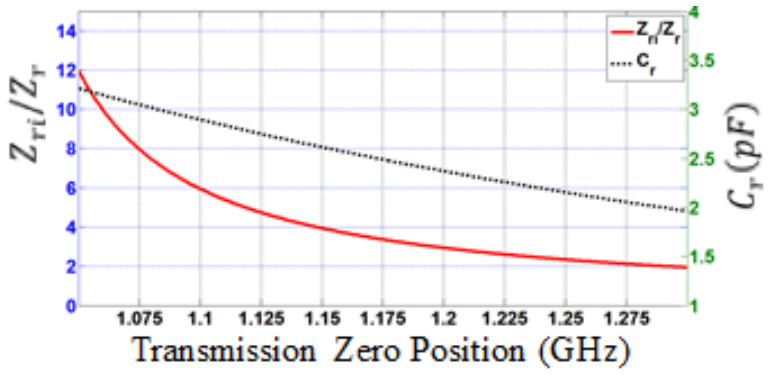

(a)

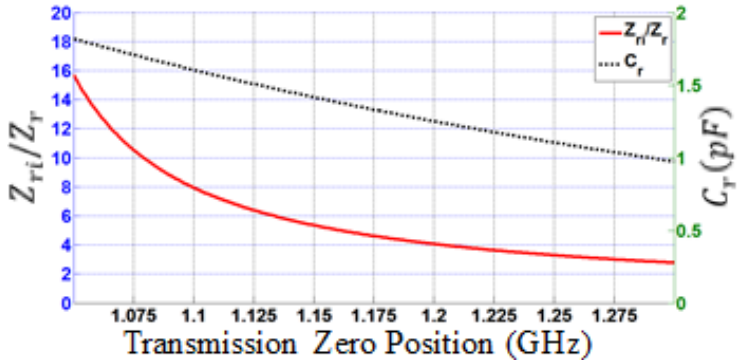

(b)

Fig. 4-28 (a) Element values vs transmission zero positions $f_o = 1\ GHz$, and $\theta_o = 30^o$and $Z_{ri} = 77\ \Omega$ (b) Element values vs transmission zero positions $f_o = 1\ GHz$, and $\theta_o = 45^o$and $Z_{ri} = 77\ \Omega$

4.5.4 Physical dimensions

With the element values known, calculation of the physical dimensions is fairly straight-forward using established methods already used for combline and interdigital bandpass filters as explained in [4, 5, 32]. The inner transmission lines are realized as circular coaxial lines which are easy to machine. One end of the inner re-entrant line is fixed to the upper metallic wall (cover) by screwing it into the wall. Metallic discs may be fitted to the other end of the inner re-entrant line to achieve the required capacitive loading. The middle transmission lines may be realized with circular or rectangular rods. The ground spacing is chosen to achieve the given unloaded Quality factor, Q_u and that there is sufficient space for the inner re-entrant conductor.

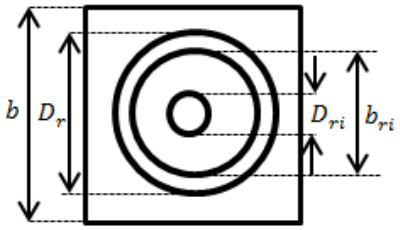

Fig. 4-29 Re-entrant resonator cross section corresponding to Fig. 4-17 structure of section 0 case 2 with square outer conductor and circular middle and inner conductors and height H (not shown)

Table 4-4 Re-entrant Resonator vs Coaxial Resonator

Air-Filled Re-entrant Resonator With $b = 35\ mm, b_{ri} = 18\ mm, D_{ri} = 4.99\ mm, H = 25\ mm$				
Middle Conductor D_r (mm)	Resonant Frequency(GHz)	First Spurious (GHz)	UnloadedQ_u	Q_u per Volume (mm^{-3})
32.14	1.02	2.82	1805	0.055
24.43	1.01	2.76	2226	0.067
Air-Filled Coaxial Resonator With $b = 35\ mm, H = 25\ mm$				
Inner Conductor D_r (mm)	Resonant Frequency(GHz)	First Spurious (GHz)	UnloadedQ_u	Q_u per Volume (mm^{-3})
13.89	1.00	6.16	3386	0.111

It is quite obvious that the advantages of the re-entrant resonator of having close-to-band transmission zeros creating high stopband rejection and simple in-line structure do have trade-offs. The theoretical spurious resonance is three times the centre frequency for $\theta_o = 30^o$. However, because of the presence of the parasitic capacitance on one end of the middle conductor, the spurious resonances actually appear closer to the first passband. Furthermore, choosing relatively large ground spacing pushes these farther down in frequency. Table 4-4 shows the unloaded Q_u and spurious performance for a re-entrant resonator compared to the normal coaxial resonator of comparative size using HFSS assuming silver plated

conductors. Following up from section 4.5.3, it may be seen that for fixed inner conductor dimensions, the transmission zero is controlled by the middle conductor dimension, i.e. D_r as shown in Fig. 4-29. Therefore, for a fixed ground plane spacing (b) and as the position of the transmission zero gets closer to the passband, D_r increases. The middle conductor dimension in Table 4-4 corresponds to a transmission zero position at 1.075 GHz (32.14 mm) and 1.2 GHz (24.43 mm) respectively. It is clear from Table 4-4 that the unloaded Q_u is lower in re-entrant resonator and further degrades for much closer-to-band transmission zeros above the passband.

The requirement to physically incorporate two conductors within the same physical structure and to improve the unloaded Q_u does mean that the re-entrant filter would require relatively large resonator size. However, in certain cellular applications where deep stopband rejections are required on the upper side of the passband, the re-entrant resonator bandpass filter would provide a good alternative solution.

4.6 Design Examples

4.6.1 Design Example I

A 5 pole re-entrant bandpass filter with centre frequency at 1 GHz, 50 MHz bandwidth and 20 dB return loss was designed. The filter was designed with the following arbitrary located transmission zeros as:

$$\omega_r = [7.1616, 3.4, 3, 3.2, 4.44, 7.1404]\ rad/s$$

corresponding to microwave frequencies:

$$f_r = [1.147, 1.077, 1.068, 1.098, 1.147]\ GHz.$$

Firstly, the pseudo-elliptic prototype lowpass filter with arbitrary transmission zeros was synthesised corresponding to the circuit of Fig. 4-26 above. The obtained element values are shown in Table 4-5 below. The bandpass element values are obtained as described in section 4.5.2. The electrical length at the centre frequency was chosen to be $\theta_o = 30^o$. After the bandpass frequency transformation and scaling so that the inner re-entrant lines are identical for all resonators (i.e.

$Z_{ri} = 77\ \Omega$), the element values were determined as shown in Table 4-6 in a $50\ \Omega$ system.

Table 4-5 Elliptic Lowpass Filter Element Values

B_r	b_r	$K_{ij}{}'$
-7.0647	48.8958	0.2192
-0.2262	0.6968	0.0440
-0.2158	0.5744	0.0331
-0.1693	0.7069	0.1658
-6.9901	48.6018	

Table 4-6 Re-entrant Bandpass Filter Element Values

$Z_{ri} = 77\ \Omega$

Middle Conductors	Capacitors	Coupling admittances	Input and Output Coupling
$Z_1 = 27.5963\ \Omega$	$C_1 = 2.6265\ pF$	$Z_{12} = 53.9827\ \Omega$	$Z_{s1} = 50\ \Omega$
$Z_2 = 15.2545\ \Omega$	$C_2 = 3.0335\ pF$	$Z_{23} = 33.9059\ \Omega$	$Z_{7l} = 50\ \Omega$
$Z_3 = 12.8267\ \Omega$	$C_3 = 3.0868\ pF$	$Z_{34} = 43.6124\ \Omega$	
$Z_4 = 20.7958\ \Omega$	$C_4 = 2.9050\ pF$	$Z_{45} = 69.1771\ \Omega$	
$Z_5 = 25.1697\ \Omega$	$C_5 = 2.6271\ pF$		

The circuit simulation is shown in Fig. 4-30. All the element values shown are realisable with the middle conductors realised in rectangular coaxial profile, while the inner transmission lines are realised with circular coaxial and are identical. The input and output feed is implemented by means of a tap near the top of the first and last resonators. The close to band transmission zero at 1.068 GHz is created by the centre resonator as evidenced by the smallest characteristic impedance ($Z_4 = 12.8267\ \Omega$). This impedance may easily be scaled up if necessary. The outermost transmission zeros at 1.145 GHz are created by the the first and last resonators. Deep stopband rejection of about 120 dB is achieved around the transmission zeros positions.

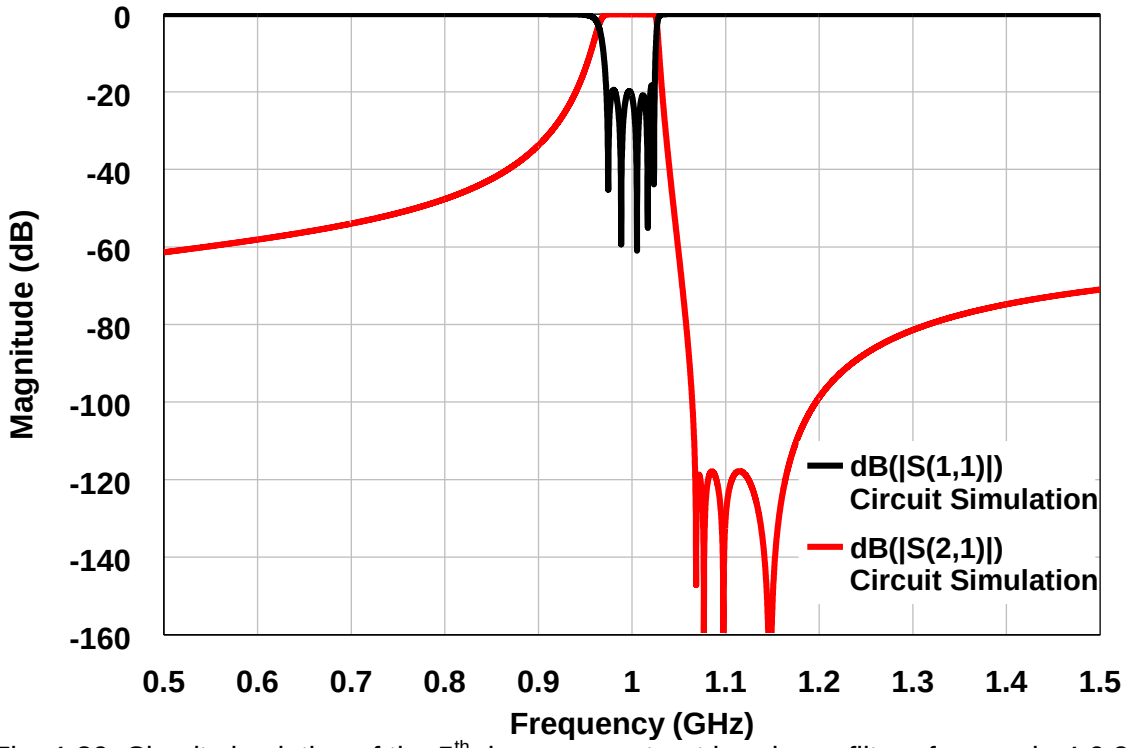

Fig. 4-30 Circuit simulation of the 5th degree re-entrant bandpass filter of example 4.6.2

4.6.2 Design Example II

A 5 pole re-entrant bandpass filter with centre frequency at 1 GHz, 85 MHz bandwidth, 20 dB return loss and 1 dB maximum insertion loss across ripple bandwidth was designed. A lowpass filter was first designed with all the transmission zeroes placed at $\omega_r = 5.5\, rad/s$, corresponding to a microwave frequency of $1.1466\, GHz$.

The Chebyshev lowpass filter with $20\, dB$ return loss was synthesized with elements values C_r and $K'_{r,r+1}$ obtained. Then (4.15)-(4.16) was used to obtain the element values of the pseudo-elliptic lowpass prototype filter required for the design of the re-entrant bandpass filter. The bandpass element values are obtained by application of (4.73)-(4.76) and (4.67) as described in section 4.5.2. The electrical length at the centre frequency was chosen to be $\theta_o = 30^o$. After the bandpass frequency transformation and scaling so that the inner re-entrant lines are identical for all resonators, the element values in a $50\,\Omega$ system were determined as shown in Table 4-7. The circuit simulation is shown in Fig. 4-31 below.

Table 4-7 Re-entrant Bandpass Filter Element Values

Inner conductors	Middle Conductors	Coupling admittances
$Z_{ri} = 77.1598\ \Omega$	$Z_1 = Z_5 = 32.9867\ \Omega$	$Z_{12} = Z_{45} = 102.84\ \Omega$
$C_r = 2.3658\ pF$	$Z_2 = Z_4 = 43.1568\ \Omega$	$Z_{23} = Z_{34} = 139.98\ \Omega$
	$Z_3 = 38.8326\ \Omega$	

Table 4-8 Filter Theoretical (Calculated) Physical Dimensions (mm)

$D_{ri} = 1.97$	$b = 40$	$sw1 = 20$	$w1 = 12.88$
$D_r = 7.14$	$H = 25$	$s12 = 8$	$w2 = 11.14$
$t = 32.00$	$h = 4.2$	$s23 = 10.4$	$w3 = 12.52$

Table 4-9 Filter Physical Dimensions after Optimization (mm)

$D_{ri} = 5.02$	$b = 40$	$sw1 = 20$	$w1 = 23.63$
$D_r = 17.88$	$H = 25$	$s12 = 7.8$	$w2 = 21.88$
$t = 32.00$	$h = 4.2$	$s23 = 10.4$	$w3 = 23.27$

The physical dimensions were determined as described in section 4.5.4 and using [32] as shown in Table 4-8. A ground spacing of 40 mm was used in the design. The physical structure was simulated using HFSS and optimized. Note as always [79], the theoretical design underestimate the actual bandwidth in combline filter design using [32]. The optimised physical dimensions are given in Table 4-9 and depicted in Fig. 4-32. Note also that the inner conductor dimensions were not optimized but were proportionally increased so that the characteristic impedance ($Z_{ri} = 77.1598\ \Omega$) is maintained. The overall filter cavity dimensions were 40 mm wide, 190.69 mm in length and 29.2 mm in height. The filter was fabricated using Aluminium with the above physical dimensions.

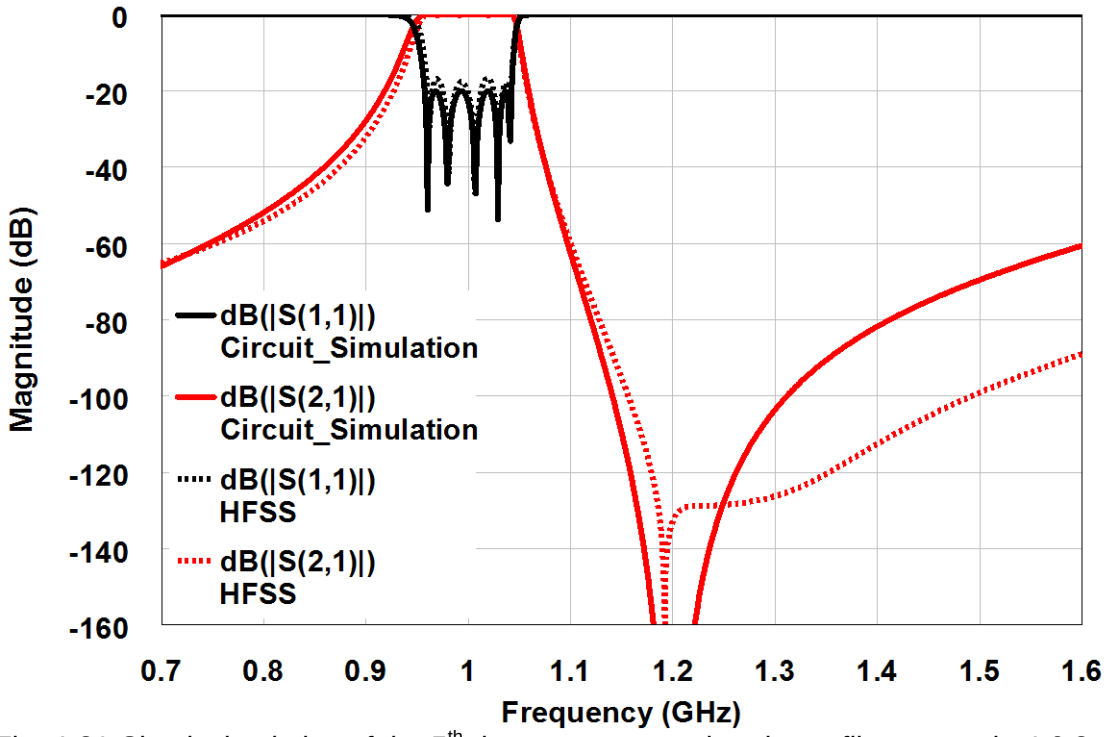

Fig. 4-31 Circuit simulation of the 5th degree re-entrant bandpass filter example 4.6.2 vs HFSS simulation

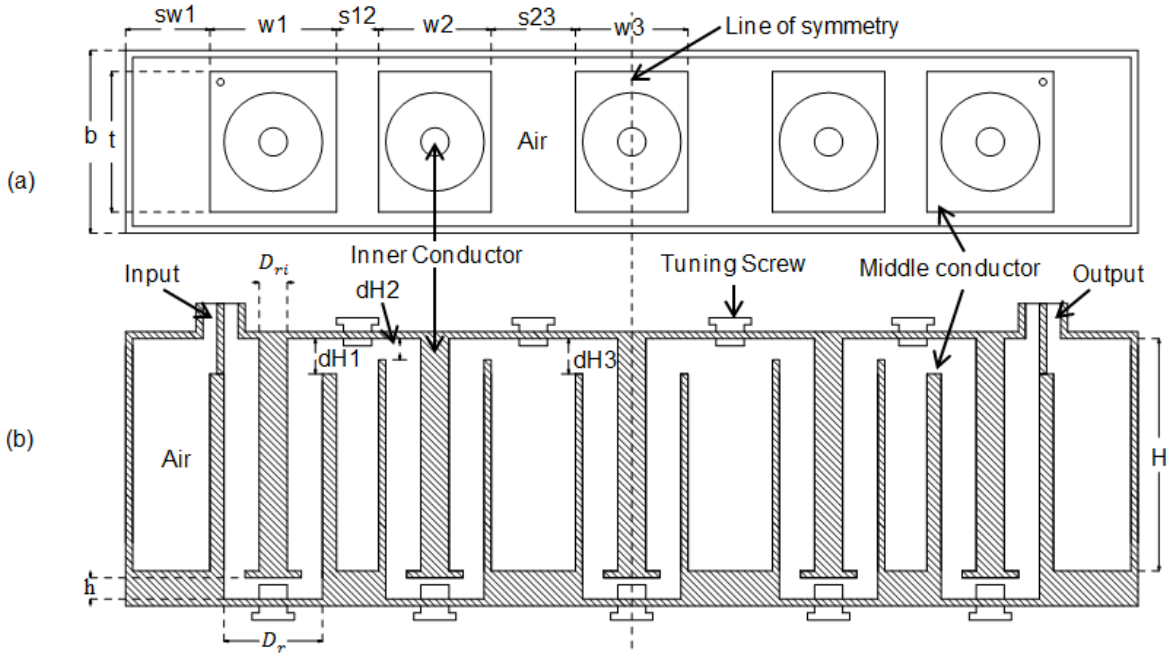

Fig. 4-32 Diagram showing the layout of the re-entrant resonators in the design example 4.6.2: (a) Top view (b) Cross section of side view - dimensions shown are as given in Table 4-9

4.7 Discussion

Fig. 4-33 shows a comparison between the measured frequency response and the HFSS (lossless) simulation whereas Fig. 4-34 shows the same simulation on a broader frequency scale. Measurements were performed on an Agilent Technologies E5071C ENA series network analyser. In the re-entrant bandpass filter, the coupling admittances are considerably smaller than in normal combline bandpass filter of comparable bandwidths. This means that the inter-resonator spacings are relatively small. Thus significant fringing capacitance between non-adjacent resonators does exist and potentially leading to the method in [32] for obtaining physical dimensions being inaccurate. Thus the bandwidth is considerably broader with initial values obtained using [8]. However, this bandwidth change also occurs in conventional combline filters. As noted in [79], the problem may be solved by utilizing full EM simulators or alternatively using bandwidth correction factors may be less time consuming. Further adjustment may be achieved by mechanical tuning using tuning screws in the fabricated filter. The fabricated filter is shown in Fig. 4-35.

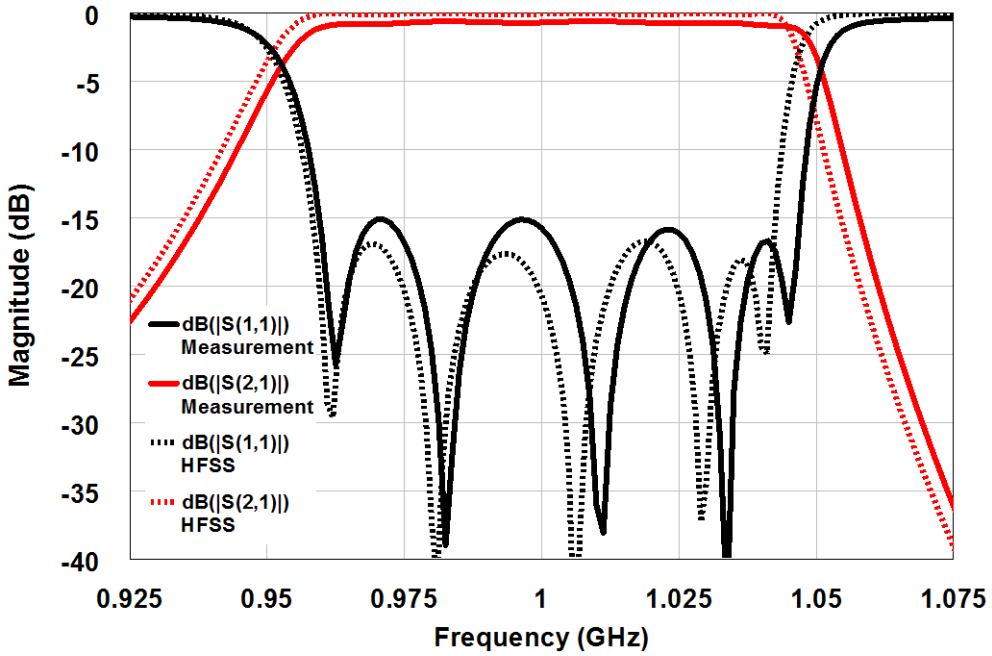

Fig. 4-33 Measured vs HFSS frequency response of the fabricated re-entrant bandpass filter

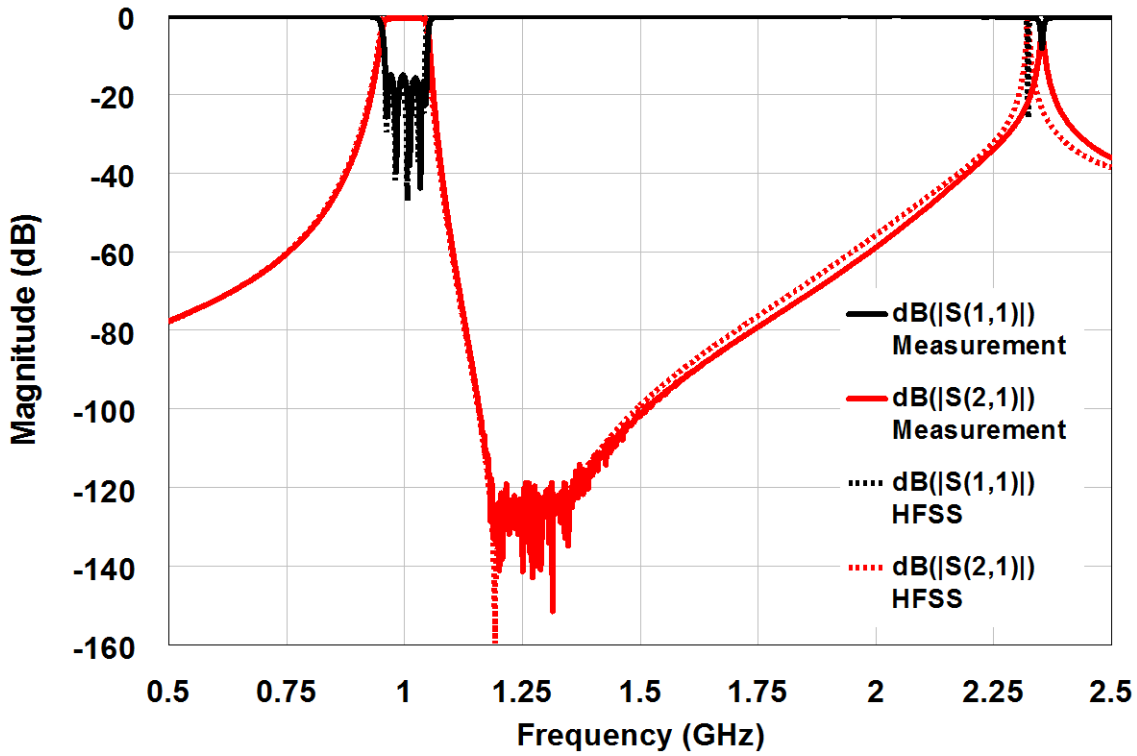

Fig. 4-34 Measured versus HFSS simulation of the fabricated re-entrant bandpass filter

4.7.1 High Selectivity

The re-entrant bandpass can realise a maximum of N transmission zeroes equivalent to the filter order making it a relatively a very selective filter compared to conventional filters. Additionally, the design presented above provides for flexibility in position of the transmission zeroes. The transmission zeros above the passband may be located as near as one passband away from the bandedge. The fundamental limit to the placement of transmission zeroes is that as the transmission zeroes become much closer to the passband edge the impedance levels are unrealizably small or large.

4.7.2 Symmetrical Design

The re-entrant bandpass may be realized using physically symmetrical or asymmetrical in-line structures depending on transmission zero placements. Physically symmetrical design may be achieved by placing transmission zeroes so that each node from the two opposite ends have the same transmission zero. For example for a 5 pole and 5 transmission zeroes filter, the lowpass transmission

zero distribution may be chosen as $\omega = 2{,}3{,}4{,}3{,}2\ rad/s$ or $\omega = 5{,}10{,}10{,}10{,}5\ rad/s$ - all produce physically symmetrical designs. Alternatively, all the transmission zeroes may be placed at a single frequency. Although this does not improve the overall stopband rejection, it does simplify the synthesis, design and tuning of the filter. Physically symmetrical structures make for easy tuning of the filter after fabrication and as well as cut down design time when optimizing using time consuming EM software such as HFSS.

4.7.3 Tunability

The filter tuning is achieved by screws that control the lumped capacitance on the inner transmission lines of the re-entrant resonators. The tuning of the lumped capacitance controls both the resonant frequency and the transmission zero location. Additional tuning screws may be inserted on top of the filter to control the resonance frequency by slight adjustment of the capacitance at the open-circuited end of the middle conductors. Coupling screws may also be inserted between the nodes to control the couplings. The fabricated filter was easy to tune as all the inner conductors' dimensions were identical, requiring identical turns in the tuning screws.

4.7.4 Compact In-Line Filter Structure

In the re-entrant bandpass filter design presented in section 4.6.2, the resonator lengths at the centre frequency may be made considerably short e.g. $\theta_o = 30^o$. The re-entrant resonators also require strong couplings for very close-to-band transmission zeroes resulting in smaller inter-resonator spacing. Thus the filter may be considerably reduced in size. However, the requirement to have an inner conductor inside the middle conductor does limit the choice of the ground spacing. In addition, the in-line filter topology makes an ideal realization for base station filters.

The highly selective re-entrant resonators may also be mixed with normal combline resonators with much wider spurious free frequency window to exploit the best attributes of each resonator. Furthermore, the re-entrant bandpass filter is easy to fabricate, similar to combline bandpass filters, as all the middle transmission lines

are fixed and short-circuited at one end whereas the inner transmission lines may be fabricated separately and fixed to the filter cover by screwing them into the cover as depicted in the fabricated filter photos in Fig. 4-35. The tuning screws located on the same side of the filter bottom wall make for easy of tuning.

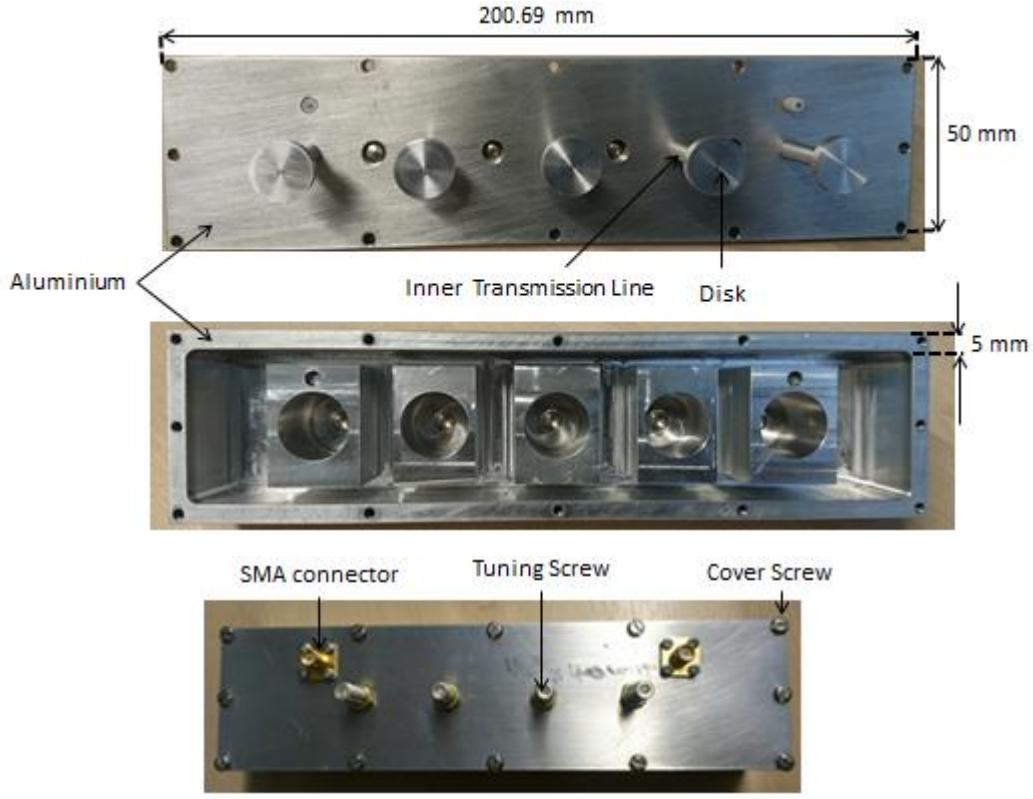

Fig. 4-35 Photo showing a fabricated re-entrant bandpass filter (a) filter with top cover removed (b) assembled filter with input and output connectors

4.8 Conclusion

In this Chapter, a re-entrant transmission line was exploited to provide both a resonance frequency and a finite frequency transmission zero. A complete design procedure was given starting from a pseudo-elliptic low-pass prototype. A prototype bandpass filter was designed and fabricated. Measurement results showed good correspondence with theory. The re-entrant bandpass filter with transmission zeros above the passband is well suited for base station receive filters where a high rejection is required in the transmit frequency band. The following Chapter gives an application of the synthesis method of Chapter 2 to synthesis of single and narrow dual bandpass filters.

Chapter 5 Synthesis Methods for Single Bandpass and (Narrow) Dual Bandpass Filters

5.1 Introduction

In this Chapter, an application of the methods of Chapter 1 and Chapter 2 are applied to the direct synthesis of bandpass and narrow dual bandpass filters. To prove the success of the proposed synthesis technique, synthesis and design procedures for combline and interdigital bandpass filters are given in section 5.2. Synthesis and design examples are given to validate the proposed synthesis technique and to demonstrate the practical realisation. Finally in section 5.3, it is shown through an example how a narrow dual bandpass filter may be synthesised from a suitable lowpass prototype filter using the proposed synthesis technique.

5.2 Direct synthesis of bandpass filters

The general Chebyshev characteristic function for direct bandpass filter synthesis was derived in Chapter 2. Each unique solution may be obtained corresponding to a linear combination of basis functions depending on the number and position of transmission zeros. The transmission zeros are required not only to increase rejection in the stopband but also for physical realisation. It will be shown how the synthesis method is both applicable in the lumped and distributed domain. This will be exemplified by the design of pseudo-combline and interdigital bandpass filters in the next sections.

5.2.1 Pseudo-combline Bandpass Filter Design

Pseudo-combline bandpass filter may be realised from lumped element network shown in Fig. 5-1. This bandpass filter is characterised by a N-0-1 transfer function and contains only a single pair of transmission zero at the origin and the rest are at infinity on the imaginary p complex plain. It may look like each shunt inductor in Fig. 5-1 provides a single transmission zero at the origin and thus the inductors

provides $N/2$ number of transmission zeros. In fact all the shunt inductors contribute to only a single transmission zero at the origin. Similarly, Table 2-5 in Chapter 2 shows the weighting numbers for each of the basis function required. This bandpass filter may be used to design pseudo-combline bandpass filters by transforming the lumped bandpass filter network of Fig. 5-1 into a distributed network.

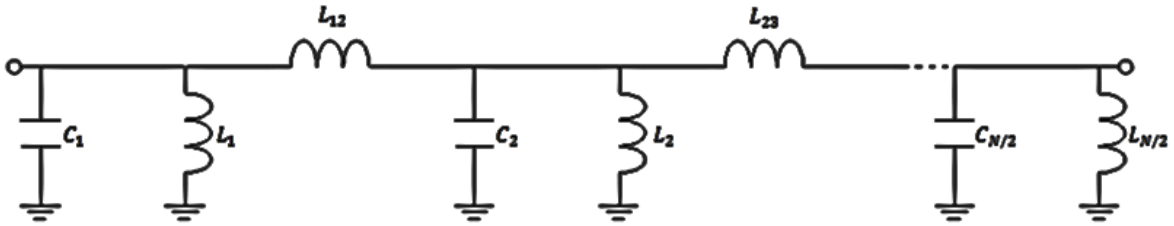

Fig. 5-1 Lumped element bandpass prototype filter used for design of pseudo-combline bandpass filter with $N_{TZ} = 1$

5.2.1.1 Network Synthesis

The characteristic function for the bandpass prototype filter to be used for the design of pseudo-combline bandpass is the unique solution to the general solution discussed in Method for Generating Generalised Chebyshev Polynomials corresponding to the second family N-0-$(N-1)$ of solution in Table 2-5 and with weighting numbers α, β and γ as

$$\alpha = N/2 - 1,\ \beta = 1 \text{ and } \gamma = 0 \tag{5.1}$$

The element values for the bandpass prototype filter shown in Fig. 5-1 may be obtained through network synthesis using the $ABCD$ matrix cascaded synthesis approach as described in Chapter 1. The following is the procedure for the network synthesis for element by element extraction from the $ABCD$ matrix. For $N \geq 6$ ($N = 2$ and 4, are trivial cases and may easily be found by inspection of the $ABCD$ matrix).

Step 1: Extract shunt capacitor with value

$$C_1 = \frac{D}{pB}\bigg|_{p\to\infty} \tag{5.2}$$

The remainder $ABCD$ is computed as

$$ABCD_{rem} = \frac{1}{P}\begin{bmatrix} A & B \\ C-(C_1p)A & D-(C_1p)B \end{bmatrix} \tag{5.3}$$

The remainder C and D polynomials are now less by 1 degree

Step 2: Extract Γ section:

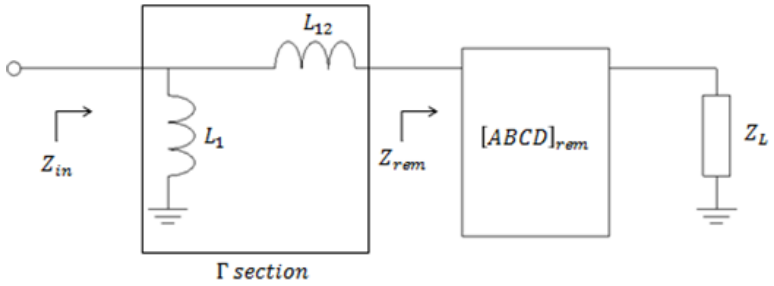

Fig. 5-2 Extraction of Γ section from the filter network

From Fig. 5-2

$$ABCD_{\Gamma} = \begin{bmatrix} 1 & L_{12}p \\ \dfrac{1}{L_1p} & 1+\dfrac{L_{12}}{L_1} \end{bmatrix} \tag{5.4}$$

The input impedance to the remainder of the network is,

$$Z_{\text{in}} = \frac{A_{\Gamma}Z_{\text{rem}} + B_{\Gamma}}{C_{\Gamma}Z_{\text{rem}} + D_{\Gamma}} = \frac{AZ_{\text{L}} + B}{CZ_{\text{L}} + D} \tag{5.5}$$

and if $Z_{\text{L}} = \infty$, and substituting for $ABCD_{\Gamma}$ elements, then the open-circuit impedance is,

$$Z_{\text{in}} = \frac{Z_{\text{rem}} + L_{12}p}{\dfrac{1}{L_1p}Z_{\text{rem}} + 1 + \dfrac{L_{12}}{L_1}} = \frac{A}{C}$$

$$\frac{\dfrac{L_1Z_{\text{rem}}}{p} + L_1L_{12}}{\dfrac{Z_{\text{rem}}}{p} + L_1 + L_{12}} = \frac{A}{pC} \tag{5.6}$$

Hence define the sum from (5.6),

$$sum = \frac{1}{L_1} + \frac{1}{L_{12}} = \left.\frac{pC}{A}\right|_{p\to\infty} \tag{5.7}$$

The value of L_{12} may be chosen so that both L_1 and the remainder polynomials are positive real functions. e.g. $L_{12} = 1$. Appropriate choice of L_{12} ensures the

remainder of the network is well scaled to avoid extreme element values. Thus L_1 is determined from,

$$L_1 = \frac{1}{sum - \frac{1}{L_{12}}} \tag{5.8}$$

The remainder ABCD is computed as,

$$ABCD_{rem} = \frac{1}{P}\begin{bmatrix} \left(1 + \frac{L_{12}}{L_1}\right)A - (L_{12}p)C & \left(1 + \frac{L_{12}}{L_1}\right)B - (L_{12}p)D \\ C - \frac{A}{L_1 p} & D - \frac{B}{L_1 p} \end{bmatrix} \tag{5.9}$$

Note that all the remainder ABCD polynomials are now 1 degree less except for the P polynomial.

Step 3: Repeat step 1 and 2 up to $N/2 - 1$ times. Note also that, because of symmetry, when the synthesis process is performed past the centre of the network, the other values of the coupling inductors must be assigned such that,

$$\begin{aligned} L_{12} &= L_{N-1,N} \\ L_{23} &= L_{N-2,N-1}, \ldots \end{aligned} \tag{5.10}$$

Step 4: Finally, the last element to be extracted is a shunt LC resonator. $P = p/\varepsilon$ is divided throughout the $ABCD$ polynomials so that A, D and P are unity, B is zero and C polynomial takes the form

$$C = c_0 p + \frac{c_1}{p} \tag{5.11}$$

Hence

$$\begin{aligned} C_N &= c_0 \\ L_N &= \frac{1}{c_1} \end{aligned} \tag{5.12}$$

This completes the synthesis process to yield the circuit in form of Fig. 5-1. Notice that in this example, the classical cascaded synthesis was applied. A more efficient method involves the use of CM synthesis method as the example in section 5.2.3.2 will show.

5.2.1.2 Lumped-to-distributed circuit Transformation

The bandpass filter circuit is obtained by transforming the lumped bandpass filter circuit of Fig. 5-1 to a distributed bandpass filter by means of Richard's lowpass transformation [9] defined parametrically as

$$p = a\rho, \qquad \rho = jt = jtan(\theta)$$

$$a = \frac{1}{tan(\theta_2)} = \frac{1}{t_2} \tag{5.13}$$

$$\omega = \frac{tan(\theta)}{tan(\theta_2)} = \frac{t}{t_2}$$

where θ_2 is the electrical length at ω_2, the upper bandedge frequency point. Thus the lumped capacitors become open circuited stubs and the lumped inductors become short circuited stubs as shown in Fig. 5-3. Redundant input and output unit phase shifters of Fig. 5-4 may be added to the network and admittance inverters may also be formed as in Fig. 5-5 to realise the circuit of Fig. 5-6. It is often the case with narrow bandpass filters that the short circuited characteristic impedance are unrealisable and thus scaling of internal nodes is required. The network of Fig. 5-6 is scaled at every internal node such that the shunt short circuited stubs characteristic admittances are unity. After scaling, the internal inverters are removed and phase shifters are formed at the input and output yielding the final realisable circuit of Fig. 5-7. The final circuit element values are given by the formulae below.

The scaling factors at nodes $1, 2, 3, \ldots \mathrm{N}/2$ are:

$$\mathrm{n}_1 = \frac{\sqrt{\mathrm{a}}}{\sqrt{\frac{1}{\mathrm{L}_1} + \frac{1}{\mathrm{L}_{12}} + \mathrm{a}}}$$

$$\mathrm{n}_2 = \frac{\sqrt{\mathrm{a}}}{\sqrt{\frac{1}{\mathrm{L}_1} + \frac{1}{\mathrm{L}_{12}} + \frac{1}{\mathrm{L}_{23}}}} \tag{5.14}$$

$$\vdots$$

$$n_r = \frac{\sqrt{a}}{\sqrt{\frac{1}{L_r} + \frac{1}{L_{r-1,r}} + \frac{1}{L_{r,r+1}}}}$$

$$\vdots$$

$$n_{N/2-1} = n_2$$

$$n_{N/2} = n_1$$

Characteristic admittances for the coupling admittances,

$$Y_{01} = n_1$$

$$Y_{12} = \frac{n_1 n_2}{a L_{12}}$$

$$\vdots$$

$$Y_{r,r+1} = \frac{n_r n_{r+1}}{a L_{r,r+1}} \tag{5.15}$$

$$\vdots$$

$$Y_{N/2-2,N/2-1} = Y_{12}$$

$$Y_{N/2-1,N/2} = Y_{01}$$

Characteristic admittances for the short circuited stubs,

$$Y_0 = 1 - n_1$$

$$Y_1 = 1 - n_1 - \frac{n_1 n_2}{a L_{12}}$$

$$\vdots$$

$$Y_r = 1 - \frac{n_{r-1} n_r}{a L_{r-1,r}} - \frac{n_r n_{r+1}}{a L_{r,r+1}} \tag{5.16}$$

$$\vdots$$

$$Y_{N/2} = Y_1$$

$$Y_{N/2+1} = Y_0$$

Characteristic admittances for the open circuited stubs

$$
\begin{aligned}
Y_{os1} &= aC_1{n_1}^2 = \frac{a^2C_1}{\frac{1}{L_1}+\frac{1}{L_{12}}+a} \\
Y_{os2} &= aC_2{n_2}^2 = \frac{a^2C_2}{\frac{1}{L_2}+\frac{1}{L_{12}}+\frac{1}{L_{23}}} \\
&\vdots \\
Y_{osr} &= aC_r{n_r}^2 = \frac{a^2C_r}{\frac{1}{L_r}+\frac{1}{L_{r-1,r}}+\frac{1}{L_{r,r+1}}} \\
&\vdots \\
Y_{osN/2-1} &= Y_{os2} \\
Y_{osN/2} &= Y_{os1}
\end{aligned}
\tag{5.17}
$$

Note that the mapping produced by transformation (5.13) is such that

$$
\begin{aligned}
\omega_c &\rightarrow \theta_1 \\
1 &\rightarrow \theta_2
\end{aligned}
\tag{5.18}
$$

where θ_1 and θ_2 are the two bandedges in degrees of the bandpass filter in the θ-plane. In the design of filters, the specifications are given in terms of the bandwidth (bw) and the centre frequency f_o. The designer chooses the appropriate electrical length at the centre frequency θ_o. Thus the bandwidth in degree (θ-plane) is

$$
d\theta = \frac{bw\theta_o}{f_o} \tag{5.19}
$$

Hence the two bandedges are defined as

$$
\begin{aligned}
\theta_1 &= \theta_o - d\theta/2 \\
\theta_2 &= \theta_o + d\theta/2
\end{aligned}
\tag{5.20}
$$

From which the lumped bandpass filter cutoff frequency in radians is computed from (5.13) as

$$
\omega_c = \frac{tan(\theta_1)}{tan(\theta_2)} \tag{5.21}
$$

Recall that, this is the inner cutoff frequency used in the generation of the characteristic polynomials.

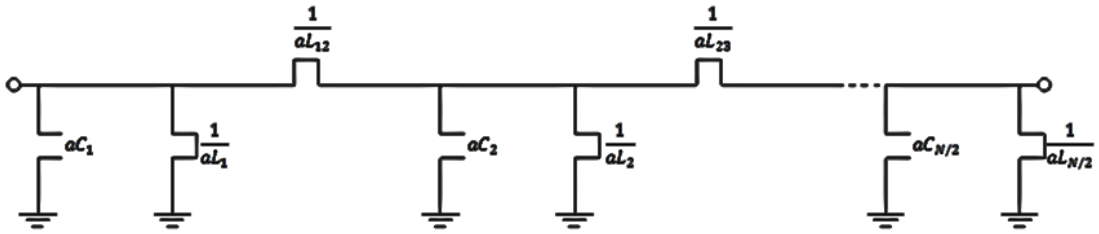

Fig. 5-3 Distributed circuit for pseudo-combline bandpass filter

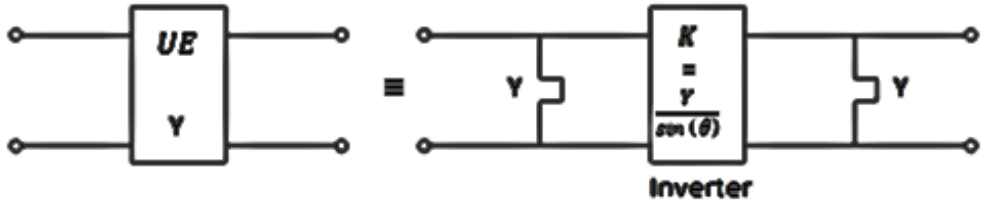

Fig. 5-4 A unit length (UE) phase shifter and its equivalent circuit consisting of an inverter between short circuited shunt stubs

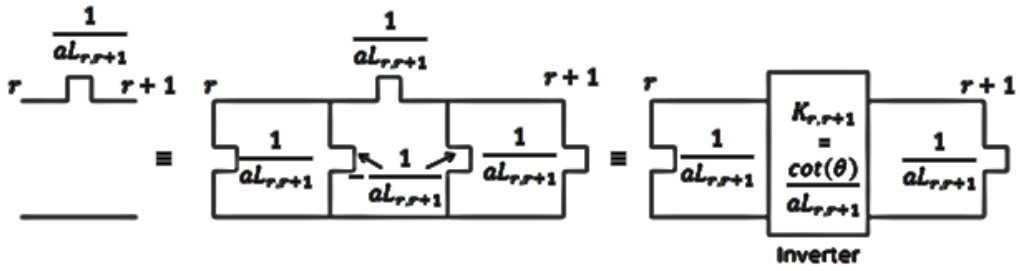

Fig. 5-5 Formulation of an inverter in the distributed pseudo-combline bandpass filter between node r and $r+1$

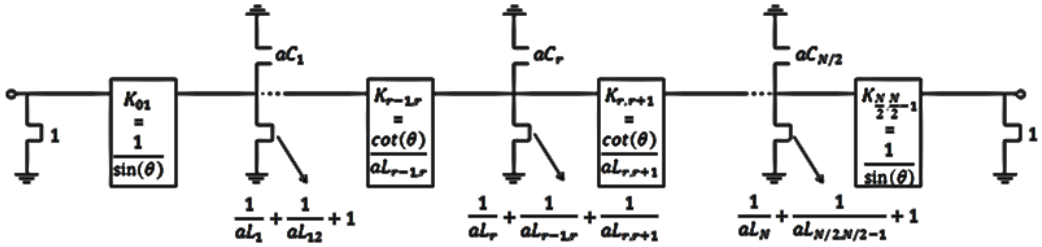

Fig. 5-6 Distributed pseudo-combline bandpass filter circuit after introduction of unit phase shifter at input/output and admittance inverters

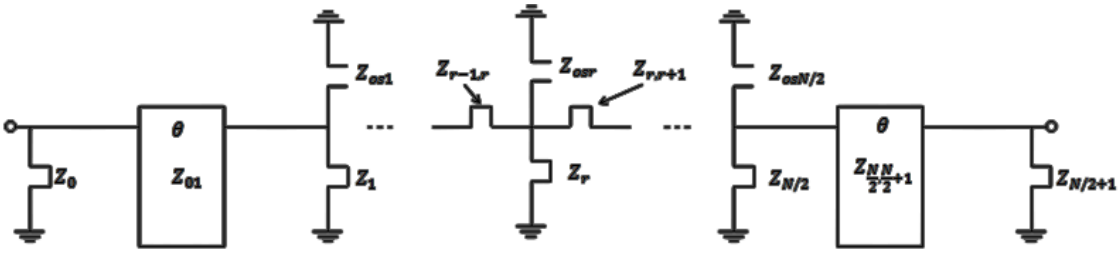

Fig. 5-7 Final distributed circuit for pseudo-combline bandpass filter after scaling internal nodes

5.2.1.3 Synthesis Illustrative Example

Firstly, an experimental pseudo-combline bandpass filter prototypes was designed using the above procedure with the specifications given in Table 5-1.

Table 5-1 Pseudo-combline Bandpass Filter Specifications

Centre frequency (f_o)	1 GHz
Bandwidth (bw)	50 MHz
Passband Return Loss (RL)	20 dB
Stopband Insertion loss (ILs) at $1.05\ GHz$	50 dB

It was established that a lumped bandpass prototype filter with $N = 10$ would meet the above specifications. Choosing $\theta_o = 45^o$, and from (5.20) $\theta_2 = 46.125^o$. Then (5.21) was used to compute $\omega_c = 0.9244$. Note that a 10th degree characteristic function ($N = 10$) corresponds to a 5th degree bandpass filter.

Table 5-2 5th Degree Lumped Bandpass Filter Characteristic Polynomials

$\mu = 1 \qquad \varepsilon = 761953$

Zeros of $P(p)$	Zeros of $F(p)$	Zeros of $E(p)$ [Poles]
0	$\pm 0.9982j$	$-0.0072 \pm 1.0047j$
	$\pm 0.9847j$	$-0.0191 \pm 0.9889j$
	$\pm 0.9627j$	$-0.0076 \pm 0.9196j$
	$\pm 0.9403j$	$-0.0240 \pm 0.9628j$
	$\pm 0.9263j$	$-0.0197 \pm 0.9363j$

Table 5-3 5th Degree Lumped Bandpass Filter Synthesized Element Values

$C_1 = 12.8805\ F$	$L_1 = 0.0913\ H$	$L_{12} = 1\ H$
$C_2 = 19.6088\ F$	$L_2 = 0.0617\ H$	$L_{23} = 1\ H$
$C_3 = 23.8887\ F$	$L_3 = 0.0496\ H$	

Table 5-4 5th Degree Pseudo-combline Bandpass Filter Impedance Values (Ω)

$Z_0 = 68.7583$	$Z_{os1} = 54.2450$	$Z_{01} = 183.2742$
$Z_1 = 75.5313$	$Z_{os2} = 50.2159$	$Z_{12} = 766.7849$
$Z_2 = 56.4968$	$Z_{os3} = 50.1736$	$Z_{23} = 1004.3$
$Z_3 = 55.5292$		

Table 5-5 5th degree Pseudo-combline Bandpass Filter Dimensions (mm)

$w_0 = 8.400$	$s_{w0} = 10.0$	$D_1 = 19.77$	$t = 8.00$	$dH_1 = 1.84$
$w_1 = 8.720$	$s_{01} = 4.70$	$D_2 = 18.49$	$b = 20.0$	$dH_2 = 5.00$
$w_2 = 11.42$	$s_{12} = 12.5$	$D_3 = 18.47$	$H = 37.5$	
$w_3 = 11.59$	$s_{23} = 14.0$			

Table 5-5 (Continued) Tune screw ($\emptyset\ 3$ mm) Height (mm)

Resonator 1 Tuning Screw Height	2
Resonator 2 Tuning Screw Height	1
Resonator 3 Tuning Screw Height	1

The characteristic polynomials are generated as described in Chapter 2 and their singularities are tabulated in Table 5-2. The $ABCD$ polynomials computation easily follows as presented in Chapter 1 and network synthesis explained in section 5.2.1.1 then follows to yield lumped elements of Table 5-3. Because of symmetry only half of the values are given in Table 5-3.

Using formulae (5.14)-(5.17) and the element values in Table 5-3, the bandpass distributed circuit elements are computed and tabulated in Table 5-4. The circuit of Fig. 5-7 may be realized in two parts - the upper part of the filter consisting of the open circuited stubs may be implemented using open circuited circular coaxial transmission lines and the all-stop network, bottom part, consisting of an array of coupled short circuited lines may be implemented using the canonical combline realization. More compact combline bandpass filter may be obtained by replacing the open circuited stubs with lumped capacitors which are realised by capacitively

loading the short circuited stubs with the top filter cover (and screw) as the example in section 5.2.3 shows. Having the required bandpass filter circuit, the physical dimensions for the bottom part are computed using Getsinger [33] method utilizing rectangular striplines [32].

Table 5-5 shows the physical dimensions for the pseudo-combline bandpass filter dimensions as depicted in Fig. 5-8. The ground plane spacing (b) and striplines thickness (t) were chosen to $b = 20\,mm$ and $t = 8\,mm$ respectively and length $H = 37.5\,mm$ were calculated corresponding to $\theta_o = 45^o$ at the centre frequency $f_o = 1\,GHz$. The inner diameters of the upper open circuited lines were chosen to be t. The high frequency structure simulator (HFSS) physical model shown in Fig. 5-9 was EM simulated with the result of the simulation shown in Fig. 5-10 and Fig. 5-11 below.

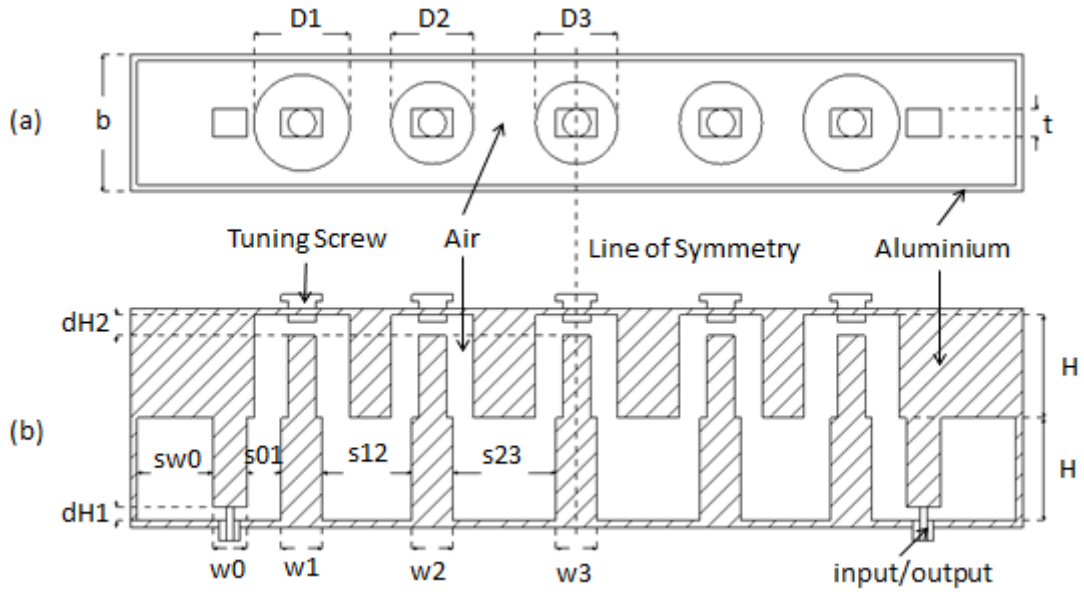

Fig. 5-8 Physical layout of the hardware for 5th degree pseudo-combline bandpass filter (a) top view (b) side view

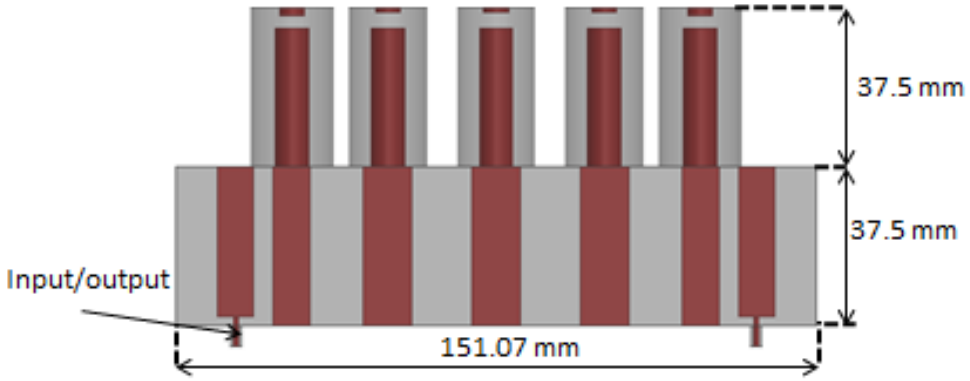

(a)

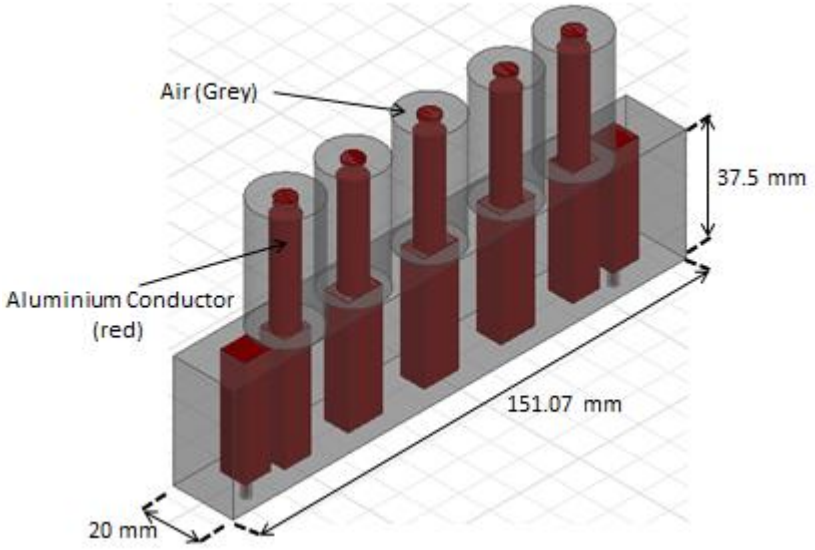

(b)

Fig. 5-9 HFSS physical model of the 5th degree pseudo-combline bandpass filter (a) side view (b) perspective view

The slightly wide bandwidth above is due to the method used to obtain physical dimension of the parallel coupled short circuited stubs. In fact this issue of bandwidth discrepancy, or indeed bandwidth expansion is a well-known problem in the history of microwave filters with design made utilizing TEM capacitance matrix in determining the physical dimensions of combline bandpass and has caused much debate even in the recent past [79, 80]. In fact it also occurs in interdigital bandpass filters although to a much lesser extent than it occurs in combline bandpass filters. The problem also tends to be worse in capacitively loaded bandpass filters than the exact realisation of a distributed TEM bandpass filter as

this example shows. To accurately determine physical dimensions, therefore, would require some EM techniques or alternatively, the problem may be solved by using appropriate bandwidth correction factors such as those proposed in [80]. Analysis showed that the pseudo-combline bandpass filter is not very sensitive to the tuning states as it requires only coarse adjustments on the shortened open circuited stubs (see tuning screw position in Table 5-5). In comparison, a capacitively loaded combline bandpass filter is very sensitive to tuning state as it would require a high level of accuracy for the tuning screw positions often to a thousandth of a millimetre accuracy to achieve equal ripple passband return loss as demonstrated in section 5.2.3.2! With the advent of efficient computer simulation software tools, this could easily be achieved, but would obviously be time consuming. Further improvements in the passband return loss may be achieved by EM fine tuning techniques such as space mapping.

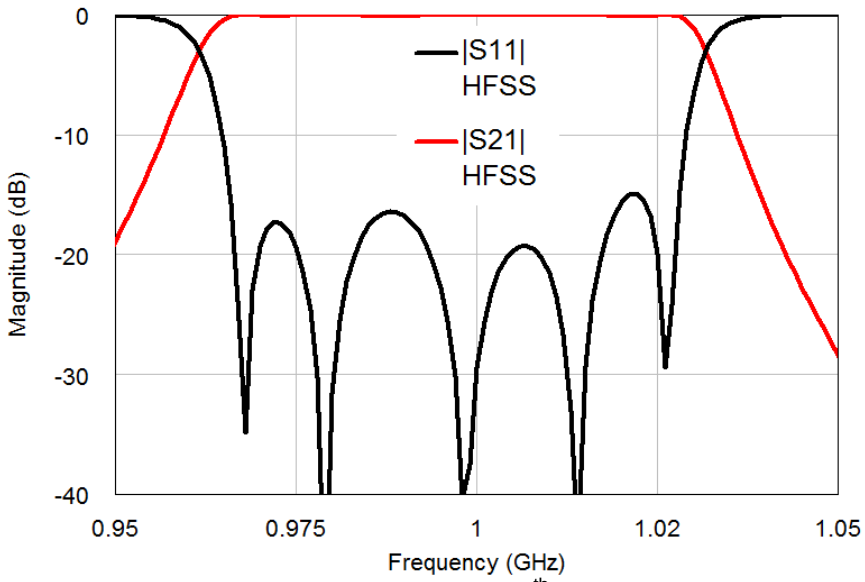

Fig. 5-10 HFSS simulated passband response of 5th degree pseudo-combline bandpass filter

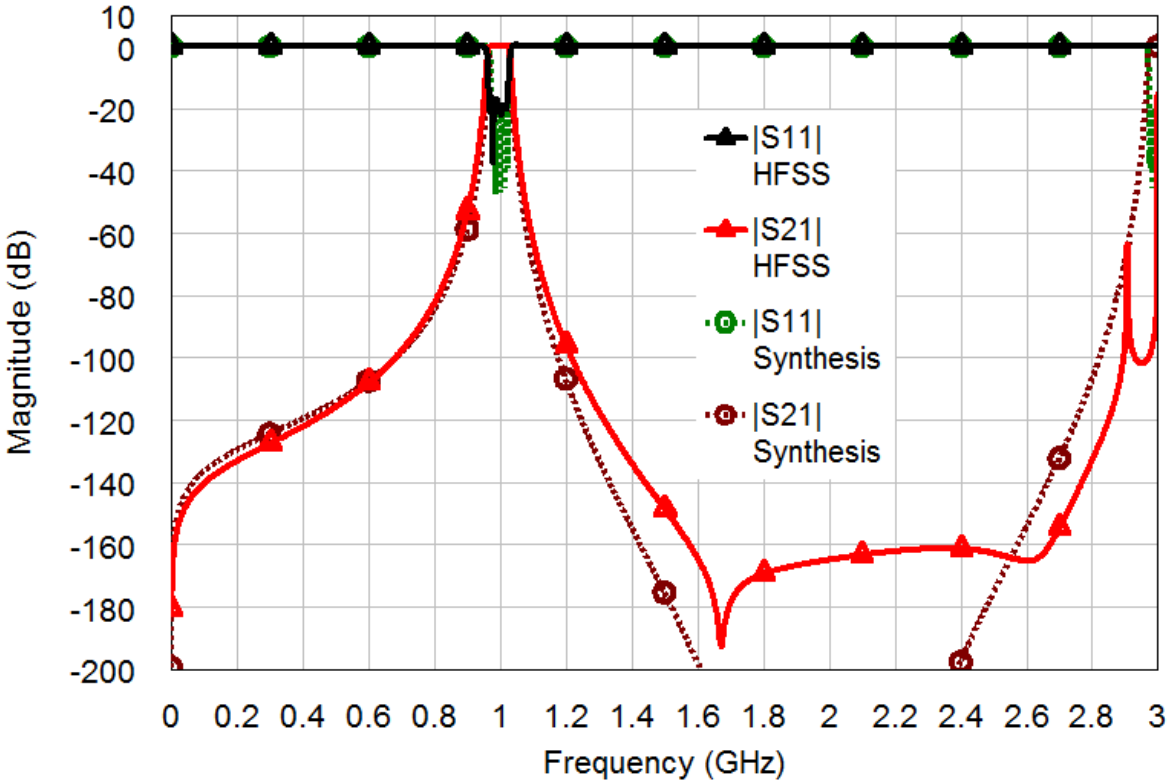

Fig. 5-11 HFSS vs synthesis wide band response of the pseudo-combline bandpass filter

5.2.2 Synthesis of the interdigital bandpass filter

An approach to the exact synthesis and design for interdigital bandpass filter will be explained. Fig. 2-4 shows an equivalent circuit used in the implementation of an interdigital bandpass filter, consisting of shunt short circuited stubs separated by unit length transmission lines. The goal now is to obtain characteristic polynomials which may be used to exactly synthesise the network of Fig. 2-4.

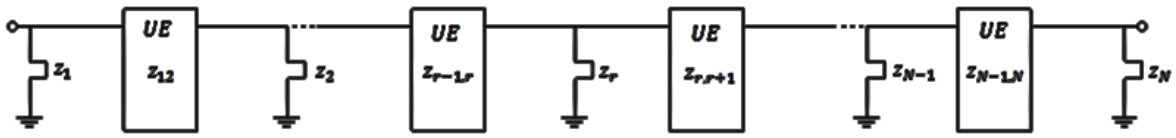

Fig. 5-12 General distributed equivalent circuit for interdigital bandpass filter

5.2.2.1 Network Synthesis

The characteristic polynomials are obtained as described in Chapter 2 section 2.4.4. Similar to the pseudo-combline bandpass, the interdigital bandwidth in degree is

$$d\theta = \frac{bw\theta_o}{f_o} \tag{5.22}$$

and

$$\theta_1 = \theta_o - d\theta/2 \tag{5.23}$$

From which the normalised cutoff parameter ω_c in rad/s is computed from section 2.4.4.1 (Chapter 2) as

$$\omega_c = \frac{tan(\theta_1)}{\sqrt{1 + tan^2(\theta_1)}} \tag{5.24}$$

This enables the computation of the characteristic polynomials as explained in section 2.4.4 of Chapter 2. Using cascaded synthesis, the synthesis to obtain the element values of Fig. 2-4 is achieved by exploiting some features of the network in Fig. 2-4. The first feature may be analysed by assuming that the internal nodes may be scaled so that $z_{ij} = K$ for all i and j in Fig. 2-4. At a quarter-wave frequency, $\theta = 90^o$ corresponding to $t = \infty$. Then all the shunt short circuited stubs become open circuited and the $N - 1$ transmission lines becomes impedance inverters with characteristic impedance K. Therefore for N even, the overall $ABCD$ matrix becomes,

$$ABCD_{t\to\infty} = \begin{bmatrix} 0 & jK \\ \frac{j}{K} & 0 \end{bmatrix}^{N-1} = j^{N-1}\begin{bmatrix} 0 & K \\ \frac{1}{K} & 0 \end{bmatrix} \tag{5.25}$$

For N odd,

$$ABCD_{t\to\infty} = \begin{bmatrix} 0 & jK \\ \frac{j}{K} & 0 \end{bmatrix}^{N-1} = j^{N-1}\begin{bmatrix} 1 & 0 \\ 0 & 1 \end{bmatrix} \tag{5.26}$$

Thus for odd degree case, K may take any arbitrary value. For even degree, however, the magnitude of the reflection parameter, $S_{11}(\rho)$ may be written as,

$$|S_{11}(\infty)| = \left|\frac{F(\rho)/\mu'}{E(\rho)}\right|\Bigg|_{\rho\to\infty} = \frac{1}{|\mu'|} = \left|\frac{K - \frac{1}{K}}{K + \frac{1}{K}}\right| \tag{5.27}$$

(5.27) may be solved for K as,

$$K = \sqrt{\frac{\mu' + 1}{\mu' - 1}}, N \text{ even} \tag{5.28}$$

Using this feature, the following procedure may be adopted for the synthesis cycle:

Step 1: Extract a Γ section of Fig. 5-13

$$ABCD_{\Gamma} = \frac{1}{\sqrt{1-\rho^2}} \begin{bmatrix} 1 & K\rho \\ \frac{1}{z_1\rho} + \frac{\rho}{K} & 1 + \frac{K}{z_1} \end{bmatrix} \tag{5.29}$$

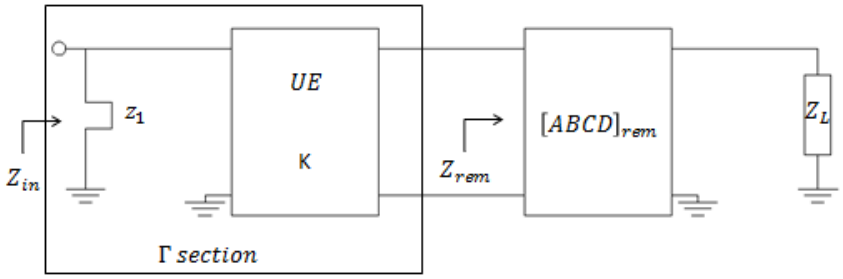

Fig. 5-13 Extraction of the Γ section

The second feature lies in the fact that the open-circuited input admittance of the entire network may be expressed as,

$$\left.\frac{1}{z_1\rho}\right|_{\rho=1} + \left.\frac{D_{rem}}{B_{rem}}\right|_{\rho=1} = \left.\frac{D}{B}\right|_{\rho=1} = sum \tag{5.30}$$

where B_{rem} and D_{rem} are the remainder B and D polynomials after extraction of the first shunt open circuited stub. But the input characteristic admittance after extraction of the first open circuited stub is given by,

$$\frac{1}{z_{12}} = \frac{1}{K} = \left.\frac{D_{rem}}{B_{rem}}\right|_{\rho=1} \tag{5.31}$$

Hence by substituting (5.31) in (5.30) and solving for z_1,

$$z_1 = \frac{1}{sum - 1/z_{12}} \tag{5.32}$$

Or a rather more general expression

$$z_r = \frac{1}{sum - 1/K}. \tag{5.33}$$

The sum is calculated from (5.30) and for even degree, the characteristic impedance for all the transmission lines K, is computed from (5.28). For odd degree, any appropriate value of K may be used. For example, $K = 1$ works for most synthesis. Once the element values of the Γ section are known, they may be removed and the remainder ABCD becomes,

$$ABCD_{rem} = \frac{1}{\left(\sqrt{1-\rho^2}\right)P}\begin{bmatrix} \left(1+\frac{K}{z_1}\right)A - KC\rho & \left(1+\frac{K}{z_1}\right)B - KD\rho \\ C - \frac{A}{z_1\rho} - \frac{A\rho}{K} & D - \frac{B}{z_1\rho} - \frac{B\rho}{K} \end{bmatrix} \tag{5.34}$$

All polynomials must then be divided by $1-\rho^2$ to complete the extraction process.

Step 2: Repeat step 1 $N-1$ times.

Step 3: The last element to be extracted is a shunt short circuited stub. A, D and P polynomials are all unity, B is zero and C is a constant c_o. Hence

$$z_N = \frac{1}{c_o} \tag{5.35}$$

Scaling of internal nodes may be performed were necessary by using the equivalent circuit of the UE shown in Fig. 5-4 and by introducing redundant unit phase shifters at the input and output, the network internal nodes may be scaled as depicted in Fig. 5-14 in a similar way as was done for the pseudo-combline bandpass filter. Finally the circuit of Fig. 5-15 may directly be realized for relatively broad bandwidths or using array of alternatively short circuited coupled lines for narrow bandwidths. The following are the formulae for the scaled final element values corresponding to Fig. 5-15:

Scaling factors at nodes $1, 2, 3, \ldots N$ are

$$n_1 = \frac{1}{\sqrt{y_1 + y_{12} + 1}}$$

$$n_2 = \frac{1}{\sqrt{y_2 + y_{12} + y_{23}}} \tag{5.36}$$

$$\vdots$$

$$n_r = \frac{1}{\sqrt{y_r + y_{r-1,r} + y_{r,r+1}}}$$

$$\vdots$$

$$n_{N-1} = n_2$$

$$n_N = n_1$$

Characteristic admittances for the coupling admittances,

$$Y_{01} = n_1$$

$$Y_{12} = n_1 n_2 y_{12}$$

$$\vdots$$

$$Y_{r,r+1} = n_r n_{r+1} y_{r,r+1} \tag{5.37}$$

$$\vdots$$

$$Y_{N-1,N} = Y_{12}$$

$$Y_{N,N+1} = Y_{01}$$

Characteristic admittances for the short circuited stubs,

$$Y_0 = 1 - n_1$$

$$Y_1 = 1 - n_1 - n_1 n_2 y_{12}$$

$$\vdots$$

$$Y_r = 1 - n_{r-1} n_r y_{r-1,r} - n_r n_{r+1} y_{r,r+1} \tag{5.38}$$

$$\vdots$$

$$Y_{N/2} = Y_1$$

$$Y_{N/2+1} = Y_0$$

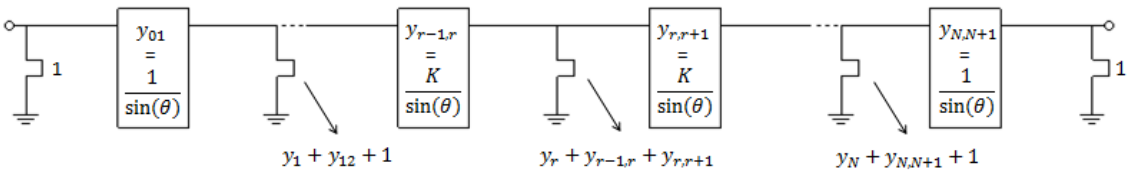

Fig. 5-14 Interdigital bandpass filter equivalent circuit after introduction of redundant unity phase shifters at input/output and formation of admittance inverters

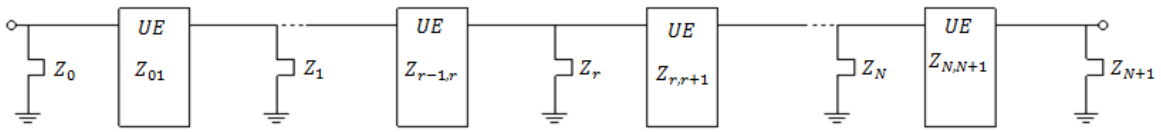

Fig. 5-15 Final interdigital bandpass filter equivalent circuit after scaling of internal nodes

A synthesis example is now used to validate the design theories in the next section.

5.2.2.2 Synthesis Illustrative Example

A 4th degree interdigital bandpass filter was designed with specifications as given in Table 5-6.

Table 5-6 4th degree interdigital bandpass specifications:

Centre frequency (f_o)	1 GHz
Bandwidth (bw)	50 MHz
Return Loss (RL)	20 dB

Table 5-7 4th Degree Lumped Bandpass Filter Characteristic Polynomials

$\mu = -1 \qquad \varepsilon = 338308$

Zeros of $F(p)$	Zeros of $E(p)$ [Poles]
$\pm 0.9999j$	$-0.0006 \pm 1.0003j$
$\pm 0.9993j$	$-0.0006 \pm 0.9990j$

Since this is an even degree filter, a 4th degree lumped bandpass filter is required. The lumped bandpass filter characteristic polynomials $F(\omega)$ and $E(\omega)$ were obtained as described in section 2.4.4.1 of Chapter 2 using $\omega_c = 0.9992$ computed from (5.24) and the corresponding ρ-plane cutoff, $\rho_c = 25.4517j$. The singularities of $F(\omega)$ and $E(\omega)$ are shown in Table 5-7. Then by applying the lumped to distributed transformation, those singularities are transferred to the ρ-plane to obtain singularities for $F(\rho)$ and $E(\rho)$ as shown in Table 5-8. Using direct distributed domain synthesis described in section 2.4.5, the same characteristic polynomials of Table 5-8 are obtained. The synthesis procedure is performed according to section 5.2.2.1 to obtain the element values as depicted in Table 5-9.

Table 5-8 4th Degree Distributed Interdigital Bandpass Filter Characteristic Polynomials

$\mu' = -10 \qquad \varepsilon' = -1.0050$

Zeros of $F(\rho)$	Zeros of $E(\rho)$ [Poles]
$\pm 66.5413j$	$-23.5699 \pm 15.3811j$
$\pm 27.5511j$	$-5.2417 \pm 19.9204j$

Table 5-9 4th Degree Interdigital Bandpass Filter Synthesised Impedances (Ω)

$K = 0.9045$

$z_1 = 0.0441$	$z_2 = 0.0263$	$z_3 = 0.0263$	$z_4 = 0.0441$

Table 5-10 4th Degree Interdigital Bandpass Filter Final Impedance Values (Ω)

$Z_0 = 62.5699$	$Z_1 = 65.4362$	$Z_2 = 53.3314$
$Z_{01} = 248.89$	$Z_{12} = 1428.4$	$Z_{23} = 1820.7$

The above synthesis procedure starts to be inaccurate for very small percentage bandwidths (e.g. less than 5%) where ω_c becomes closer to unity, but increases in accuracy for all the impedance values for moderate to broad bandwidths even for higher order interdigital filters. Where accuracy is lost, better results are achieved by using the first half of the impedance values.

In this example, it is necessary to scale the network as the short circuited stubs may be directly unrealizable. Therefore, unity phase shifters are introduced at the input and output according to Fig. 5-14 and admittance inverters are formed from the UE using the equivalent circuit in Fig. 5-4. The entire network is then scaled as described in section 5.2.2.1. Using formulae (5.36)-(5.38), the final elements in 50 ohms system are shown in Table 5-10 corresponding to the circuit in Fig. 5-15. Note only half of the values are shown in Table 5-10 because of symmetry.

5.2.3 Direct Synthesis for Combline Bandpass Filter

5.2.3.1 Network Synthesis

The pseudo-combline bandpass filter of section 5.2.1 may easily be synthesised using direct distributed bandpass filter basis functions. The basis functions are

chosen according to Table 5-11 and the general recursive technique may be applied according to the methods in Chapter 2 to obtain the characteristic polynomials. Then methods in Chapter 1 are applied to determine the coupling matrix in distributed domain.

Table 5-11 Basis Functions Selection for Combline Bandpass Filters

α_r	N-N_{FTZ}-N_{OTZ}	Purpose
$N_r - 1$	$2 - 0 - 0$	Provide $2(N_r - 1)$ transmission zeros at infinity
1	$2 - 0 - 1$	Provide a single transmission zeros at the origin and a single transmission zero at infinity

Note: $N_r = N/2$ is the degree of the bandpass filter network

5.2.3.2 Synthesis Illustrative Example

A 5th degree ($N = 2N_r = 10$) purely distributed bandpass was designed with the specifications given in Table 5-12.

Table 5-12 Specification for Combline Bandpass Filter Synthesis Example 5.2.3.2

Centre frequency (f_o)	1 GHz
Bandwidth (bw)	150 MHz
Passband Return Loss (RL)	20 dB

Using Table 5-11, the basis functions were used to yield a 10-0-1 characteristic function corresponding to a 5th degree bandpass filter. After the formation of the transverse coupling matrix, it was reconfigured to a canonical form and the remnant $N_r \times N_r$ matrices, M_{Ts} M_{Cs} and M_{Ls} are shown in Table 5-13.

To enable realisation as capacitively loaded bandpass filters, the technique by Wenzel [57] may be used to eliminate the shunt open circuited stubs. The value of the short circuited stub admittance (Y_r) and capacitors (C_r) are computed from the short circuited admittance (Y_{sc}) and open circuited admittance (Y_{oc}) at the two bandedges frequencies (ω_1 and ω_2) as

$$C_r = \frac{Y_{oc}\left(tan^2(a\omega_2) - tan^2(a\omega_1)\right)}{\omega_2 tan(a\omega_2) - \omega_1 tan(a\omega_1)}$$
$$Y_r = Y_{sc} - Y_{oc} tan^2(a\omega_1) + \omega_1 C_r tan(a\omega_1) \quad (5.39)$$

Table 5-13 Final Coupling Matrix for Distributed Bandpass Filter in 1 Ohm System

$$Y_{BP} = M_{Ts} + \rho M_{Cs} + \frac{1}{\rho} M_{Ls}, \qquad \rho = jt = jtan(a\omega), \qquad a = \frac{T_o}{\omega_o}$$

$$M_{Ts} = \begin{bmatrix} 0.2433 & 0 & 0 & 0 & 0 \\ 0 & 0.0000 & 0 & 0 & 0 \\ 0 & 0 & 0.0000 & 0 & 0 \\ 0 & 0 & 0 & 0.0000 & 0 \\ 0 & 0 & 0 & 0 & 0.2433 \end{bmatrix}$$

$$M_{Cs} = \begin{bmatrix} 1 & 0 & 0 & 0 & 0 \\ 0 & 1 & 0 & 0 & 0 \\ 0 & 0 & 1 & 0 & 0 \\ 0 & 0 & 0 & 1 & 0 \\ 0 & 0 & 0 & 0 & 1 \end{bmatrix}$$

$$M_{Ls} = \begin{bmatrix} +1.0377 & -0.2067 & 0 & 0 & 0 \\ -0.2067 & +1.0392 & -0.1512 & 0 & 0 \\ 0 & -0.1512 & +1.0316 & -0.1512 & 0 \\ 0 & 0 & -0.1512 & +1.0392 & -0.2067 \\ 0 & 0 & 0 & -0.2067 & +1.0377 \end{bmatrix}$$

Using this technique, the purely distributed network with coupling matrix of Table 5-13 is converted to a capacitively loaded combline bandpass filter as illustrated in Fig. 5-16. The final scaled circuit elements in 50 Ohm system are shown as in Table 5-14. By using the theory developed in Chapter 1, the resonant frequencies, inter-resonator coupling and the 3 dB bandwidths for the input and output couplings may be computed as shown in Table 5-15 to Table 5-17.

Initial physical dimensions were obtained as explained in Chapter 1. Fine tuning is necessary to achieve equal ripple Chebyshev response and aggressive space mapping techniques were applied. After 11 iterations the final screw positions were obtained and the final dimensions are shown in Table 5-18. Fig. 5-18 shows the simulated HFSS simulation after fine tuning using space mapping techniques.

Table 5-14 Final Combline Bandpass Filter Element Values

Inter-resonator Coupling Impedances (Ω)	Capacitors	Short-Circuited Stubs Impedance (Ω)
Input/Output $K = 139.2719$ $Z_{12} = 456.9484$ $Z_{23} = 623.2374$	$C_1 = 2.0729\ pF$ $C_2 = 2.0705\ pF$ $C_3 = 2.0830\ pF$	$Z_r = 75$

Table 5-15 10-0-1 Combline Bandpass Filter Resonance Frequencies

All combline Resonators $75\ \Omega$

Physical length $\lambda/8$ long at $f_o = 1\ GHz$

Resonator	Frequency (GHz)
1	1.0091
2	1.0096
3	1.0072
4	1.0096
5	1.0091

Table 5-16 10-0-1 Combline Bandpass Filter Inter-resonator Couplings using two combline resonators model

Coupling	Coefficient K_m (GHz)	f_{ev} (MHz)	f_{od} (MHz)	Coupling Bandwidth (MHz)
1-2	0.1681	940.4	1069.3	128.8914
2-3	0.1230	958.9	1053.1	94.2419
3-4	0.1230	958.9	1053.1	94.2419
4-5	0.1681	940.4	1069.3	128.8914

Table 5-17 10-0-1 Combline Bandpass Filter Input/Output Couplings

Resonator	Frequency (MHz)
$f_{3dBupper}$	1088.5
$f_{3dBlower}$	935.4
f_{3dB}	153.0729

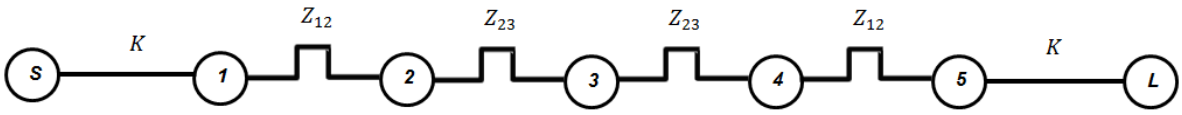

(a) Combline bandpass filter circuit realisation

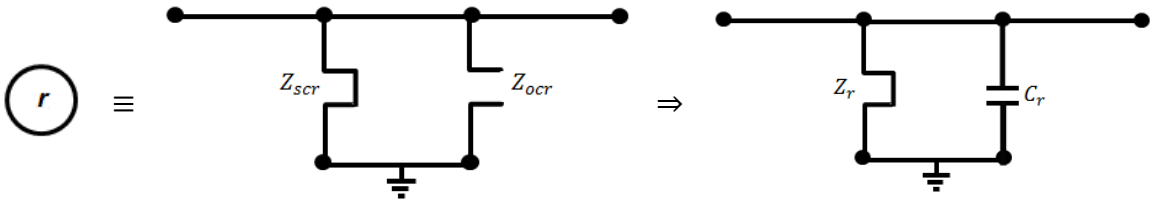

(b) Distributed resonator and conversion to combline resonator

Fig. 5-16 Topology of the 5th degree combline bandpass filter

Table 5-18 Physical Dimensions (mm)

Ground plane spacing	25
Resonators' Height	37.5
Resonator diameters	7.73
Tuning screw diameter	3
Capacitive loading gap on resonators	2
Re-entrant depth and diameter	4×10
Resonator 1 tuning screw height	9.9636
Resonator 2 tuning screw height	7.7316
Resonator 3 tuning screw height	7.6106
inter-resonator tuning screw heights 1-2	5.6913
inter-resonator tuning screw heights 2-3	7.1800
Wall to first/last resonator centre spacing	12.5
Centre-to-centre inter-resonator spacing 1-2	17.7004
Centre-to-centre inter-resonator spacing 2-3	20.6385

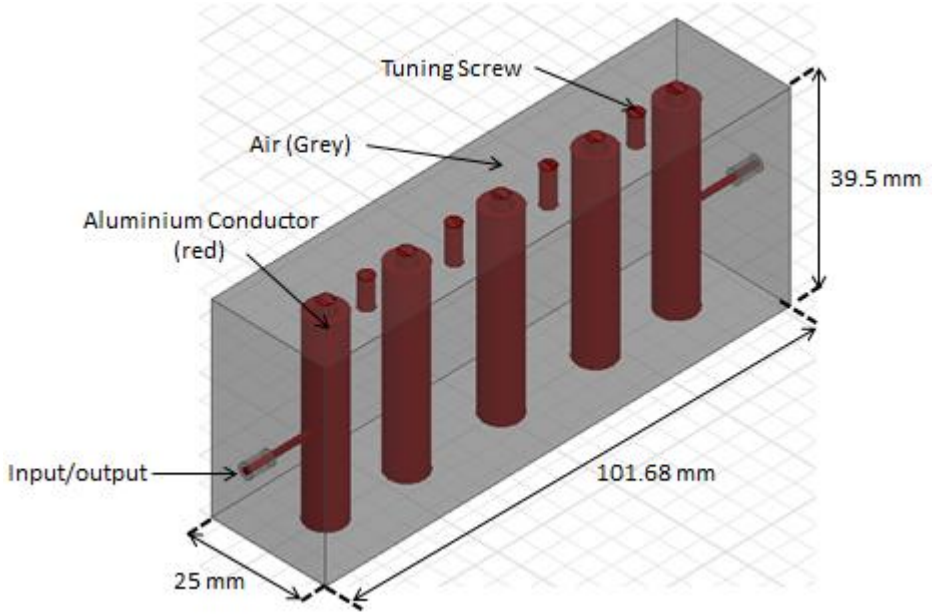

Fig. 5-17 HFSS modelling of the combline bandpass filter in example 5.2.3.2

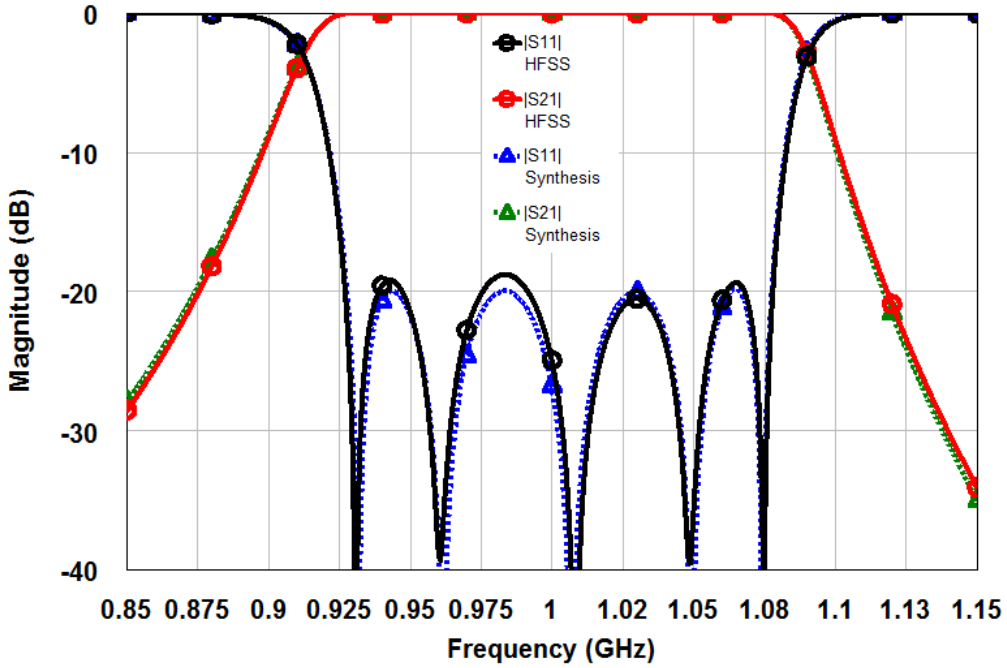

Fig. 5-18 Comparison between synthesised and HFSS fine-tuned simulation for combline bandpass filter response

5.3 Synthesis of Narrow Dual Bandpass Filters

A more complete coverage of dual bandpass filters is given in Chapter 6. In this section, it is demonstrated how dual bandpass filters may be synthesised from suitable lowpass prototype filters. Because the transformation used from lowpass

to bandpass filter is valid only for narrow band filters, the technique in this section is more suitable for narrow (less than 20% fractional bandwidth) dual bandpass filters. The basis functions for synthesis of narrow dual bandpass filters were derived in section 0 of Chapter 2.

The synthesis is fairly straight forward. Using the basis functions for asymmetrical or symmetrical dual bandpass filter, the characteristic polynomials are obtained based on the transmission zero positions to meet a given filter specifications as described in Chapter 1 and Chapter 2. Because the filter is first synthesised in lowpass domain, the lowpass coupling matrix is used as opposed to bandpass coupling matrix. An illustrative example is given in the next section.

5.3.1 Synthesis Illustrative Example

A dual passband filter with cut-offs at 1710-1785 MHz and 1920-1995 MHz and 20 dB passband return loss was designed. The normalised cutoffs are at $\alpha = -0.5025$, $\beta = 0.5025$, and $\delta = 1$ (corresponding to $\omega_c = 0.5025$). Five transmission zeros were prescribed at $\omega_z = \pm 0.25, 0, \pm 1.75$.

Table 5-19 Basis Functions Selection for a Dual Band Lowpass Characteristic Function

α_r	N-N_{FTZ}-N_{OTZ}	Purpose
2	$2-0-0$	Provide four transmission zeros at infinity
1	$2-0-1$	Provide a single transmission zero at the origin and a single transmission zero at infinity
2	$2-2-0$	Provide two symmetrical pairs of transmission zeros at $\omega_z = \pm 0.25, \pm 1.75$

Since the dual band is symmetrical, the following lowpass prototypes were linearly combined according to the method described in Chapter 2 based on the basis functions as follows: 2-0-0, 2-0-1 and 2-2-0 basis function with weighting numbers $\alpha_1 = 2$, $\alpha_2 = 1$ and $\alpha_3 = 2$ respectively. The first basis function only provides transmission zeros at infinity, the second provides the required single transmission zero at the origin and the last basis function provides the two pairs of symmetrical

transmission zeros. Table 5-19 shows the summary of the basis functions chosen and the transmission zeros they provide. This gives an overall 10-4-1 lowpass characteristic function corresponding to a 10th degree dual bandpass filter. Using the general recursive formulae algorithm of Chapter 2 the characteristic polynomials were determined as in Table 5-20 in complex variable $p\ (= j\omega)$. Then cascaded synthesis was used to extract the element values and the coupling matrix generated is as shown below in Table 5-21. The dual bandpass filter topology is shown in Fig. 5-19 and the circuit simulation is shown in Fig. 5-20.

Table 5-20 10-4-1 Lowpass Filter Prototype Characteristic Polynomials

($\mu = -1$ and $\varepsilon = 197.6872$)

$$P(p) = p^5 + 3.1250p^3 + 0.1914p$$
$$F(p) = p^{10} + 2.9564p^8 + 3.3175p^6 + 1.7564p^4 + 0.4373p^2 + 0.0410$$
$$E(p) = p^{10} + 1.0152p^9 + 3.4717p^8 + 2.5759p^7 + 4.2763p^6 + 2.2206p^5 + 2.2900p^4 + 0.7535p^3 + 0.5238p^2 + 0.0842p + 0.0410$$

Table 5-21 10-4-1 Lowpass Filter Prototype Coupling Matrix

$$M = \begin{bmatrix} 0 & 0.7124 & 0 & 0 & 0 & 0 & 0 & 0 & 0 & 0 & 0 & 0 \\ 0.7124 & 0 & 0.6601 & 0 & -0.4907 & 0 & 0 & 0 & 0 & 0 & 0 & 0 \\ 0 & 0.6601 & 0 & 0.0643 & 0 & 0 & 0 & 0 & 0 & 0 & 0 & 0 \\ 0 & 0 & 0.0643 & 0 & 0.6752 & 0 & 0 & 0 & 0 & 0 & 0 & 0 \\ 0 & -0.4907 & 0 & 0.6752 & 0 & 0.3150 & 0 & 0 & 0 & 0 & 0 & 0 \\ 0 & 0 & 0 & 0 & 0.3150 & 0 & 0.6816 & 0.3276 & 0 & 0 & 0 & 0 \\ 0 & 0 & 0 & 0 & 0 & 0.6816 & 0 & 0 & 0 & 0 & 0 & 0 \\ 0 & 0 & 0 & 0 & 0 & 0.3276 & 0 & 0 & 0.7038 & 0 & -0.0984 & 0 \\ 0 & 0 & 0 & 0 & 0 & 0 & 0 & 0.7038 & 0 & 0.4841 & 0 & 0 \\ 0 & 0 & 0 & 0 & 0 & 0 & 0 & 0 & 0.4841 & 0 & 0.8167 & 0 \\ 0 & 0 & 0 & 0 & 0 & 0 & 0 & -0.0984 & 0 & 0.8167 & 0 & 0.7124 \\ 0 & 0 & 0 & 0 & 0 & 0 & 0 & 0 & 0 & 0 & 0.7124 & 0 \end{bmatrix}$$

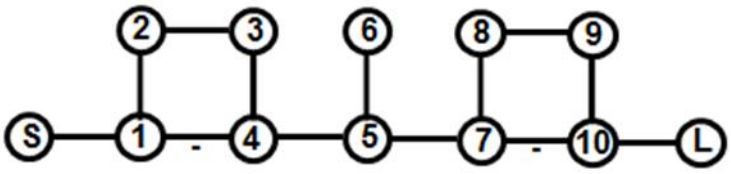

Fig. 5-19 10th Degree Dual Bandpass Filter Topology

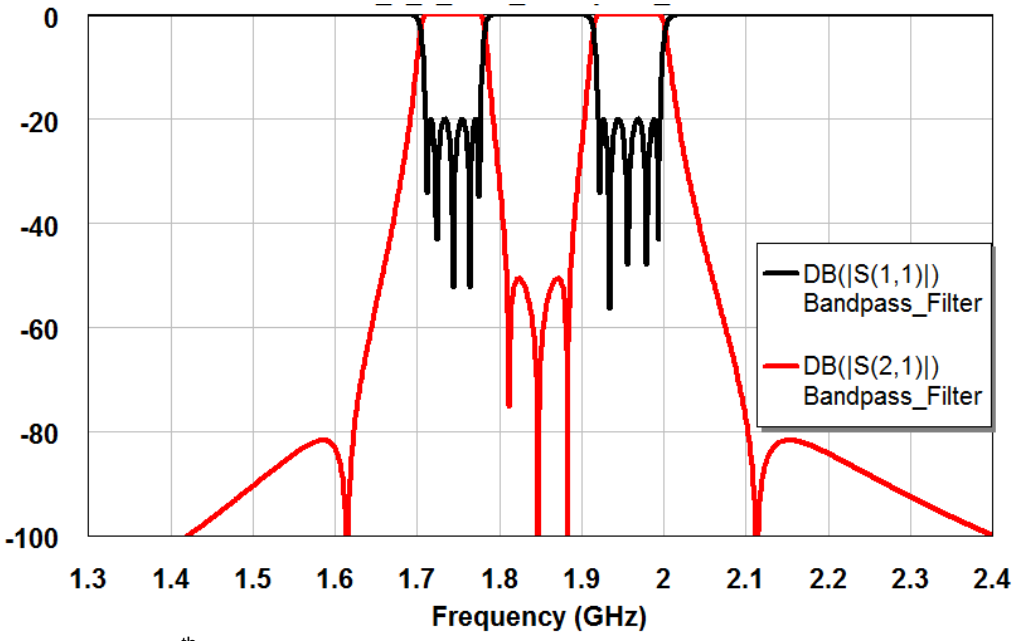

Fig. 5-20 10th Degree Dual Bandpass Filter Simulated Frequency Response

5.4 Conclusion

The method of direct synthesis of bandpass filters and narrow band dual bandpass filters has been presented. Synthesis and design of interdigital and combline bandpass were given in section 5.2. Then in section 5.3, synthesis of narrow dual bandpass filter was given based on the basis functions computed in Chapter 2. Chapter 5 highlighted the different applications of the method of generating Chebyshev characteristic function as presented in Chapter 2. The next Chapter makes the final application of the synthesis technique of Chapter 2 to the direct synthesis of dual bandpass filters of arbitrary bandwidth and separation.

Chapter 6 Direct Synthesis and Design for Dual Band Filters

6.1 Introduction

In the past decade, there has been increasing interest in the area of multi-passband filters. In particular dual passband filters offer flexibility as well as efficiency in the utilization of communication resources. The efficiency comes in terms of simplified circuit networks thereby reducing mass and volume of filters and hence the cost of the filters. Many important contributions have been made to the methods of designing dual passband filters.

In this work, methods for the direct generation of general Chebyshev transfer functions for dual passband filters will be explained. The method outlined offers a simple and intuitive approach to the synthesis of symmetrical and asymmetrical dual band filter networks by linearly combining simple elementary characteristic functions given in Chapter 2, where the dual bandpass behaviour is achieved by carefully placed reflection and transmission zeros.

Two different physical realisations are examined. The first one consists of cascaded n-tuplets sections. The dual bandpass may be synthesised in the same way as was done for a single bandpass filter, except that some transmission zeros are placed in-band to separate the two bands.

In the second physical realisation, the dual bandpass filter is synthesised in the same way as for cascaded n-tuplets realisation but decomposed into two separate parallel connected bandpass filters by adding extra complex transmission zeros. The extra complex transmission zeros enables physical separation of the two constituent bandpass filters. The two parallel connected filters interact in a complicated way that produces these extra transmission zeros. Understanding the complex interaction between the two parallel connected bandpass filters is key to determining how the separation is achieved. This realisation offers advantages over the former because coupling bandwidths are confined to each individual bandpass filter as opposed to wide coupling bandwidths in the cascaded n-tuplets

realisation in which some couplings may be difficult to realise especially for wide dual bandpass filters. The disadvantage is that extra transmission zeros are required to achieve the decomposition which limits the stopband attenuation as these transmission zeros are at complex frequencies.

6.2 Existing Methods for Dual Bandpass Synthesis

There are a number of narrow band approximations to the synthesis of dual bandpass filters. The simplest dual bandpass characteristic may be obtained from Zolotarev lowpass transfer function approximation [81-83]. This class is characterised by a dip in between the two passband as all the transmission zeros are at the origin or infinity frequencies. Thus there is no control over the attenuation between the two passbands. The attenuation produced by the dip depends on the network order and the relative bandwidths between the two bands.

Advanced optimisation techniques may also be employed to synthesise dual bandpass filters [84-86]. The number of poles and zeros of the characteristic function may be imposed and determined through optimisation. However, the convergence of such numerical optimization techniques is not always guaranteed and this may compromise their usefulness.

Another way of designing dual passband filter is cascading a wide passband filter and a narrow stopband filter. There is no better control over the rejection levels in the stopbands and because there are two separate filters, this requires matching to enable integration into a single unit. Alternatively a single wide bandpass may be designed and the attenuation poles added in-between the passband to create the required passband separation [87]. Unfortunately, these techniques also require optimisations to yield the required response.

However, the most common design method makes use of frequency transformations. The methods outlined in [88, 89] involve some form of frequency transformations to generate a lowpass prototype filter transfer function suitable for dual band filters. Symmetrical lowpass prototype filters for dual band filters may be designed using change of variable based on classical work in [90]. The general

asymmetrical lowpass prototype filter, however, may also be synthesised using the proposed method utilising basis functions as demonstrated in Chapter 1 and Chapter 5. Since the design of such lowpass prototype filters with attenuation poles in-band is easily achieved [91, 92], frequency transformation to bandpass domain of the lowpass prototype filter produces the desired separation between the two passbands of interest. As alluded to earlier, the frequency transformation is only suitable for narrow bandpass filters because of the dispersive nature of the coupling elements. The synthesis example of Chapter 5 is one such good example.

For wide dual bandpass filters (usually higher than 20% overall fractional bandwidth, considering the outer cutoff frequencies), direct synthesis provides a better approximation since the coupling elements are frequency variant. Xiao in [93] proposes a superposition approach. The synthesis here is achieved by directly synthesising two separate bandpass filters, one for each band, with allocated finite frequency transmission zeros in the vicinity of each band and then the overall characteristic function is obtained by inverse combination of the individual characteristic functions. This means the two filters maintain their reflections zeros in the overall filter, but the transmission zeros are changed, and additional transmission zeros are added in the process. Unless the required transmission zeros are known initially, there is no direct control on the position of the transmission zeros. The synthesis is therefore more useful for transverse network realisations.

The next section shows how the proposed method enables control over the reflection zeros and transmission zeros in the passbands and stopbands respectively using the basis functions derived in Chapter 2.

6.3 Cascaded quadruplets (CQ) Dual Bandpass Filters

In this proposed method it is shown by means of examples how the direct synthesis of dual bandpass filter may be achieved. This section also shows how transfer functions of a dual bandpass filter with the two bands which are symmetrical and asymmetrical are generated and realised using cascaded quadruplet (CQ) sections. In general cascaded n-tuplets sections may be used, for

illustrative purposes, however, only CQ sections are used in the following examples.

6.3.1 Symmetric Dual Bandpass Filter Example

In this illustrative example, consider an 8th degree $(N = 16)$ symmetrical dual bandpass filter with each band of degree $N_1 = N_2 = N/2 = 8$, with the specifications as in Table 6-1. The normalized cutoff points may easily computed as $\alpha = 0.8680$, $\beta = 0.8934$, $\gamma = 0.9746$ and $\delta = 1$. Two symmetrical pairs of transmission zeros were prescribed at $\omega_{r1} = \pm 1.01$ and $\omega_{r2} = \pm 0.9546$, a single transmission zero at the origin and seven transmission zeros at infinity.

Table 6-1 Symmetrical Dual Bandpass Filter Specifications

Passband 1	1710-1760 MHz
Passband 2	1920-1970 MHz
Passband Return Loss (RL)	20 dB

Table 6-2 Basis Functions Selection 16-8-1 Direct Synthesised Dual Bandpass Filter

α_r	N-N_{FTZ}-N_{OTZ}	Purpose
1	$4-0-1$	Provide a single transmission zero at the origin and 3 transmission zeros at infinity
1	$4-4-0$	Provide a pair of prescribed symmetrical transmission zeros at $\omega_{r1} = \pm 1.01$ and a pair of dependent symmetrical transmission zeros at $\omega_{z1} = \pm 0.8580$
1	$8-4-0$	Provide a pair of prescribed symmetrical transmission zeros at $\omega_{r2} = \pm 0.9546$, a pair of dependent symmetrical transmission zeros at $\omega_{z2} = \pm 0.9111$ and four transmission zeros at infinity

Since this is a symmetrical transfer function ($\delta - 1 = \beta - \alpha$), the other dependent pairs $(\pm\omega_{zr})$ of symmetrical transmission zeros generated are approximately

symmetrically located in the lower and upper stopbands and inner stopband with the use of appropriate basis functions.

Working out the required basis functions from the tables of Chapter 2 (Table 2-10 to Table 2-12) the following basis functions may be used: 4-0-1, 4-4-0 and 8-4-0 with weighting numbers $\alpha_1 = 1$, $\alpha_2 = 1$ and $\alpha_3 = 1$ respectively. This gives an overall 16-8-1 dual bandpass characteristic function. Table 6-2 shows the summary of the basis functions chosen and the transmission zeros they provide. The rest of synthesis procedure is done as described in Chapter 2. The characteristic polynomials obtained after application of general recursive technique are shown in Table 6-3.

Table 6-3 16-8-2 Dual Bandpass Filter Characteristic Polynomials

($\mu = \pm 1$ and $\varepsilon = 1.1127 \times 10^5$)

$P(p) = p^9 + 3.4977p^7 + 4.5659p^5 + 2.6364p^3 + 0.5681p$
$F(p) = p^{16} + 7.0037p^{14} + 21.4185p^{12} + 37.3561p^{10} + 40.6406p^8 + 28.2412p^6 + 12.2414p^4 + 3.0262p^2 + 0.3266$
$E(p) = p^{16} + 0.1070p^{13} + 7.0094p^{14} + 0.6560p^{13} + 21.4486p^{12} + 1.7200p^{11} + 37.4218p^{10} + 2.5000p^9 + 40.7170p^8 + 2.1757p^7 + 28.2911p^6 + 1.1337p^5 + 12.2588p^4 + 0.3275p^3 + 3.0287p^2 + 0.0405p + 0.3266$

Y Matrix Polynomials

$Y_{11n}(p) = 0.1070p^{15} + 0.6560p^{13} + 1.7200p^{11} + 2.5000p^9 + 2.1757p^7 + 1.1337p^5 + 0.3275p^3 + 0.0405p = Y_{22n}(p)$
$Y_{21n}(p) = Y_{12n}(p) = -(p^9 + 3.4977p^7 + 4.5659p^5 + 2.6364p^3 + 0.5681p)/\varepsilon$
$Y_{den}(p) = 2p^{16} + 14.0132p^{14} + 42.8671p^{12} + 74.7779p^{10} + 81.3576p^8 + 56.5323p^6 + 24.5002p^4 + 6.0548p^2 + 0.6533$

This filter may easily be realized with two cascaded quadruplets. The transverse coupling matrix is generated from the Y matrix polynomials of Table 6-3 from which the coupling matrix of two cascaded quadruplets may be obtained as described in

Chapter 1. The final coupling matrix is shown in Table 6-4 corresponding to the topology as illustrated in Fig. 6-1. Negative inductive coupling elements may be replaced by capacitive couplings elements if required. The simulated magnitude response is shown in Fig. 6-2.

Table 6-4 $N_r \times N_r$ Normalised Coupling Matrix of a Symmetrical 16-8-1 Dual Bandpass Filter

$$Y_{BP} = M_{Ts} + pM_{Cs} + \frac{1}{p}M_{Ls}$$

$$M_{Ts} = \begin{bmatrix} 0.0535 & 0 & 0 & 0 & 0 & 0 & 0 & 0 \\ 0 & 0.0000 & 0 & 0 & 0 & 0 & 0 & 0 \\ 0 & 0 & 0.0000 & 0 & 0 & 0 & 0 & 0 \\ 0 & 0 & 0 & 0.0000 & 0 & 0 & 0 & 0 \\ 0 & 0 & 0 & 0 & 0.0000 & 0 & 0 & 0 \\ 0 & 0 & 0 & 0 & 0 & 0.0000 & 0 & 0 \\ 0 & 0 & 0 & 0 & 0 & 0 & 0.0000 & 0 \\ 0 & 0 & 0 & 0 & 0 & 0 & 0 & 0.0535 \end{bmatrix}$$

$$M_{Cs} = \begin{bmatrix} 1 & 0.0000 & 0 & 0 & 0 & 0 & 0 & 0 \\ 0.0000 & 1 & 0.0000 & 0 & 0 & 0 & 0 & 0 \\ 0 & 0.0000 & 1 & 0.0000 & 0 & 0 & 0 & 0 \\ 0 & 0 & 0.0000 & 1 & 0.0000 & 0 & 0 & 0 \\ 0 & 0 & 0 & 0.0000 & 1 & 0.0000 & 0 & 0 \\ 0 & 0 & 0 & 0 & 0.0000 & 1 & 0.0000 & 0 \\ 0 & 0 & 0 & 0 & 0 & 0.0000 & 1 & 0.0000 \\ 0 & 0 & 0 & 0 & 0 & 0 & 0.0000 & 1 \end{bmatrix}$$

$$M_{Ls} = \begin{bmatrix} +0.8763 & -0.0938 & 0 & -0.0454 & 0 & 0 & 0 & 0 \\ -0.0938 & +0.8787 & +0.0809 & -0.0018 & 0 & 0 & 0 & 0 \\ 0 & +0.0809 & +0.8740 & -0.0812 & 0 & 0 & 0 & 0 \\ -0.0454 & -0.0018 & -0.0812 & +0.8758 & -0.0353 & 0 & 0 & 0 \\ 0 & 0 & 0 & -0.0353 & +0.8861 & -0.0891 & -0.0011 & -0.0523 \\ 0 & 0 & 0 & 0 & -0.0891 & +0.8646 & +0.0099 & 0 \\ 0 & 0 & 0 & 0 & -0.0011 & +0.0099 & +0.8749 & -0.0901 \\ 0 & 0 & 0 & 0 & -0.0523 & 0 & -0.0901 & +0.8763 \end{bmatrix}$$

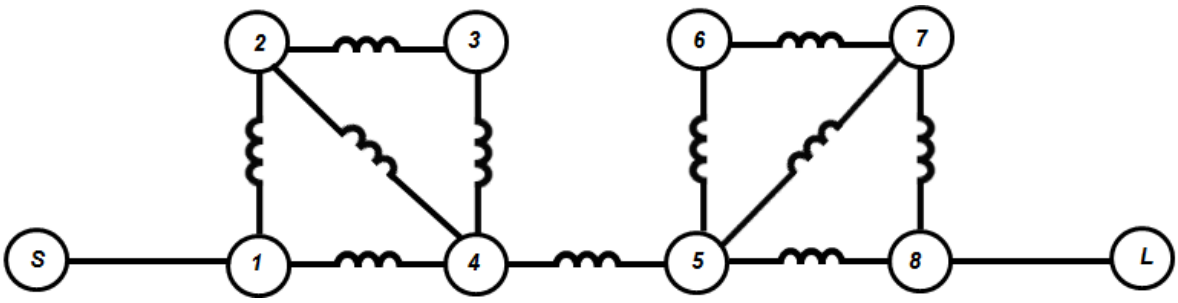

Fig. 6-1 Symmetrical 16-8-1 dual bandpass filter topology

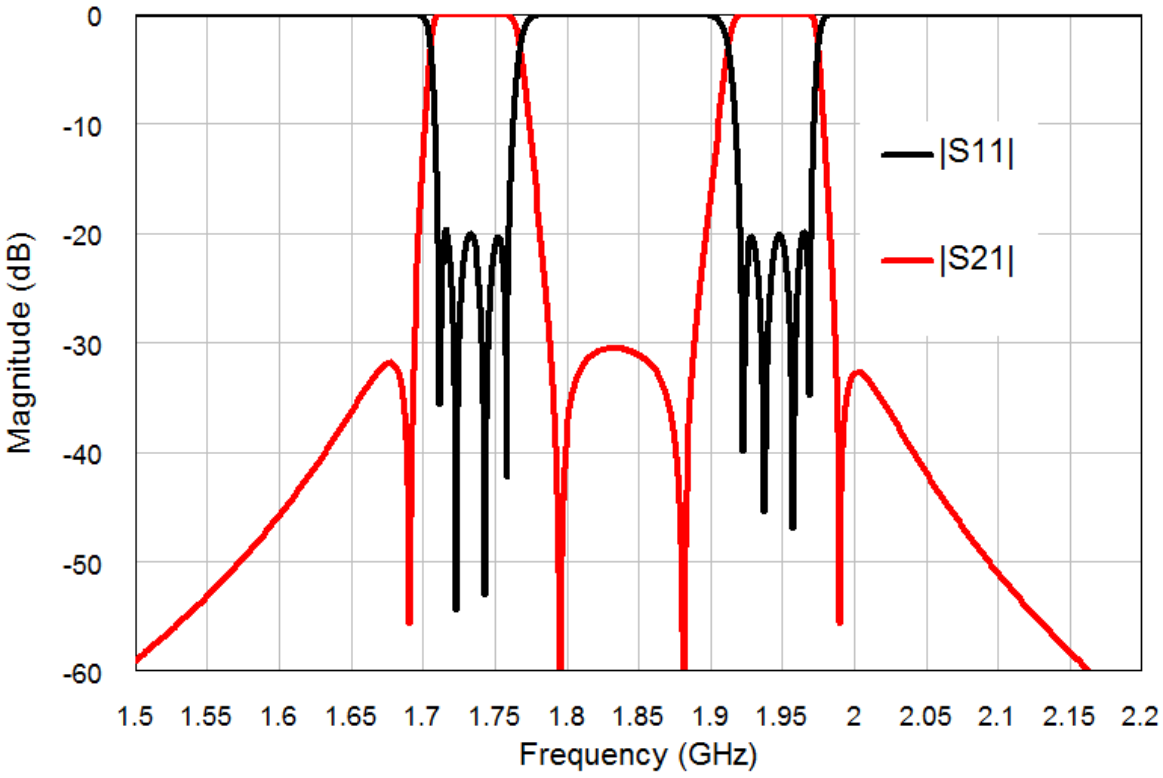

Fig. 6-2 Simulated magnitude response for 16-8-2 symmetric dual bandpass filter

6.3.2 Asymmetric Dual Bandpass Filter Example

Consider a dual bandpass filter with the specifications shown in Table 6-5. This example will be synthesised in the lumped domain but realised using distributed elements. To enable this requires the use of the following normalised lumped to distributed transformation,

Table 6-5 Asymmetrical Dual Bandpass Filter Specifications

Passband 1	1700-1770 MHz
Passband 2	1900-1960 MHz
Stopband Insertion Loss $IL \geq 40$ dB	1800-1850 MHz
Stopband Insertion Loss $IL \geq 80$ dB	2100-2160 MHz
Passband Return Loss (RL)	20 dB
Electrical length at Centre Frequency	45^{o}

$$\omega = \frac{\tan(a\omega)}{\tan(a\omega_{u2})} = \frac{t}{t_{u2}} \tag{6.1}$$

where

$$\omega_{u2} = 2\pi f_{u2} \tag{6.2}$$

is the upper most cutoff frequency (f_{u2}) of the dual bandpass filter. Using the (6.1), the normalised cutoff points in the lumped domain may be calculated as $\alpha = 0.7996$, $\beta = 0.8493$, $\gamma = 0.9496$ and $\delta = 1$. To meet the specifications an 8th degree $(N = 16)$ asymmetrical dual bandpass filter with each band of degree $N_1 = N_2 = N/2 = 8$ and a single prescribed transmission zero at $\omega_{r1} = \pm 1.142$ is synthesised. The following basis functions were used: 4-2-1, 4-4-0 and 8-2-0 with weighting numbers $\alpha_1 = 1$, $\alpha_2 = 1$ and $\alpha_3 = 1$ respectively as shown in Table 6-6. The other finite transmission zero pairs are dependent transmission zeros that result from the basis functions used. This yielded a 16-8-1 characteristic function which meets the filters specifications. As before the overall characteristic function was obtained by application of general recursive technique. The filter polynomials are shown in Table 6-7.

Table 6-6 Basis Functions Selection 16-8-1 Direct Synthesised Asymmetrical Dual Bandpass Filter

α_r	N-N_{FTZ}-N_{OTZ}	Purpose
1	$4-2-1$	Provide a single transmission zero at the origin, a single transmission zero at infinity and a dependent finite frequency transmission zero pair at $\omega_{z1} = \pm 0.9019$
1	$4-4-0$	Provide a prescribed single pair of symmetrical transmission zero at $\omega_{r1} = \pm 1.142$ and a pair of dependent symmetrical transmission zeros at $\omega_{z1} = \pm 0.8782$
1	$8-2-0$	Provide a dependent pair of symmetrical transmission zeros at $\omega_{r2} = \pm 0.8903$ and six transmission zeros at infinity

Table 6-7 16-8-1 Dual Bandpass Filter Polynomials

Characteristic Polynomials

$(\varepsilon = 3.5444 \times 10^4, \mu = 1)$

$P(p) = p^9 + 3.6814p^7 + 4.9837p^5 + 2.9535p^3 + 0.6485p$
$F(p) = p^{16} + 6.5343p^{14} + 18.6048p^{12} + 30.1464p^{10} + 30.4045p^8 + 19.5446p^6 + 7.8199p^4 + 1.7806p^2 + 0.1767$
$E(p) = p^{16} + 0.2133p^{15} + 6.5571p^{14} + 1.2216p^{13} + 18.7165p^{12} + 2.9851p^{11} + 30.3738p^{10} + 4.0344p^9 + 30.6507p^8 + 3.2568p^7 + 19.6939p^6 + 1.5704p^5 + 7.8680p^4 + 0.4188p^3 + 1.7870p^2 + 0.0476p + 0.1767$

Y Matrix Polynomials

$Y_{11n}(p) = 0.2133p^{15} + 1.2216p^{13} + 2.9851p^{11} + 4.0344p^9 + 3.2568p^7 + 1.5704p^5 + 0.4188p^3 + 0.0476p = Y_{22n}(p)$
$Y_{21n}(p) = Y_{12n}(p) = -(p^9 + 3.6814p^7 + 4.9837p^5 + 2.9535p^3 + 0.6485p)/\varepsilon$
$Y_{den}(p) = 2p^{16} + 13.0914p^{14} + 37.3212p^{12} + 60.5202p^{10} + 61.0552p^8 + 39.2385p^6 + 15.6880p^4 + 3.5675p^2 + 0.3533$

This filter may also be easily realized with two cascaded quadruplets as the coupling matrix in Table 6-8 and topology as in Fig. 6-3 shows. The filter elements are re-normalised to distributed domain by dividing by $\tan(a\omega_{u2})$. The final elements are shown in Table 6-9 for realisation as capacitively loaded dual bandpass filter. Fig. 6-4 shows the simulated circuit response of the synthesised 16-8-1 dual bandpass filter. Empirical EM based techniques may then be applied to obtain the filter's physical dimensions.

Table 6-8 $N_r \times N_r$ Coupling Matrix of an Asymmetrical 16-8-1 Dual Bandpass Filter

$$Y_{BP} = M_{Ts} + pM_{Cs} + \frac{1}{p}M_{Ls}$$

$$M_{Ts} = \begin{bmatrix} 0.1067 & 0 & 0 & 0 & 0 & 0 & 0 & 0 \\ 0 & 0.0000 & 0 & 0 & 0 & 0 & 0 & 0 \\ 0 & 0 & 0.0000 & 0 & 0 & 0 & 0 & 0 \\ 0 & 0 & 0 & 0.0000 & 0 & 0 & 0 & 0 \\ 0 & 0 & 0 & 0 & 0.0000 & 0 & 0 & 0 \\ 0 & 0 & 0 & 0 & 0 & 0.0000 & 0 & 0 \\ 0 & 0 & 0 & 0 & 0 & 0 & 0.0000 & 0 \\ 0 & 0 & 0 & 0 & 0 & 0 & 0 & 0.1067 \end{bmatrix}$$

$$M_{Cs} = \begin{bmatrix} 1 & 0.0000 & 0 & 0 & 0 & 0 & 0 & 0 \\ 0.0000 & 1 & 0.0000 & 0 & 0 & 0 & 0 & 0 \\ 0 & 0.0000 & 1 & 0.0000 & 0 & 0 & 0 & 0 \\ 0 & 0 & 0.0000 & 1 & 0.0000 & 0 & 0 & 0 \\ 0 & 0 & 0 & 0.0000 & 1 & -0.1056 & 0 & 0 \\ 0 & 0 & 0 & 0 & -0.1056 & 1 & 0.0000 & 0 \\ 0 & 0 & 0 & 0 & 0 & 0.0000 & 1 & 0.0000 \\ 0 & 0 & 0 & 0 & 0 & 0 & 0.0000 & 1 \end{bmatrix}$$

$$M_{Ls} = \begin{bmatrix} +0.8188 & -0.1306 & 0 & -0.0747 & 0 & 0 & 0 & 0 \\ -0.1306 & +0.8093 & -0.0168 & -0.0119 & 0 & 0 & 0 & 0 \\ 0 & -0.0168 & +0.7337 & -0.0848 & 0 & 0 & 0 & 0 \\ -0.0747 & -0.0119 & -0.0848 & +0.8953 & -0.0799 & 0 & 0 & 0 \\ 0 & 0 & 0 & -0.0799 & +0.7304 & 0 & -0.0538 & -0.0219 \\ 0 & 0 & 0 & 0 & 0 & +0.8821 & -0.0429 & 0 \\ 0 & 0 & 0 & 0 & -0.0538 & -0.0429 & +0.8391 & -0.1488 \\ 0 & 0 & 0 & 0 & -0.0219 & 0 & -0.1488 & +0.8188 \end{bmatrix}$$

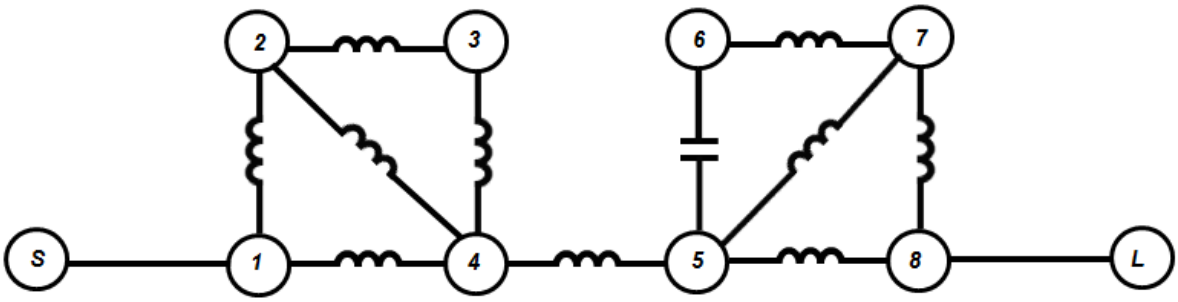

Fig. 6-3 Asymmetrical 16-8-1 dual bandpass filter topology

Table 6-9 Final Element Values of a Capacitively Loaded Dual Bandpass Filter

Inductive Inter-resonator Coupling Impedances (Ω)	Capacitors	Short-Circuited Stubs Impedance (Ω)
$Z_{12} = 569.10$	$C_1 = 1.1444\ pF$	$Z_r = 75$
$Z_{14} = 1037.8$	$C_2 = 1.1554\ pF$	Input/Output Coupling Impedance (Ω)
$Z_{23} = 4235.5$	$C_3 = 1.2513\ pF$	
$Z_{24} = 6463.2$	$C_4 = 1.0627\ pF$	$K_{output} = 197.8455$
$Z_{34} = 873.70$	$C_5 = 1.2559\ pF$	$K_{input} = 197.8454$
$Z_{45} = 925.30$	$C_6 = 1.0759\ pF$	Capacitive Inter-resonator Coupling Impedance (Ω)
$Z_{57} = 1337.2$	$C_7 = 1.1214\ pF$	
$Z_{58} = 3252.3$	$C_8 = 1.1444\ pF$	$Z_{56} = 870.3142$
$Z_{67} = 1812.4$		
$Z_{78} = 507.00$		

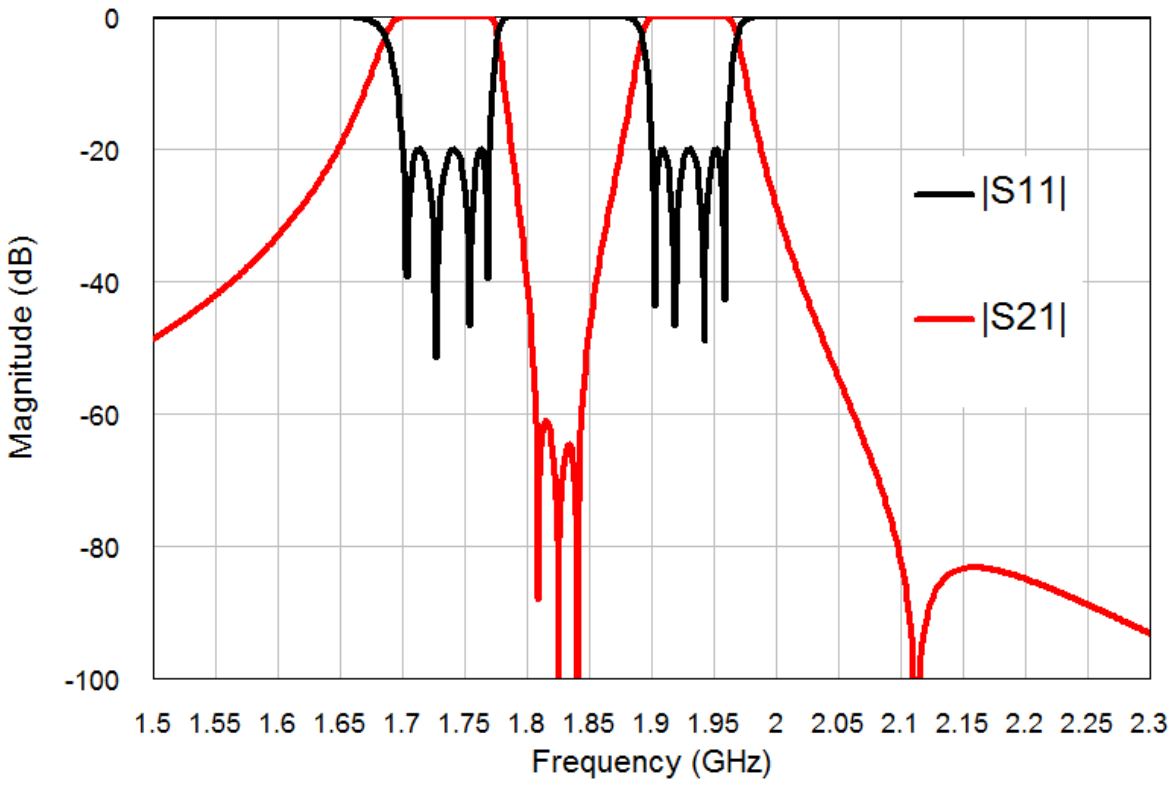

Fig. 6-4 Simulated magnitude response for 16-8-1 asymmetric dual bandpass filter

6.4 Decomposition into Parallel Connected Filters

In the foregoing section, it was demonstrated using linear combination of low degree elementary functions how direct synthesis of dual bandpass filter may be achieved. The dual bandpass filter illustrative examples were realised using CQ sections. In general cascaded n-tuplets dual bandpass filter networks present two challenges: (1) The coupling values tend to be unrealizably strong especially for widely separated dual bandpass filters [94, 95]. (2) Changes in every resonator and coupling element values have strong effect on frequency response of the two bands especially for relatively narrow dual bandpass filters. The two problems above may be mitigated by having two bandpass filters, one for each band, connected in parallel so that the resultant filter produces the desired dual bandpass frequency response. Using a technique similar to the one used in [94], it is now shown how an overall dual bandpass filter synthesized using the novel direct synthesis method may be separated into two bandpass filters - one filter for each band with prescribed number of reflection and transmission zeros.

6.4.1 Dual Bandpass Filter Analysis

It is assumed that the synthesis of the required characteristic polynomials has been done. Let the overall filter $[ABCD]_T$ matrix be

$$[ABCD]_T = \frac{1}{P_T}\begin{bmatrix} A_T & B_T \\ C_T & D_T \end{bmatrix} \tag{6.3}$$

It is evident from direct dual bandpass synthesis that both polynomials B_T and C_T are both even, while the polynomials A_T and D_T are both old. All the transmission zeros P_T are all symmetrical except the transmission zeros at the origin. Now for symmetrical and reciprocal filter networks, the following properties of $[ABCD]_T$ matrix holds true:

$$\begin{aligned} A_T &= D_T \\ {A_T}^2 - B_T C_T &= {P_T}^2 \end{aligned} \tag{6.4}$$

The overall filter $[ABCD]_T$ matrix in (6.3) is converted to admittance matrix $[Y]_T$ as follows:

$$[Y]_T = \begin{bmatrix} \frac{A_T}{B_T} & -\frac{P_T}{B_T} \\ -\frac{P_T}{B_T} & \frac{A_T}{B_T} \end{bmatrix} \tag{6.5}$$

Let

$$B_T = 2B_1B_2 \tag{6.6}$$

where the polynomials B_1 and B_2 are all monic polynomials with indices 1 and 2 referring to lower and upper band filter 1 and 2 respectively. B_1 is associated with the lower band filter 1 and B_2 is associated with the upper band filter 2. It is assumed (when the total number of transmission zeros are less than the degree of the network), as is normally the case, that the coefficient of the highest term in B_T is 2. B_1 and B_2 are found by simply sorting the zeros of B_T in ascending order and assigning lower values (around filter 1 band $\pm\alpha \rightarrow \pm\beta$) to B_1 and upper values (around filter 2 band $\pm\gamma \rightarrow \pm 1$) to B_2. Substituting (6.6) into (6.5) yields,

$$[Y]_T = \begin{bmatrix} \frac{A_T}{2B_1B_2} & -\frac{P_T}{2B_1B_2} \\ -\frac{P_T}{2B_1B_2} & \frac{A_T}{2B_1B_2} \end{bmatrix} \tag{6.7}$$

Then polynomials in (6.7) may be separated by grouping the residues and poles of rational polynomials in (6.7) as

$$[Y]_T = \frac{1}{2}\begin{bmatrix} \frac{A_1}{B_1} + \frac{A_2}{B_2} & -\left(\frac{P_1}{B_1} + \frac{P_2}{B_2}\right) \\ -\left(\frac{P_1}{B_1} + \frac{P_2}{B_2}\right) & \frac{A_1}{B_1} + \frac{A_2}{B_2} \end{bmatrix} \tag{6.8}$$

Where A_1 and P_1 are associated to filter 1 and A_2 and P_2 are associated to filter 2. Furthermore (6.8) may be decomposed into two separate filters by re-writing as

$$[Y]_T = \frac{1}{2B_1}\begin{bmatrix} A_1 & -P_1 \\ -P_1 & A_1 \end{bmatrix} + \frac{1}{2B_2}\begin{bmatrix} A_2 & -P_2 \\ -P_2 & A_2 \end{bmatrix} = [Y]_1 + [Y]_2 \tag{6.9}$$

so that,

$$[Y]_1 = \frac{1}{2B_1}\begin{bmatrix} A_1 & -P_1 \\ -P_1 & A_1 \end{bmatrix}$$
$$[Y]_2 = \frac{1}{2B_2}\begin{bmatrix} A_2 & -P_2 \\ -P_2 & A_2 \end{bmatrix} \quad (6.10)$$

Comparing (6.7) and (6.8), for the total transmission zeros yields,

$$P_1B_2 + P_2B_1 = P_T \quad (6.11)$$

Since (6.11) holds true for any given dual bandpass filter, then the dual bandpass filter is separable into filter 1 and filter 2 represented by (6.10). Unfortunately, there is no control on the number of transmission zeros of filter 1 (P_1) and filter 2 (P_2) and in general these are equivalent to or a degree less than the degree of each filter so that their realization is impractical [96]. By allowing certain complex transmission zeros in P_T to exist, the number of transmission zeros of filter 1 (P_1) and filter 2 (P_2) may be controlled according to (6.11). By imposing the number of transmission zeros in each filter, it is now shown how to determine the unique complex transmission zeros that would satisfy the relationship in (6.11).

6.4.2 Parallel Connected Bandpass Filters

To achieve the separation and find a unique set of complex transmission zeros to satisfy (6.11), first recognize that to achieve certain selectivity requirements or group delay equalization there is need to specify at least some of the transmission zeros of the overall filter at some finite frequency or in general complex frequency. To do this, (6.11) is re-written as

$$P_1B_2 + P_2B_1 = P_T = (1/\varepsilon)P_UP_K \quad (6.12)$$

where the monic polynomial P_U contains all the unknown complex transmission zeros and the monic polynomial P_K contains all the known transmission zeros and $1/\varepsilon$ is the coefficient of the highest term in P_T. In fact the transmission zeros in P_U occurs in complex conjugate pairs in the complex plane. The polynomials B_1 and B_2 for each individual filter are determined as in section 6.4.1 by simple root assignment. Note that for direct synthesis of dual bandpass filters, the polynomials B_1, B_2 and P_U are all even polynomials. It is now necessarily to define the following integers.

N_1 is the degree of filter 1 (degree of B_1)

N_2 is the degree of filter 2 (degree of B_2)

N_{Z1} is the degree of P_1 less 1

N_{Z2} is the degree of P_2 less 1

N_{ZU} is the degree of P_U

N_{ZK} is the degree of P_K less 1

$N = N_1 + N_2$ is the degree of the overall filter characteristic function

$N_{TZ} = N_{ZK} + N_{ZU} + 1$ is the overall filter total number of transmission zeros

(6.13)

Also let

$1/\varepsilon_1$ be the coefficient of the highest term in P_1

$1/\varepsilon_2$ be the coefficient of the highest term in P_2

(6.14)

It is assumed for simplicity and for physical realisability that the overall filter and hence filter 1 and filter 2 have a single transmission zero at the origin. When N_1 and N_2 are given, N_{Z1} and N_{Z2} may be imposed on each of the sub-filters. Thus the following relationships may be used:

1. Equal Partition $(N_1 = N_2 = N/2 \text{ and } N_{Z1} = N_{Z2})$

$$N_{ZU} = \frac{N}{2} - N_{Z1} = \frac{N}{2} - N_{Z2}$$
$$\frac{1}{\varepsilon_1} = \frac{1}{\varepsilon_2} = \frac{1}{2\varepsilon} \tag{6.15}$$

2. Unequal Partition $(N_1 \neq N_2 \text{ and } N_{Z1} \neq N_{Z2})$

$$N_{ZU} = \max(N_{Z1} + N_2, N_{Z2} + N_1) - N_{ZK}$$
$$1/\varepsilon_1 = 1/\varepsilon_2 = 1/(2\varepsilon) \text{ , for } N_{Z1} + N_2 = N_{Z2} + N_1 \tag{6.16}$$
$$1/\varepsilon_1 = 1/\varepsilon_2 = 1/\varepsilon, \text{ for } N_{Z1} + N_2 \neq N_{Z2} + N_1$$

In both cases above, it is assumed that

$$N_{ZK} = N_{Z1} + N_{Z2} \tag{6.17}$$

With (6.15) - (6.17) in view, (6.12) is now simply $(N_{ZK} + N_{ZU})/2$ system of linear equations in $(N_{ZK} + N_{ZU})/2$ unknown variables with conditions in (6.15) - (6.17)

imposed. The unknown transmission zeros in P_1, P_2 and P_U required for the separation using (6.12) are found using an iterative approach.

First starting with $P_U = 1$, then B_1 and B_2 may be obtained as describe in 6.4.1 with P_K containing the prescribed $N_{ZK}/2$ pairs of symmetrical transmission zeros and a single transmission zero at the origin. The linear system (6.12) is then solved for the $(N_{ZK} + N_{ZU})/2$ unknowns from which P_1, P_2 and P_U are obtained. Using these known transmission zeros in P_K and P_U, the synthesis is repeated so that again new B_1 and B_2 are determined. The linear system in (6.12) is evaluated again and P_U formed. This is performed iteratively until (6.12) converges. The technique is proved with some illustrative examples for equal and unequal number of reflection zeros (equal and unequal partition) in each band of the dual bandpass filter. The procedure normally takes a few iterations to converge although this largely depends on the relative bandwidths and separation of the two bands as well as the level of accuracy required in the polynomial coefficients.

6.4.3 Parallel Connected Dual Bandpass Filter Example 1

Consider a dual bandpass filter with specifications as shown in Table 6-10. Because the synthesis is done in lumped domain (6.1) apply so that the normalised cutoff points in lumped domain are calculated as $\alpha = 0.7508$, $\beta = 0.7940$, $\gamma = 0.9532$ and $\delta = 1$.

Table 6-10 Parallel Connected Dual Bandpass Filter Example 1 Specifications

Passband 1	1800-1870 MHz
Passband 2	2100-2160 MHz
Stopband Insertion Loss $IL \geq 40$ dB	1700-1755 MHz
Stopband Insertion Loss $IL \geq 40$ dB	1940-2000 MHz
Passband Return Loss (RL)	20 dB
Electrical length at Centre Frequency	45^o

To meet the specifications an 8th degree $(N = 16)$ dual bandpass filter with equal partition assumed ($N_1 = N_2 = N/2 = 8$) is used. The initial prescribed transmission zeros and two basis functions used are shown in Table 6-11. The other two pairs of

symmetrical transmission zeros are dependent and are assigned to the inner stopband. This yields an initial 16-8-1 transfer function that may even be realised using two cascaded quadruplets (CQ) as was illustrated in the examples given in section 6.2.

Now, $N_{Z1} = 4$ and $N_{Z2} = 4$ is imposed so that from (6.17) $N_{ZK} = 8$. Furthermore, according to (6.15) the number of transmission zeros required for the decomposition into parallel connected bandpass filter networks is $N_{ZU} = 4$. By solving the linear system (6.12) for six unknowns, the initial positions of the complex transmission zeros were determined as $\omega_{r3} = \pm(0.9128 + j0.1771)$ and $\omega_{r4} = \pm(0.9128 - j0.1771)$. These transmission zeros were used as the starting point to the iterative procedure described in section 6.4.2. The initial 8-2-0 basis function was replaced by 8-6-0 to accommodate for the extra complex quadruplet of transmission zeros. The iteration was initiated and after 17 iterations with absolute error on the coefficients of (6.12) defined to be less than 1e-11 so that (6.12) converges. The final complex quadruplet transmission zeros location were $\omega_{r3} = \pm(0.9127 + j0.1764)$ and $\omega_{r4} = \pm(0.9127 - j0.1764)$. Notice the small change in the position of the dependent transmission zero in Fig. 6-5. The positions of the prescribed transmission zeros are maintained and it is clear from Fig. 6-5 that the stopband rejection levels are slightly worse for the parallel filter network configurations because of the introduction of the complex quadruplet transmission zeros required for the dual bandpass filter separation.

Once the dual bandpass filter has been decomposed into parallel connected filter networks, the rest of the synthesis process is fairly straight forward as it has been demonstrated in many examples before. Table 6-12 shows the filter's polynomials. The coupling matrices for each individual parallel path network may be computed as shown in Table 6-13 using (6.10) and polynomials in Table 6-12. Notice that in the parallel connected dual bandpass filter, the element values are localised to each filter band as opposed to the CQ realisation. Fig. 6-7 shows the individual frequency magnitude response for each parallel filter path. The transmission zeros positions for each individual filter are only slightly altered in the final dual band

response shown in Fig. 6-8. As before, conventional numerical EM techniques may then be applied to obtain the filter's physical dimensions starting from the element values given in Table 6-14.

Table 6-11 16-12-1 Parallel Connected Dual Bandpass Filter Basis Functions

(a) Initial Basis Functions (16-8-1)

α_r	N-N_{FTZ}-N_{OTZ}	Purpose
1	$8-6-1$	Provide a single transmission zero at the origin, a two pairs of symmetrical prescribed transmission zero at $\omega_{r1}=\pm 0.7208$ and $\omega_{r2}=\pm 0.9040$, a dependent pair of symmetrical transmission zero at $\omega_{z1}=\pm 0.9176$ and a single transmission zero at infinity
1	$8-2-0$	Provide a dependent pair of symmetrical transmission zeros at $\omega_{z2}=\pm 0.8500$ and six transmission zeros at infinity

(b) Final Basis Functions Used in the Iterative Procedure (16-12-1)

α_r	N-N_{FTZ}-N_{OTZ}	Purpose
1	$8-6-1$	Provide a single transmission zero at the origin, a two pairs of symmetrical prescribed transmission zero at $\omega_{r1}=\pm 0.7208$ and $\omega_{r2}=\pm 0.9040$, a dependent pair of symmetrical transmission zero at $\omega_{z1}=\pm 0.9176$ and a single transmission zero at infinity
1	$8-6-0$	Provide two pairs of symmetrical prescribed transmission zero at $\omega_{r3}=\pm(0.9127+j0.1764)$ and $\omega_{r4}=\pm(0.9127-j0.1764)$, a pair of symmetrical dependent transmission zero at $\omega_{z2}=\pm 0.8435$ and two transmission zeros at infinity

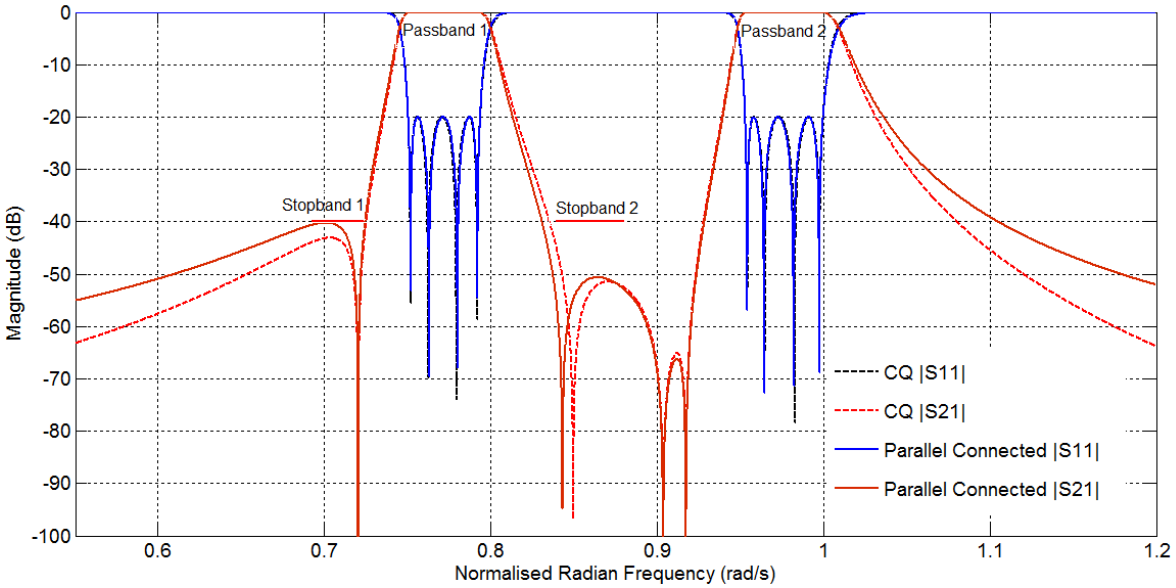

Fig. 6-5 Simulated magnitude response of a dual bandpass filter before and after decomposition into parallel connected filter networks

Table 6-12 16-12-1 Parallel Connected Dual Bandpass Filter Polynomials

Filter 1

$(\varepsilon = 4.2637 \times 10^3, \mu = 1)$

$P_1(p) = p^5 + 1.2308p^3 + 0.3695p$
$A_1(p) = 0.0908p^7 + 0.1622p^5 + 0.0964p^3 + 0.0191p$
$B_1(p) = p^8 + 2.3797p^6 + 2.1213p^4 + 0.8395p^2 + 0.1245$

Filter 2

$(\varepsilon = 4.2637 \times 10^3, \mu = 1)$

$P_2(p) = p^5 + 1.5611p^3 + 0.6042p$
$A_2(p) = 0.1012p^7 + 0.2887p^5 + 0.2742p^3 + 0.0868p$
$B_2(p) = p^8 + 3.8164p^6 + 5.4572p^4 + 3.4653p^2 + 0.8245$

Table 6-13 $N_r + 2 \times N_r + 2$ Coupling Matrix of a 16-12-1 Dual Bandpass Filter

$$M = M_T + pM_C + \frac{1}{p}M_L$$

$$M_{T1} = \begin{bmatrix} 0.0000 & 0.2131 & 0 & 0 & 0 & 0 \\ 0.2131 & 0.0000 & 0 & 0 & 0 & 0 \\ 0 & 0 & 0.0000 & 0 & 0 & 0 \\ 0 & 0 & 0 & 0.0000 & 0 & 0 \\ 0 & 0 & 0 & 0 & 0.0000 & 0.2131 \\ 0 & 0 & 0 & 0 & 0.2131 & 0.0000 \end{bmatrix}$$

$$M_{T2} = \begin{bmatrix} 0.0000 & 0.2249 & 0 & 0 & 0 & 0 \\ 0.2249 & 0.0000 & 0 & 0 & 0 & 0 \\ 0 & 0 & 0.0000 & 0 & 0 & 0 \\ 0 & 0 & 0 & 0.0000 & 0 & 0 \\ 0 & 0 & 0 & 0 & 0.0000 & 0.2249 \\ 0 & 0 & 0 & 0 & 0.2249 & 0.0000 \end{bmatrix}$$

$$M_{C1} = M_{C2} = \begin{bmatrix} 0.0000 & 0 & 0 & 0 & 0 & 0 \\ 0 & 1.0000 & 0 & 0 & 0 & 0 \\ 0 & 0 & 1.0000 & 0 & 0 & 0 \\ 0 & 0 & 0 & 1.0000 & 0 & 0 \\ 0 & 0 & 0 & 0 & 1.0000 & 0 \\ 0 & 0 & 0 & 0 & 0 & 0.0000 \end{bmatrix}$$

$$M_{L1} = \begin{bmatrix} +0.0000 & 0 & 0 & 0 & 0 & 0 \\ 0 & +0.5940 & -0.0295 & 0 & -0.0026 & 0 \\ 0 & -0.0295 & +0.5986 & -0.0242 & -0.0034 & 0 \\ 0 & 0 & -0.0242 & +0.5930 & +0.0293 & 0 \\ 0 & -0.0026 & -0.0034 & +0.0293 & +0.5940 & 0 \\ 0 & 0 & 0 & 0 & 0 & +0.0000 \end{bmatrix}$$

$$M_{L2} = \begin{bmatrix} +0.0000 & 0 & 0 & 0 & 0 & 0 \\ 0 & +0.9634 & -0.0418 & 0 & -0.0023 & 0 \\ 0 & -0.0418 & +0.9581 & -0.0273 & +0.0182 & 0 \\ 0 & 0 & -0.0273 & +0.9315 & -0.0376 & 0 \\ 0 & -0.0023 & +0.0182 & -0.0376 & +0.9634 & 0 \\ 0 & 0 & 0 & 0 & 0 & +0.0000 \end{bmatrix}$$

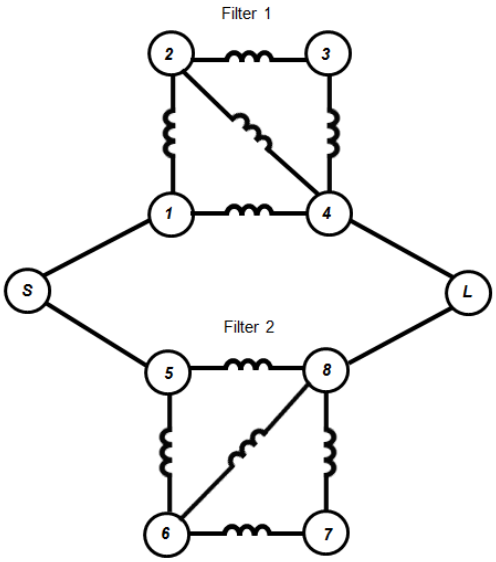

Fig. 6-6 16-12-1 Parallel Connected dual bandpass filter topology

Table 6-14 Final Element Values of a Capacitively Loaded Parallel Connected Dual Bandpass Filter

Filter 1 (Lower)		
Inductive Inter-resonator Coupling Impedances (Ω)	Capacitors	Short-Circuited Stubs Impedance (Ω)
$Z_{12} = 1799.0$ $Z_{14} = 20521$ $Z_{23} = 2195.0$ $Z_{24} = 15535$ $Z_{34} = -1804.0$	$C_1 = 1.3022\ pF$ $C_2 = 1.2938\ pF$ $C_3 = 1.3041\ pF$ $C_4 = 1.3022\ pF$	$Z_r = 75$ Input/Output Coupling Impedance (Ω) $K_{s1} = 259.4880$ $K_{l1} = 259.4880$
Filter 2 (Upper)		
Inductive Inter-resonator Coupling Impedances (Ω)	Capacitors	Short-Circuited Stubs Impedance (Ω)
$Z_{56} = 2170.0$ $Z_{58} = 39176$ $Z_{67} = 3270.0$ $Z_{68} = -4970.0$ $Z_{78} = 2386.0$	$C_5 = 0.8770\ pF$ $C_6 = 0.8809\ pF$ $C_7 = 0.9007\ pF$ $C_8 = 0.8770\ pF$	$Z_r = 75$ Input/Output Coupling Impedance (Ω) $K_{s2} = 321.8633$ $K_{l2} = 321.8633$

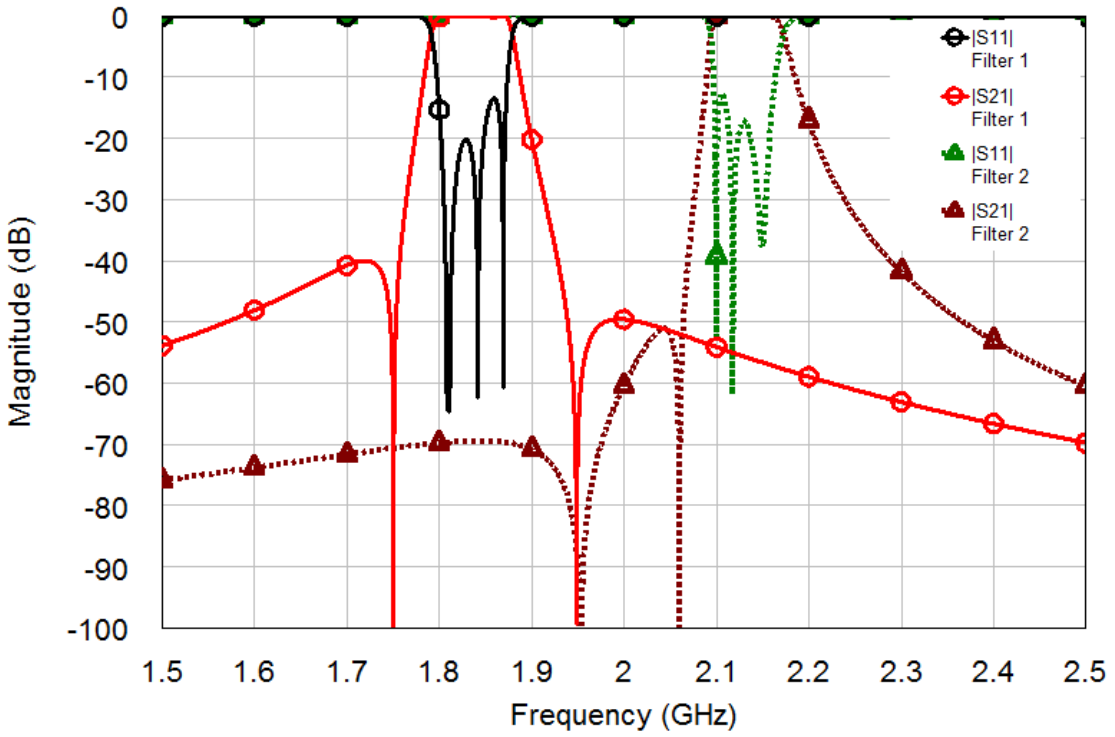

Fig. 6-7 Individual filter's magnitude response for the 16-12-1 parallel connected dual bandpass filter

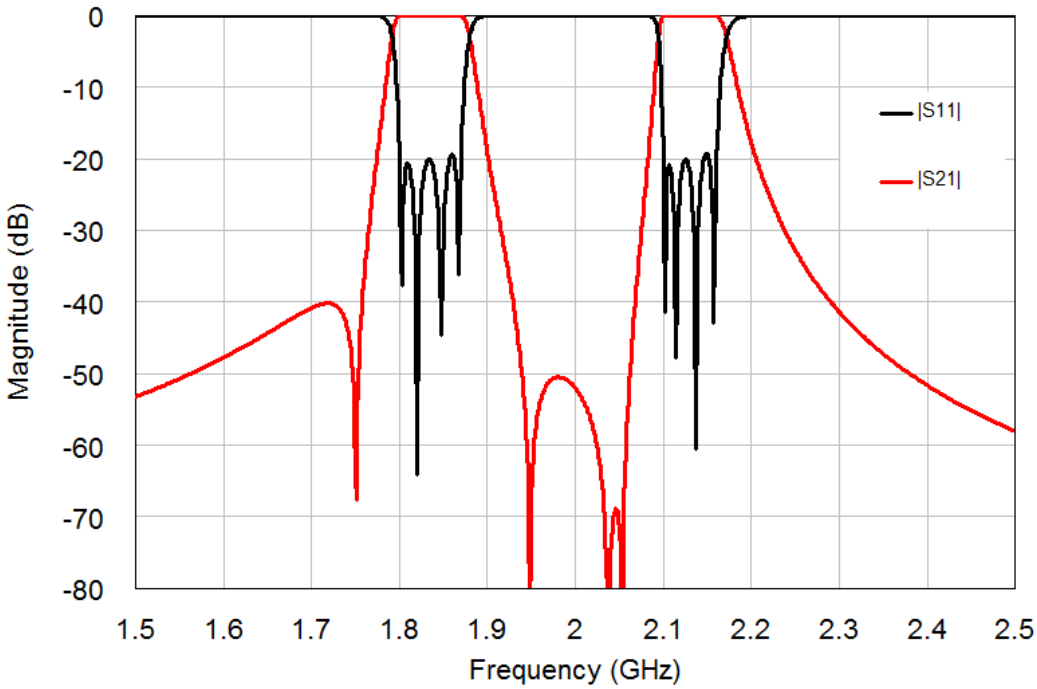

Fig. 6-8 Circuit simulation for the 16-12-1 parallel connected dual bandpass filter with element values of Table 6-14

6.4.4 Parallel Connected Dual Bandpass Filter Example 2

In this example an unequal partition ($N_1 \neq N_2$) dual bandpass will be considered with specifications as shown in Table 6-15. As before, (6.1) will be applied so that the normalised cutoff points in lumped domain are calculated as $\alpha = 0.7454$, $\beta = 0.7819$, $\gamma = 0.9457$ and $\delta = 1$.

Table 6-15 Parallel Connected Dual Bandpass Filter Example 2 Specifications

Passband 1	1800-1860 MHz
Passband 2	2100-2170 MHz
Stopband Insertion Loss $IL \geq 40$ dB	1925-2010 MHz
Passband Return Loss (RL)	20 dB
Electrical length at Centre Frequency	45^o

To meet the specifications a 7th degree $(N = 14)$ dual bandpass filter with unequal partition was used such that $N_1 = 6$ and $N_2 = 8$. The initial prescribed transmission zeros and two basis functions used are shown in Table 6-16. Each of the basis function provides a dependent pair of symmetrical transmission zeros which are assigned to the inner and upper stopband respectively. This yields an initial 14-6-1 transfer function that may be realised using a trisection cascaded with a quadruplet section.

In this example, it is imposed that $N_{Z1} = 2$ and $N_{Z2} = 4$ and from (6.17) $N_{ZK} = 6$. Thus according to (6.16), the number of transmission zeros required for the decomposition into parallel connected bandpass filter networks is $N_{ZU} = 4$. By solving the linear system (6.12) for five unknowns, the initial positions of the complex transmission zeros were determined as $\omega_{r3} = \pm(0.8891 + j0.1664)$ and $\omega_{r4} = \pm(0.8891 - j0.1664)$. The iterative procedure of section 6.4.2 was then applied using these transmission zeros. The initial 6-2-0 basis function was replaced by a 6-6-0 basis function to accommodate for the extra complex quadruplet of transmission zeros. The iteration was initiated and after 6 iterations with absolute error on the coefficients of (6.12) defined to be less than 1e-11 so that (6.12) converges. The final complex quadruplet transmission zeros locations

were $\omega_{r3} = \pm(0.8887 + j0.1656)$ and $\omega_{r4} = \pm(0.8887 - j0.1656)$. Fig. 6-9 shows the simulated response before and after the introduction of quadruplet transmission zeros. Notice the slight difference in the rejection levels in the stopband in the two filters. This change must be accounted for to obtain the desired stopband rejection levels.

Table 6-16 14-10-1 Parallel Connected Dual Bandpass Filter Basis Functions

(a) Initial Basis Functions (14-6-1)

α_r	N-N_{FTZ}-N_{OTZ}	Purpose
1	$8-4-1$	Provide a single transmission zero at the origin, a two pairs of symmetrical prescribed transmission zero at $\omega_{r1} = \pm 0.8749$, a dependent pair of symmetrical transmission zero at $\omega_{z1} = \pm 0.8236$ and three transmission zero at infinity
1	$6-2-0$	Provide a dependent pair of symmetrical transmission zeros at $\omega_{z2} = \pm 1.0075$ and four transmission zeros at infinity

(b) Final Basis Functions Used in the Iterative Procedure (14-10-1)

α_r	N-N_{FTZ}-N_{OTZ}	Purpose
1	$8-4-1$	Provide a single transmission zero at the origin, a two pairs of symmetrical prescribed transmission zero at $\omega_{r1} = \pm 0.8749$, a dependent pair of symmetrical transmission zero at $\omega_{z1} = \pm 0.8236$ and three transmission zero at infinity
1	$6-6-0$	Provide two pairs of symmetrical prescribed transmission zero at $\omega_{r3} = \pm(0.8887 + j0.1656)$ and $\omega_{r4} = \pm(0.8887 - j0.1656)$ and a pair of symmetrical dependent transmission zero at $\omega_{z2} = \pm 1.0072$

The rest of the synthesis is done as described before with the filter's polynomials shown in Table 6-17. Additionally, the coupling matrices for each individual parallel

filter network may be computed as shown in Table 6-18 using (6.10) and polynomials in Table 6-17. The corresponding topology is shown in Fig. 6-10. Finally the magnitude response for each filter network is shown in Fig. 6-11.

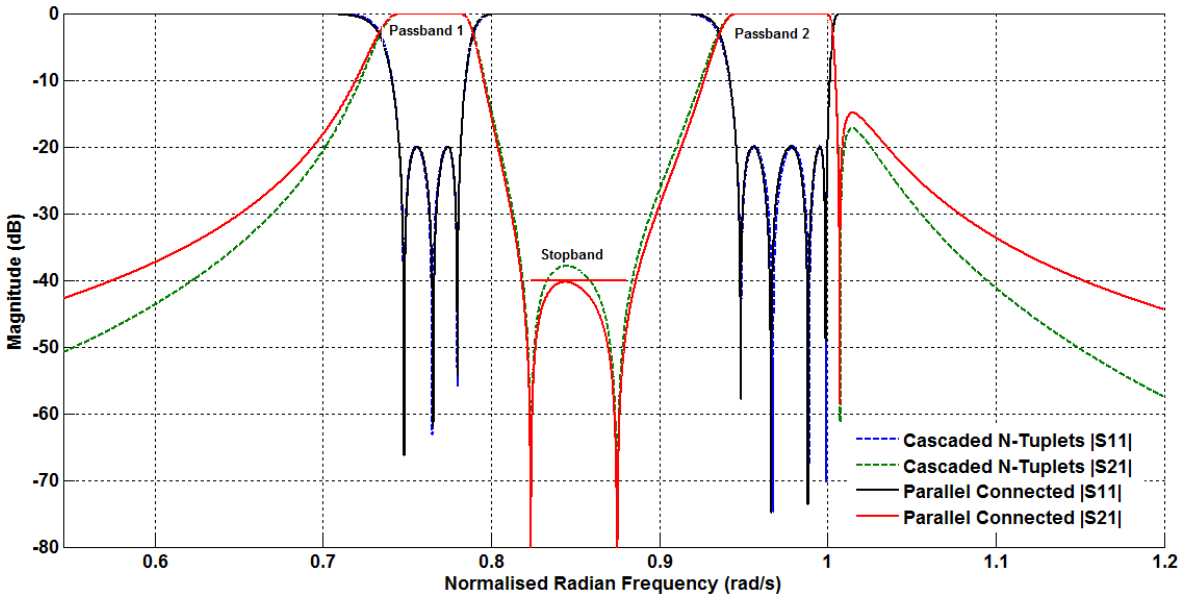

Fig. 6-9 Simulated magnitude response of a dual bandpass filter before and after decomposition into parallel connected filter networks

Table 6-17 14-10-1 Parallel Connected Dual Bandpass Filter Polynomials

Filter 1

$(\varepsilon = 1.3543 \times 10^3, \mu = 1)$

$P_1(p) = p^3 + 0.6793p$
$A_1(p) = 0.0853p^5 + 0.0999p^3 + 0.0292p$
$B_1(p) = p^6 + 1.7483p^4 + 1.0172p^2 + 0.1969$

Filter 2

$(\varepsilon = 1.3543 \times 10^3, \mu = 1)$

$P_2(p) = p^5 + 1.7144p^3 + 0.7101p$
$A_2(p) = 0.1144p^7 + 0.3286p^5 + 0.3142p^3 + 0.1000p$
$B_2(p) = p^8 + 3.8241p^6 + 5.4781p^4 + 3.4839p^2 + 0.8300$

Table 6-18 $N_r + 2 \times N_r + 2$ Coupling Matrix of a 14-10-1 Dual Bandpass Filter

$$M = M_T + pM_C + \frac{1}{p}M_L$$

$$M_{T1} = \begin{bmatrix} 0.0000 & 0.2066 & 0 & 0 & 0 \\ 0.2066 & 0.0000 & 0 & 0 & 0 \\ 0 & 0 & 0.0000 & 0 & 0 \\ 0 & 0 & 0 & 0.0000 & 0.2066 \\ 0 & 0 & 0 & 0.2066 & 0.0000 \end{bmatrix}$$

$$M_{T2} = \begin{bmatrix} 0.0000 & 0.2391 & 0 & 0 & 0 & 0 \\ 0.2391 & 0.0000 & 0 & 0 & 0 & 0 \\ 0 & 0 & 0.0000 & 0 & 0 & 0 \\ 0 & 0 & 0 & 0.0000 & 0 & 0 \\ 0 & 0 & 0 & 0 & 0.0000 & 0.2388 \\ 0 & 0 & 0 & 0 & 0.2388 & 0.0000 \end{bmatrix}$$

$$M_{C1} = \begin{bmatrix} 0.0000 & 0 & 0 & 0 & 0 \\ 0 & 1.0000 & 0 & 0 & 0 \\ 0 & 0 & 1.0000 & 0 & 0 \\ 0 & 0 & 0 & 1.0000 & 0 \\ 0 & 0 & 0 & 0 & 0.0000 \end{bmatrix}$$

$$M_{C2} = \begin{bmatrix} 0.0000 & 0 & 0 & 0 & 0 & 0 \\ 0 & 1.0000 & 0 & 0 & 0 & 0 \\ 0 & 0 & 1.0000 & 0 & -0.0318 & 0 \\ 0 & 0 & 0 & 1.0000 & -0.0382 & 0 \\ 0 & 0 & -0.0318 & -0.0382 & 1.0000 & 0 \\ 0 & 0 & 0 & 0 & 0 & 0.0000 \end{bmatrix}$$

$$M_{L1} = \begin{bmatrix} +0.0000 & 0 & 0 & 0 & 0 \\ 0 & +0.5778 & -0.0274 & -0.0087 & 0 \\ 0 & -0.0274 & +0.5927 & -0.0274 & 0 \\ 0 & -0.0087 & -0.0274 & +0.5778 & 0 \\ 0 & 0 & 0 & 0 & +0.0000 \end{bmatrix}$$

$$M_{L2} = \begin{bmatrix} +0.0000 & 0 & 0 & 0 & 0 & 0 \\ 0 & +0.9513 & -0.0466 & 0 & -0.0050 & 0 \\ 0 & -0.0466 & +0.9377 & -0.0295 & 0 & 0 \\ 0 & 0 & -0.0295 & +0.9838 & 0 & 0 \\ 0 & -0.0050 & 0 & 0 & +0.9466 & 0 \\ 0 & 0 & 0 & 0 & 0 & +0.0000 \end{bmatrix}$$

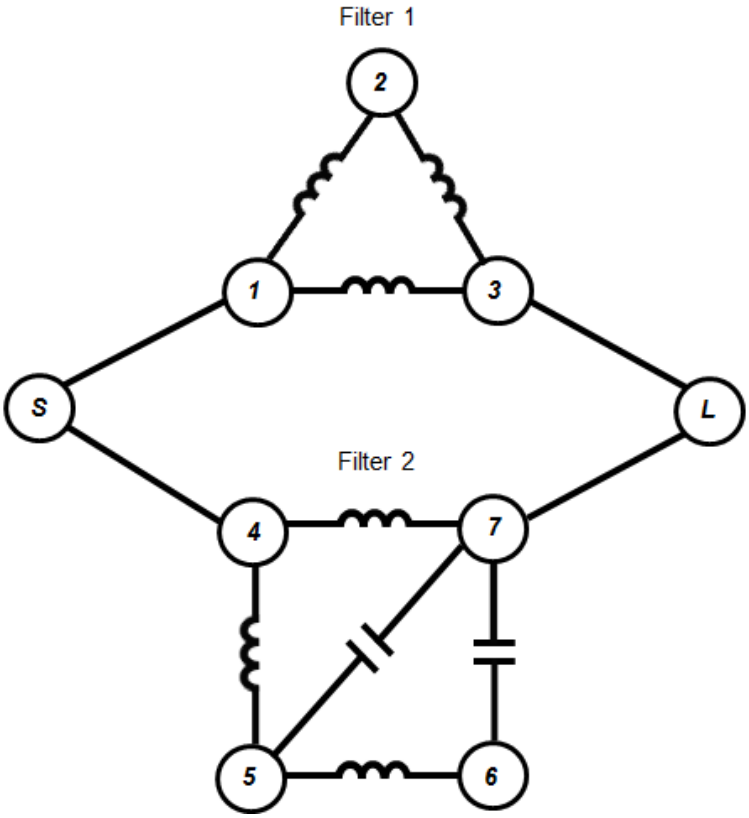

Fig. 6-10 14-10-1 Parallel Connected dual bandpass filter topology

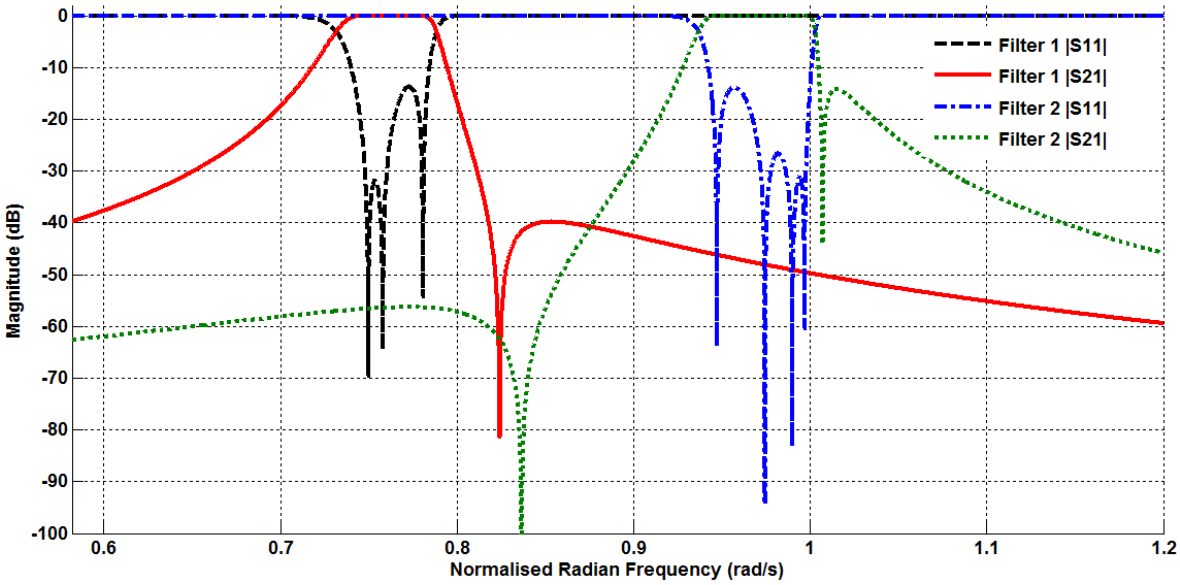

Fig. 6-11 Individual filter's magnitude response of the 14-10-1 parallel connected dual bandpass filter

6.4.5 Comparison Between Cascaded N-tuplets and Parallel Connected Dual Bandpass Realisations

The example in section 6.4.4 was used to compare the coupling bandwidths for the two different physical realisations. The two filters have topologies as shown in Fig. 6-12. It can be noted from Table 6-19 that the cascaded n-tuplets sections realisation resonant frequencies are much more spread out than in the parallel connected realisation. It also clear that the resonant frequencies for filter 1 and filter 2 are within their respective bandwidths in the parallel connected network realisation.

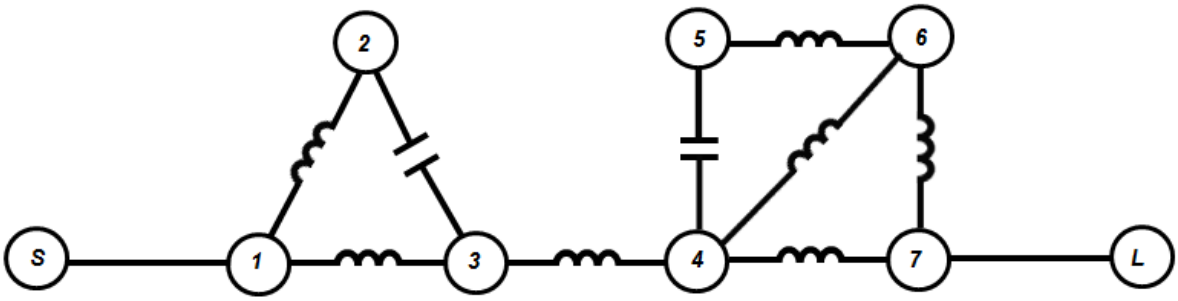

(a) 14-6-1 Filter Cascaded N-tuplets Sections Realisation

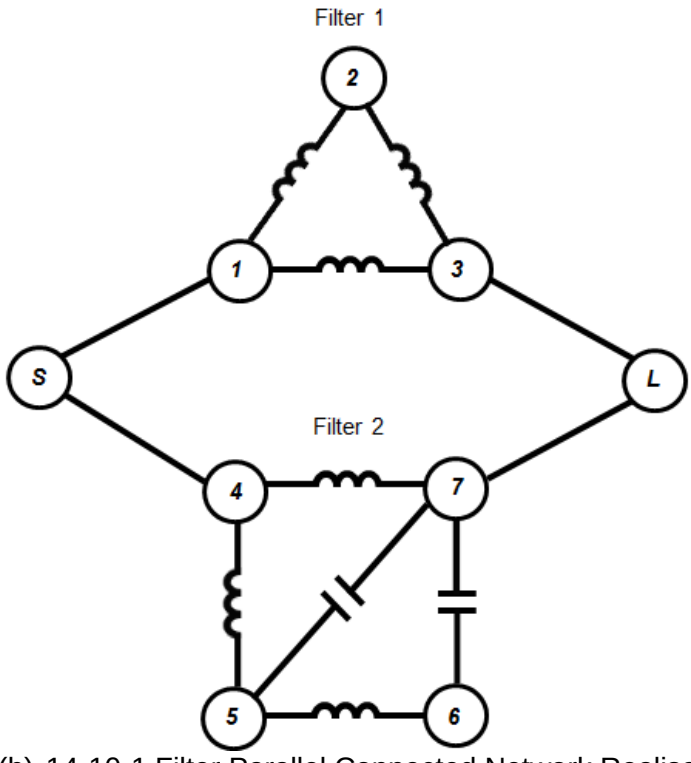

(b) 14-10-1 Filter Parallel Connected Network Realisation

Fig. 6-12 Two possible physical realisation of dual bandpass filter

Table 6-19 Dual Bandpass Filter Resonance Frequencies

All combline Resonators $75\ \Omega$

Physical length $\lambda/8$ long at $f_o = 1.985\ GHz$

14-6-1 Cascaded N-tuplets		14-10-1 Parallel Connected Networks	
Resonator	Frequency (GHz)	Resonator	Frequency (GHz)
1	2.0158	1	1.8243
2	1.9656	2	1.8403
3	1.9420	3	1.8243
4	2.0438	4	2.1384
5	2.1471	5	2.1294
6	1.9843	6	2.1596
7	2.0158	7	2.1353

Table 6-20 14-6-1 Cascaded N-tuplets Dual Bandpass Filter Inter-resonator Couplings using two combline resonators model

Coupling	Coefficient K_m (GHz)	f_{ev} (MHz)	f_{od} (MHz)	Coupling Bandwidth (MHz)
1-2	0.3614	1837.0	2122.8	285.8189
1-3	0.1726	1899.3	2053.5	154.2296
2-3	0.0612	1928.1	1980.6	52.5401
3-4	0.3637	1831.8	2132.1	300.3593
4-5	0.0445	2041.0	2150.6	109.5521
4-6	0.0398	1980.6	2047.3	66.6491
4-7	0.1316	1977.8	2079.2	101.4609
5-6	0.1445	1967.9	2160.5	192.5830
6-7	0.3847	1838.8	2137.2	298.3703

This could simplify numerical analysis when determining physical dimensions in parallel connected networks. In general the parallel connected network realisation has narrow coupling bandwidths compared to the cascaded n-tuplets realisation as evident from the results in Table 6-20, Table 6-21 and Table 6-22. Certainly some of the couplings in cascaded n-tuplets would require close proximity couplings or

other mechanisms to be practically realised [95]. This is worsened in very wide dual bandpass filters, making the cascaded n-tuplets realisation impractical [94]. The parallel connected network realisation therefore, provides a better realisation for moderate to wide bandwidth filters. The additional complex transmission zeros only slightly affect the filter's group delay and thus merely used for physically separating the two filtering paths in the parallel connected dual bandpass filter.

Table 6-21 14-10-1 Parallel Connected Dual Bandpass Filter Inter-resonator Couplings using two combline resonators model

Coupling	Coefficient K_m (GHz)	f_{ev} (MHz)	f_{od} (MHz)	Coupling Bandwidth (MHz)
Filter 1				
1-2	0.0640	1801.4	1862.3	60.9030
1-3	0.0202	1814.9	1833.6	18.7286
2-3	0.0640	1801.4	1862.3	60.9030
Filter 2				
4-5	0.0940	2102.1	2164.6	62.5434
4-7	0.0100	2133.2	2140.5	7.2627
5-6	0.0595	2119.7	2168.9	49.1275
5-7	0.0478	2112.6	2152.9	40.2689
6-7	0.0575	2121.1	2175.1	54.0165

Table 6-22 Dual Bandpass Filter Input/Output Couplings Bandwidths Comparisons (MHz)

14-6-1 Cascaded N-tuplets (Input=Output)	14-10-1 Parallel Connected Networks Filter 1 (Input=Output)	14-10-1 Parallel Connected Networks Filter 2 (Input/Output)
$f_{3dBupper} = 2088.9$	$f_{3dBupper} = 1859.7$	$f_{3dBupper} = 2175.5/2172.4$
$f_{3dBlower} = 1945.3$	$f_{3dBlower} = 1789.5$	$f_{3dBlower} = 2101.9/2098.8$
$f_{3dB} = 143.5767$	$f_{3dB} = 70.1797$	$f_{3dB} = 73.6691/73.5675$

6.5 Dual Bandpass Filter Design Example

In this section, a prototype dual bandpass filter will be designed with specifications shown in Table 6-23. Using (6.1) the normalised cutoff points in lumped domain are calculated as $\alpha = 0.7508$, $\beta = 0.7940$, $\gamma = 0.9532$ and $\delta = 1$.

Table 6-23 Dual Bandpass Filter Specifications

Passband 1	1800-1870 MHz
Passband 2	2100-2160 MHz
Insertion Loss	< 1 dB
Stopband Insertion Loss $IL \geq 40$ dB	1950-2000 MHz
Passband Return Loss (RL)	20 dB
Electrical length at Centre Frequency (1.98 GHz)	45^{o}

Table 6-24 12-4-1 Dual Bandpass Filter Basis Functions

α_r	N-N_{FTZ}-N_{OTZ}	Purpose
1	$4-2-1$	Provide a single transmission zero at the origin, a dependent pair of symmetrical transmission zero at $\omega_{z1} = \pm 0.8760$ and a single transmission zero at infinity
1	$8-2-0$	Provide a dependent pair of symmetrical transmission zeros at $\omega_{z2} = \pm 0.8500$ and six transmission zeros at infinity

To meet the specifications a 6[th] degree $(N = 14)$ dual bandpass filter with $N_1 = 6$ and $N_2 = 6$. The two basis functions used are shown in Table 6-24. Each of the basis function provides a dependent pair of symmetrical transmission zeros which are assigned to the inner stopband. This yields an overall 12-4-1 transfer function shown in Fig. 6-13.

The filter's polynomials were then computed as tabulated in Table 6-25. The transverse coupling matrix were generated and reduced to the folded canonical

topology shown in Fig. 6-14. The resulting $N_r \times N_r$ coupling matrix is shown in Table 6-26. The element values in Table 6-26 coupling matrices were converted to a distributed network and re-normalised by dividing by $\tan(a\omega_{u2})$. Finally, the element values were converted to capacitively loaded resonators as shown in Table 6-27.

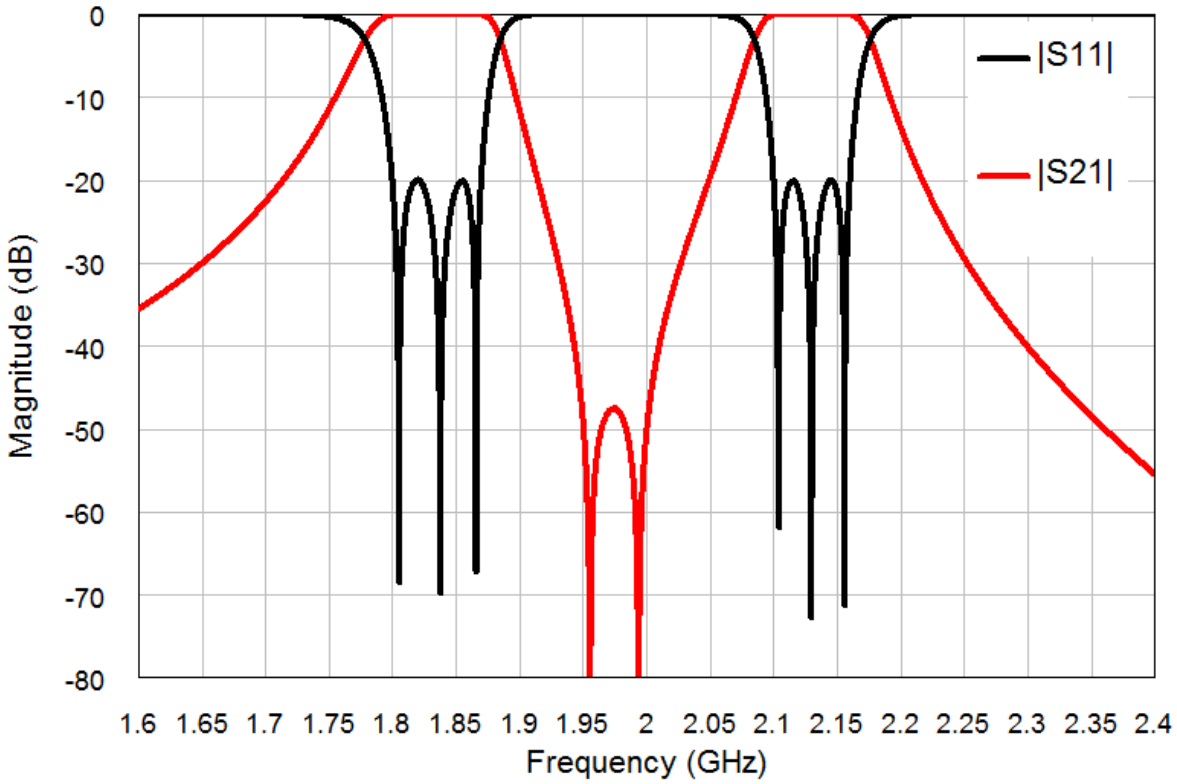

Fig. 6-13 Simulated magnitude response of a 12-4-1 dual bandpass filter

By employing the method as described in Chapter 1, the resonance frequencies, coupling bandwidths and 3 dB bandwidths for the input and output couplings were computed according to Table 5-15 , Table 5-16 and Table 5-17 respectively. EM modelling techniques were used to compute the initial physical dimension of the course model. Further fine tuning would be required to obtain equal ripple passband return loss in both bands. Fig. 6-15 shows the EM model for the dual bandpass filter and the corresponding EM simulation is shown in Fig. 6-16.

Table 6-25 12-4-1 Dual Bandpass Filter Polynomials

Characteristic Polynomials

$(\varepsilon = 3.9105 \times 10^3, \mu = 1)$

$P(p) = p^5 + 1.4899p^3 + 0.5545p$
$F(p) = p^{12} + 4.6549p^{10} + 8.9309p^8 + 9.0372p^6 + 5.0861p^4 + 1.5097p^2 + 0.1847$
$E(p) = p^{12} + 0.2095p^{11} + 4.6768p^{10} + 0.8130p^9 + 8.9988p^8 + 1.2471p^7 + 9.1153p^6 + 0.9452p^5 + 5.1256p^4 + 0.3539p^3 + 1.5171p^2 + 0.0524p + 0.1847$

Y Matrix Polynomials

$Y_{11n}(p) = 0.2095p^{11} + 0.8130p^9 + 1.2471p^7 + 0.9452p^5 + 0.3539p^3 + 0.0524p = Y_{22n}(p)$
$Y_{21n}(p) = Y_{12n}(p) = -(p^5 + 1.4899p^3 + 0.5545p)/\varepsilon$
$Y_{den}(p) = 2p^{12} + 9.3317p^{10} + 17.9297p^8 + 18.1524p^6 + 10.2118p^4 + 3.0267p^2 + 0.3694$

Table 6-26 $N_r \times N_r$ Coupling Matrix of a 12-4-1 Dual Bandpass Filter

$$Y_{BP} = M_{Ts} + pM_{Cs} + \frac{1}{p}M_{Ls}$$

$$M_{Ts} = \begin{bmatrix} 0.1048 & 0 & 0 & 0 & 0 & 0 \\ 0 & 0.0000 & 0 & 0 & 0 & 0 \\ 0 & 0 & 0.0000 & 0 & 0 & 0 \\ 0 & 0 & 0 & 0.0000 & 0 & 0 \\ 0 & 0 & 0 & 0 & 0.0000 & 0 \\ 0 & 0 & 0 & 0 & 0 & 0.1048 \end{bmatrix}$$

$$M_{Cs} = \begin{bmatrix} +1.0000 & 0 & 0 & 0 & 0 & 0 \\ 0 & 1.0000 & 0 & 0 & 0 & 0 \\ 0 & 0 & +1.0000 & 0 & -0.0290 & 0 \\ 0 & 0 & 0 & +1.0000 & 0 & 0 \\ 0 & 0 & -0.0290 & 0 & +1.0000 & 0 \\ 0 & 0 & 0 & 0 & 0 & +1.0000 \end{bmatrix}$$

$$M_{Ls} = \begin{bmatrix} +0.7859 & -0.1900 & 0 & 0 & 0 & 0 \\ -0.1900 & +0.7770 & -0.0713 & 0 & -0.0317 & 0 \\ 0 & -0.0713 & +0.8199 & -0.1409 & 0 & 0 \\ 0 & 0 & -0.1409 & +0.7202 & -0.0631 & 0 \\ 0 & -0.0317 & 0 & -0.0631 & +0.7757 & -0.1899 \\ 0 & 0 & 0 & 0 & -0.1899 & +0.7859 \end{bmatrix}$$

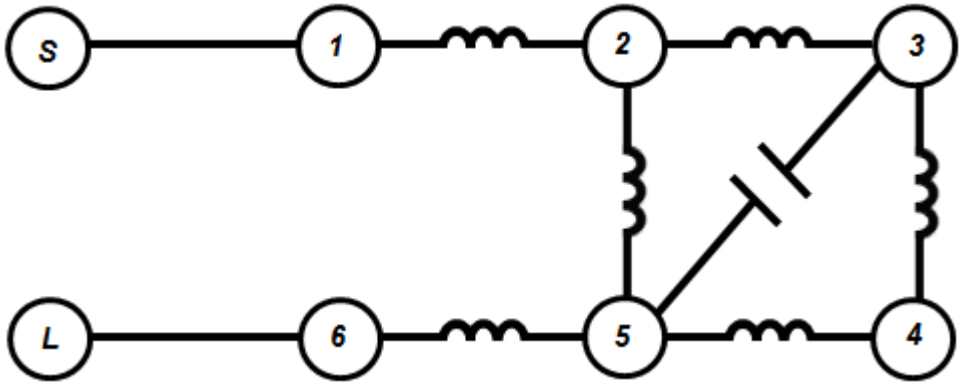

Fig. 6-14 12-4-1 Dual Bandpass Filter Topology

Table 6-27 Final Element Values of a Capacitively Loaded Dual Bandpass Filter

Inductive Inter-resonator Coupling Impedances (Ω)	Capacitors	Short-Circuited Stubs Impedance (Ω)
$Z_{12} = 373.90$	$C_1 = 1.0429\ pF$	$Z_r = 75$
$Z_{23} = 1013.8$	$C_2 = 1.0527\ pF$	Input/Output Coupling Impedance (Ω)
$Z_{25} = 2225.7$	$C_3 = 1.0069\ pF$	
$Z_{34} = 497.10$	$C_4 = 1.1203\ pF$	$K_{output} = 198.2380$
$Z_{45} = 1085.1$	$C_5 = 1.0542\ pF$	$K_{input} = 198.2380$
$Z_{56} = 373.70$	$C_6 = 1.0429\ pF$	Capacitive Inter-resonator Coupling Impedance (Ω)
		$Z_{35} = 3318.8$

Table 6-28 12-4-1 Dual Bandpass Filter Resonance Frequencies

All combline Resonators $75\ \Omega$

Physical length $\lambda/8$ long at $f_o = 1.98\ GHz$

Resonator	Frequency (GHz)
1	2.0011
2	1.9938
3	2.0283
4	1.9460
5	1.9927
6	2.0011

Table 6-29 12-4-1 Dual Bandpass Filter Inter-resonator Couplings using two combline resonators model

Coupling	Coefficient K_m (GHz)	f_{ev} (MHz)	f_{od} (MHz)	Coupling Bandwidth (MHz)
1-2	0.4063	1827.6	2140.4	312.8530
2-3	0.1525	1949.3	2069.1	119.8209
2-5	0.0679	1966.9	2018.9	52.0633
3-4	0.3014	1855.7	2103.6	247.8932
3-5	0.0465	1985.3	2036.4	51.1467
4-5	0.1350	1909.8	2025.9	116.1516
5-6	0.4061	1827.0	2139.9	312.9401

Table 6-30 12-4-1 Dual Bandpass Filter Input/Output Couplings

Resonator	Frequency (MHz)
$f_{3dBupper}$	2077.5
$f_{3dBlower}$	1927.4
f_{3dB}	150.0603

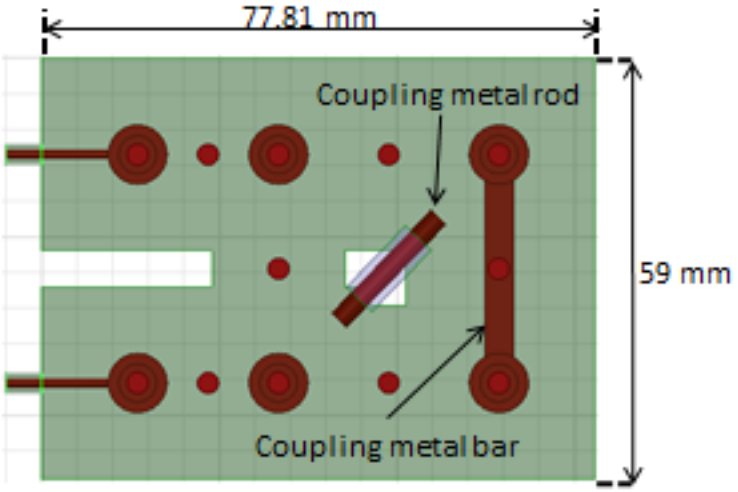

(a) Top view

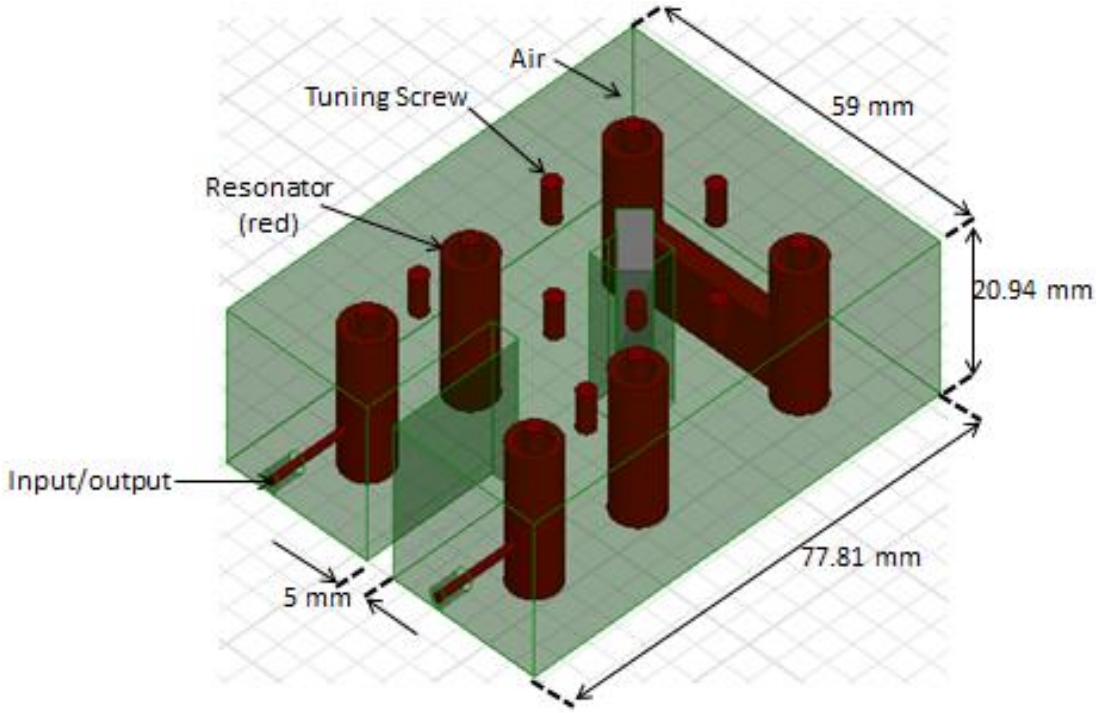

(b) Perspective view

Fig. 6-15 12-4-1 dual bandpass filter EM model

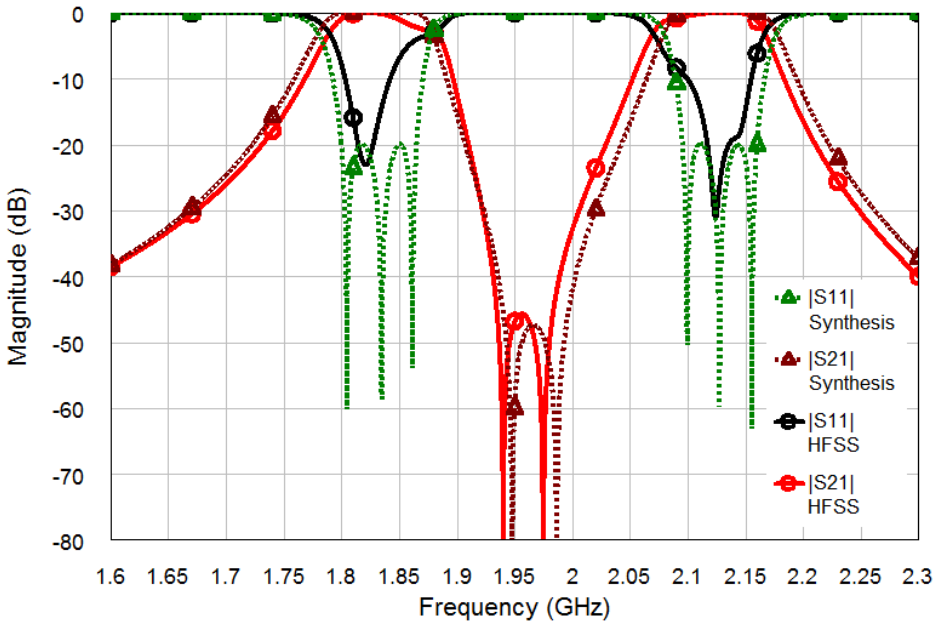

Fig. 6-16 Coarse EM vs Circuit simulation for the 12-4-1 dual bandpass filter

6.6 Conclusion

A method of direct synthesis of dual bandpass filter has been given. Section 6.2 highlighted the different methods used when synthesising dual bandpass filters. Then in section 6.3 the proposed method was described with the dual bandpass filter realised as cascaded n-tuplet. The alternative realisation using parallel connected bandpass networks were given in section 6.4 together with some design examples. Comparison was drawn between the two physical realisations and their merits were given. In section 6.5 an illustrative example of dual bandpass filter synthesis and design was given. Finally, a thesis conclusion and future work are presented in Chapter 7.

Chapter 7 Conclusion and Future Work

Filter synthesis is at the root of microwave filter design. Many decades of research has produced a conventional design process. The rapid development of information and technology has led to more challenges in the communication industry. This has meant that the design of filters needs to adapt to the dynamic requirements impossed by the wireless communications industry.

This research has produced some advanced work in filter synthesis and physical realisations suitable for selective microwave filters which are required to improve performance and reduce weight, volume and costs. Not only can the synthesis techniques be used for BTS filter designs but could also be used in many RF and microwave filter designs.

Chapter 1 begun with the overview description of filter synthesis and design techniques. This formed the foundation for the work presented in the rest of the Chapters. The synthesis is presented in a way suitable for easy computer programming.

In Chapter 2, the method of generating the generalised Chebyshev characteristic function used in the design of Chebyshev microwave filters was demonstrated. This allows different Chebyshev characteristic functions with arbitrary bandwidths to be synthesised. Linear combinations of the elementary characteristic functions, based on reflection and transmission zeros placement, allow high order symmetrical and asymmetrical characteristic functions to be determined. The demonstrated method is applicable to the synthesis of lumped and distributed, single or multi-band electrical filters. Typical and practical synthesis examples are given to show the power of this method.

An exact design technique for realising generalised Chebyshev distributed low-pass filters using coupled line/stub without approximating the series short circuited stubs has been demonstrated in Chapter 3. These low-pass filters have better selectivity and overall stopband response with quarter-wave transmission zeros.

The physical realisation I has a simple equivalent circuit, however, it requires isolation walls to eliminate coupling between basic sections. Since a single basic section may realise a pair of finite frequency transmission zero, a maximum of $(N-1)/2$ pairs of symmetrically located transmission zeros is achievable.

A more general meander-like structure, physical realisation II, with optimal number of elements and simple physical layout of transmission lines has also been presented. Its physical realisation does not require decoupling walls between the parallel coupled line section and hence is easier to construct. However, only certain forms of transfer functions are realisable as described in Chapter 3. Synthesis of a few realisations up to 9^{th} degree together with the required transmission zeros locations of their canonical forms have been illustrated.

A low-pass filter design example utilising the later physical realisation was fabricated and measurement results showed good agreement with theory. Comparison with other low-pass filter realisations reviewed that the proposed low-pass filter has a much higher roll-off rate and deeper effective stopband.

Future work could focus on general extension of the synthesis approach to an N^{th} meander-like low-pass filter. It would also be interesting to see how the stopband could further be extended in this physical realisation within realisable element values. One possible solution is to change the filter impedance and use of impedance matching circuits at both the input and output of the filter network. This would allow small electrical lengths to be used and thus much broader stopband width. Another alternative solution is to shorten the open circuited stubs and compensate the resulting effect by lumped capacitive loading at the ends of the shortened stubs. This broadens the effective stopband with minimum effect on the passband return loss while providing close-to-theoretical rejection in the stopband as was demonstrated in Chapter 3. Future work could also investigate the possibility of using this known synthesis approach in design of meander-line phase-shifters [97].

In Chapter 4, a new method for synthesis of pseudo-elliptic bandpass filter with integrated transmission zeros has been described. Pseudo-elliptic filters described in this Chapter make an important application in the design of filters with

transmission zeros at finite frequency to increase close-to-band rejection. These sorts of filters could suitably be used in cellular BTS where a high rejection is required in the transmitter band of the receiver filter and conversely the receiver band of the transmitter filter.

Two suitable low-pass prototypes were considered together with their merits. The asymmetrical-frequency-transformed pseudo-elliptic low-pass prototype filter provides an easy design for pseudo-elliptic bandpass filters with all transmission zeros at a single finite frequency. The advantage provided is that, although the filtering response is asymmetrical, the pseudo-elliptic low-pass filter itself is symmetrical and thus produces a symmetrical physical structure. Nevertheless, the rejection is not well distributed across the stopband and generally will require higher filter order to improve the stopband rejection than the general pseudo-elliptic low-pass prototype filter. The general pseudo-elliptic low-pass prototype filter with distributed transmission zeros in the stopband is therefore preferred. Such a prototype, moreover also generally produces a physically asymmetrical filter. In addition it requires fewer elements for the same attenuation in the stopband than its asymmetrical-frequency-transformed elliptic low-pass prototype filter counterpart.

Integrated transmission zeros were achieved using re-entrant transmission line elements. The design of microwave bandpass filters using re-entrant resonators with arbitrarily placed transmission zeros above the passband had been demonstrated. A five pole re-entrant bandpass filter was designed and fabricated. The measured results showed good agreement with established theories. Such a simple physical construction offers significant advantages over conventional design when very high stopband attenuation is required.

Chapter 5 showed the general application of the synthesis methods of Chapter 1 and Chapter 2 to the synthesis of bandpass filters and narrow dual bandpass filters. The synthesis is based on linear combination of Chebyshev elementary characteristic functions based on the number and position of the transmission zeros.

Applications for the design of practical bandpass filters have been examined. Explicit design procedures for exact synthesis of pseudo-combline and interdigital bandpass filter have been given. Two experiment 5^{th} degree combline bandpass filters were designed. A similar design procedure has been demonstrated for interdigital bandpass filters. Furthermore, the method of synthesising relatively close-spaced Chebyshev dual passband filters was outlined. A 10^{th} degree symmetrical dual bandpass filter was synthesised to illustrate the principles.

Multiband filters are important in modern communication systems that ensure effective filtering for multi-bands in diplexer architectures. An alternative method for direct synthesis of dual bandpass filters was presented in Chapter 6 that allows better control over out-of-band rejection levels as opposed to [93]. The outlined method provides a simple direct synthesis method for design of dual bandpass filter by using pre-determined basis functions. The method allows control over the number and position of both the reflection and transmission zeros in both passbands and stopbands. It also provides a better alternative to other approximation methods where transformations and optimisations are used.

Practical Limitations of the dual bandpass filter are clearly understood. This is due to increased permutation of the number and position of reflection and transmission zeros - because of increased number of passbands and stopbands compared to single bandpass filters. Some of the transmission zeros of the basis functions are dependant transmission zeros in order to control the four passband edges of the dual bandpass filter. However, the synthesis method enables these transmission zeros to be allocated to the desired stopbands to meet the filter's specifications.

The method also allows synthesis of dual bandpass filters with arbitrary bandwidths and separations of the two bands. Finally the method could also be used for different physical topological realisations. It has been demonstrated how cascaded n-tuplets section realisation may be achieved. The parallel connected filter networks also provides alternative realisation especially when the two bands are wide apart. The decomposition of a dual bandpass filter into parallel connected filter networks has clearly been demonstrated with examples. The merits of both

topologies in terms of coupling bandwidth realisations have also been shown and a practical design example given.

Since much of the work involved synthesis, future work would perhaps focus on implementing the synthesis of dual bandpass in different technologies. Further miniaturisation could be achieved by use of multi-mode ceramic filters. This is another area being exploited to increasing performance of microwave filters. However, it must be mentioned here that not all facets of microwave filter are simultaneously improved as filter design often involves various trade-offs.

Another area that could be exploited in future is implementing the dual band filter parallel sub-networks using different unloaded quality factors. This is possible because the two filter sub-networks dimensions and hence the unloaded quality factor is frequency dependant thus allowing different dimensions for the networks to be used. Different technology implementation could also be exploited for the two sub-networks.

Sometimes, other multiband filters such as triple and quadruplet bandpass filters may be required. The low-pass prototype filter networks for such filtering function may easily be generated using the concept developed in Chapter 2.

Future research could also focus on finding other simple physical structures that could be used to implement strong couplings in wide dual bandpass filters dealt with in Chapter 6. As it has been demonstrated before, it is one thing to develop filter circuit networks through synthesis and quite another to be able to physically realise the circuit model. Even though EM simulators provide close to real performance of the physical filter, it would be imperative to fabricate some prototype designs to see the measured performance and validate some of the synthesised dual bandpass filters, especially the parallel connected network.

List of References

1. *RF Front-End Technology Challenges*. ICT Knowledge Transfer Network and Cambridge Wireless joint positioning paper 2012; Available from: https://connect.innovateuk.org/documents/2849135/3712563/04Dec12+RF+Front+End+Technologies+Challenges+Paper+ICTKTN+%26+CW+FINAL.pdf/b39ee4e9-bfce-4cdc-abea-36a85755b064.
2. Mansour, R.R., *Filter technologies for wireless base stations.* Microwave Magazine, IEEE, 2004. **5**(1): p. 68-74.
3. Cameron, R.J., C.M. Kudsia, and R.R. Mansour, *Microwave filters for communication systems: fundamentals, design, and applications*. 2007, Hoboken, N.J: Wiley-Interscience.
4. Hunter, I., *Theory and design of microwave filters*. 2001: IET.
5. Matthaei, G.L., L. Young, and E.M.T. Jones, *Microwave filters, impedance-matching networks, and coupling structures*. 1980, Dedham, MA: Artech House.
6. Hong, J.-S. and M.J. Lancaster, *Microstrip filters for RF/microwave applications*. 2001, Chichester; New York: Wiley.
7. Youla, D.C., *A tutorial exposition of some key network-theoretic ideas underlying classical insertion-loss filter design.* Proceedings of the IEEE, 1971. **59**(5): p. 760-799.
8. Saal, R. and E. Ulbrich, *On the Design of Filters by Synthesis.* Circuit Theory, IRE Transactions on, 1958. **5**(4): p. 284-327.
9. Richards, P.I., *Resistor-transmission-line circuits.* Proceedings of the IRE, 1948. **36**(2): p. 217-220.
10. Hunter, I., et al., *Microwave filter design from a systems perspective.* Microwave Magazine, IEEE, 2007. **8**(5): p. 71-77.
11. Rhodes, J.D. and S. Alseyab, *The generalized chebyshev low-pass prototype filter.* International Journal of Circuit Theory and Applications, 1980. **8**(2): p. 113-125.
12. Meng, M., *Design and synthesis of lossy microwave filters*. 2014: Leeds
13. Cameron, R.J., *Advanced Filter Synthesis.* Microwave Magazine, IEEE, 2011. **12**(6): p. 42-61.
14. Atia, A. and A. Williams, *New types of waveguide bandpass filters for satellite transponders.* Comsat Tech. Review, 1971. **1**(1): p. 20-43.
15. *Coupling Matrix Software*. Available from: http://www.guidedwavetech.com/.
16. Cameron, R.J., *General coupling matrix synthesis methods for Chebyshev filtering functions.* Microwave Theory and Techniques, IEEE Transactions on, 1999. **47**(4): p. 433-442.
17. Cameron, R.J., *Advanced coupling matrix synthesis techniques for microwave filters.* Microwave Theory and Techniques, IEEE Transactions on, 2003. **51**(1): p. 1-10.
18. Bell, H.C., Jr., *Canonical Asymmetric Coupled-Resonator Filters.* Microwave Theory and Techniques, IEEE Transactions on, 1982. **30**(9): p. 1335-1340.

19. Cameron, R.J., A.R. Harish, and C.J. Radcliffe, *Synthesis of advanced microwave filters without diagonal cross-couplings.* Microwave Theory and Techniques, IEEE Transactions on, 2002. **50**(12): p. 2862-2872.
20. Macchiarella, G., *Accurate synthesis of inline prototype filters using cascaded triplet and quadruplet sections.* Microwave Theory and Techniques, IEEE Transactions on, 2002. **50**(7): p. 1779-1783.
21. Tamiazzo, S. and G. Macchiarella, *An analytical technique for the synthesis of cascaded N-tuplets cross-coupled resonators microwave filters using matrix rotations.* Microwave Theory and Techniques, IEEE Transactions on, 2005. **53**(5): p. 1693-1698.
22. Wei, M., et al., *Synthesis of Wideband Multicoupled Resonators Filters.* Microwave Theory and Techniques, IEEE Transactions on, 2011. **59**(3): p. 593-603.
23. Wei, M., et al. *Synthesis of multi-coupled resonator filters with frequency-dependent couplings*. in *Microwave Symposium Digest (MTT), 2010 IEEE MTT-S International*. 2010.
24. Yildirim, N., et al., *A revision of cascade synthesis theory covering cross-coupled filters.* Microwave Theory and Techniques, IEEE Transactions on, 2002. **50**(6): p. 1536-1543.
25. Kinayman, N. and M.I. Aksun, *Modern microwave circuits*. 2005, Boston; London: Artech House.
26. Montejo-Garai, J.R., *Synthesis of filters with transmission zeros at real frequencies by means of trisections including source/load to resonator coupling.* Electronics Letters, 2000. **36**(19): p. 1629-1630.
27. Montejo-Garai, J.R., et al., *Synthesis and design of in-line N-order filters with N real transmission zeros by means of extracted poles implemented in low-cost rectangular H-plane waveguide.* Microwave Theory and Techniques, IEEE Transactions on, 2005. **53**(5): p. 1636-1642.
28. Rhodes, J.D. and R.J. Cameron, *General Extracted Pole Synthesis Technique with Applications to Low-Loss TE₀₁₁ Mode Filters.* Microwave Theory and Techniques, IEEE Transactions on, 1980. **28**(9): p. 1018-1028.
29. Rhodes, J.D., *Theory of electrical filters*. 1976, London: Wiley.
30. Swanson, D.G. *RF and Microwave Filter Design with EM Simulation*. Annual International Courses in Telecommunications Semiconductor Technology Nanotechnology, 2010.
31. Ness, J.B., *A unified approach to the design, measurement, and tuning of coupled-resonator filters.* Microwave Theory and Techniques, IEEE Transactions on, 1998. **46**(4): p. 343-351.
32. Gunston, M.A.R., *Microwave transmission-line impedance data*. 1972, London Van Nostrand Reinhold.
33. Getsinger, W.J., *Coupled rectangular bars between parallel plates.* Microwave Theory and Techniques, IRE Transactions on, 1962. **10**(1): p. 65-72.
34. Cristal, E.G., *Coupled Circular Cylindrical Rods Between Parallel Ground Planes.* Microwave Theory and Techniques, IEEE Transactions on, 1964. **12**(4): p. 428-439.

35. Rhodes, J.D. and S.A. Alseyab, *Simple design technique for TEM-networks having equal-diameter coupled circular cylindrical rods between parallel ground planes.* Microwaves, Optics and Acoustics, IEE Journal on, 1979. **3**(4): p. 142-146.
36. Hong, J.S., *Couplings of asynchronously tuned coupled microwave resonators.* Microwaves, Antennas and Propagation, IEE Proceedings, 2000. **147**(5): p. 354-358.
37. Bakr, M.H., et al., *A trust region aggressive space mapping algorithm for EM optimization.* Microwave Theory and Techniques, IEEE Transactions on, 1998. **46**(12): p. 2412-2425.
38. Bakr, M.H., et al., *A hybrid aggressive space-mapping algorithm for EM optimization.* Microwave Theory and Techniques, IEEE Transactions on, 1999. **47**(12): p. 2440-2449.
39. Bandler, J.W., et al., *Electromagnetic optimization exploiting aggressive space mapping.* Microwave Theory and Techniques, IEEE Transactions on, 1995. **43**(12): p. 2874-2882.
40. Bandler, J.W., et al., *Design optimization of interdigital filters using aggressive space mapping and decomposition.* Microwave Theory and Techniques, IEEE Transactions on, 1997. **45**(5): p. 761-769.
41. Bandler, J.W., et al. *Aggressive space mapping for electromagnetic design*. in *Microwave Symposium Digest, 1995., IEEE MTT-S International*. 1995.
42. Bandler, J.W. and Q.J. Zhang. *Next generation optimization methodologies for wireless and microwave circuit design*. in *Technologies for Wireless Applications, 1999. Digest. 1999 IEEE MTT-S Symposium on*. 1999.
43. Bandler, J.W., et al., *Space mapping technique for electromagnetic optimization.* Microwave Theory and Techniques, IEEE Transactions on, 1994. **42**(12): p. 2536-2544.
44. WOLANSKÝ, D. and R. Tkadlec, *Coaxial filters optimization using tuning space mapping in CST studio.* RADIOENGINEERING, 2011. **20**(1): p. 289.
45. Garcia-Lamperez, A., et al., *Efficient electromagnetic optimization of microwave filters and multiplexers using rational models.* Microwave Theory and Techniques, IEEE Transactions on, 2004. **52**(2): p. 508-521.
46. Traina, D. and G. Macchiarella. *Novel Formulations of the Cauchy Method Suitable for the Synthesis of Microwave Filters and Duplexers*. in *Microwave Conference, 2006. 36th European*. 2006.
47. Macchiarella, G. and D. Traina, *A formulation of the Cauchy method suitable for the synthesis of lossless circuit models of microwave filters from lossy measurements.* Microwave and Wireless Components Letters, IEEE, 2006. **16**(5): p. 243-245.
48. Esmaeili, M. and A. Borji. *Diagnosis and tuning of multiple coupled resonator filters*. in *Electrical Engineering (ICEE), 2010 18th Iranian Conference on*. 2010.
49. Zhang, Y.-L., et al., *A Hybrid Computer-Aided Tuning Method for Microwave Filters.* Progress In Electromagnetics Research, 2013. **139**: p. 559-575.
50. Swanson, D. and G. Macchiarella, *Microwave filter design by synthesis and optimization.* Microwave Magazine, IEEE, 2007. **8**(2): p. 55-69.

51. Swanson, D.G., *Narrow-band microwave filter design.* Microwave Magazine, IEEE, 2007. **8**(5): p. 105-114.
52. Musonda, E. and I. Hunter. *Synthesis of general Chebyshev characteristic function for dual (single) bandpass filters*. in *Microwave Symposium (IMS), 2015 IEEE MTT-S International*. 2015.
53. Snyder, R.V., et al., *Present and Future Trends in Filters and Multiplexers.* Microwave Theory and Techniques, IEEE Transactions on, 2015. **63**(10): p. 3324-3360.
54. Abramowitz, M. and I. Stegun, *Legendre functions and orthogonal polynomials. Ch. 22 in Chs. 8 and 22.* Handbook of mathematical functions with formulas, graphs, and mathematical tables, 1972: p. 331-339.
55. Levy, R., *A New Class of Distributed Prototype Filters with Applications to Mixed Lumped/Distributed Component Design.* Microwave Theory and Techniques, IEEE Transactions on, 1970. **18**(12): p. 1064-1071.
56. Jeffrey, A., *Handbook of mathematical formulas and integrals*. 2004, London: Elsevier Acdemic Press.
57. Wenzel, R.J., *Synthesis of Combline and Capacitively Loaded Interdigital Bandpass Filters of Arbitrary Bandwidth.* Microwave Theory and Techniques, IEEE Transactions on, 1971. **19**(8): p. 678-686.
58. Jaradat, H.M. and W.M. Fathelbab. *Selective lowpass filters realizing finite-frequency transmission zeros*. in *Radio and Wireless Symposium, 2009. RWS '09. IEEE*. 2009.
59. Chen, C.J., C.H. Sung, and Y.D. Su, *A Multi-Stub Lowpass Filter.* Microwave and Wireless Components Letters, IEEE, 2015. **25**(8): p. 532-534.
60. Alseyab, S.A., *A Novel Class of Generalized Chebyshev Low-Pass Prototype for Suspended Substrate Stripline Filters.* Microwave Theory and Techniques, IEEE Transactions on, 1982. **30**(9): p. 1341-1347.
61. Musonda, E. and I. Hunter. *Design of generalised Chebyshev lowpass filters using coupled line/stub sections*. in *Microwave Symposium (IMS), 2015 IEEE MTT-S International*. 2015.
62. Musonda, E. and I.C. Hunter, *Exact Design of a New Class of Generalized Chebyshev Low-Pass Filters Using Coupled Line/Stub Sections.* Microwave Theory and Techniques, IEEE Transactions on, 2015. **PP**(99): p. 1-11.
63. Sato, R., *A Design Method for Meander-Line Networks Using Equivalent Circuit Transformations.* Microwave Theory and Techniques, IEEE Transactions on, 1971. **19**(5): p. 431-442.
64. Wang, J., et al., *Compact quasi-elliptic microstrip lowpass filter with wide stopband.* Electronics Letters, 2010. **46**(20): p. 1384-1385.
65. Musonda, E. and I.C. Hunter, *Microwave Bandpass Filters Using Re-Entrant Resonators.* Microwave Theory and Techniques, IEEE Transactions on, 2015. **63**(3): p. 954-964.
66. Amari, S. and G. Macchiarella, *Synthesis of inline filters with arbitrarily placed attenuation poles by using nonresonating nodes.* Microwave Theory and Techniques, IEEE Transactions on, 2005. **53**(10): p. 3075-3081.
67. Lapidus, A. and C. Rossiter, *Cross-coupling in microwave bandpass filters.* Microwave Journal, 2004. **47**(11): p. 22-24.

68. Thomas, J.B., *Cross-coupling in coaxial cavity filters - a tutorial overview.* Microwave Theory and Techniques, IEEE Transactions on, 2003. **51**(4): p. 1368-1376.
69. Amari, S., U. Rosenberg, and J. Bornemann, *Singlets, cascaded singlets, and the nonresonating node model for advanced modular design of elliptic filters.* Microwave and Wireless Components Letters, IEEE, 2004. **14**(5): p. 237-239.
70. Amari, S. and U. Rosenberg, *Synthesis and design of novel in-line filters with one or two real transmission zeros.* Microwave Theory and Techniques, IEEE Transactions on, 2004. **52**(5): p. 1464-1478.
71. Glubokov, O. and D. Budimir, *Extraction of Generalized Coupling Coefficients for Inline Extracted Pole Filters With Nonresonating Nodes.* Microwave Theory and Techniques, IEEE Transactions on, 2011. **59**(12): p. 3023-3029.
72. Macchiarella, G. and M. Politi. *Use of generalized coupling coefficients in the design of extracted-poles waveguide filters with non-resonating nodes*. in *Microwave Symposium Digest, 2009. MTT '09. IEEE MTT-S International*. 2009.
73. Amari, S. and U. Rosenberg. *A third order in-line pseudo-elliptic filter with a transmission zero extracted at its center*. in *Microwave Symposium Digest, 2004 IEEE MTT-S International*. 2004.
74. Macchiarella, G., *Synthesis of an in-line prototype filter with two transmission zeros without cross couplings.* Microwave and Wireless Components Letters, IEEE, 2004. **14**(1): p. 19-21.
75. Cohn, S.B., *The Re-Entrant Cross Section and Wide-Band 3-db Hybrid Couplers.* Microwave Theory and Techniques, IEEE Transactions on, 1963. **11**(4): p. 254-258.
76. Horton, M.C. and R.J. Wenzel, *The Digital Elliptic Filter - A Compact Sharp-Cutoff Design for Wide Bandstop or Bandpass Requirements.* Microwave Theory and Techniques, IEEE Transactions on, 1967. **15**(5): p. 307-314.
77. Ruiz-Cruz, J.A., M.M. Fahmi, and R.R. Mansour, *Triple-Conductor Combline Resonators for Dual-Band Filters With Enhanced Guard-Band Selectivity.* Microwave Theory and Techniques, IEEE Transactions on, 2012. **60**(12): p. 3969-3979.
78. Sato, R. and E.G. Cristal, *Simplified Analysis of Coupled Transmission-Line Networks.* Microwave Theory and Techniques, IEEE Transactions on, 1970. **18**(3): p. 122-131.
79. Abramowicz, A., *Modelling of wide band combline and interdigital filters.* Mikrotalasna revija, 2010. **16**(1): p. 15-22.
80. Shapir, I., V.A. Sharir, and D.G. Swanson, *TEM modeling of parasitic bandwidth expansion in combline filters.* Microwave Theory and Techniques, IEEE Transactions on, 1999. **47**(9): p. 1664-1669.
81. Levy, R., *Generalized rational function approximation in finite intervals using Zolotarev functions.* Microwave Theory and Techniques, IEEE Transactions on, 1970. **18**(12): p. 1052-1064.
82. Bell, H.C., *Zolotarev bandpass filters.* Microwave Theory and Techniques, IEEE Transactions on, 2001. **49**(12): p. 2357-2362.

83. Latif, M., et al. *Synthesis and full-wave EM Simulation of Ku-band direct-coupled 10th order dual-band Zolotarev bandpass filter and performance comparison with Chebyshev bandpass filter*. in *Satellite Telecommunications (ESTEL), 2012 IEEE First AESS European Conference on*. 2012.
84. Lunot, V., et al., *Certified Computation of Optimal Multiband Filtering Functions.* Microwave Theory and Techniques, IEEE Transactions on, 2008. **56**(1): p. 105-112.
85. Lunot, V., S. Bila, and F. Seyfert. *Optimal Synthesis for Multi-Band Microwave Filters*. in *Microwave Symposium, 2007. IEEE/MTT-S International*. 2007.
86. Bila, S., et al. *Chebyshev Synthesis for Multi-Band Microwave Filters*. in *Microwave Symposium Digest, 2006. IEEE MTT-S International*. 2006.
87. Mokhtaari, M., et al., *Coupling-Matrix Design of Dual and Triple Passband Filters.* Microwave Theory and Techniques, IEEE Transactions on, 2006. **54**(11): p. 3940-3946.
88. Juseop, L. and K. Sarabandi, *A Synthesis Method for Dual-Passband Microwave Filters.* Microwave Theory and Techniques, IEEE Transactions on, 2007. **55**(6): p. 1163-1170.
89. Macchiarella, G. and S. Tamiazzo, *Design techniques for dual-passband filters.* Microwave Theory and Techniques, IEEE Transactions on, 2005. **53**(11): p. 3265-3271.
90. Orchard, H. and G.C. Temes, *Filter design using transformed variables.* Circuit Theory, IEEE Transactions on, 1968. **15**(4): p. 385-408.
91. Yunchi, Z., et al. *Analytical Synthesis of Generalized Multi-band Microwave Filters*. in *Microwave Symposium, 2007. IEEE/MTT-S International*. 2007.
92. Juseop, L. and K. Sarabandi, *Synthesizing microwave resonator filters.* Microwave Magazine, IEEE, 2009. **10**(1): p. 57-65.
93. Fei, X., *Direct Synthesis Technique for Dual-Passband Filters: Superposition Approach.* Circuits and Systems II: Express Briefs, IEEE Transactions on, 2013. **60**(5): p. 267-271.
94. Macchiarella, G. and S. Tamiazzo. *Synthesis of dual-band filters with parallel-connected networks*. in *European Microwave Conference (EuMC), 2014 44th*. 2014.
95. Snyder, R.V. and S. Bastioli. *Transmission zero generation for wideband high frequency evanescent mode filters*. in *Microwave Symposium (IMS), 2014 IEEE MTT-S International*. 2014.
96. Macchiarella, G. and S. Tamiazzo. *Dual-Band Filters for Base Station Multi-Band Combiners*. in *Microwave Symposium, 2007. IEEE/MTT-S International*. 2007.
97. Bulja, S. and D. Mirshekar-Syahkal, *Meander line millimetre-wave liquid crystal based phase shifter.* Electronics Letters, 2010. **46**(11): p. 769-771.